Characterization of translational mechanisms in astrocytes

Marc Oudart

Sorbonne Université

Ecole doctorale n° 158 – Cerveau Cognition Comportement (ED3C)

Centre Interdisciplinaire de Recherche en Biologie (CIRB), Collège de France

Equipe de recherche – Physiologie et physiopathologie de l'unité gliovasculaire

Characterization of translational mechanisms in astrocytes

Par Marc Oudart

Thèse de doctorat de Neurosciences et sciences cognitives

Dirigée par Martine Cohen-Salmon

Présentée et soutenue publiquement le 28 septembre 2022

Devant un jury composé de :	
Alain Trembleau, PU, Institut de Biologie Paris Seine	Président
Jimena Baleriola, DR, Achucarro Basque Center for Neuroscience	Rapportrice
Olivier Namy, DR, Institut de Biologie Cellulaire Intégrative	Rapporteur
Hervé Le Hir, DR, Institut de Biologie de l'Ecole Normale Supérieure	Examinateur
Célia Plisson-Chastang, CR, Laboratoire de Biologie Moléculaire Eucaryotes	Examinatrice
Clément Chapat, CR, Ecole Polytechnique	Invité
Martine Cohen-Salmon, DR, Collège de France	Directrice de thèse

Remerciements

Je voudrais remercier les membres du jury pour avoir engagé une discussion passionnante lors de la soutenance ainsi que mes rapporteurs, Clément Chapat et Jimena Baleriola, pour leur lecture attentive de ce manuscrit.

Merci à Clément Chapat de s'être plongé dans le monde des astrocytes lors de mes comités de suivi de thèse et de notre collaboration fructueuse. Merci également à Cyril Hanus pour ses précieux retours sur ma thèse lors des 2 CSI.

Martine, tu m'as engagé sur un projet ambitieux au départ car avec une approche ouverte où on ne savait pas trop ce qu'on allait trouver. Et finalement on a trouvé RACK1 (grâce à toi) et ça a été le jackpot. Même si je croyais que rien ne se passait dans cette souris au début, on a été très content d'obtenir de beaux résultats. Ce qui est bien avec toi c'est que tu nous assures un article tôt dans la thèse comme ça on peut s'engager sur quelque chose de plus risqué sur la suite. Notre papier AstroDot est toujours aussi utilisé. Je pense que tu m'appris à être le scientifique que je suis devenu aujourd'hui dans l'efficacité et la rigueur de travail.

J'ai vraiment eu l'impression d'avoir créé le laboratoire aux côtés de Martine, Anne-Cécile, Noémie et Alice. Je me suis approprié tous les aspects du labo et ça m'a beaucoup plu. Ça va être dur de partir dans un labo inconnu !

Je suis content d'avoir pu partager ça avec toi Anne-Cécile. J'ai toujours pu discuter avec toi au labo ou autour d'une bière. Merci de m'avoir aussi bien accueilli.

J'aimerais aussi remercier Noémie et Alice avec qui j'ai partagé une bonne partie de ma thèse, on a partagé des projets, des soirées, un mariage et en restera pleins de bons souvenirs. Merci Noémie pour ces parties de jeux de société et toutes ces soirées. Merci Alice pour tous ces gouters ! Vous m'avez bien intégré au CIRB.

Je remercie tous mes étudiants qui étaient honnêtement de supers étudiants et qui ont tous contribué dans ma thèse. Robin a été le 1er suivi d'Ines, vous m'avez grandement aidé dans l'étude des ARNs associés à RACK1. Katia tu m'as aidé sur tous les aspects du projet et enfin Mathis tu t'es pris au jeu du volume astrocytaire et à m'embêter (merci pour ton initiation au wordle, lewdle, globle et compagnie)!

J'aimerais remercier la nouvelle (pas si nouvelle) génération du labo. Leila avec qui j'ai partagé 2 semaines dans le labo de Schuman où on s'est bien amusé à peindre des gateaux de Noël, à manger

de la choucroute et du Glüwein et des trucs bizarres. Merci Katia pour ton aide sur mes projets. Désolé si je t'embête tout le temps sur ton accent mexicain et sur ta taille, tu parles très bien français ! On peut compter sur toi dans le labo et tu es d'un très grand soutien. Merci à toutes les deux pour les gouters revivifiants. Merci Rodrigo pour tes histoires passionnantes et ta bonne humeur. Merci Barbara avec tes blagues un peu bizarres.

Je tiens aussi à remercier Xabi, on s'entendait bien et j'avais plaisir à discuter avec toi. Merci Romain et tes humeurs toujours aussi marquantes, on s'est bien amusé avec toi au labo (à coup d'AstroDot h24). Merci aussi à Emma, vous étiez là au tout début de ma thèse et c'était une chouette entrée en matière.

En dehors du labo je veux remercier mes potes de Bordeaux : Alex, Tommy, Raph, Rémi et Arnaud. Vous êtes merveilleux. Le confinement s'est beaucoup mieux passer grâce à nos visios jusqu'à 2h du mat' le samedi à jouer à la belotte. Vous êtes toujours là et vous êtes ma famille.

Je remercie aussi ma famille : ma mère, mon beau-père, mon père, Véronique et ma sœur. Je n'ai pas été présent pour vous pendant ces 4 ans de thèse mais vous avez toujours été là et c'est grâce à vous si j'ai pu aller à Paris et faire une thèse dans les meilleures conditions.

Merci à Carole qui me supporte tous les jours et m'écoute parler IP et blot à longueur de journée sans jamais décrocher. Merci !

Merci à mes colocs Laure et Quentin, vous m'avez supporté au jour le jour pendant 4 ans et j'ai beaucoup aimé notre cohabitation et les soirées jeux. Merci aussi aux potes d'Ulm : Brieuc, Alban, Lucas, Victor et Coline pour toutes nos soirées à l'ENS et les sorties le weekend !

Je voudrais remercier aussi toute l'équipe Rouach et plus particulièrement : Rachel, tu es la personne la plus gentille du monde, tu es d'un soutien sans faille. Eléonore, merci pour ces soirées et ces moments au club med et ton aide pour le patch (heureusement que tu es là) ! Merci aussi à Jeff , Giam et Josien, il est facile de discuter avec vous et vous êtes toujours à l'écoute. Merci au trio Noémie, Flora et Anna qui m'ont tout de suite intégré. Merci aussi à Augustin pour tous les moments qu'on a partagé en M2 et après et avec Adam. Merci aussi au reste de l'équipe, Pascal tu es toujours prêt à aider, Julien, Charles, Elena, Isabelle, Noémie C, Armelle, Nathalie, Jérome, Danijela, Daria, David et Glenn.

Merci aussi aux anciens de l'équipe Joliot Edmond et Irène.

Merci à nos voisins Belen et Alessya avec qui on a partagé de bons moments à la retraite étudiante, Richard, David et Gilles.

Merci à Camille ! On a partagé énormément de choses et de soirées. Tu es venue jusque dans mon labo pour me sortir et m'introduire à tout le CIRB. Tu as créé mon cercle d'amis au Collège. Tu as toujours été à l'écoute tout en me confrontant sur mes décisions telle une vraie amie.

Enfin, je tenais à remercier les potos du bâtiment B. Vous m'avez accepté parmi vous en un clin d'œil malgré la séparation des bâtiments. J'ai tellement de bons souvenirs (et des souvenirs de ne plus me souvenir) avec Pierre, P-E, Juliette, Sonia, Camille, Marie, Emma et Solène. Vous êtes tellement bienveillant et ça a vraiment contribué à me sentir bien au Collège. Merci aussi à Noémie Brassard, Maëla, Camille Curantz, Camille Compère, Omar, Beetsi, Théo, Shayan, Sabrina, Isabelle, Brenna et chacha.

Publication list

Research articles

Oudart, M., Avila-Gutierrez, K., Moch, C., Dossi, E., Milior, G., Boulay, A.-C., Gaudey, M., Moulard, J., Lombard, B., Loew, D., Bemelmans, A.-P., Rouach, N., Chapat, C., Cohen-Salmon, M. (2022). Translational regulation by RACK1 in astrocytes represses KIR4.1 expression and regulates neuronal activity. Under review. In BioRxiv: https://doi.org/10.1101/2022.07.16.500292. *Presented in this thesis.*

Tortuyaux, R., Avila-Gutierrez, K., **Oudart, M.**, Mazaré, N., Mailly, P., Deschemin, J.-C., Vaulont, S., Escartin, C., and Cohen-Salmon, M. (2022). Physiopathological changes of ferritin mRNA density and distribution in hippocampal astrocytes in the mouse brain. 2022.04.01.486678. BioRxiv https://doi.org/10.1101/2022.04.01.486678. *Not presented here. I contributed in the development of the main method used in this study: AstroDot.*

Mazaré, N., **Oudart, M.**, Moulard, J., Cheung, G., Tortuyaux, R., Mailly, P., Mazaud, D., Bemelmans, A.-P., Boulay, A.-C., Blugeon, C., Jourdren, L., Le Crom, S., Rouach, N., Cohen-Salmon, M. (2020a). Local Translation in Perisynaptic Astrocytic Processes Is Specific and Changes after Fear Conditioning. Cell Reports *32*, 108076. https://doi.org/10.1016/j.celrep.2020.108076. *Not presented here. I helped in the experiments and analyses. I contributed in the reviewing process.*

Oudart, M.*, Tortuyaux, R.*, Mailly, P.*, Mazaré, N., Boulay, A.-C., and Cohen-Salmon, M. (2020). AstroDot – a new method for studying the spatial distribution of mRNA in astrocytes. J Cell Sci *133*. https://doi.org/10.1242/jcs.239756. *: co-authors. *Presented in this thesis.*

Reviews

Mazaré, N., **Oudart, M.**, and Cohen-Salmon, M. (2021). Local translation in perisynaptic and perivascular astrocytic processes – a means to ensure astrocyte molecular and functional polarity? Journal of Cell Science *134*, jcs251629. https://doi.org/10.1242/jcs.251629. *Presented in this thesis in appendix. I contributed in the RNA-binding protein part and in the writing.*

Cohen-Salmon, M., Slaoui, L., Mazaré, N., Gilbert, A., **Oudart, M.**, Alvear-Perez, R., Elorza-Vidal, X., Chever, O., and Boulay, A. (2020). Astrocytes in the regulation of cerebrovascular functions. Glia glia.23924. https://doi.org/10.1002/glia.23924. *Not presented here.*

Protocols

Mazaré, N., **Oudart, M.**, Cheung, G., Boulay, A.-C., and Cohen-Salmon, M. (2020b). Immunoprecipitation of Ribosome-Bound mRNAs from Astrocytic Perisynaptic Processes of the Mouse Hippocampus. STAR Protocols *1*, 100198. https://doi.org/10.1016/j.xpro.2020.100198. *Not presented here. I contributed in writing the protocol and in the figures.*

Abbreviations

Aβ : Amyloid beta
AchE : Acetylcholinesterase
AD : Alzheimer's disease
AHA : Azidohomoalanine
AGO : Argonaute
ALS : Amyotrophic Lateral Sclerosis
AMPAR : α-amino-3-hydroxy-5-methyl-4-isoxazoleproprionic acid receptor
ANL : Azidonorleucine
APA : Alternative Polyadenylation
AQP4 : Aquaporin 4
ATP : Adenosine Triphosphate
BBB : Blood Brain Barrier
BDNF : Brain Derived Neurotrophic Factor
BG : Bergmann Glia
BONCAT : Bioorthogonal Non-canonical Amino Acid Tagging
Ca2+ : Calcium ion
CDS : Coding Sequence
CLIP : Cross-linking immunoprecipitation
CNS : Central Nervous System
CSF : Cerebrospinal Fluid
CPEB1 : Cytoplasmic Polyadenylation element-binding protein 1
CUIC : CIS-element upstream of the initiation codon
CX30 : Connexin 30
CX43 : Connexin 43
Da : Dalton
DNA : Desoxyribonucleic Acid
DSH : Dishevelled
EC : Endothelial Cell
ECM : Extracellular Matrix
eIF : Eukaryotic Initiation Factor
EM : Electron Microscopy
ER : Endoplasmic Reticulum
FAK : Focal Adhesion Kinase
FASS : Fluorescence Activated Synaptosome Sorting
FISH : Fluorescence in situ Hybridization
FMRP : Fragile X Mental Retardation Protein
FRAP : Fluorescence Recovery After Photobleaching
FTO : Fat-mass and Obesity Associated Protein
FUNCAT : Fluorescence non-canonical Amino Acid Tagging
FUS : Fused Sarcoma
FXS : Fragile X Syndrome
GABA : γ-Aminobutyric Acid
GECI : Genetically Encoded Calcium Indicators
GFAP : Glial Fibrillary Acidic Protein
GFP : Green Fluorescent Protein
GLAST : Glutamate Aspartate Transporter
GLT1 : Glutamate Transporter 1
GluR : Glutamate Receptor
GNP : Granule Neural Progenictors
GPCR : G-Protein Coupled Receptor
GS : Glutamine Synthetase
GTP : Guanosine Triphosphate
GVU : Gliovascular Unit
HuR : Human Antigen R
IRES : Internal Ribosome Entry Site
ITAF : IRES Trans-acting Factor
K+ : Potassium ion
KH : K-homology
KIR4.1 : Potassium Inward Rectifier 4.1
KO : Knock Out
LARP4 : La-related Protein 4
LTD : Long Term Depression
LTP : Long Term Potentiation
m6A : N6-Methyladenosine
MetRS : Methionine tRNA Synthetase
MBP : Myelin Basic Protein
MCT : Monocarboxylate Transporter
MFC : Multi-Factor Complex
MOG : Myelin Oligodendrocyte Glycoprotein
MS : Mass Spectrometry
NGF : Nerve Growth Factor
NMDAR : N-Methyl-D-Aspartate Receptor
NRP1 : Neuropilin 1
NSC : Neural Stem Cell
Nt : Nucleotide
NVU : Neurovascular Unit
OPC : Oligodendrocyte Precursor Cell
P : Postnatal day
PABP : PolyA Binding Protein
PAP : Perisynaptic Astrocytic Processes
PC : Purkinje Cell
PeMP : Peripheral Microglial Processes
PGE : Prostaglandin E
PIP2/3 : Phosphatidylinositol bis/triphosphate
PKC : Protein Kinase C

PLA : Phospholipase A or Proximity Ligation Assay
PLP : Proteolipid Protein
PNS : Peripheral Nervous System
POE : Purity of Essence
pSILAC : pulsed Stable Isotope Labeling by Amino Acid in Cell Culture
PUF6 : Pumillo
PvAP : Perivascular Astrocytic Processes
PTZ : Pentylenetetrazol
QBM : Quaking Binding Motif
QKI : Quaking
QRE : Quaking Response Element
RACK1 : Receptor for Activated C Kinase 1
RBP : RNA-binding Protein
RER : Rough Endoplasmic Reticulum
RF : Release Factor
RNA : Ribonucleic Acid
mRNA : messenger RNA
miRNA : micro RNA
rRNA : ribosomal RNA
tRNA : transfer RNA
RNP: Ribonucleoparticle
hnRNP : heterogeneous RNP
RP : Ribosomal Protein
RQC : Ribosome Quality Control
RRM : RNA Recognition Motif
S : Svedberg
Sema3A : Semaphorin 3A
SERBP1 : Plasminogen Activator Inhibitor 1
SG : Stress Granule
SHH : Sonic Hedgehog
TCA : Tricyclic Antidepressant
TDP43 : TAR DNA-binding Protein 43
TOM : Translocase of the Outer Membrane
TRAP : Translating Ribosome Affinity Purification
UTR : Untranslated Region
VGLUT1 : Vesicular Glutamate Transporter 1
ZBP1 : ZIP-code Binding Protein 1

Figures and Tables

Introduction

Supplementary results

Tables

Table of Contents

Introduction

I. The central nervous system contains key cells: Astrocytes

In mammals, the nervous system can be divided between the peripheral nervous system (PNS) including nerves and ganglia and the central nervous system (CNS) including the brain and the spinal cord. The brain is a complex organ composed of the cerebrum (or telencephalon, the main part of the brain divided into 2 hemispheres controlling emotions, senses or voluntary movement for instance), the cerebellum (at the back of the brain, responsible for movement coordination and balance for instance) and the brain stem connecting the brain to the spinal cord (involved in cardiac and respiratory functions) (**Fig. 1, left**) (Purves et al., 2012).

I.a) Astrocytes are integrated glial cells

In the CNS, different cell types are interdependent and include the neurons, the glial cells and the blood vessels (**Fig. 1, right**). Neurons are electrically excitable cells that communicate through synapses. Neurons are very complex cells with processes receiving information, the dendrites, and a process responsible for collecting and transmitting the information, the axon. Of note, axons can be very long, up to millimeters and centimeters (for instance, a neuron located in our spinal cord can extend its axon to innervate our toes). Neurons come up with very different morphologies and can be excitatory or inhibitory. The communication between neurons is called the synapse and consists in a presynaptic axon terminal apposed to a postsynaptic dendritic bouton. The electric nervous signal or action potential in the axon reaches the presynaptic terminal, is converted in the synaptic cleft (the space between 2 neurons) in a chemical signal as a release of neurotransmitters and neuromodulators. These molecules bind to receptors at the postsynaptic terminal of dendrites and this chemical signaling is converted back into an electrical pulse. The neuronal cell body integrates the different signaling from its dendrites to send another message through its axon etc… (Purves et al., 2012). The neuronal transmission also involves glial cells and will be developed later.

Glial cells consist in astrocytes, microglia, oligodendrocytes (**Fig. 1, right**) and ependymal cells. Astrocytes participate in regulating neuronal and cerebrovascular functions will be developed later. Microglia are small ramified cells involved in particular in the brain immunity. They are highly dynamic cells and react when the brain is injured (trauma, stroke, epilepsy, infection, neurodevelopmental and neurodegenerative diseases). Microglia reactivity consists in proliferation and migration toward the injured site (infection site, leaky blood brain barrier, cell death, amyloid beta plaque). Microglia are also involved in the synaptogenesis during development. They participate in synaptic pruning (remove of the excess of synapses during development) by phagocyting weak

synapses or tagging them to be phagocyted by astrocytes. Microglia functions are reviewed in (Wolf et al., 2017). Oligodendrocytes are also ramified cells participating in the myelin sheath formation around axons of neurons. The myelin is a lipid insulating axons for the nerve signal to be transmitted faster. Oligodendrocytes produce myelin wrapped in sheaths around the axons. The spaces between each myelin segments are called ‘Noeud de Ranvier’ or node of Ranvier. Hence, the action potentials in axons ‘jump’ from node to node, called saltatory conduction, increasing the information transmission speed which was an evolutionary advantage. Oligodendrocytes participate also in the metabolic support of neurons through channels in the myelin sheath by exporting lactate or pyruvate. Oligodendrocytes physiology is reviewed in (Simons and Nave, 2016). Finally, ependymal cells are located in the borders of the brain ventricles (large cavities in the middle of the brain containing the cerebrospinal fluid (CSF)), regulate the CSF flow with cilia and support neurogenesis. Ependymocytes roles are reviewed in (Del Bigio, 2010).

Although some teams evaluated the glial cells to be 10 times more numerous than neurons in the human brain (Allen and Barres, 2009), recent studies with new fractionation techniques computed glial cells as numerous as the neurons in the human brain and 35% in the mouse brain (von Bartheld et al., 2016; Herculano-Houzel, 2014).

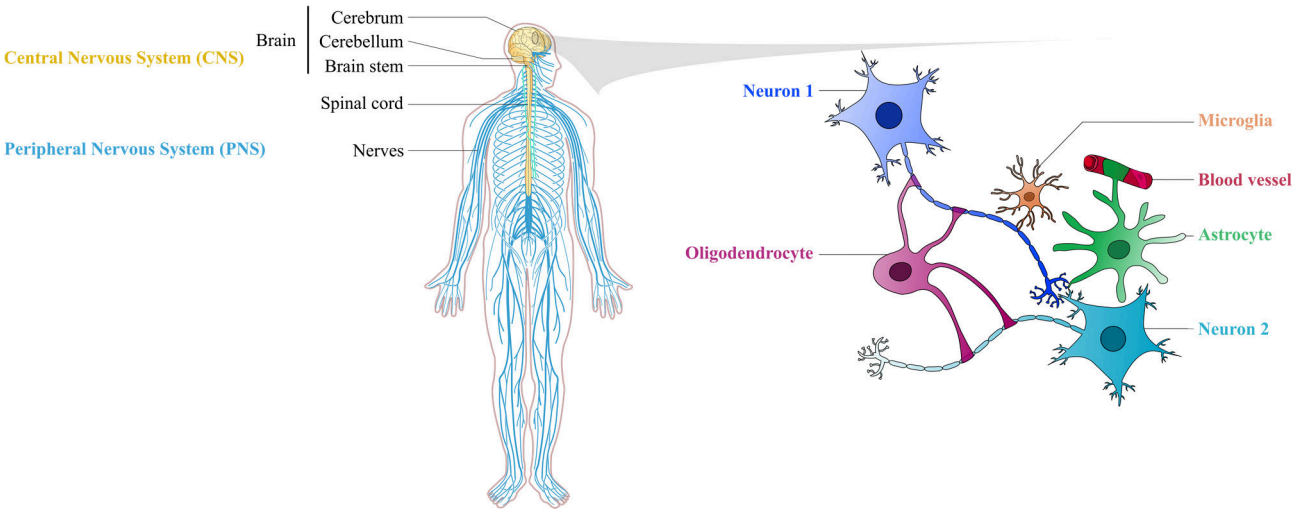

Figure 1. ***Cells of the central nervous system (CNS). (Left)*** *The CNS contains the brain and the spinal cord whereas the PNS contains the peripheral nerves.* ***(Right)*** *Neurons interplay with glial cells in the brain: microglia, oligodendrocytes and astrocytes. The CNS is highly vascularized (right).*

I.b) Astrocytes are rising stars: from depreciation to high interest

Astrocytes and glia in general were discovered after neurons in 1858 by Rodolph Virchow (1821-1902) (Hubbard and Binder, 2016). He referred to neuroglia as a cement, a cell-free glue to support

the nerve cells. Neuroglia was considered as cells with the silver-chromate staining technique of Camillo Golgi (1843-1926) in the 1870s when he drew stellate cells (astrocytes). Importantly, Golgi already assumed a metabolic support role of astrocytes because of the astrocytic endfeet contacting blood vessels. The word astrocyte (from ancient greek 'αστρον', star and 'κυτοσ', cell) was used by Michael von Lenhossék (1863-1937) in 1893 and comes from their star shape with Golgi staining (**Fig. 2, left**). Nowadays, we would consider a 'bushy' shape rather than a star shape. Indeed, the Golgi astrocyte staining only show the intermediate filament structure whereas the staining of fluorescent reporter mouse lines with the astrocyte cytoplasm filled with the fluorescent protein show a high morphological complexity (**Fig. 2, right**) (Verkhratsky and Nedergaard, 2018). Santiago Ramon y Cajal (1852-1934) described astrocyte morphology with its own astrocyte-specific gold and mercury chloride-sublimate staining technique. He described astrocyte heterogeneity as well as potential functional roles of astrocytes in the control of blood flow (Hubbard and Binder, 2016). However, astrocyte functions were still unknown and they were still considered as 'glue' despite Golgi and Cajal hypotheses.

As electrically non-excitable cells, scientists lacked tools to study these cells. In 1980s and 1990s, studies on astrocytes described ions channels and receptors (Kettenmann et al., 1984) as well as their propensity to communicate with calcium waves (Cornell-Bell et al., 1990). However, astrocytes were still considered as passive supporting cells compared to neurons. We had to wait until the late 1990s for Ben Barres (1957-2017), a pioneer in glial cell biology, to describe astrocytes as active players in the brain physiology in the development, neuronal communications and diseases (Allen and Barres, 2009). From his studies, the astrocyte community has grown to be almost as valued as the neuron one. However, still today, astrocytes roles are not well understood especially at the vascular interface although Golgi described endfeet in the 1870s! The neural community remains neuron-centered and I think it is time to start integrating all brain cells if we want to tackle fundamental and applied long lasting unresolved questions.

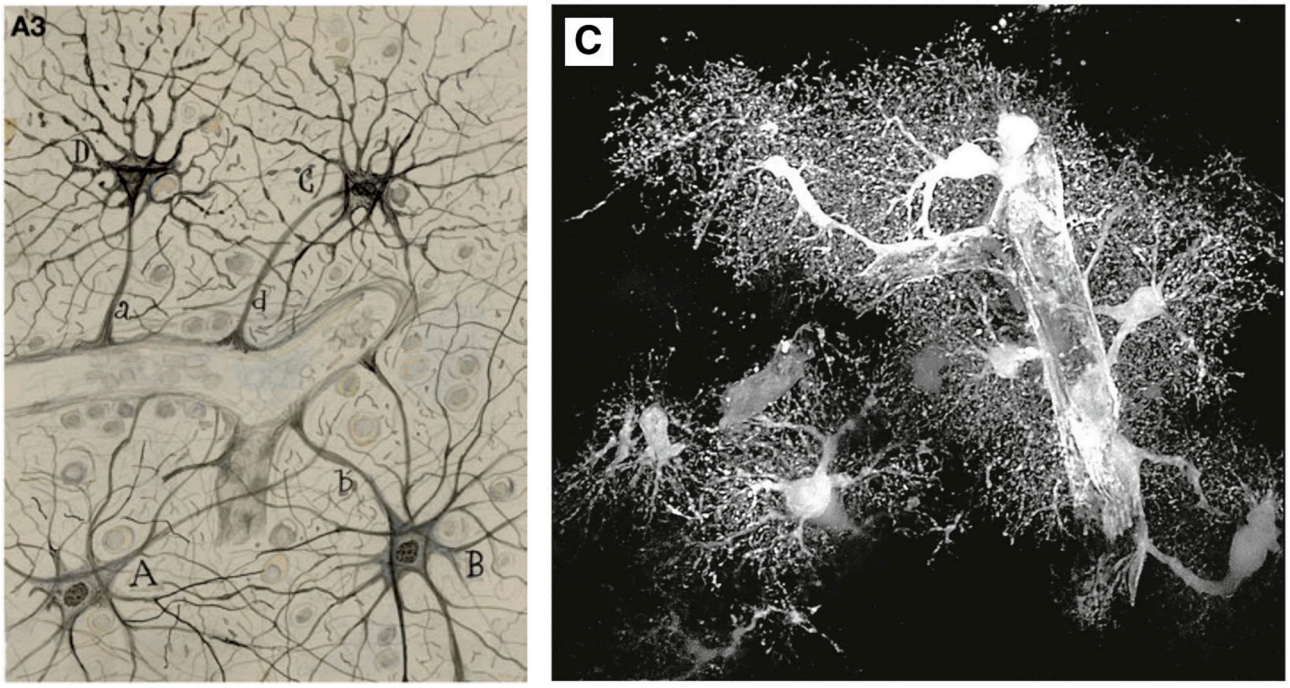

Figure 2. ***Astrocytes through the history. (Left)*** *Drawing of Ramon y Cajal (1852-1934) of astrocytes stained with modified Golgi techniques. The astrocytes processes correspond to the intermediate filaments GFAP. Astrocytes were already shown to contact blood vessels.* ***(Right)*** *EGFP-filled astrocytes in the cortex (outer layer of the brain). Astrocytes have, in fact, a bushy morphology with ramified processes and totally ensheath blood vessels. Adapted from (Verkhratsky and Nedergaard, 2018).*

I.c) Astrocytes display unique properties

Astrocytes are considered the most numerous glial cells in the brain although recent studies have highlighted that this statement could be wrong. Oligodendrocytes would be the most abundant (75%) in the white matter (deep in the brain, with a high density in axons) as well as in the grey matter (at the brain surface with neuronal cell bodies) in the human brain compared to astrocytes (20%) and microglia (5%) (von Bartheld et al., 2016; Pelvig et al., 2008). However, numbers of glial cells could depend on the brain region and on the species. Astrocyte morphology complexity increases with evolution especially in the human brain where astrocytes display a larger domain, a larger cell body and more processes than its mouse counterpart (Oberheim et al., 2006, 2009).

For a complete review of astrocytic functions read “Physiology of Astroglia” of Alexei Verkhratsky and Maiken Nedergaard (Verkhratsky and Nedergaard, 2018). The following sections only point out what I think are the most important and interesting functions.

I.c.i. Astrocytes increase their contact surface with a bushy morphology

Astrocyte morphology described in Golgi and Cajal drawings reveals only part of the entire cell. In fact, the protein stained by this technique is the intermediate filament expressed in astrocytes and radial glia: glial fibrillary acidic protein (GFAP). The GFAP staining reveals the soma and only large processes of astrocytes. Bushong et al. calculated that it only accounts for 15% of the entire volume (Bushong et al., 2002). When filled with a cytoplasmic dye, either by pipette loading or in transgenic mice, astrocytes look like a bush. We understand the multitude of cells and processes an astrocyte can contact when we look at this bushy structure (**Fig. 2, right**) (Verkhratsky and Nedergaard, 2018).

This bushy structure is heterogeneous between brain regions as well as inside the same region. In the cerebellum, resident astrocytes are called Bergmann glia, in the retina, Müller cells and in the hypophyse (a hormone-secreting gland near the hypothalamus deep in the brain), pituicytes. Within the brain, astrocytes can be protoplasmic (bushy structure with a lot of processes) in the grey matter, fibrous (fewer processes but longer) in the white matter, pial at surfaces and perivascular around blood vessels. In terms of processes length, protoplasmic have 50 µm ramified processes whereas fibrous have long 300 µm less complex processes (Verkhratsky and Nedergaard, 2018). Within one region of the brain such as the hippocampus (a region involved in memory formation and spatial navigation), astrocytes are bigger in the CA3 than the CA1 regions. Molecular signatures of astrocytes determine their heterogeneity. Recent studies investigating the astrocytic molecular identities (Batiuk et al., 2020) revealed a more complex heterogeneity than expected in the brain. For instance, GFAP is expressed at high levels in the hippocampus, contrary to the cortex (Zhang et al., 2019b). The molecular identity of an astrocyte population could match the neuronal network they are integrated in.

I.c.ii. Astrocytes have non-overlapping domains

Astrocytes overlap in a restricted manner. In the hippocampus, a well-known structure in the cerebrum involved in memory and space navigation, protoplasmic astrocytes only overlap with their very fine processes by 4.6% in average of their volume (**Fig. 3**) (Bushong et al., 2002; Ogata and Kosaka, 2002). It is considered that protoplasmic astrocytes have exclusive domains meaning that 1 astrocyte controls all contacted neuronal fibers in its domain. Fibrous astrocytes in the white matter do not have such exclusivity and can extensively overlap. Although the non-overlapping domains have been described 20 years ago, the physiological relevance of this property remain unclear.

However, it is now clear that astrocyte domains undergo changes in different neuropathologies such as traumas, strokes and neurodegenerative diseases (Sofroniew and Vinters, 2010). Astrocytes in neurological disorders become reactive underlying morphological, functional and molecular changes.

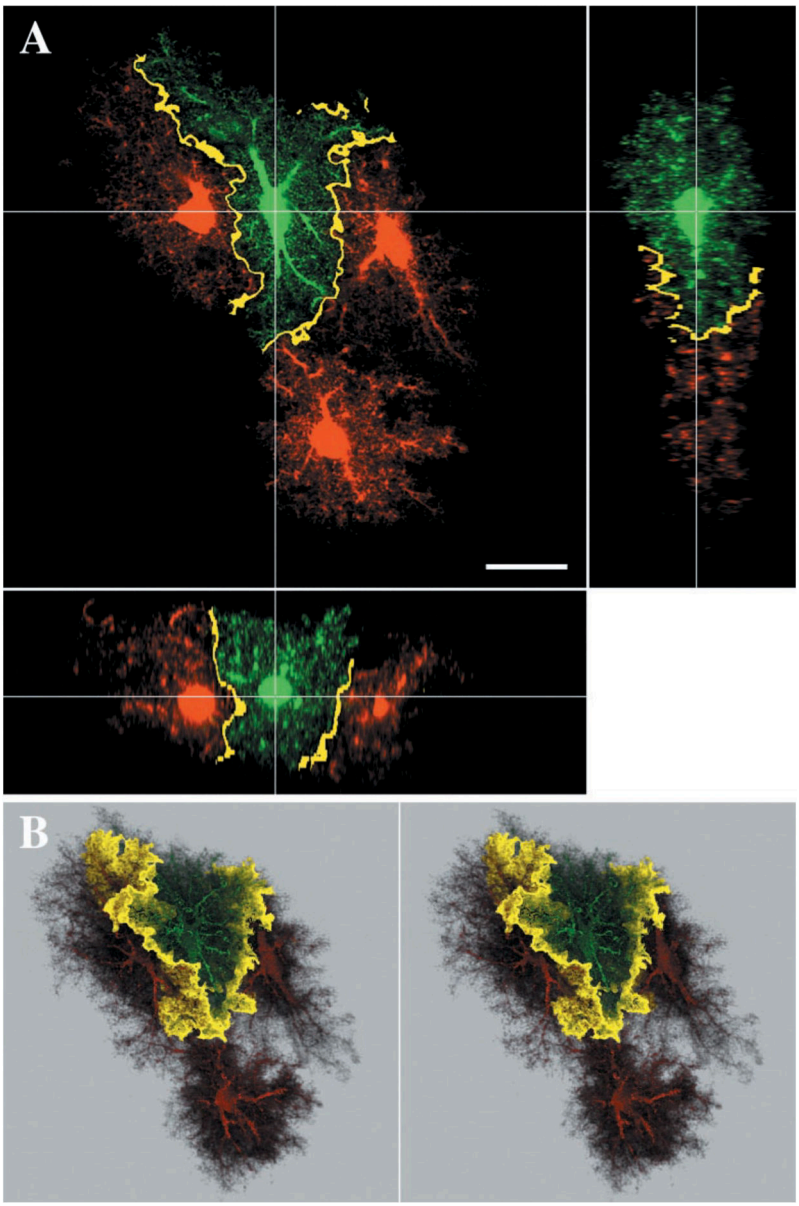

Figure 3. ***Astrocytes have non-overlapping domains. (Upper panel)*** *Green protoplasmic astrocyte only overlap with 4.6% of very fine processes volume (yellow part) with the red neighbor cells.* ***(Lower panel)*** *3D reconstruction of the overlapping. Adpated from (Bushong et al., 2002).*

These changes appear to be dependent on the context and the brain region and are highly heterogeneous (Escartin et al., 2021). For instance, in epilepsy, reactive astrocytes in the epileptic foci increase their processes to overlap with neighbors domains (Oberheim et al., 2008). Disorganized astrocytic domains may account for neuronal susceptibility. Interestingly, not in every cases reactive astrocytes overlap their domains, for instance in Alzheimer's disease (Oberheim et al., 2008).

I.c.iii. Astrocytes are electrically non-excitable cells but communicate with calcium

Unlike neurons, astrocytes can not be excitable electrically. It means that they do not convey messages through action potentials. Their membrane can depolarize (increase in the membrane potential) and hyperpolarize (decrease in the membrane potential) (Membrane potential are changes in the cation and anion composition between intra and extracellular spaces near the membrane and can be measured by electrodes) but never triggers high voltage pics and astrocytes are considered electrically passive cells (Verkhratsky and Nedergaard, 2018). However, astrocytes main way of communication is through calcium ions (Ca^{2+}). The calcium is coming from outside the cell or from internal storage. For instance, neurotransmitters released in the synapse from presynaptic terminals bind receptors in the astrocyte process at the synaptic level. G-protein coupled receptors (GPCR) signaling will convert phosphatidylinositol bisphosphate (PIP_2) into phosphatidylinositol triphosphate (PIP_3) by phosphorylation. PIP_3 can bind to its receptor (inositol triphosphate IP3R) at the endoplasmic reticulum (ER) surface. The activation of IP3R by PIP3 will release Ca^{2+} from the ER to the cytoplasm because the concentration of Ca^{2+} is very high in the ER compared to the intracellular space. The elevation of intracellular Ca^{2+} concentration will depolarize the cell (elevation of potential due to increase of positive charges) and trigger the release of gliotransmitters because of the calcium-dependent fusion of vesicles (**Fig. 4, left**) (Agulhon et al., 2012). Gliotransmitters are neurotransmitters released from the astrocyte (developed later) that can influence the synaptic transmission.

Another aspect of calcium communication is the neurovascular coupling. The neuronal metabolic support by astrocytes is regulated. The metabolic demand is directly coupled with the metabolite uptake of astrocytes from the blood stream. Calcium increase in the astrocyte processes after neuronal excitation will elevate in the whole astrocyte. In particular, it will reach the astrocyte endfeet where calcium increase will activate enzymes such as the phospholipase A (PLA) to contribute in the release of lipid derivatives as prostaglandins (PGE). PGE are vasodilators molecules activating the dilation of mural contractile cells and thus, of the blood vessels. An increased blood let the astrocyte to uptake more metabolites (**Fig. 4, middle**) (Petzold and Murthy, 2011).

Therefore, astrocytes decode inputs from the environment with calcium to impact on synaptic plasticity and integrity (Guerra-Gomes et al., 2018) and to couple metabolic needs with blood flow regulation.

Astrocytes, as bushy cells, have a complex network of ramification. Calcium transients activated by a synapse activation can be very localized in the arborization. Recently, microdomains have been

investigated as restricted spaces of functional units. These microdomains have been studied in the processes contacting the synapses (Lia et al., 2021) and the blood vessels (Lind et al., 2018). The relevance of calcium microdomains in astrocytes is still not understood but could participate in synaptic plasticity and cerebral blood flow regulation.

Interestingly, Ca^{2+} signaling has been used to track activity of astrocytes with calcium indicators. For instance, the family of GCaMP proteins (the fusion of modified Green Fluorescent Protein (GFP) and Calmodulin (a calcium sensor protein)) belonging to the Genetically Encoded Calcium Indicators (GECI) has been widely used.

I.c.iv. Astrocytes form a connecting network through gap junctions

Another feature of astrocytes is their connection through gap junction between each other forming a network of cells linked by their cytoplasm (**Fig. 4, middle**). Gap junctions form the channel linking 2 connexons of 2 cells constituted by 6 connexins. Astrocytic connexins (Cx), mostly Cx43 and Cx30, form homotypic and heterotypic gap junction channels creating a bridge between cells allowing molecules <1 kiloDalton (kDa) to pass and to share metabolites and signaling molecules. This network allows a group of astrocytes, more or less restricted depending on the brain region, to be functionally coupled. The astrocyte connexins and network contribute to share nutrients (**Fig. 4, middle, yellow lines**), buffer potassium (Pannasch and Rouach, 2013) and regulate synaptic activity and plasticity (Han et al., 2014; Pannasch et al., 2014; Rouach et al., 2008). The aforementioned calcium can travel the network through gap junctions and create calcium waves (**Fig. 4, middle, blue lines**). Calcium waves are generated by the calcium and IP3 travel through gap junctions that trigger more calcium to be released in the next cell rather than the travel of calcium alone that would dilute in the network (Sanderson et al., 1994). Calcium waves in a given astrocyte network could help synchronize the neurons as connexins helps neuronal coordination (Chever et al., 2016).

In addition, the astrocytic network allows the sharing of metabolites taken from the blood or from storage. For instance, astrocytes redistribute glucose (**Fig. 4, middle, yellow lines**) (180 Da) and lactate (90 Da) to nourish neurons and sustain neuronal activity (Giaume et al., 2010; Rouach et al., 2008). However, a recent study showed that all astrocytes were associated with a blood vessel (Hösli et al., 2022), refuting the need of a metabolic coupling if every single astrocyte can take up metabolites from the blood. But this study shows that some astrocytes in the hippocampus were not associated to a blood vessel, this region being studied in the previous references. Finally, this study does not distinguish between arteriole, veins and capillaries that could contribute differently to metabolic support.

Another role for astrocyte coupling is potassium (K+) spatial buffering that will be further described in the KIR4.1 section. Because the concentration of potassium in astrocytes needs to be maintained low to be able to uptake K+ from the synaptic cleft, K+ is redistributed through the network to be diluted in the network volume and to be released at the blood vessel interface.

Astrocytic hemichannels can create heterotypic gap junctions with hemichannels from oligodendrocytes. Cx43 and Cx30 from astrocyte can associate with Cx47 and Cx32 from oligodendrocytes respectively (Griemsmann et al., 2015). This coupling is believed to support axon metabolism via nutrients distribution.

Astrocytic connexins have also hemichannel functions such as the release of ATP and glutamate to control neuronal activity (Sáez et al., 2003). Finally, Cx30 and Cx43 have non-channel functions that could mediate the synapse invasion (Clasadonte and Haydon, 2014; Pannasch et al., 2014; Ribot et al., 2021).

I.d) Astrocyte's polarity connects blood vessels and neurons

I.d.i. Astrocytes display perivascular endfeet and regulate vascular functions

Astrocytes contact blood vessels with a specialized structure, endfeet or perivascular astrocytic process (PvAP) (**Fig. 4, right**). Endfeet are large structures wrapping the blood vessels (Mathiisen et al., 2010). These structures are the least studied in astrocyte history. A recent study (Hösli et al., 2022) showed that all astrocytes connect at least 1 blood vessel with 3 blood vessels on average except in the hippocampus where vessel density is low and where some astrocytes (2,6%) do not contact vessels. Blood vessels are heterogeneous, from big arteries/veins with big PvAP to small capillaries with small PvAP (Wang et al., 2021). Astrocytes apposed to the vessel are called perivascular astrocytes, although this definition is not clear in the literature.

Astrocyte endfeet are part of a specialized structure: the gliovascular unit (GVU) (**Fig. 4, right**) (sometimes called the neurovascular unit (NVU)). The gliovascular unit is composed, from the vessel lumen to the edge, by the endothelial cells (EC), an EC-secreted basal lamina (special extracellular matrix), mural cells (vascular smooth muscle cells for arterioles and venules, and pericytes for capillaries), an astrocyte-secreted basal lamina and finally PvAPs (Cohen-Salmon et al., 2020). In capillaries the 2 basal lamina from EC and astrocytes are fused and in big vessels, an extracellular space is filled with cerebrospinal fluid present between mural cells and astrocytes.

Astrocytes-vascular functions are numerous and recapitulated in Cohen-Salmon et al. (Cohen-Salmon et al., 2020). The enrichment of a specific protein repertoire in the endfeet allows the astrocyte to

regulate vascular functions. For instance, astrocytes regulate the blood brain barrier (BBB) integrity. The BBB separates the blood from the brain parenchyma allowing only specific molecules to enter or to leave by selective transporters and pumps. For instance, a Glucose Transporter GLUT1 mediates glucose uptake in ECs and the Permeability GlycoProtein PgP is an efflux pump making hard the delivery of drugs in the CNS. The principal cell components of the BBB are endothelial cells (EC) tightened together by tight junctions composed by specific claudins, occludin and cadherins (Li et al., 2022). This endothelial barrier is regulated by mural cells and astrocytes that secrete factors which regulate tight junction protein expression. In addition, astrocytes regulate the ion homeostasis at the GVU. The polarized expression of Aquaporin 4 (AQP4), a water channel, and the Inward-rectifying K+ channel KIR4.1 regulate water flow and potassium homeostasis (**Fig. 4, right**). The CSF flow in the brain allows clearance of waste such as protein aggregates (Aβ for instance) regulated by the AQP4-mediated water flow called the glymphatic system (Mestre et al., 2018). KIR4.1 mediates the efflux and circulation of potassium accumulated around synapses. Connexins, such as Connexin 30 and 43 (Cx30 and Cx43) form gap junctions between astrocyte endfeet and are enriched at the vascular interface. Cx43 also regulates the brain immune quiescence, which is the ability for brain vessel to NOT recruit immune cells from the blood circulation. Deletion of Cx43 leads to aberrant immune recruitment in the brain parenchyma (Boulay et al., 2015a). Metabolites are taken up from the blood by specific transporters such as the glucose transporter GluT1 expressed in endothelial cells and astrocyte endfeet (Morgello et al., 1995).

I.d.ii. Astrocytes regulate synaptic functions with perisynaptic processes (PAP)

In the mouse, each astrocyte contacts up to 100,000 synapses and in the human, up to 2,000,000 synapses (Oberheim et al., 2009) with very fine structures, compared to PvAPs, with a diameter of 50 nm called Perisynaptic Astrocytic Processes (PAP) (**Fig. 4, left**). Given their size, they represent only 10% of the astrocyte volume but given their shape they count for 70-80% of the astrocyte surface area (Semyanov and Verkhratsky, 2021).

PAPs are dynamic structures. In physiology, in the hypothalamus, PAPs can be inside the synaptic cleft, avoiding 2 neurons to communicate. During parturition and lactation, PAPs retract from the cleft and allow the synaptic transmission to stimulate the production of milk for instance (Oliet et al., 2001, 2004). It has been shown in slices and *in vivo* that PAP motility depends on the synaptic activity (Bernardinelli et al., 2014a, 2014b). Ezrin, a protein linking the plasma membrane and the actin cortex, is highly expressed in the PAPs and was suspected to be involved in the PAP motility (**Fig. 4, left**) (Derouiche and Geiger, 2019). Interestingly, *Ezrin* mRNA is more abundant in the PAPs than the astrocyte soma and is locally translated at this interface supporting a functional role of ezrin in the

PAP dynamism regulation (Mazaré et al., 2020a). Another protein involved in PAP morphology is Cx30. Cx30 knock out mice display a disruption of the synapse coverage with an invasion of the synapse and a decrease in the synaptic strength (Pannasch et al., 2014).

A specific pool of enriched proteins defines PAP identity and regulate neuronal functions. Astrocytes regulate synaptic transmission, which is related to ion homeostasis as well. Apart from Cx30 described above, KIR4.1 is involved in the synaptic transmission regulation. As neurons rely on K+ to generate action potentials, buffering extracellular K+ at the synaptic level is critical to avoid undesired neuronal firing (we refer as neuronal firing when neurons burst) and to be able to communicate properly. Astrocytes regulate neuronal transmission also by releasing gliotransmitters (**Fig. 4, left**). Upon synaptic transmission, neurotransmitters secreted by the presynapse (the axon terminal) can be fixed by receptors in PAPs. Calcium elevation after the signaling cascade triggered by the receptor activation will cause gliotransmitter release from the PAP such as glutamate, ATP (excitatory transmitters), GABA and Glycine (inhibitory transmitters) (Agulhon et al., 2012; Araque et al., 2014). It has been proposed that D-serine, the chiral opposite of L-serine, can be released from PAPs to bind the glycine-binding site of NMDA receptors at postsynaptic dendrites and could be a mandatory co-agonist for NMDA dependent transmission. However, D-serine release from astrocytes has been the subject of controversies (astroglial D-serine (Papouin et al., 2017) or neuronal D-serine (Wolosker et al., 2017)) and teams have proposed that astrocytes released L-serine to neurons to convert it in D-serine (Martineau et al., 2014).

Astrocytes support neurons in their metabolism and matches their metabolic demand by sensing the synaptic activity. Glutamate release in the synaptic cleft can bind glutamate receptors on the PAP and provoke glucose uptake from the blood by the neurovascular coupling seen above. The extracellular glucose (can be from glycogen storage as well) is converted in lactate through glycolysis in astrocytes. Lactate is then shuttled to neurons via Monocarboxylate Transporter (MCT) and converted into energy via the oxidative phosphorylation as neurons have high demands to sustain their activity (**Fig. 4, left**) (Bélanger et al., 2011). The astrocyte to neuron lactate transport is necessary for long term synaptic plasticity and memory formation (Suzuki et al., 2011). This is the lactate shuttle hypothesis (Pellerin and Magistretti, 1994) still debated today (Bonvento et al., 2005) especially because neurons can also use glucose in an activity dependent manner and lactate enzyme are expressed in both cells (Bak and Walls, 2018; Ivanov et al., 2014).

Finally, astrocytes are capable of recycling neurotransmitters (**Fig. 4, left**). For instance, glutamate is taken up from the synaptic cleft by glutamate transporters such as GLT1 and GLAST. In the cell, glutamate is converted into glutamine by the glutamine synthetase (GS). Glutamine is then exported to neurons to replenish their storage in glutamate by the glutaminase enzyme (Schousboe et al., 2014).

Interestingly, GS is an astrocyte specific marker supporting the fact that neurons are incapable of transforming glutamate into glutamine (Anlauf and Derouiche, 2013). However, they can reuptake glutamate directly from the cleft as well.

Other important roles of PAPs during the brain development such as synaptogenesis will not be discussed here.

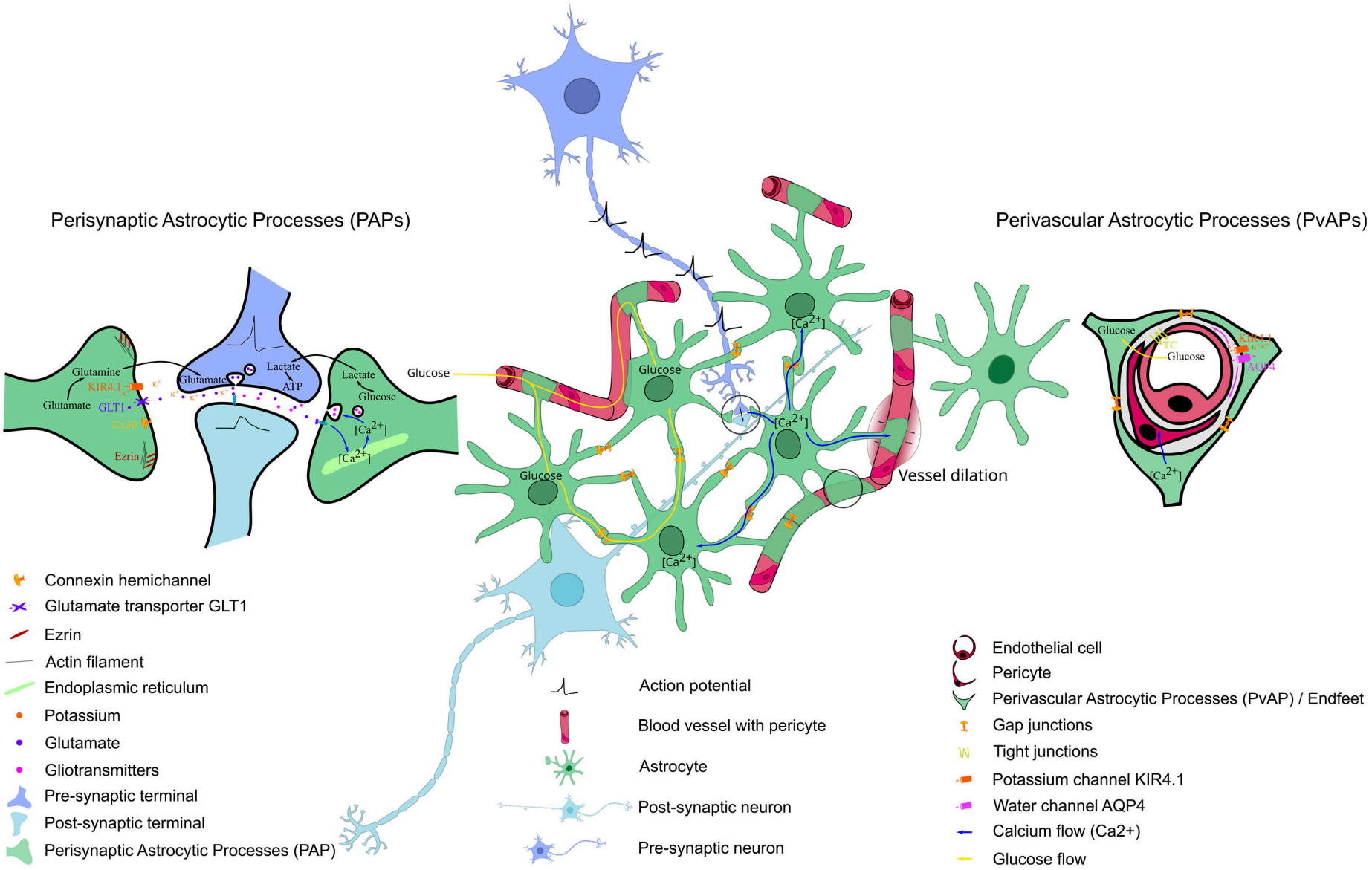
Perisynaptic Astrocytic Processes (PAPs)
Perivascular Astrocytic Processes (PvAPs)
Glutamine
Glutamate
KIR4.1
GLT1
Cx30
Ezrin
Glutamate
Lactate
ATP
Lactate
Glucose
[Ca2+]
[Ca2+]
Glucose
Glucose
[Ca2+]
Glucose
[Ca2+]
[Ca2+]
Vessel dilation
Glucose
TC
Glucose
KIR4.1
AQP4
[Ca2+]
Connexin hemichannel
Glutamate transporter GLT1
Ezrin
Actin filament
Endoplasmic reticulum
Potassium
Glutamate
Gliotransmitters
Pre-synaptic terminal
Post-synaptic terminal
Perisynaptic Astrocytic Processes (PAP)
Action potential
Blood vessel with pericyte
Astrocyte
Post-synaptic neuron
Pre-synaptic neuron
Endothelial cell
Pericyte
Perivascular Astrocytic Processes (PvAP) / Endfeet
Gap junctions
Tight junctions
Potassium channel KIR4.1
Water channel AQP4
Calcium flow (Ca2+)
Glucose flow

Figure 4. ***Astrocyte functions at the synapse, at the blood vessels and at the network level. (Left)*** *Astrocytes contact synapses between 2 neurons with their perisynaptic processes (PAPs). At this level, astrocytes regulate neuronal transmission by releasing gliotransmitters after receptor-mediated Ca2+ elevation, they recycle neurotransmitters with GLT1 transporter, they regulate potassium homeostasis with KIR4.1 channel and participate in metabolism with lactate shuttling. PAPs are also motile with CX30 and ezrin proteins.* ***(Middle)*** *Astrocyte network mediated by connexins-forming gap junctions distribute metabolites such as glucose uptaken from the blood stream, and Ca2+ increased after neuronal activity. Ca2+ participates in the neurovascular coupling with dilation of blood vessels to increase nutrients uptake.* ***(Right)*** *Astrocytes contact blood vessels with perivascular processes (PvAPs) also called endfeet. PvAPs are integrated in the gliovascular unit with mural cells (Pericytes here), endothelial cells and basal lamina. At this level, nutrients such as glucose are transported from the blood to the astrocyte, potassium and water homeostasis occur with the expression of KIR4.1 and AQP4 channels and calcium regulates neurovascular coupling.*

I.e) Astrocytes express a critical protein for brain homeostasis: KIR4.1

I.e.i. KIR4.1 is a major potassium channel in astrocytes

The inwardly-rectifying K+ channel KIR4.1 is only expressed in glia in the central nervous system. KIR4.1 is a homo- or heteromeric tetramer with 4 KIR4.1 or 2 KIR4.1 and 2 KIR5.1/KIR2.1 subunits (**Fig. 5, left**) (Ohno et al., 2018). KIR4.1 has affinity for K+. It is mostly expressed in astrocytes in the CNS with strong expression in the PAPs and in PvAPs as described above. However, it is also expressed in oligodendrocyte precursor cells (OPC), Müller cells (a type of astrocyte in the retina) and oligodendrocytes. The *kcnj10* gene coding for KIR4.1 is two times more expressed in astrocytes than OPC or oligodendrocytes (Zhang et al., 2014) in the cerebral cortex and is largely believed to be almost astrocytic-specific in the hippocampus .

Electrophysiological properties of KIR4.1 gives resting membrane potential to astrocytes. Glia are highly permeable to K+ and have a very negative resting membrane potential of -85 mV. The membrane potential of a cell is the electrical charge difference between the outside and the inside of a biological lipid membrane. It is due to the difference of distribution of cations and anions on both sides of the membrane. This distribution is mediated by channels, pumps and transporters that can be passive and active (against the passive flow). It depends also on the charge of the ion: cations will be attracted to negative intracellular compartment and anion towards positive compartments. Ions movements are described by the Nernst equation taking into account the ion charge and its

extracellular and intracellular concentrations. In the case of K+, its equilibrium potential of -90 mV is very close from the astrocyte resting membrane potential highlighting that astrocytes are permeable to K+ with the predominance of KIR4.1 channels. Intracellular concentrations of potassium are very high (150 mM) and let the extracellular space almost empty (4 mM). During a neuronal excitation in the form of action potential, neurons release a high concentration of K+. For another action potential to happen, K+ must be removed to keep the extracellular concentration low. KIR4.1 is here to take K+ into the astrocytes. Pharmacological blockade of KIR4.1 has been traditionally performed by application of Barium Ba2+ (Nwaobi et al., 2016) although it blocks all the Kir family including some in the neurons. Recently, a more specific KIR4.1 blocker has been developed : VU0134992 (Kharade et al., 2018).

I.e.ii. KIR4.1 regulates potassium homeostasis in PAPs and PvAPs

KIR4.1 is highly expressed in PAPs and PvAPs. K+ is taken up by PAPs from the synaptic cleft and redistributed in the astrocyte network. As numerous astrocytes are coupled by gap junctions, the local increase of intracellular K+ will diffuse in the network (**Fig. 5, right**). This phenomenon is called the K+ spatial buffering or siphoning and helps the PAPs to have a steady K+ concentration to be able to take K+ again (Kinboshi et al., 2020; Nwaobi et al., 2016; Ohno et al., 2021). Another feature of the spatial buffering comes from the KIR4.1 expression in the PvAPs. The K+ concentration around blood vessels is low, and KIR4.1 at this interface has an outward flow. Therefore, the entry of potassium in the astrocytes can be directly released in the perivascular space (Higashi et al., 2001; KOFUJI and NEWMAN, 2004).

In Müller cells in the retina, KIR4.1 co-immunoprecipitates with AQP4 (Connors and Kofuji, 2006). Ion homeostasis is tightly linked with water flow in the cell. Therefore it has been proposed that KIR4.1 and AQP4 might work together as the deficiency in KIR4.1 causes retina swelling (Pannicke et al., 2004). However, this might be unique to the retina as hippocampal KIR4.1 current is not perturbed in the AQP4 KO astrocytes (Nwaobi et al., 2016; Zhang and Verkman, 2008). KIR4.1 is also associated with GLT1-mediated glutamate uptake. Indeed, GLT1 relies on anti-transportation of Na+ permitted by the low potential of astrocytes mediated by KIR4.1. Hence, the loss of KIR4.1 leads to glutamate accumulation in the synapses and causes neurological diseases as described below.

I.e.iii. KIR4.1 is perturbed in several neurological diseases

KIR4.1 is altered in a large amount of brain diseases from neurodevelopmental, traumas and neurodegenerative diseases (**Fig. 5, right**). KIR4.1 knock-out mouse model provokes ataxia and epilepsy and is lethal at post-natal day 24 (P24) (Djukic et al., 2007). Epilepsy is a disease caused by

the synchronized excitation or firing of a significant number of neurons included in a network. If targeted neurons are in the motor cortex, body tremor and movement are seen in the mouse or the patient. If elsewhere it can be seen as absence. KIR4.1 and *kcnj10* gene expression have been studied in epilepsy in mice and patients where it was reduced and the reduction was proportional to the symptom severity (Kinboshi et al., 2020; Nwaobi et al., 2016). KIR4.1 decrease implies a reduction of K+ buffering. As the spatial K+ buffering is perturbed, GLT1 transporters do not work properly due to high extracellular K+ and the impossibility for Na+ to be released. Therefore, glutamate release after synaptic transmission is not uptaken by astrocytes and accumulates in the synaptic cleft. Accumulation of glutamate can fix neurotransmitter receptors longer and can stimulate the post synaptic compartment a longer time. The consequence is a constant neuronal firing.

KIR4.1 has also been involved in the pathogenesis of Alzheimer's disease (AD). AD is a neurodegenerative disease characterized by accumulative deposition of amyloid beta (Aβ) proteins forming plaques in the extracellular space and the formation of Tau protein tangles inside neurons. Aβ and tau lead to BBB and neurovascular disruptions, astrocytes and microglia reactivity, and neuronal death. These defects result in cognitive decline, dementia and eventually death. No curative treatment is available as the understanding of the disease is still limited. A KIR4.1 decrease by 60 to 70% in post mortem human tissues has been described (Wilcock et al., 2009). This decrease is correlated with plaques and symptoms apparition. Even though it could only be a consequence of the neurovascular unit defect, loss of KIR4.1 could speed up the disease. Interestingly, AD is an increased factor to develop epilepsy and could correspond to the progressive decrease of KIR4.1. A recent study investigated the KIR4.1 expression by immunofluorescence in AD mouse model. In this model, KIR4.1 expression was increased by a maximum of 60% in astrocytes close to Aβ plaques compared to non-plaques-associated astrocytes disputing previous statements (Huffels et al., 2021).

Accumulative evidence have shown a KIR4.1 decrease in neurodevelopmental, traumas and neurodegenerative diseases. Therapeutical investigations aim therefore to overexpress KIR4.1 in those diseases (Ohno, 2018).

Physiological or pathological increase of KIR4.1 expression remain rare. One pathology in which KIR4.1 is overexpressed is depression (**Fig. 5, right**). Depression is a mental illness or mood disorder characterized by a loss of interest in activity and increased risk of suicidal behavior. In a congenic rat model of depression, KIR4.1 levels were increased by 50% in the lateral habenula (Cui et al., 2018), a small deep brain structure involved in nociception (sensation of pain), sleep-wake cycles and mood. Interestingly, depressive-like behavior could be repeated in overexpressing astrocytic KIR4.1 in the mouse habenula. Finally, silencing KIR4.1 in depressive rats rescued the depressive phenotype. In patients, KIR4.1 increase in post mortem tissues has been correlated with depressive disorders (Della

Vecchia et al., 2021; Xiong et al., 2019). Antidepressant drugs such as tricyclic antidepressants (TCA) and selective serotonin reuptake inhibitors (SSRI) block KIR4.1 channel to try to lower potassium buffering. Interestingly, antidepressants have seizure side effects and anti-epileptic drugs have depressive-like impacts highlighting the opposite hallmarks between epilepsy with KIR4.1 decrease and depression with KIR4.1 increase.

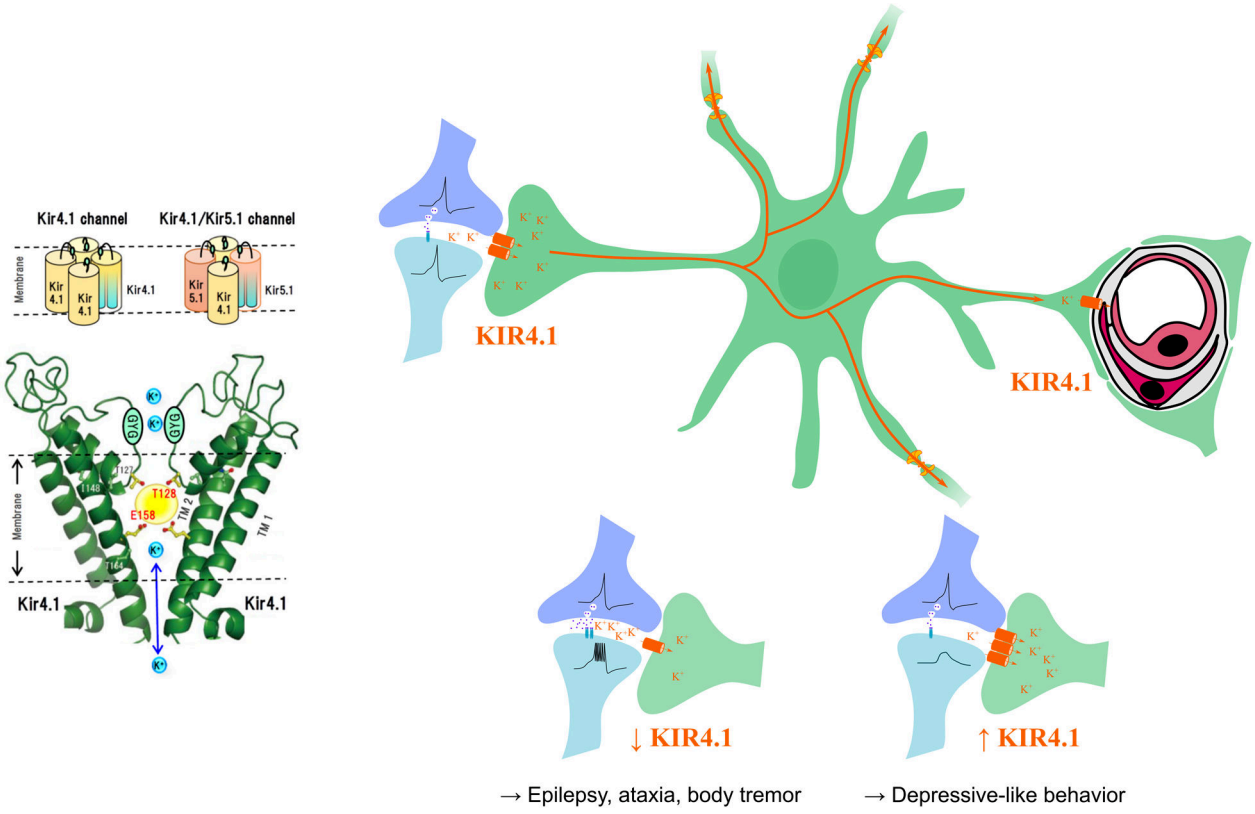

Figure 5. ***Astrocytic potassium channel KIR4.1 has crucial roles in the brain. (Left)*** *KIR4.1 structure in homotetramere (4 KIR4.1) or heterotetramere (2 KIR4.1 and 2 KIR5.1). This tetramere is selective for the potassium ion K+. Adapted from (Ohno et al., 2021).* ***(Right)*** *Potassium released in the synaptic cleft after neuronal excitation is uptaken by PAPs. Spatial buffering of K+ is mediated by low K+ concentration near blood vessels and diffusion through the astrocytic network. When KIR4.1 is downregulated, K+ remains in the synaptic cleft leading to neuronal bursts and is encountered in epilepsy. When KIR4.1 is upregulated, K+ buffering is stronger and leads to post-synaptic regime modifications encountered in depression.*

I.f) Other brain cellular interactions

Astrocytes do not connect only with blood vessels and synapses. Astrocytes interact with all other brain cells (Yu and Khakh, 2022). K+ buffering by astrocytic processes around neurons cell body is also crucial and ion homeostasis by astrocytes is vital for the saltatory conduction on noeud de Ranvier to occur properly.

Astrocytes contact oligodendrocytes by gap junctions as connexons of both cells can interact. This allows metabolic support of oligodendrocytes but also to axons wrapped by oligodendrocytes processes (Nagy et al., 2003). Astrocytes – microglia interactions have been demonstrated in development in their role in synaptogenesis. Interleukin-33 secreted by astrocytes, binds to receptors in microglia to promote synapse engulfment and phagocytosis (Vainchtein et al., 2018).

At the vascular levels, neurons also contact blood vessels to take up metabolites and control neurovascular coupling (Cauli and Hamel, 2010). Microglia also contact the vessels and can regulate the blood flow (Bisht et al., 2021).

Finally, microglia can contact synapses and noeud de ranvier to sense neuronal activity and controlling remyelination (Ronzano et al., 2021).

Generally, few labs investigate the communication between the brain cells. Apart from the astrocyte-synapse and the oligodendrocyte-axon interfaces, most studies on the CNS focus on one cell type. It is time for neuron-, astrocyte-, microglia- and oligodendrocyte-centered lab to consider the other cells and the blood vessels especially in diseases that usually affect the whole system and not just one cell. Non-cellular elements are also of great interest such as the extracellular matrices (basal lamina around vessels, perineuronal nets …) and the glymphatic system.

PART I in summary:

- Astrocytes are glial cells in the central nervous system, contacting neurons, microglia and oligodendrocytes, and highlighted only recently
- Astrocytes have long processes shaped in a bushy structure integrated in non-overlapping domains
- Astrocytes are connected by gap junctions in a network to distribute calcium influx, nutrients and K^+
- Astrocytes contact blood vessels with perivascular astrocytic processes (PvAP) to regulate the blood-brain-barrier integrity, ion homeostasis, neurovascular coupling and immune quiescence
- Astrocytes contact synapses with perisynaptic astrocytic processes (PAP) to regulate synaptic transmission, ion homeostasis, neurotransmitter recycling and neuronal metabolism
- KIR4.1, an astrocytic potassium channel, regulates potassium buffering at the synapse and is involved in epilepsy and depression

II. Local translation is a mechanism for cell polarity

Local translation is the synthesis of proteins occurring at distance from the cell body or soma. The central dogma of protein synthesis describes the translation taking place in the soma of cells and the newly synthesized proteins are transported to their final destination. However, evidence have highlighted translation in distal part of the cell especially in ramified and complex cells such as neurons and astrocytes. Moreover, researchers were puzzled on how fast adaptative responses to environmental cues can be processed by proteins travelling long distances in the cell (see **Box 1**).

We have seen in the previous section that astrocytes, and ramified cells in general, are molecularly polarized at their interfaces by enrichment of specific pools of proteins. The local protein synthesis is a mechanism to restrain the expression of some proteins that have a dedicated role at a given place.

II.a) Local translation studies focused on neurons

Local translation has been extensively studied in the CNS in neurons for 60 years. However, local translation in astrocytes has only been described for the first time in 2017 (Boulay et al., 2017) ...

II.a.i. First insights

In 1960, Edward Koenig and George B. Koelle investigated the regeneration of the acetylcholinesterase activity in distal regions of the cranial nerves (nerves are axon bundles) of cats after its irreversible inactivation (Koenig and Koelle, 1960). They showed that this regeneration was occurring faster than the time for the enzyme to be transported from the soma to the nerve. Thus, they hypothesized that the translation of this enzyme occurs distally in the nerves.

The giant squid has been a study model in neuroscience for the big size of its axons (~1 mm in diameter), 1000 times bigger than a typical axon in the mouse (~1 µm in diameter) making it easier to study especially in electrophysiology. Scientists have demonstrated that isolated giant squid axons from their soma can incorporate radiolabeled amino acids (Giuditta et al., 1968). This incorporation could be blocked by translation inhibitors.

In 1996, Hyejin Kang and Erin M. Schuman investigated local protein synthesis in rat hippocampal slices in the context of synaptic plasticity (Synaptic plasticity is the potentiation or depression of synapses according to their activity) (Kang and Schuman, 1996). Brain Derived Neurotrophic Factor (BDNF) – induced plasticity was significantly reduced when translation inhibitors were applied (anisomycin and cyclohexymide) in lesioned slices where pre or post-synaptic or both compartments were isolated. They concluded that local protein synthesis was required for synaptic plasticity.

Since then, more and more studies on local translation in axons, dendrites and growth cone in various contexts have been conducted.

II.a.ii. RNA, ribosomes and maturation organelles are templates for local translation

Early on, evidence have shown the presence of RNA distally in neuronal processes (**Fig. 6**). For instance in 1988, the authors have shown the *Map2* RNA coding for a Microtubule-Associated Protein MAP2 in the dendrites of neurons in the developing rat cortex by *in situ* hybridization (Garner et al., 1988). Since then, the list of RNA transported in distal processes has grown by techniques such as RNA sequencing. For instance, the transcriptome of the neuropil in the hippocampus has been studied. The hippocampus, a brain region involved in memory and spatial navigation, has a stereotyped structure where neurons cell bodies are all stacked in a fine layer and their processes are sent in the neuropil where no neuronal cell bodies can be found (except for interneurons). The dissection of the neuropil and its transcriptomic analysis allowed the authors to find 2,550 mRNAs enriched in neuronal processes (Cajigas et al., 2012). The neuropil contains also glial cells and blood vessels and interneurons, therefore they filtered out these cell's-enriched genes by data mining of other datasets. More recently, the team of Erin Schuman identified the transcriptome of a subset of synapses: excitatory pre-synaptic compartment. They used a mouse with a fluorescent tag on vesicular Glutamate Transporter 1 (vGLUT1). VGLUT1 is a glutamate transporter responsible for the uptake of the glutamate into vesicles at the presynaptic terminal. The sorting of these terminals after synaptosome preparation by Fluorescence Activated Synaptosome Sorting (FASS), a derivative of FACS but for smaller particles,

Box 1: Matters of timing!

In mammalian cells, the average molecular motor speed is 1 µm/s. Lets take an extrinsic cue requiring new proteins at a distance of 1 mm from the cell body (some neuronal axons). If translation would only occur in the soma, a retrograde transport would take ~16 min. A transcription factor would activate the gene transcription taking another 10 min at a rate of 10-100 nucleotide/s. Translation average rate is 10 amino-acids per seconds, thus ~1 min for its protein synthesis. Then the newly synthetized protein has to go back to the distal location by anterograde transport, another 16 min. For the first protein to arrive, ~43 minutes had passed since the trigger …

Translation is still a limited factor in the local translation triggering. Therefore, it only affects "long-term" protein homeostasis rather than an immediate regulator acting within the millisecond.

let them determine its transcriptome by sequencing (Hafner et al., 2019). A total of 468 transcripts was identified in vGLUT1+ pre-synaptic terminals.

The presence of mRNA in distal processes is an important clue for local translation. Nonetheless, translational machinery needs to be present as well.

Ribosomes and polyribosomes have been shown to be present *in vivo* by electron microscopy in the axon and presynaptic terminals (Shigeoka et al., 2016), in dendrites and spines (postsynaptic structures along dendrites in the shape of a mushroom) (Ostroff et al., 2017) and in growth cones by *in vitro* immunofluorescence (**Fig. 6**) (Koppers et al., 2019).

Proteins have to undergo post-translational modifications for proper function, membrane insertion and secretion for instance. These modifications are brought by the endoplasmic reticulum (ER) and Golgi apparatus. It was a puzzling question for the local translation legitimacy as neuronal process are very fine and do not seem to support large structure as Golgi apparatus. However ER and Golgi components called Golgi outposts (not full apparatus) were observed in culture in dendrites (Horton and Ehlers, 2003) and axons (**Fig. 6**) (Merianda et al., 2009). Other studies also found that membrane proteins can bypass the Golgi by glycosylation processes (González et al., 2018; Hanus et al., 2016).

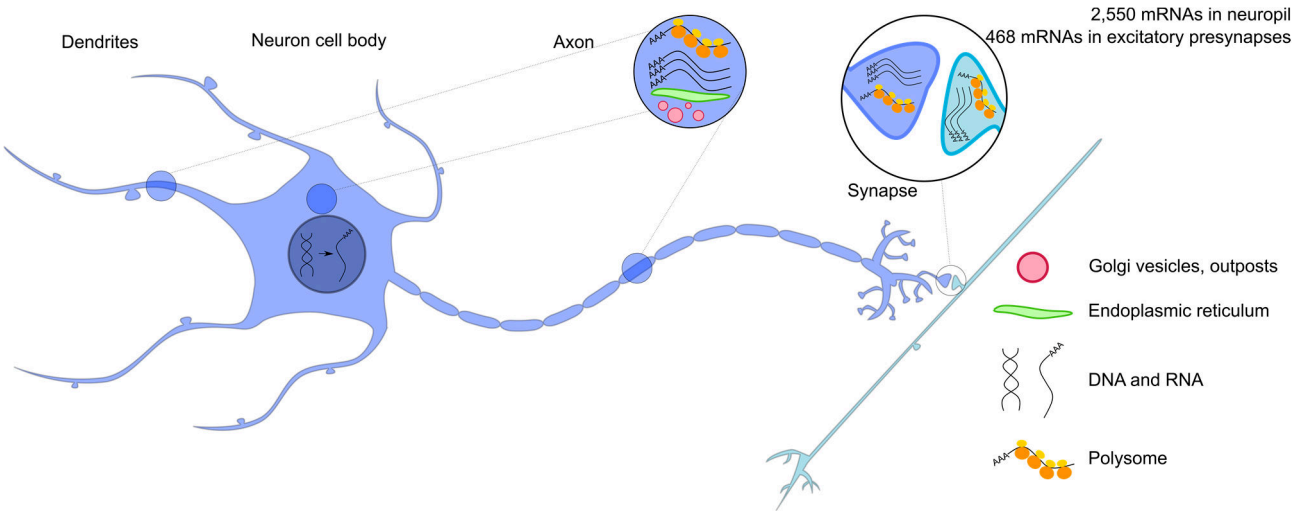

Figure 6. ***RNAs are transported and locally translated in neurons.*** *RNAs, exported from the nucleus to the cytosplam, are translated by ribosomes. RNAs can be transported in dendrites, axon and synapses of neurons to be locally translated. Post-translational modifications are mediated by golgi vesicles and outposts, and endoplasmic reticulum located in neuronal processes.*

II.a.iii. Local translation participates in the growth cone guidance

During development, axons of neurons are extending to reach their target. They sense environmental cues to guide through the brain and sometimes reach destination far from the cell body. The tip of the

axon, called the growth cone, extends protrusions called lamelipodes and filopodia to sense the different attractive or repelling molecules to guide the axon.

The Christine E. Holt's team, among others, showed that local translation is required for the axonal growth cone guidance of retinal neurons from the frog *Xenopus laevis* (**Fig. 7, top left**). The guidance cue, Netrin 1, binds to DCC receptors at the growth cone membrane. Signaling cascade will activate the kinase Src that will phosphorylate the RNA binding protein Zipcode Binding Protein 1 (ZBP1). Phosphorylated ZBP1 releases its *β-actin* mRNA into the ribosome to be translated (Campbell and Holt, 2001; Jung et al., 2012; Leung et al., 2006; Lin and Holt, 2007). β-actin local translation at one side of the growth cone will increase cytoskeleton polymerization only at this sub-location and will direct the protrusions toward the Netrin-1 cue. This regulation of translation on the β-actin mRNA involves its 3'UTR (Leung et al., 2006, 2018).

On the contrary, repelling cues provoke the actin cytoskeleton to collapse. Semaphorin3A (Sema3A) is secreted and can bind the neuropilin1 (Nrp1) on growth cones (Wu et al., 2005). The resulting signaling pathway leads to local translation of RhoA GTPase involved in the actin cytoskeleton depolymerization. The actin collapses and prevents the protrusions to continue in the Semaphorin3A gradient direction (Campbell et al., 2001; Jung et al., 2012; Lin and Holt, 2007).

II.a.iv. Local translation participates in synaptic plasticity

Synaptic plasticity is a fundamental process involved in memory formation for instance. Plasticity can either strengthen or weaken given synapses depending on the activity of their inputs. For instance, higher activity will strengthen the synapse in the long time and is part of the Long Term Potentiation (LTP). On the contrary, Long Term Depression (LTD) is the decrease of synaptic activity. Plasticity involves the recruitment or recycling of neurotransmitter receptors present at the membrane surface.

It has been shown that local translation participates in the long-term synaptic plasticity (contrary to short term) by regulating receptors on site (**Fig. 7, top right**). Application of drugs can elicit LTD in the hippocampus of acute brain slices. When the neuronal somas are disconnected from their dendrites by micro dissecting the CA1 region of the hippocampus, the LTD in the dendrite region can still be elicited. This plasticity was blocked by translation inhibitors (Huber et al., 2000). A yet unknown protein thus mediates the level of neurotransmitter receptor internalization. Activity-dependent activation of receptors lead to signaling cascades affecting the level of activated initiation factors crucial for translation. It was shown that the activation of GABAergic neurons (inhibitory neurons) in the hippocampus triggers local translation in pre-synaptic terminals. When in contact with translational inhibitors, the LTD-induction was abolished and was dependent on the mTOR pathway activating initiation translation factors (Younts et al., 2016).

A recent study, (Sun et al., 2021) investigated the levels of translation in synapses of cultured neurons in basal conditions as well as after global or more local plastic conditions. After synaptic protocols there was an increase in the newly synthetized protein in synapses. More impressive, they were able to detect local translation events in single spines of dendrites by eliciting their activity by local calcium uncaging.

RNA translation is often described as multiple ribosomes translating the same RNA in single file called polyribosomes or polysomes. However, the team of Erin Schuman investigated the relevance of monosome translation in neuronal processes (Biever et al., 2020). Using ribosome fractionation (a method based on separation between small and large subunits, monosomes and polysomes by their sedimentation coefficient), they showed that monosomes were in fact more abundant in the neuronal processes than polysomes. They also demonstrated the translational capacity of monosomes and their translatome (**Fig. 7, top right**). Among monosome-enriched transcripts (compared to polysome), several neurotransmitter receptors were identified suggesting a role for monosomes in synaptic plasticity.

II.b) Local translation in radial glia regulates cortical development

Radial glia cells are progenitor cells in the brain development giving rise to neurons first then to the glial lineage of astrocytes and oligodendrocytes. The radial glia are scaffold elements for the neurons that use them to migrate along their processes to grow the brain. Radial glia have a process attached to the apical side toward ventricles of the brain and another longer basal process connected to the pial surface of the brain with an endfoot.

Pilaz and colleagues exploited the polarity of the radial glia to investigate local translation in the basal endfoot (**Fig. 7, bottom left**) (Pilaz et al., 2016). It is one of the first evidence for local translation in glia. In their experiments, the authors isolated the radial glia endfeet by peeling off the pial surface. With irreversible photoswitchable fluorophores from green to red, Dendra2, they showed the recovery of the green

Box 2: Advantages of local translation

Local translation restricts protein expression in space and time.
Proteins are sometimes needed during a limited amount of time in a particular location. Transport of somatic-encoded proteins would not allow time and space constraints. Furthermore, proteins that are involved in organelle degradation for instance would be harmful if expressed in the whole cell.

Local translation costs less energy compared to the ATP-demanding transport with molecular motors. In addition, RNA can be translated multiple times. Finally, replacement of old proteins is easier.

fluorescence of a Dendra2 construct fused to a 3'UTR of a gene, *Ccnd2*, showed to be transported specifically in the radial glia endfoot (Pilaz et al., 2016). It shows that specific mRNAs are transported in the processes and their local translation occurs in the radial glia endfoot.

The RNA-binding protein (RBP) Fragile Mental Retardation Protein (FMRP) was shown to be present in endfeet and to bind to a specific local RNA repertoire. Interestingly, the knock-out (KO) of FMRP in the brain leads to defect in the active transport of some RNAs at the basal interface. It points out a mechanism for the regulation of local translation by FMRP, controlling the transport of RNA in processes in radial glia.

In a preprint (Pilaz et al., 2020), the same team investigated the consequences of local translation in endfoot on the cortical development. They showed that the Rho-GTPase ARHGAP11A was locally translated in endfeet and its disruption lead to radial glia morphology defect and lamination (neuronal layers) perturbations. This disruption was rescued by the *arghap11a* mRNA on the contrary to a construct lacking the 5'UTR restricted to the cell body. It means that the local translation of ARHGAP11A in the endfoot regulates cortical development.

II.c) Myelin coding RNA are transported in oligodendrocyte sheaths

Oligodendrocytes extend long processes toward neuronal axons to wrap them with insulating myelin sheaths. The myelin is composed of lipids and proteins and participates in the saltatory conduction of the action potentials to make nervous transmission faster. Myelin contains proteins as the Myelin Basic Protein (MBP), the Myelin Oligodendrocyte Glycoprotein (MOG) and the ProteoLipid Protein (PLP).

The myelin proteins are enriched in the sheaths. Interestingly, *mbp* RNA has been shown to be actively transported and locally translated in the sheaths (**Fig. 7, bottom right**) (Meservey et al., 2021; Müller et al., 2013). *Mbp* RNA is transported along the microtubules toward the myelin sheath (anterograde transport) thanks to molecular motors Kinesins and Dyneins (retrograde transport) (Herbert et al., 2017). Once at the sheath, local translation of MBP depends on the axonal activity during myelin formation and maintenance (Müller et al., 2013; Wake et al., 2011). Nervous transmission in the axon releases glutamate sensed by the oligodendrocyte. Signaling cascade will activate the Fyn kinase to phosphorylate RBP associated with the *mbp* RNA such as heterogeneous ribonucleoparticles (hnRNP) that were repressing their translation. The phosphorylation leads to a de-repression and the local translation of MBP (Müller et al., 2013; Wake et al., 2011). The activity dependent local translation of MBP is one of the few examples in oligodendrocytes that maintains the polarity of the cell in an

active manner. Recently, it was shown that the 3'UTR of the *mbp* RNA regulates its transport and active translation and was the target of the RBP (Torvund-Jensen et al., 2018).

Other myelin protein-coding mRNA have been shown to be transported in the myelin sheaths such as the *mog* mRNA.

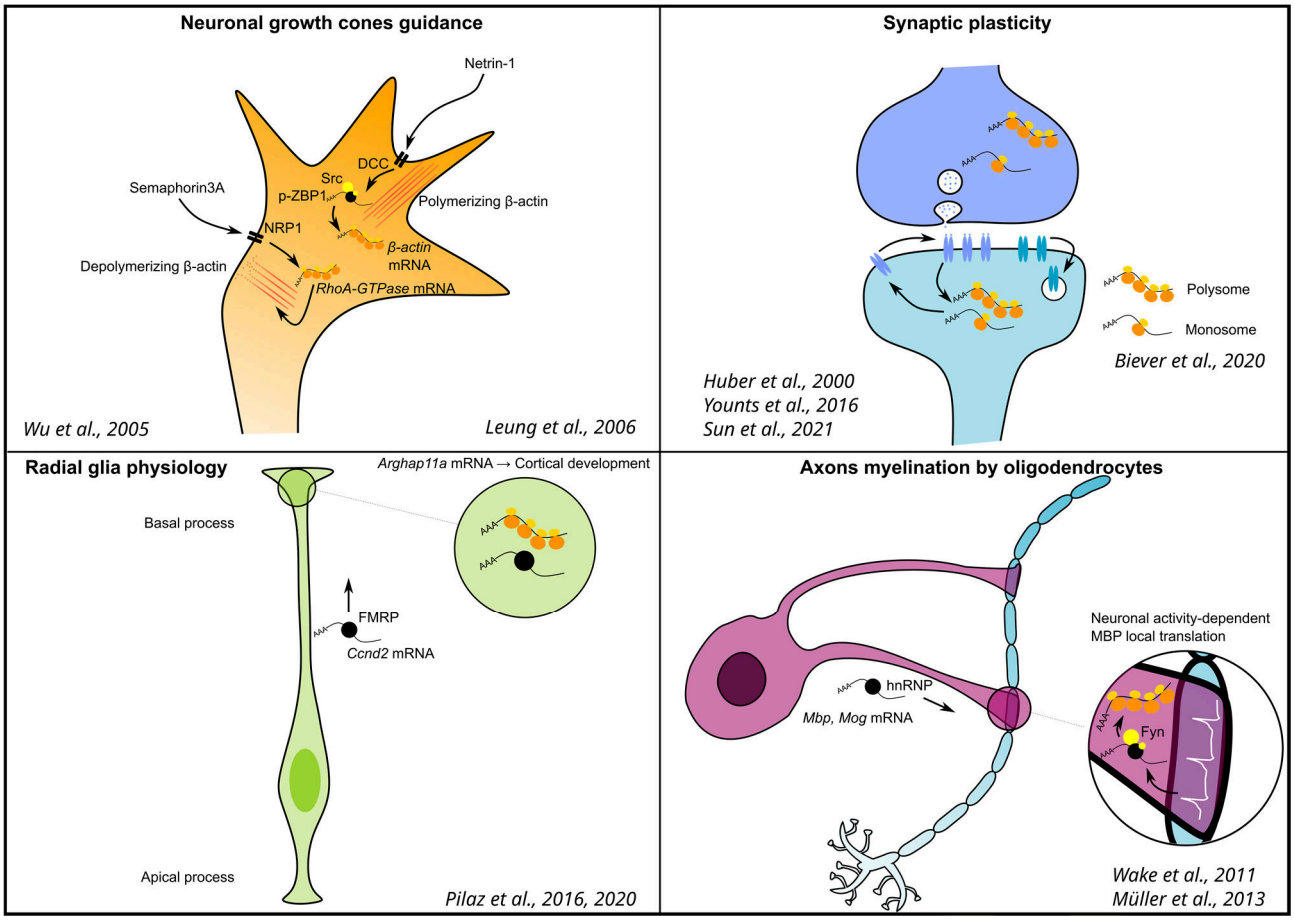

Figure 7. ***Local translation in neurons, radial glia and oligodendrocytes. (Top left)*** *Netrin-1 source binds to DCC receptor activating Src kinase to phosphorylate the RBP ZBP1 (p-ZBP1) releasing its mRNA for β-actin local translation. The growth cone is guided toward Netrin-1. On the contrary, Semaphorin3A binds to NRP1 triggering local translation of RhoA-GTPase to depolymerize β-actin and avoiding Sema3A source.* ***(Top right)*** *Local translation occurs in pre- and post-synaptic terminals by polysomes and monosomes. Neuronal transmission triggers local translation to induce neurotransmitter recruitment at the synaptic cleft or receptor internalization both in synaptic plasticity.* ***(Bottom left)*** *FMRP regulates mRNA transport in basal processes of radial glia where local translation occurs. For instance, local translation in radial glia endfeet of Arghap11a regulates cortical development.* ***(Bottom right)*** *Myelin-coding mRNA are transported to myelin sheaths in oligodendrocytes. Neuronal activity is sensed by this cell and triggers phosphorylation of RBP by Fyn kinase to induce local translation of MBP.*

II.d) Local translation occurs in perisynaptic and perivascular processes of astrocytes

The enrichment of proteins in the astrocyte interfaces (seen above) is accompanied by an enrichment of a pool of mRNAs enriched and locally translated in the processes. Even if the transport of an mRNA does not involve translation necessarily, its local protein synthesis induces the molecular polarity of the astrocyte.

II.d.i. Local translation sets molecular heterogeneity in Perivascular Astrocytic Processes (PvAP)

One of the first example of local translation in astrocytes was shown by the lab in the PvAP and only very recently (Boulay et al., 2017).

First, the authors described the pool of RNAs present in endfeet. Microvessel purification technique allows the mechanical isolation of the cerebral vasculature along with the endfeet detached from their soma due its associated with extracellular matrix (Boulay et al., 2015b). Enzyme digestion of the basal lamina detaches the endfeet from the vessels. The differential transcriptome analysis of both digested and non-digested vessels allowed to identify for the first time the pool of RNA transported in endfeet. Fluorescence In Situ Hybridization (FISH) confirmed the presence of a subset of genes such as *Aqp4* mRNA coding for the water channel AQP4. AQP4, described above, is part of the enriched molecule in PvAP to regulate water homeostasis.

To know if the mRNAs were locally translated, the authors performed astrocytic polyribosomes RNAs immunoprecipitation from isolated astrocyte endfeet. They used a transgenic mouse model, Aldh1l1-Rpl10a:eGFP (BacTRAP mouse) in which GFP is fused to a ribosomal protein from the 60S subunit, RPL10A. Translating Ribosome Affinity Purification (TRAP) (Heiman et al., 2014) of endfeet isolation from this mouse was performed with a GFP immunoprecipitation and the RNAs were identified by RNA sequencing. Among locally translated RNA in PvAP, called the endfeetome, we can find *Aqp4* but also *Kcnj10* coding for the potassium channel KIR4.1 described above, *Gja1* coding for CX43 involved in gap junction and immune quiescence and *Agt* coding for the angiotensinogen AGT involved in the neurovascular coupling (**Fig. 8**). Those proteins are essentials for vascular functions highlighting the role of local translation in the astrocyte polarity. Finally, the authors described global translational events in isolated PvAP with the staining of incorporated modified methionine. The newly synthetized proteins were not coming from the soma that is detached and had to come from local translation.

Interestingly, they described the presence of machineries for post-translational modifications in endfeet such as the endoplasmic reticulum and Golgi apparatus by electron microscopy although not in all structures for the Golgi (**Fig. 8**). They also described the vicinity of synapses at the PvAP level confronting the stereotyped image of the 2 astrocytic interfaces separated at 2 distinct places.

II.d.ii. Local translation in Perisynaptic Astrocytic Processes (PAPs) is dynamic

The same year as the PvAP local translation paper, the team of Joseph D. Dougherty described the local translatome (locally translated mRNAs) in PAPs (Sakers et al., 2017). They showed the presence of ribosomes and translational events in the peripheral astrocytic arborization suggesting local translation in PAPs (**Fig. 8**). Using the TRAP technique on the BacTRAP mouse shown previously on synaptosomes preparation, isolated PAPs along with the synapses, they identified PAP enriched locally translated transcripts such as *Kcnj10* coding for KIR4.1 and *Slc1a2* coding for GLT1. Globally, this local PAP translatome corresponds to neurotransmitter (GABA and Glutamate) and fatty acid metabolic process. This relates to the gliotransmission properties of PAPs and its new potential roles in lipid regulation.

Interestingly, the authors investigated translational regulatory mechanisms of these genes. They showed that the PAP enriched RNAs have longer 3' UnTranslated Regions (3'UTRs) than PAP-depleted ones. Among this 3'UTRs, a significant part had a motif, Quaking Response Element (QRE), recognized by the RNA-binding protein Quaking (QKI). This motif was responsible for the localization and translation regulation of the RNAs. QKI was already shown to regulate *Mbp* mRNA localization in oligodendrocytes (Li et al., 2000). Furthermore, QKI7, a QKI isoform, has been shown to bind *Gfap* mRNA in primary human cortical astrocytes to promote QKI expression (Mazaré et al., 2021; Radomska et al., 2013). More recently, the team of Joseph D. Dougherty identified the subset of astrocytic mRNAs bound to QKI6, another QKI isoform (Sakers et al., 2021). QKI6 deletion lead to a delay in maturation of some astrocyte genes.

We recently addressed the question of the PAP translatome dynamism (Mazaré et al., 2020a). After describing RNAs, ribosomes, protein maturation machinery and translational events in astrocytes processes close to synapses, we first characterized the PAP translatome, we called the PAPome, in the dorsal hippocampus with a refined TRAP technique from the bacTRAP mice (**Fig. 8**). Interestingly, some mRNAs were more translated in PAPs than in the whole astrocyte and included metabolism or cell signaling for instance. For example, ferritin-subunit-encoding mRNAs as *Ftl1* and *Fth1* could highlight iron homeostasis in PAPs and cytoskeleton-encoding mRNAs as *Ezrin* could highlight a role for local translation in the PAP dynamics. Surprisingly, ribosome subunits-encoding mRNAs

were also highly enriched in the PAPome such as *Rpl4* or *Gnb2l1* coding for RACK1. As shown in the next section, ribosome subunits are assembled together with ribosomal RNA (rRNA) in the nucleus. However, recent data from neurons suggested that replacement of ribosomal subunits could occur when proteins are too old or it could be an adaptative ribosomal stoechiometry to translate subsets of genes (Fusco et al., 2021). Is the PAPome dynamic ? To tackle this question, we compared the PAP translatome between control and fear-conditioned mice. Fear-conditioning involves memory formation and the dorsal hippocampus structure. A mouse is placed in cued-environment and electrically shocked on the paws. 24 h later, the mouse is placed again in the same cued-environment and freezing time is measured. The mouse remembered being shocked in that cage and froze as a defense mechanism. Interestingly, a subset of mRNAs from the PAPome changed upon fear-conditioning. For instance Gnb2l1 mRNA was less associated with polysomes in PAPs and was redistributed in larger process and soma and RACK1 (its encoding protein) level was decreased. This led us to hypothesize that local translation in PAPs is dynamic and could be involved in learning and memory formation. Astrocyte's functional polarity is sustained by this local translation.

Dougherty's lab investigated the activity dependent translation in the whole astrocyte (preprint Sapkota et al., 2020). 10 min after the injection of a pro-epileptic drug, pentylenetetrazol (PTZ) (which induce a high neuronal activity), in the bacTRAP mouse, they performed TRAP and described a translational profile change compared to saline-injected mice. *Ex vivo*, they stimulated neurons with Brain Derived Neurotrophic Factor (BDNF) application on slices and observed an increase in the global translation events in astrocytes.

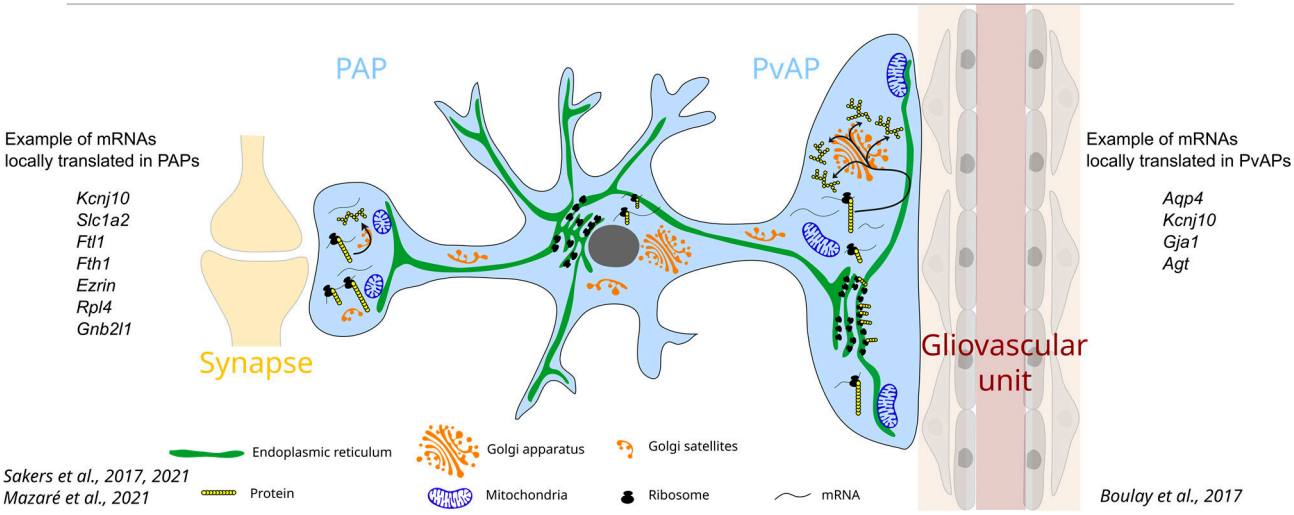

Figure 8. ***Local translation occurs in PvAPs and in PAPs.*** *mRNAs, polysomes and endoplasmic reticulum are found in PvAP and PAPs. Full Golgi apparatus can be present in few PvAP whereas only Golgi outposts are present in PAPs. Local translation occurs in both compartments on specific subsets of mRNAs.*

II.e) Local translation in microglia remains poorly understood

As in all ramified cells, local translation should occur in microglia but has never been investigated yet. However, few studies brought hints toward that direction.

The lab of Joseph D. Dougherty investigated the local translation characteristics of microglia and its functional relevance with the same line as the previous study in PAPs (preprint Vasek et al., 2021). They first showed that ribosomes and translational events occurred in microglial processes contacting the synapses. Next, using an inducible bacTRAP mouse specific of microglia (CX3CR1-creERT2:lxl-RPL10a-GFP expressing GFP fused to RPL10a in microglia upon Cre recombinase activation by tamoxifen injection) they were able to compare the translatome of whole microglia versus peripheral microglia processes (PeMP). Among the PeMP enriched RNAs, some were involved in microglia crucial functions as immune response, cell motility, chemotaxis, phagocytosis and synapse pruning. As microglia is involved in immunity, they tested the microglia translation role in phagocytosing foreign objects. *Ex vivo*, in acute brain slices, the inhibition of translation by anisomycin decreased the microglial phagocytosis capacity of beads coated with *E. coli* particles. However, global translation and not local translation was addressed and other cells could be involved as anisomycin targets the whole slice.

II.f) Outside the brain, local translation occurs also in non-complex cells

Local translation has been investigated in complex ramified cells because it was clearly not conceivable that proteins travel such a long distance in a short time to adapt to the environment. However, evidence of local translation were given for non-ramified cells and even single-cell organisms (Das et al., 2021). Almost all cells have some kind of polarity and as local translation sustain these polarities, it seems easier for the cell to transport RNAs that can be translated multiple times and be stocked than to transport proteins after a retrograde signaling pathway (see **Box 1**).

In bacteria, transcription and translation are thought to be coupled as there are no organelles. However, studies showed that some RNAs translation was uncoupled from their synthesis and were translated in cell location where the protein was needed (**Fig. 9, top left**). For instance, the *bglg* RNA was present only at the cell poles where its protein, BglG, is present (Nevo-Dinur et al., 2011).

The budding yeast *S. cerevisiae* reproduces by forming buds which stay attached to the mother cell until the mitosis is complete. ASH1 is a transcriptional factor involved in the mating system of the yeast. Its mRNA *Ash1* is transcribed in the mother cell and transported in the bud via the cytoskeleton

(**Fig. 9, top right**). The phosphorylation of its RNA-binding protein (RBP) Pumillo (PUF6) leads to its translation in the bud (Gu et al., 2004).

During the embryogenesis of the fly *D. melanogaster*, the embryo adopts a anterio-posterior axis early on. By FISH, studies have shown that the B*cd* mRNA coding for the bicoid protein was polarized at the anterior part and that *Osk* mRNA coding for oskar protein was polarized at the posterior part. The local translation of these 2 RNAs determine the antero-posterior axis of the fly (**Fig. 9, bottom left**) (Kugler and Lasko, 2009).

In mammals, not only cells in the nervous system are capable of local translation. Epithelial cells in the gut, enterocytes, have a strong apico-basal polarization. It was shown that mRNA localization was also polarized. Very interestingly, upon feeding, local translation of ribosomal proteins in the apical side increased the translational rate to support the increase of nutrient absorption (**Fig. 9, bottom right**) (Moor et al., 2017).

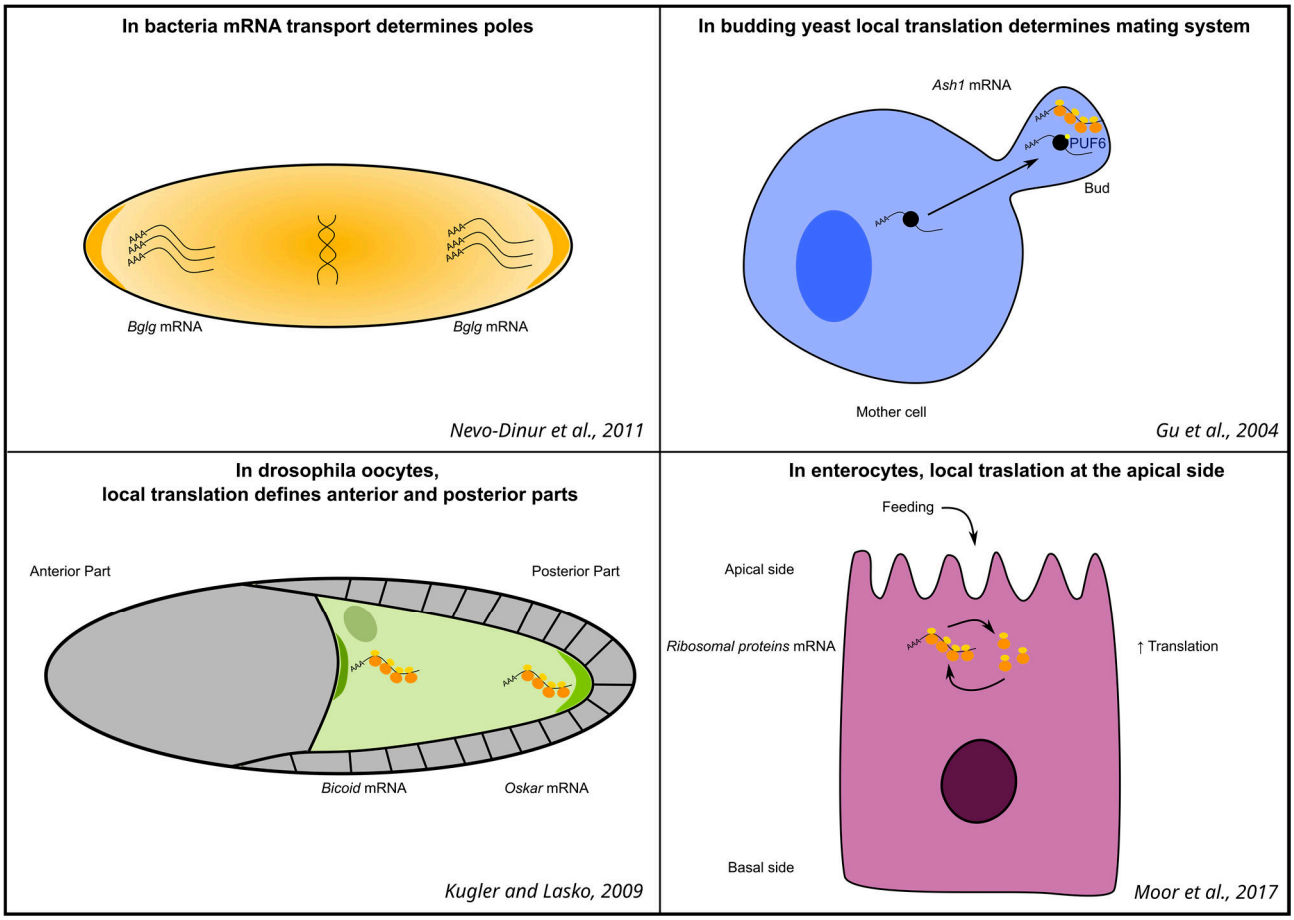

Figure 9. ***Local translation occurs in other cell models. (Top left)*** *In bacteria, translation can be decoupled from transcription to enable Bglg mRNA transport in both cell poles.* ***(Top right)*** *In yeasts, Ash1 mRNA can be transported via the cytoskeleton in the bud to be locally translated after its RBP PUF6 phosphorylation and regulate the mating system.* ***(Bottom left)*** *In oocytes of flies, bicoid mRNA and oskar mRNA are locally translated in the anterior and posterior part respectively to determine*

the organism development axis. ***(Bottom right)*** *Enterocytes in the intestine are polarized from the basal to the apical side. Upon feeding, microvilli on the apical side sense the increase of nutrients activating local translation of ribosomal proteins to support more translation and absorb those nutrients.*

II.g) Local translation occurs in sub-cellular organelles

Translation near organelles can be seen also as local because it is efficient protein addressing (Béthune et al., 2019). For instance, translation of mitochondrial protein can occur at the outer membrane surface of mitochondria with the docking of the ribosomes to the Translocase of the Outer Membrane (TOM) complex (Lesnik et al., 2015). As an organelle coming from endosymbiosis, mitochondria have their own ribosomes and translates mitochondrial mRNAs. Translation of membrane and secreted proteins occurs at the Rough Endoplasmic Reticulum (RER) membrane where ribosomes are docked at its surface. More recently, it was shown that translation at nuclear pores regulates its biogenesis (Lautier et al., 2021). Endosome-associated mRNAs are also translated at the endosomal surface (Müntjes et al., 2021). Finally, some studies have identified translational events in the nucleus but these mechanisms need further investigations (Dahlberg, 2003; David et al., 2012; Reid and Nicchitta, 2012; Yewdell and David, 2013).

Recently, studies have shown that local translation in synapses support mitochondria functions by providing its proteins (Cioni et al., 2019; Kuzniewska et al., 2020; Lee et al., 2022). Mitochondria proper function is essential for synaptic functions as nervous transmission is highly demanding in energy. Using mitochondrial translation event reporter, an unpublished study showed that translation inside presynaptic mitochondria was increased during synaptic activity and that its inhibition using chloramphenicol altered synaptic functions (Yousefi et al., 2020). Local translation of PINK1 near distal mitochondria support mitophagy in a controlled manner (Harbauer et al., 2022). Finally, it was shown that mitochondria are the energy suppliers for local translation to occur and to support synaptic plasticity (Rangaraju et al., 2019). In this study, authors were able to kill mitochondria in single spines by laser activation of mitochondria killer protein. They showed that in those mitochondria-depleted spines, plasticity was unable to elicit local translation as it normally does.

II.h) Multiplication of tools to study local translation

The tools to study protein synthesis *in vitro* and *in vivo* are recapitulated in a review from Shintaro Iwasaki and Nicholas T. Ingolia (Iwasaki and Ingolia, 2017). The difficulty in studying the local translation relies on the ‘local’ part, especially *in vivo* where the isolation of compartment becomes hard.

However, here are some of the techniques used to study localized protein synthesis:

In vitro: Most work have been done in neurons because they polarize well in culture in contrast to astrocytes which flatten in the absence of neurons.

- First by metabolic labeling of translation with short pulse of methionine analogs or puromycine for instance. The incorporation of a modified methionine such as the azidonorleucine (ANL) or the azidohomoalanine (AHA) in nascent chains through a mutated methionyl-tRNA synthetase (MetRS*) can be followed by Fluorescent non-canonical amino-acid tagging (FUNCAT) which consists in a click chemistry reaction detected by fluorescence (Alvarez-Castelao et al., 2017). Puromycin is an antibiotic protein synthesis inhibitor that incorporates into nascent chains and can be targeted by immunofluorescence (Gamarra et al., 2020). The short incubation time (5-10 min) in neuronal culture is not sufficient for nascent chains to travel a long distance. The fluorescent labelling in the neuronal processes reflects the local translation events. FUNCAT and puromycilation assays can be combined with proximity ligation assays (FUNCAT-PLA or Puro-PLA) to target only specific proteins.

- Another way to assess local translation events by fluorescence is by using photoswichable reporters or Fluorescence Recovery After Photobleaching (FRAP) technique. First, the compartment has to be isolated by laser dissection, for instance the axon or the growth cone. The assessment of the FRAP fluorescence or the recovery of the green fluorescence after irreversible green to red photoswitch are clues for local translation as no proteins can come from the isolated rest of the cell (Ströhl et al., 2017).

- Boyden chambers are cylindrical inserts nested inside a well of a culture plate. The bottom of the insert have a membrane with a defined pore size. Neurons can be cultured on this membrane and their processes extend through the pores to reach the lower part. The membrane can be removed to detach the cell body from the processes and cultivated with heavy amino acids for 5 min. The newly synthetized local proteome can be assessed by Mass Spectrometry in a technique called pulsed stable isotope labeling by amino acid in cell culture (pSILAC) (Cagnetta et al., 2018).

- Finally, protein synthesis reporters such as GFP flanked with 5’ and 3’ UTRs localize the RNA in cultured neuron processes. When mechanically detached from the cell body, local protein synthesis in the isolated process can be assessed by measuring the level of GFP after stimulation for instance (Aakalu et al., 2001).

In vivo: Challenges are to isolate local cell specific compartments.

- Ribo-tag or TRAP techniques consist in cell-specific tagging of ribosomal proteins with tags that can be immunoprecipitated. Synaptosome preparations are isolation of synapses along with the PAPs. Synaptosomes combined with the TRAP can help decipher local translation in synapses of certain

neuronal cell type (Ouwenga et al., 2018) and from PAPs (Mazaré et al., 2020a). Microvessels purification that isolates PvAPs can be used before the TRAP to investigate PvAP local translation (Boulay et al., 2017).

- FUNCAT signals can be assessed by cell-specific metabolic labeling of translation in acute slices. High resolution microscopy can detect fluorescence in cellular processes (Alvarez-Castelao et al., 2017). Likewise, puromycine can be used. However, the signal will not be specific to any cell and will be hard to assess in astrocytes as neurons have a strong puromycine signal compared to astrocyte processes.

- For neurons, it is sometimes easy to physically separate the cell body from the processes by microdissection. For instance, in the cerebellum, the cell body of Purkinje cells, a type of cerebellar neuron, are aligned in the same layer and can be microdissected from their dendrite located in another layer. The local translatome can be accessed by TRAP (Kratz et al., 2014). Another team investigated local translated mRNA dynamics in dendrites of neurons from the CA1 region of the hippocampus by tissue punches within the dendritic region using a needle (Ainsley et al., 2014). No such method could be used for astrocytes as they do not organize in stereotypical layers with cell bodies on one hand and processes on the other hand.

PART II summary :

- RNAs, ribosomes, endoplasmic reticulum (ER) and Golgi vesicles are present in neuronal dendrites, axon and synapses
- Local translation occurs in neuronal processes, in radial glia endfoot and in myelin sheaths of oligodendrocytes. This local translation is dynamic
- RNAs, polysomes, ER, Golgi vesicles and local translation are present in PAPs and PvAPs
- Local translation is also taking place in non brain and non polarized cells. It is also encoutered in and near organelles

III. A fundamental biological process coordinated by multiple partners: Translation

Local translation, described in the previous section, is tightly regulated to set the molecular and functional polarity of neurons and astrocytes for instance. The mechanisms involved in the regulation of local translation has, once again, almost only been addressed in neurons. It involves ribosomes, translation factors, RNAs and multiple protein partners.

III.a) From nucleus to cytoplasm: Translation involves proteins and RNAs

III.a.i. Ribosomes are composed of two subunits and four ribosomal RNA (rRNA)

Eukaryotic ribosomes are big complexes with 79 proteins and 4 rRNA divided into 2 subunits: the large subunit comprises 46 proteins and 3 rRNA and the small subunit 33 proteins and 1 rRNA. Ribosomes are also known as 80 S ribosomes referring to their sedimentation coefficient in Sverdberg units (S) when ultracentrifuged. The large subunit becomes 60 S with 28 S, 5.8 S and 5 S rRNA, and the small subunit becomes 40 S with its 18 S rRNA. The ribosome nomenclature for eukaryotes names large subunit ribosomal proteins RPLx, with RP for Ribosomal Proteins and L for large subunit, and x for a number and letter (e.g. RPL10a). The small subunit RP are named RPSx in the same manner. However, no consensus was used early on, therefore the prokaryote's naming is different and there are also different names for one protein among eukaryotes. For instance, RPS15a in humans is RPS22 in yeast and RPS8 in bacteria. Hence, a new nomenclature emerged (Ban et al., 2014) to take all the reigns into account. Now, for the small subunit, it is bSx for bacteria only, eSx for eukaryotes only and uSx for universal. For the large one, it is bLx, eLx or uLx. Although more and more used, the literature sticks to the old nomenclature (including this thesis).

Ribosomal RNA (rRNA) are essential for translation as they bind messenger RNA (mRNA) and transfer RNA (tRNA) to facilitate their entry in the ribosome. rRNAs also form the ribosome binding sites, A, P, and E sites, which are 'pockets' in the ribosome used in the translation process. The A site, for aminoacyl, allows the entry of the tRNA carrying the amino acid and its recognition to the mRNA. The P site, for peptidyl, facilitates the elongation of the nascent chain with the formation of the peptidic bond. Finally, the E site, for exit, releases the amino acid free tRNA.

Ribosomes were thought to be an invariable complex with the same RPs across the same cells throughout time. However, recent findings showed that the ribosome can be heterogeneous even

within one cell. This heterogeneity could come from a difference in the RP stoichiometry with more or less 1 RP, or post-translational modifications of RPs and rRNA (Emmott et al., 2019). For instance, the protein RACK1 has been shown to be a core RP and crystallized with the whole ribosome. However, RACK1 has also a free form outside the ribosome and can jump on and off the ribosome (Johnson et al., 2019). In cultured neurons, RACK1, RPS30, RPLP2 and RPLP0 have been shown to be more or less present in the ribosome according to oxydative stress (Fusco et al., 2021). Does this heterogeneity have a physiological effect? In a mass spectrometry study conducted in embryonic stem cells, RPs were shown to have different stoichiometry (Shi et al., 2017). For instance, RPL10a had a stoichiometry below 1, indicating that it is not present in all ribosomes (interestingly they showed RACK1 with a stoichiometry of 1 in this model in contrast to Fusco et al., 2021). Ribo-seq of RPL10a-enriched versus -depleted transcripts revealed distinct subpools of regulated mRNA potentially with different functional roles.

III.a.ii. Ribosome biogenesis and assembly occur in the nucleus but some ribosomal proteins are locally translated

The 80 S ribosome formation is a multi-step process involving the nucleus. Ribosomal proteins (RPs) are translated in a classic way: In the nucleus, the RNA polymerase 2 transcribes mRNAs coding for RPs that are translated by ribosomes in the cytoplasm (**Fig. 10, left**). However, ribosomal subunits assemble in the nucleus together with the rRNAs. Thus, RPs are imported back into the nucleus. The rRNA are transcribed in the nucleolus (sub-region of the nucleus) by the RNA polymerase 1 for the 35 S rRNA and by the RNA polymerase 3 for the 5 S rRNA. The polycistronic 35 S rRNA is post-processed to give the 28 S, 18 S and 5.8 S rRNA. RPs, together with pre-rRNA, assemble to form the pre-40 S and pre-60 S ribosomal subunits. Further maturation steps and exportation into the cytoplasm form the mature 40 S and 60 S subunits that can assemble on a mRNA as the 80 S ribosome. Importantly, RACK1, a ribosomal protein, only assembles lately with the pre-40 S particle in the cytoplasm. RACK1 participates in the maturation of the human pre-40 S particle and of the 18 S rRNA observed by high-resolution cryo-Electron microscopy (cryo-EM) (Cerezo et al., 2019; Larburu et al., 2016). Interestingly, the deletion of RACK1 by siRNA in human HEK293 cells slows down the pre-40 S maturation but does not change the 40 S subunit quantity. This late incorporation in ribosomes and its non-essential property in cultured human cells led to suggest that RACK1 is involved in translation initiation and is an accessory factor regulating translation at will.

The nucleus mandatory step to assemble ribosomal subunits is *a priori* not compatible with a distal ribosome biogenesis. Therefore, researchers were surprised to encounter locally translated RPs in neurons and astrocytes processes. For instance, mRNAs coding for RPs are found in the neuropil local transcriptome in the hippocampus (Cajigas et al., 2012), axons of neurons in the visual cortex

(Shigeoka et al., 2016) and perisynaptic astrocytic processes (PAPs) in the dorsal hippocampus (Mazaré et al., 2020a). The lab of Christine Holt showed that RP local translation was taking place in the axon in neuronal culture. Interestingly, they suggested that RPs localized at the outer surface of the ribosome would be more distally translated than those deep inside suggesting that RP locally synthesized were replacing those in existing ribosomes (**Fig. 10, right**) (Shigeoka et al., 2019). The inhibition of RP local translation decreased local protein synthesis and altered axonal branching. Translating ribosomes are almost immobile while RPs can diffuse freely, therefore, single molecule tracking of RPs dynamics could reveal exchanges with polysomes (Dastidar and Nair, 2022).

Distally translated RPs could finally play other roles. It has been shown that free ribosomal proteins could have extra-ribosomal functions such as tumorigenesis by activating p53, immune signaling and development and diseases (Zhou et al., 2015). RACK1, a scaffold protein that can associate with the 40 S subunit, is also present in a free form. As a receptor of activated C kinase 1, it binds to the PKC protein and regulates multiple signaling pathways (Adams et al., 2011). RACK1 functions will be further detailed in the RACK1 section (part IV).

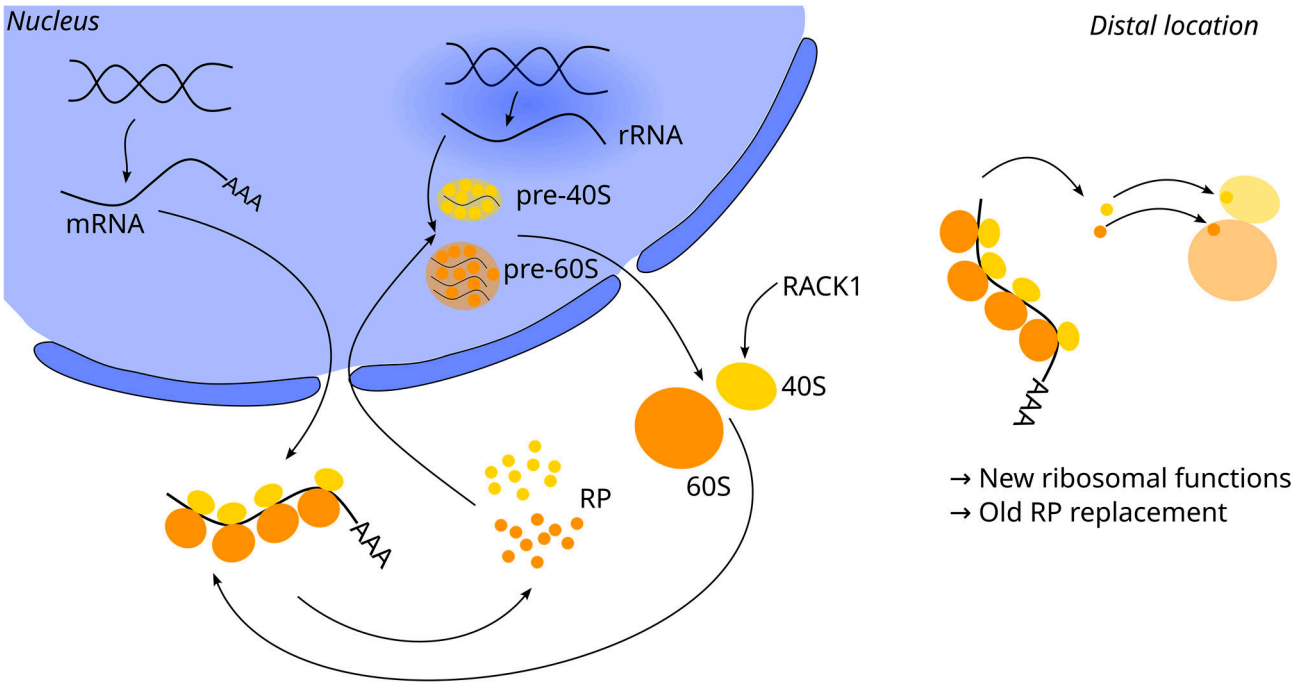

Figure 10. ***Ribosome biogenesis occurs in the nucleus but some RPs are locally translated. (Left)*** *mRNAs coding for ribosomal proteins are exported in the cytoplasm and translated into RPs. RPs are imported back to the nucleus to be assembled as pre-40S and pre-60S with rRNA transcribed in the nucleolus. These particles mature and are exported in the cytoplasm where RACK1 integrates the 40S subunit. Mature 40S and 60S can then be used for translation.* ***(Right)*** *In distal location such as in cell processes, some RPs are also locally translated to replace old ribosome parts and to set ribosome heterogeneity translating subsets of mRNAs.*

III.a.iii. RNA sequences are recognized before translation

The protein synthesis involves several steps and multiple partners (**Fig. 11**) (Browning and Bailey-Serres, 2015). The mRNA is recruited by complexes of proteins recognizing the cap at the 5' end: the eukaryotic Initiation Factor 4F (eIF4F) cap-binding complex, and the poly-Adenosine (poly-A) tail at the 3' end by the Poly A Binding Protein (PABP). The interaction of these complexes with the mRNA allows the recruitment of the 40 S subunit along with other initiation factors, the Multi-Factor Complex (MFC) and the first tRNA carrying the first methionine amino acid. The 40 S subunit can then scan the 5'UTR of the mRNA to find the AUG start codon from 5' to 3'. Once at the start position, the 60 S subunit binds the mRNA-40 S complex to form the 80 S and starts with the translation of the mRNA coding sequence (CDS). Interestingly, RACK1 regulates the formation of the 80 S complex. EIF6 is an initiation factor at 60 S surface blocking the association with the 40 S. It has been proposed that RACK1 binds to a kinase, PKC, to phosphorylate eIF6 and release it from the 60 S allowing the 80 S formation (Gallo and Manfrini, 2015; Rollins et al., 2019). Then, the elongation process can occur: tRNA with a given amino acid can enter the A site of the ribosome. If the tRNA anticodon matches the mRNA codon, a peptide bond will be formed with the previous amino acid in the P site. The tRNA with the nascent chain will translocate from the A to the P site, and the previous empty tRNA from the P to the E site for its exit. When a STOP codon is recognized by release factors (RFs), the peptide is released for further post-translational modifications and the ribosomal subunits are dissociated to be reused or degraded. On a given mRNA, multiple ribosomes can participate to its translation at the same time forming a polysome. However, we have seen earlier that monosomes, only one ribosome on the mRNA, can translate too (Biever et al., 2020).

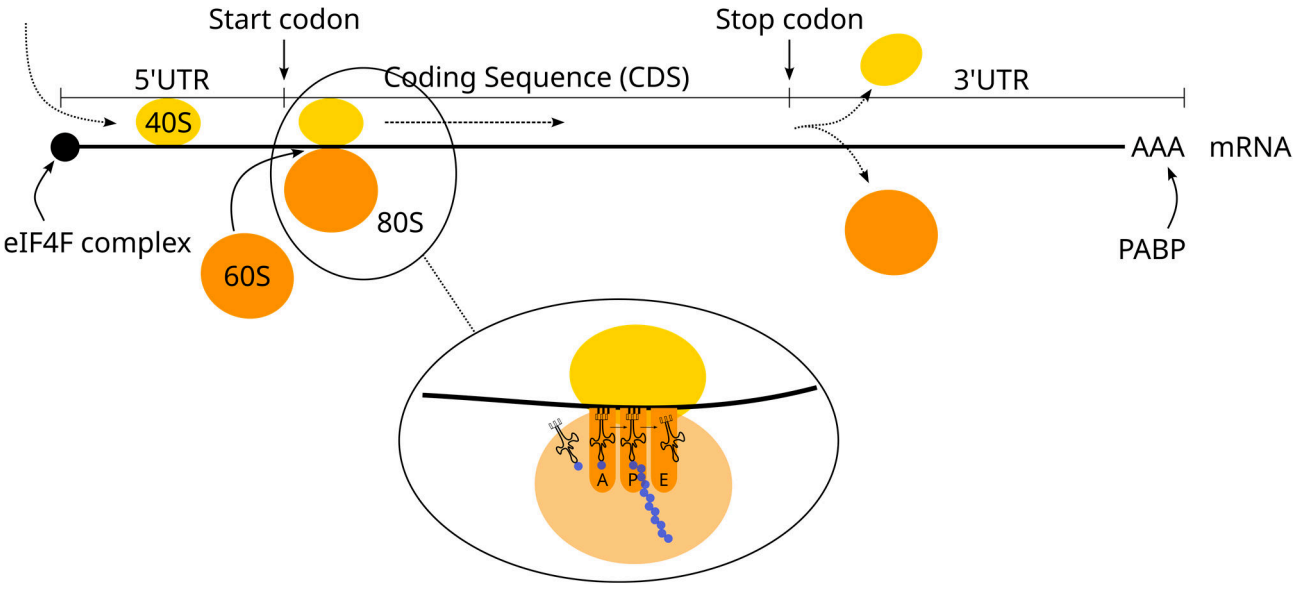

Figure 11. ***Eukaryotic cytoplasmic translation.*** *5' cap and 3' polyA tail are recognized by eIF4F complex and PABP respectively to recruit further regulators. The 40S ribosomal subunit scans the*

5'UTR of the mRNA to reach the start codon where the 60S assemble to form the 80S. While translating the mRNA CDS, tRNA carrying amino acids enter in the A site of the ribosome and match their anti-codon with the mRNA codon. When hybridized, a peptide bond is formed with the nascent chain in the P site and translocate in this site. The empty tRNA exit the ribosome via the E site. At the stop codon, the 80S is disassemble to be recycled or degraded.

Other translation mechanisms exist in eukaryotes. It is the case of the cap-independent Internal Ribosome Entry Site (IRES) translation. The recognition of the beginning of the mRNA does not rely on the cap but on a secondary structure in the 5'UTR, called IRES, recognized by IRES trans-acting factors (ITAFs) (Komar and Hatzoglou, 2011). Although mostly studied in viral RNA, IRES are also found in some mRNA in eukaryotic cells. Interestingly, RACK1 is used by viruses to enhance the translation of their viral RNA. It is the case for the hepatitis C virus (Majzoub et al., 2014) and the poliovirus (LaFontaine et al., 2020) which contain 2 IRES.

III.b) Translation is regulated by RNAs and proteins

Translation is regulated at all steps in the mRNA life. Once transcribed, the mRNA is recruited by proteins involve in the regulation of its half-life (degradation / stabilization balance). The mRNA is packed in RNA granules and transported to reach a specific destination. The mRNA is stored until its translation. The mRNA is translated at a specific rate under specific cues. The mRNA is degraded under specific conditions.

III.b.i. CIS-acting elements involve sequences in the RNA

Translation regulation in CIS means that the regulation comes from inside the RNA. It involves specific mRNA sequences, mostly in the UTRs (**Fig. 12, top**). These sequences include motifs and 2D conformations (loops, hairpin …) recognized by trans-acting elements to stabilize and transport the mRNAs. As the 5'UTR is the sequence scanned by the ribosome, it is involved mostly in the translation rate whereas the 3'UTR, after the coding sequence, regulates the stability and localization of the mRNA but also its translation efficiency. For instance, localization of the β-*actin* mRNA is Netrin1-dependent in growth cones *in vitro*, and relies on its 3'UTR. Deletion of the 3'UTR does not induce its localization upon Netrin1 application (Leung et al., 2018). The β-*actin* mRNA 3'UTR contains a zipcode sequence of 54 nucleotide (nt) forming a stem-loop including a critical sequence ACACCC recognized by the Zipcode Binding Protein 1 (ZBP1) (Andreassi and Riccio, 2009). In oligodendrocytes, the 3'UTR of *Mbp* coding for a myelin protein MBP mediates *Mpb* localization in the myelin sheaths and regulate its translation upon BDNF and PTZ application in a zebrafish model (Torvund-Jensen et al., 2018). They used the Dendra2 system to investigate the 3'UTR of *mbp*. No specific sequence was found crucial for this mRNA metabolism but rather multiple sequences across

the mRNA. In astrocytes, the lab of Joseph D. Dougherty determined that a Quaking Response Element (QRE) was present in almost 1/3 rd of the 3'UTR of transcripts present in PAPs (Sakers et al., 2017). QRE is composed of 2 Quaking Binding Motifs (QBM) recognized by the RBP Quaking (QKI). They showed that this QRE controls transport and translation efficiency of the *Sparc* mRNA (Sakers et al., 2017). Interestingly, the QRE motif is also found in the *Mbp* 3'UTR mRNA (Sakers et al., 2021). The team of Christine E. Holt found translating mRNA coding for ribosomal proteins in the axons of retinal ganglion cells of the frog embryo (Shigeoka et al., 2019). In 70% of them, a motif, a *cis-element upstream of the initiation codon* (CUIC), was found in 5'UTR and contained YYYYTTYC (Y for pyrimidine nucleotide C or T).

The team of Erin Schuman investigated the global 3'UTR features of mRNAs in the neuropil versus the somata of neurons in the hippocampus by microdissection and 3'end sequencing (Tushev et al., 2018). They found that neuron-enriched mRNAs had longer 3'UTR in the neuropil (neuronal processes) than in the somata (**Fig. 12, bottom**). In addition, these mRNAs had multiple 3'UTRs isoforms compared to non-enriched mRNAs. For instance, the CaMK2a mRNA was identified with 3 different 3'UTR isoforms: long, middle and short. With GFP reporters, the long UTR was found to localize GFP at distance from the cell body whereas the short one restricted it near the nucleus. Importantly, long 3'UTRs had longer half-lives certainly due to the increase of factor binding to stabilize it. Neuronal activity shortened 3'UTR certainly to allow the translation and to remove inhibiting factors. RNA isoforms can be created by alternative polyadenylation (APA) consisting in upstream or downstream polyadenylation shortening or lengthening the 3'UTR (Arora et al., 2022). The *Bdnf* mRNA has 2 sites of APA in its 3'UTR. It has been shown that the long isoform is imported in the dendrite whereas the short is restricted to the soma. A disruption in the long isoform leads to BDNF-induced protein mis-localization, disruption of dendritic spine morphology and impairment of plasticity (An et al., 2008).

III.b.ii. TRANS-acting elements involve multiple proteins

RNA-binding proteins (RBP) recognize RNA structures and sequences.

As RBP-binding motifs and RNA secondary structures, RBPs are often binding 5' and 3'UTRs (**Fig. 12, top**). RBPs have RNA-binding domains interacting with specific nucleotide sequences or to secondary structures. For example, RNA Recognition Motifs (RRM) or K-homology (KH) domains recognize single stranded RNA and the SAM domain recognizes stem loops (Re et al., 2014).

The Fragile-X Mental Retardation protein (FMRP) is one of the most studied RBP in the CNS. Loss of FMRP causes Fragile X Syndrome (FXS), a genetic disorder of mental retardation characterized by an autistic spectrum, seizures and dendritic spines with aberrant morphology. With a KH RNA-

binding domain, FMRP has been shown to associate with more than 400 mRNAs in the neuronal dendrites of the hippocampic CA1 region by Cross-Linking Immunoprecipitation (CLIP) of FMRP (Hale et al., 2021). Interestingly, FMRP represses the translation of mRNAs linked to synaptic function (Darnell et al., 2011). A loss in FMRP destabilizes synaptic proteins leading to disruption in spine morphology, autism behavior and FXS. Furthermore, FMRP has been shown to regulate mRNA transport in neurons upon synaptic activation (Dictenberg et al., 2008). In FMRP KO mice, FMRP-targeted mRNAs displayed less dynamics upon metabotropic Glutamate Receptors (mGluRs) activation mediated by kinesin-dependent transport (see **Box 3**). FMRP is also expressed in astrocytes and has been shown to control the GLT1 protein level (Higashimori et al., 2016). We have seen previously that FMRP was associated with mRNAs in radial glia and was controlling their transport in the processes (Pilaz et al., 2016).

Box 3: How does the mRNA know where to stop in the process?

One puzzling question is how does an mRNA transported along the microtubule know at which place it should wait to trigger its translation? No answer has been given yet but scientists formulated models for neurons in which synapses are tagged. This tag anchors the mRNAs to the desired spine, which has a high activity for instance. Another model, formulated by Michael Doyle and Michael A Kiebler in 2011, describes the scanning of several spines by the mRNAs with a bidirectional transport. This Sushi-Belt model allows an active spine to stop the transport of an mRNA for its local translation.

The amyotrophic lateral sclerosis (ALS) is a neurodegenerative disease resulting in the progressive loss of motor neurons that controls voluntary muscles. Familial or genetic causes represent 5 to 10% of ALS cases and are linked to genes coding for Fused Sarcoma (FUS) and TAR DNA-binding protein 43 (TARDBP or TDP43) which are 2 RBPs. In ALS, mutated TDP-43 and FUS are misfolded and create aggregates in the cell leading to its death. TDP43 has 2 RRM and FUS has 1 RRM and 1 zinc-finger motif to bind RNAs. Both proteins are involved in the whole life of the mRNA from its transcription and splicing to its transport and local translation (Lagier-Tourenne et al., 2010). It was hypothesized that mis-regulation of transport and translation in neurons by TDP-43 mutations would lead to neurodegeneration. TDP-43 was found to regulate the transport of ribosomal proteins (RP) mRNAs and thus to regulate local translation in axons of cortical neurons (Nagano et al., 2020). TDP-43 binds to their 5'UTR on the Terminal OligoPyrimidine (TOP) motif. Importantly, neuronal processes from ALS patients had reduced RP-coding mRNAs. TDP-43 is also expressed in astrocytes and appears as inclusions in ALS. Astrocytes deficits due to TDP-43 misfolding could lead to motor neuron degeneration (Izrael et al., 2020), however, no studies have yet investigated the translation regulation of TDP-43 in astrocytes.

To date, a vast number of RBPs have been studied in neurons especially in the context of neurodegenerative diseases (De Conti et al., 2017) but only few of them have been investigated in astrocytes (Mazaré et al., 2021).

Translation machinery-interacting proteins regulate translation.

Another level of translation regulation concerns the factors involved in the initiation and elongation of translation as well as ribosomal proteins themselves (**Fig. 12, top**). The initiation factor eIF2 is carrying the starting methionine amino acid when active. Phosphorylation of eIF2 leads to its inactivation and to protein synthesis impairment (Kapur et al., 2017). Interestingly, it was shown that eIF2 phosphorylation impaired protein synthesis-mediated memory formation and that its dephosphorylation induced memory consolidation (Sharma et al., 2020). Another initiation factor, eIF4E-BP (4E-BP) is crucial for the assembly of the cap-dependent complex. Mammalian Target of Rapamycin Complex (mTORC) phosphorylates this complex for its assembly (Kapur et al., 2017). It was shown that mTORC-dependent phosphorylation of 4E-BP2 regulates epileptogenesis in mice (Sharma et al., 2021). Another target of mTORC is the ribosomal protein RPS6. Phosphorylation of RPS6 (p-RPS6) has been used to evaluate neuronal activity but its molecular impact remains elusive. Recent studies showed that p-RPS6, rather than playing a role in the global translation rate, regulates the translation of subsets of mRNAs, for instance mitochondrial protein encoding mRNAs in the Nucleus Accumbens (Puighermanal et al., 2017) and short coding sequence mRNAs (Bohlen et al., 2021). Finally, RACK1, a ribosomal protein located at the small subunit of ribosomes, has been shown to regulate translation by promoting the 80 S formation, recruiting specific mRNAs or participating in RNA and nascent chains quality control (Gallo and Manfrini, 2015). RACK1 roles will be detailed in the next section.

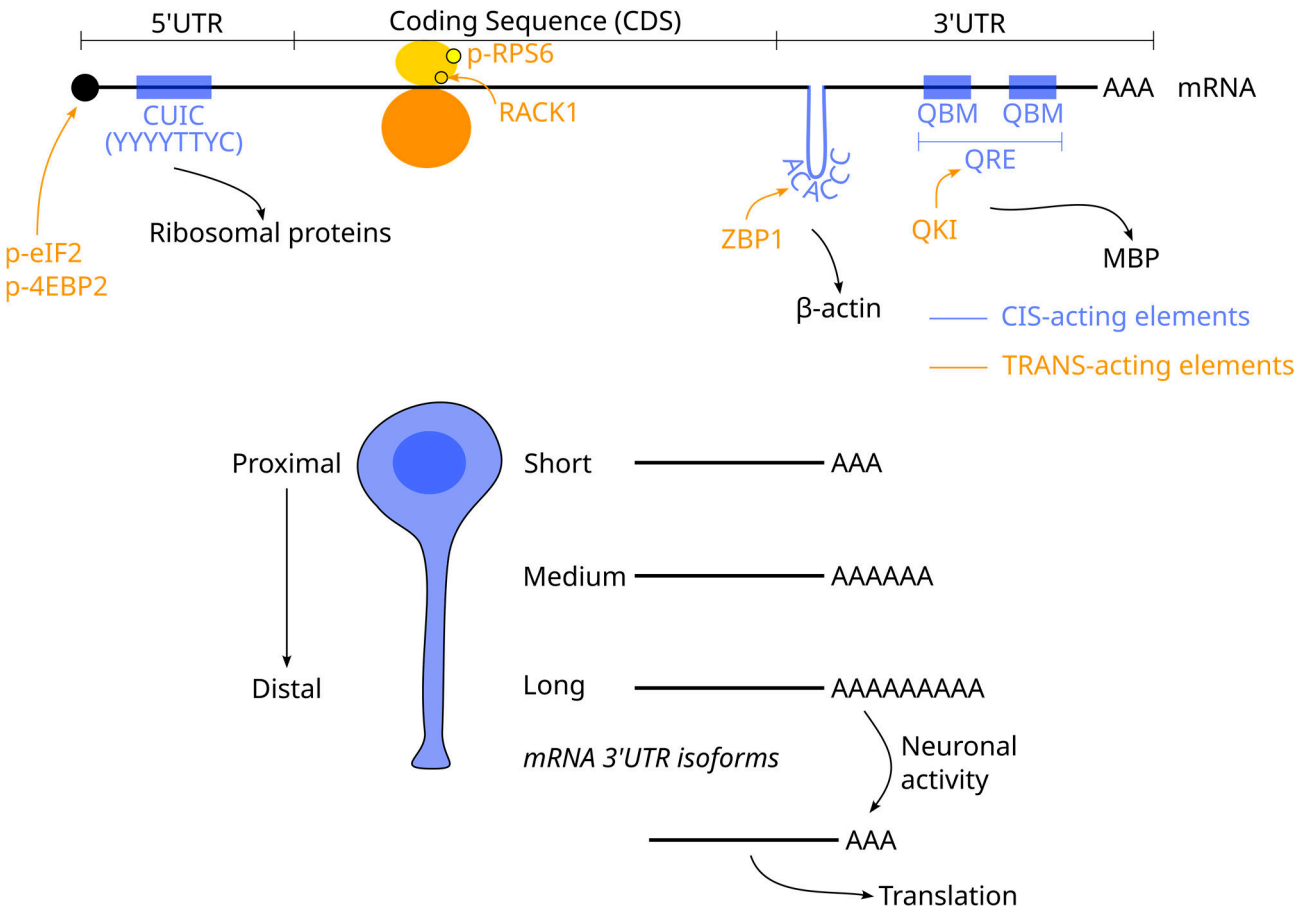

Figure 12. ***Translation is regulated by CIS and TRANS-acting elements. (Top)*** *CIS-acting elements can be sequence motifs such as CUIC and QBM or secondary structures such as loops. TRANS-acting elements can be phosphorylated initiation factors (p-eIF2 and p-4EBP2), RBP (ZBP1, QKI), phosphorylated RPS6 (p-RPS6) and RACK1.* ***(Bottom)*** *Alternative polyadenylation regulates 3'UTR length. 3'UTR length mediates mRNAs location with short isoforms in the soma and long isoforms in more distal parts. Upon neuronal activity, 3'UTR is shortened to remove inhibitory elements and allow local translation.*

Cytoskeleton proteins regulate RNA localization.

RNA distribution in the cell, especially in neurons, is allowed by the cytoskeleton and molecular motors (**Fig. 13**). Specifically, microtubules and actin filaments are the frames of RNA localization and dynamics are allowed by molecular motors: kinesins, dyneins and myosins (Buxbaum et al., 2015). Interestingly, the link between neuronal activity and mRNA distribution is mediated by RBPs. For instance, FMRP has been shown to mediate mRNA transport after mGluR stimulation in a kinesin-dependent manner (Dictenberg et al., 2008). In FMRP KO mice, mRNA transport mediated by neuronal activity was abolished. In addition, FMRP has been associated with mRNA transport in radial glia (Pilaz et al., 2016). FMRP has been shown to interact with kinesins such as KIF3C in neurons and to make the link between the mRNA and microtubules (Davidovic et al., 2007). Kinesins 'walk' toward the '+' end of microtubules corresponding to an anterograde transport. On the contrary,

dyneins go retrogradely toward the '-' end and are also known to carry cargoes such as mRNAs (Reck-Peterson et al., 2018). *Mbp* mRNA has been shown to be transported to myelin sheaths in oligodendrocytes by kinesins but also by dyneins (Herbert et al., 2017). Curiously, dynein/dynactin complex transports *Mbp* mRNA anterogradely toward the sheaths in zebrafish and mammalian oligodendrocytes in culture. LIS1, a dynein cofactor, has been shown to be locally translated at '+' end microtubules upon Nerve Growth Factor (NGF) stimulation in axons of cultured neurons (Villarin et al., 2016). Thus, mRNA can be transported to specific areas of the cell thanks to the local translation of molecular motor cofactors. Actin filaments are also prone to interact with mRNAs. F-actin is a type of actin forming a dynamic network just below the membrane to regulate neuronal spine morphology for instance. F-actin can act as a storage anchor for mRNAs for them to wait translation signals. Stabilizing or destabilizing this network in spines led to anchorage loss of β-*actin* mRNA in spines (Yoon et al., 2016). Local translation of β-actin feeds this actin network to anchor more mRNAs. Molecular motors on actin are myosins and make the link between the actin and mRNAs. Myosin-Va (Myo5a) has been shown to anchor mRNAs in fibroblast and to release them for translation in a calcium-dependent manner (Canclini et al., 2020). In neurons, Myo5a was found to regulate mRNA dynamics into dendritic spines as its silencing impairs accumulation of some mRNAs in this compartment (Yoshimura et al., 2006).

III.b.iii. RNA granules transport and compact RNAs and proteins

mRNAs do not travel alone in the cell processes but are complexed with proteins to form ribonucleoparticles (RNP). Even more complex, multiple RNPs travel together to form granules (**Fig. 13**). Granules comprises RNAs, RBPs, ribosomal subunit 40 S (not 60 S) and enzymes (Khandjian et al., 2015). Granules, as RNP condensates, enable RNA protection to be transported over long distances on microtubules and to be docked at the final destination and wait for local translation signals. Granules allow the transport of a large amount of RNAs at the same distal place.

RNA granules are heterogeneous and can be classified in different classes: 1) Processing bodies (P-bodies) are translation repression sites that transport RNAs in physiological conditions; 2) Stress Granules (SG) are P-bodies that modified their composition to repress other mRNAs to focus on stress-response genes. They are not mobile; 3) Neuronal granules are specialized granules transporting mRNAs along the cell processes. They contain RNAs, RBP and ribosomes. Interestingly, granules can exchange proteins and RNAs. Under physiological conditions stalled RNAs are stored in P-bodies. Under stress conditions, stalled RNAs and P-bodies are forming stress granules with slightly different compositions (Kedersha et al., 2005).

Granules are considered membrane-less organelles as they have a defined composition and density. These "droplets" of RNA and proteins are formed by liquid-liquid phase separation due to these strong

composition differences, like the nucleolus in the nucleus for instance (Langdon and Gladfelter, 2018). These structures are permitted by the RBP-RNA, RBP-RBP and RNA-RNA interactions. Interestingly, if RNAs are absent from the granules, proteins aggregate like TDP43 in ALS for instance (Huang et al., 2013).

When an environmental cue such as neuronal activity occurs, the granule decondensates by post-translational modifications and let mRNAs to be translated (Khandjian et al., 2015). For instance, synaptic plasticity induces granules de-condensation and the exit of synaptic proteins-coding mRNAs in polysomes for their translation (Krichevsky and Kosik, 2001).

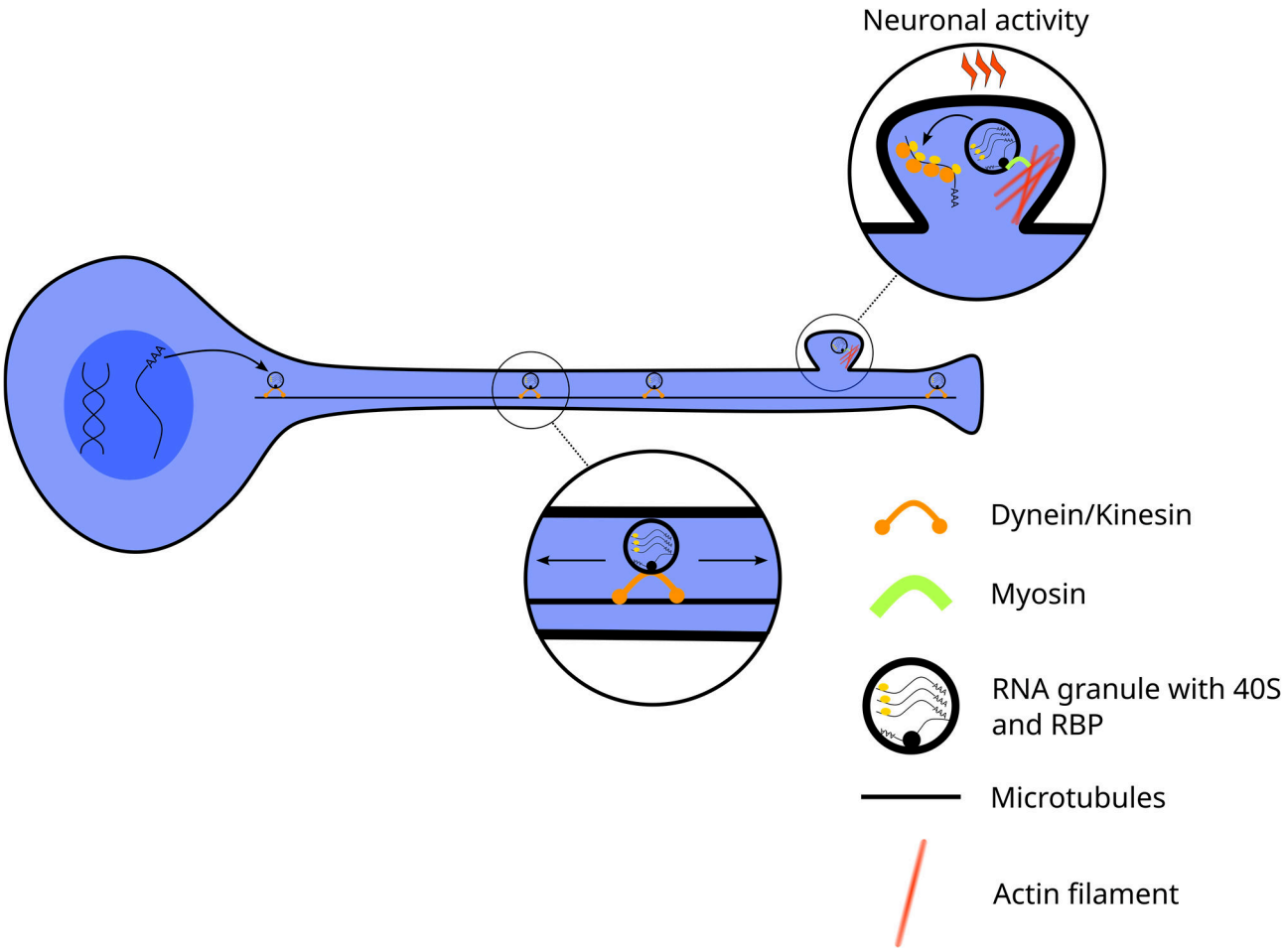

Figure 13. ***mRNAs are compacted into granules and transported along the cytoskeleton.*** *RNAs with RPs and RBPs are compacted into RNA granules. They are docked on molecular motors, dyneins and kinesins that transport them along the cell processes via the microtubule cytoskeleton network. RNA granules can be stored in particular places on the actin cytoskeleton via myosins and wait for cues such as neuronal activity to decondensate and induce local translation.*

III.b.iv. Signaling pathways regulate translation in development, plasticity and diseases

Axonal branching is a key process for the neuron to find the right path during development. Guidance cues are released and sensed by the growth cone of the axon to be targeted at the right place. Netrin-1 and BDNF, for instance, bind DCC and TrkB receptors respectively and activate the protein kinase Src. Src will phosphorylate the RBP ZBP1 releasing its mRNA *β-actin* into the ribosomes to be translated. Newly synthetized actin filament will guide the axon toward the netrin-1 source (Agrawal and Welshhans, 2021; Lin and Holt, 2007).

Synaptic plasticity requires local protein synthesis in pre and post synaptic compartments. Long term depression (LTD), for instance, reduces the number of neurotransmitter receptors in dendrites for synapses that need less activity in a process mediated by metabotropic Glutamate Receptors (mGluR). Glutamate, an excitatory neurotransmitter, is released in the synaptic cleft and binds mGluR at the post synapse spine. MGluR activation leads to phosphorylation of the initiation factor eIF2α to promote translation. Among mRNAs translated in a phospho-eIF2α-dependent manner, oligophrenin1 helps the endocytosis and internalization of AMPA Receptors (AMPAR) reducing neurotransmitter receptor at the membrane (Di Prisco et al., 2014).

Local translation is also altered in neurological disorders. For instance, in a model of nerve injury (where the nerve is sectioned), mTOR is locally translated to activate further local translation. MTOR mRNA is transported by nucleolin to axons based on its 3' UTR. When the axon is injured, mTOR signaling locally translates its own mRNA to amplify local

Box 4: The local translation regulation curiosities

The nerve injury local translation regulation article emphasizes curious events :

1- Auto regulation of its own mRNA. Here mTOR signaling pathways increase mTOR mRNA translation in a feed-forward loop to amplify the translation rates. It has been reported multiple levels of translation rates feeding each other in a time-dependent manner.

2- Retrograde transport of transcription factors. As seen in Box 1, axons can be very long and transport could take several minutes to reach the cell body for the axon tip. Why not locally translate cell survival molecules ?

3- Nucleus proteins locally translated. As for ribosomal protein, here, nucleolin, is associated with chromatin in the nucleolus. However it has been found to be an RBP as well. Several DNA binding proteins are also found away from the nucleus. It can be explained by the non-canonical functions of these proteins that are yet to determined.

translation. Transcription factors, such as STAT3, are also locally translated and are retrogradely transported to the cell body and promotes cell-survival genes transcription (Koley et al., 2019; Terenzio et al., 2018) (see **Box 4**).

In Amyotrophic Lateral Sclerosis (ALS), a neurodegenerative disease, RBPs TDP43 and FUS form aggregates and their functions are altered. In consequence, transport of RNA and granules are perturbed leading to cytoskeletal deregulation and stress granules formation (Gamarra et al., 2021).

Finally, in Alzheimer's disease, another neurodegenerative disease, Aβ oligomers are found in the extracellular space and can form Aβ plaques in the brain. Aβ was found to trigger local translation in axons of neurons and in particular the translation of a transcription factor ATF4 (see **Box 4, point 2**). ATF4 is retrogradely transported to the neuronal cell body to promote cell death mediated gene transcription (Baleriola et al., 2014; Gamarra et al., 2021).

III.b.v. Other translation regulation mechanisms involve microRNAs (miRNA), codon usage and m^{6}A modifications

Other levels of translation regulation exist and will be briefly depicted here.

RNA levels are dependent on miRNA activity. MiRNAs are small non-coding RNAs complementary to a specific sequence of specific mRNAs to repress their translation or to degrade them. The RNA-induced silencing complex (RISC), containing AGO proteins, induces translation repression when miRNA recognize an mRNA. Therefore, miRNA local concentration is important in the regulation of local translation. Indeed, neuronal activity has been shown to induce the degradation of RISC and to destabilize miRNAs leading to a de-repression of the mRNA that can be locally translated (Thomas et al., 2018). miRNA participate also in synaptic plasticity. During LTP, more GABA Receptors (GABAR) are locally translated in dendrites because of miR376C transcriptional repression (Rajgor et al., 2020). Interestingly, miRNAs can be transferred from neurons to astrocytes to regulate astrocyte local proteome. For instance, miR-124a is transferred from neuron to astrocyte processes via exosomes and regulate GLT1 expression (Morel et al., 2013).

Translation efficiency can be affected by codon usage bias. The redundancy of the genetic code allows multiple codons for the same amino acid. However, depending on the protein, the cell or the species, mRNA will have a preference for a specific codon for a given amino acid: it is the codon usage bias (Liu, 2020). This bias depends on the tRNA abundance, the GC content, the environment and other factors. It determines RNA level homeostasis, protein folding, ribosome speed regulation and secondary structure formation. Optimal codon will have fast reading whereas non-optimal codon will have slow reading. For instance, ribosomes reading optimal codon because tRNA availability is high will be fast. On the contrary, the passage over non-optimal codons because tRNAs are rare, will slow

down the ribosome. Optimal codons induce mRNA stability and longer half-lives. In a recent study, authors described an RBP, FMRP, as a sensor of these optimal codon by an unknown mechanism to stabilize its mRNA targets (Shu et al., 2020). Indeed, in FMRP KO, RNAs have shorter half-lives and the link between optimal codon and stability was disrupted.

Finally, post-transcriptional modification of RNAs can regulate translation, for instance, the methylation of adenosine, N^6-Methyladenosine (m^6A). M^6A modifications are reversible and mediated by methyltransferase and demethylase and can be recognized by RBP such as the YTH family. A study showed that a demethylase, Fat mass and obesity-associated protein (FTO), was locally translated in neuronal axons to modulate m^6A modifications on *Gap43* mRNA resulting in its local translation to promote axon elongation (Yu et al., 2018).

III.b.vi. In astrocytes, mechanisms of translation are not understood

As shown in this section, most work on local translation regulation has been performed in neurons. In fact, very little is known about translation mechanisms in astrocytes. Some RBPs have been characterized in this cell type but not all in the context of translation. In a review we recently published (Mazaré et al., 2021), we describe, among others, the sparse translation mechanisms we know in astrocytes.

I already described FMRP in radial glial cells, astrocytes precursors, as an mRNA transporter modulator. FMRP has also been involved in the GLT1 protein level, an astrocytic-specific marker, regulation to control neuronal excitability (Higashimori et al., 2016).

I also described Quaking as an RBP expressed in astrocytes to regulate Quaking Recognition Element (QRE)-containing mRNAs such as *Gfap* and *Sparc* (Radomska et al., 2013; Sakers et al., 2020). Recently, quaking has been shown to be determinant in the glial differentiation in neural stem cells (NSC) by upregulating astrocytes and oligodendrocytes genes (Takeuchi et al., 2020).

Human antigen R (HuR) binds to AU-rich elements and stabilizes RNAs. Interestingly, HuR has been shown *in vitro* to control *tardbp* and *fus* translation by binding to their 3'UTR. These 2 mRNAs code for 2 other RBPs TDP43 and FUS (Lu et al., 2014). It links potentially HuR with ALS but also highlight a complex translation regulation with RBP regulating other RBPs.

Another RBP, the cytoplasmic polyadenylation element binding protein 1 (CPEB1) regulates the 3'UTR of mRNAs specifically the polyA tail. A study showed that CPEB1 could control the polyA tail length in a time-of-day dependent manner of mRNAs in PAPs (Gerstner et al., 2012). It reveals that circadian rhythm could control translational levels in astrocytes.

Finally, KH type-splicing regulatory protein (KSRP) destabilizes ARE-containing mRNAs such as cytokines to mediate inflammatory responses in cultured astrocytes (Li et al., 2012).

PART III summary :

- Ribosomes have 2 subunits with 79 RPs and 4 rRNA and assemble in the nucleus. Some RPs are also locally translated to integrate or replace RP in distal ribosomes
- Translation is tightly regulated by CIS- (RNA sequences and structure) and TRANS-acting elements (RBP, RPs, Factors and cytoskeleton)
- RNAs are transported as RNA granules in cell processes via the cytoskeleton
- Signaling pathways and environmental cues trigger local translation via granule decondensation and RBP signaling
- Regulation of translation in astrocytes is not understood

IV. Receptor for activated C kinase 1 (RACK1) is a multifaceted protein involved in translation regulation

RACK1 is one of the translation regulators studied in this thesis. RACK1 stands for Receptor of activated C kinase 1 because it has been first described as a protein kinase C (PKC) partner. RACK1 is involved in multiple cell processes including translation.

IV.a) RACK1 structure allows multiple protein interactions

Gnb2l1 is the gene coding for RACK1, a 36 kiloDalton (kDa) highly conserved protein found in all eukaryote cells. RACK1 structure is a propeller with 7 blades represented by 7 tryptophan-aspartate (WD) repeats (Adams et al., 2011). These blades allows RACK1 to interact with several proteins at the same time including itself to form a hub of signaling pathways (**Fig. 14, Top**). These interactions allow the connection between membrane receptors, signaling proteins, the ribosomes and the cytoskeleton. For instance, when PKC becomes active, it can bind RACK1 to stabilize its enzymatic property and to be shuttled to a specific cell place such as the membrane to phosphorylate its substrate (Adams et al., 2011). RACK1 can also interact with G-protein coupled receptors (GPCR). Once the receptors are triggered, RACK1 is released and shuttled to the nucleus to act on BDNF transcription for instance (He et al., 2010).

RACK1 partners are multiple : kinases such as PKC and Src; translation factors such as eIF6; cytoskeleton-associated proteins such as β-actin and Spectrin; adhesion molecules such as integrins; receptors such as NMDAR and Acetylcholinesterase-Receptors (AchE-R); viral proteins (Sklan et al., 2006).

An interesting property of RACK1 is its capacity to associate with RNPs (Angenstein et al., 2002) as a core component of the 40 S ribosomal subunit (Sengupta et al., 2004). At the ribosomal level, RACK1 can thus link the membrane, signaling pathways, receptors and the cytoskeleton to the translational machinery.

IV.b) RACK1 is a signaling hub and interacts with ribosomes

IV.b.i. RACK1 is involved in cell physiology

RACK1 knock-out in mice is lethal at gastrulation stage highlighting a mandatory and developmental role for RACK1 (Volta et al., 2013). Interestingly, in the yeast *S. cerevisiae*, the knock-out of the

RACK1 orthologous, Asc1, is not lethal but displays abnormal responses to the environment (Gerbasi et al., 2004).

Given the high number of interactors, RACK1 is involved in several fundamental cell processes including cell division, cell migration and adhesion, and development for instance. RACK1 is controlling the G0/G1 phase of the cell cycle by interacting with the G1 checkpoint in immortalized cell culture. Indeed, RACK1 inhibits Src activity that cannot activate the cell cycle regulators. Overexpression of RACK1 leads to cell cycle arrest whereas RACK1 knock-down accelerates it (Mamidipudi et al., 2004). In addition, RACK1 interacts with Aurora-A to mediate its phosphorylation causing G2 to mitosis progression (Shen et al., 2019).

RACK1 can localize signaling molecules where it needs to be. For instance, RACK1 can bind integrins and bring PKC and Src to allow integrin downstream signaling mediating cell migration (Buensuceso et al., 2001). In glioma cells, depletion of RACK1 lead to decreased in PKC-induced cell adhesion and migration (Besson et al., 2002). RACK1 can bind to focal adhesion kinase (FAK), hotspots of cell adhesion, and bring enzymes such as the phosphodiesterase PDE4D5 to degrade the extracellular matrix (ECM) (Serrels et al., 2010). This pathway is used by cancer cells to invade tissues. In line with cell adhesion and movement, RACK1 is also involved in development, for instance, the closure of the neural tube in the frog *Xenopus*. PTK7, a planar cell polarity regulator, has been shown to bind RACK1 and mediate dishevelled (DSH) membrane localization through the recruitment of PKC necessary for the CNS development (Wehner et al., 2011).

IV.b.ii. RACK1 regulates translation in interaction with ribosomes

As described above, RACK1 is also part of the 40 S ribosomal subunit and is part of mRNP. The roles shown above can be attributed to the free form of RACK1. However some studies showed that ribosomal RACK1 can also act in cellular adhesion and migration. In addition, RACK1 has been shown to go on and off the ribosome (Johnson et al., 2019) and that it can be an adaptative parameter for the ribosome to changing environment (Fusco et al., 2021). The ribosomal RACK1 has been shown to regulate several aspects of translation (**Fig. 14, bottom**).

RACK1 associates specifically with subtypes of RNAs

RACK1 is not an RBP, as it does not have an RNA binding domain. If RACK1 would be a “basic” ribosomal protein, in all ribosomes, in all compartments of the cell, it would not be associated with specific RNAs. On the contrary, if RACK1 is not a mandatory ribosomal protein but rather adapts to signaling cues and acts with multiple factors, it is regulating specifically the translation of some mRNAs in specific contexts (**Fig. 14, bottom A**).

In vitro, in HeLa cells, the team of Stefano Biffo investigated the mRNA specificity of RACK1. With luciferase reporter of different 5'UTR and RACK1 rescue in RACK1 shRNA cells, they showed that RACK1 was more associated with IRES as previously shown but also strongly with capped RNA, TOP mRNAs and the polyA tail (Gallo et al., 2018). Curiously, RACK1 shRNA cells have decreased capped and TOP mRNA translation but no changes for the IRES reporter. They also found that RACK1 was bound to eIF4E, an important translation initiation factor. Next they used a construct where RACK1 is mutated and cannot bind the ribosome anymore (RACK1 R36D K38E (Coyle et al., 2009)) and explored the free RACK1 functions. MutRACK1 cells diplayed deficits in cell cycle progression and a global inhibition of translation.

RACK1 regulates the formation of the 80 S ribosome

The 40 S subunit, containing RACK1, scans the 5'UTR of mRNAs to the start codon. The 60 S subunit is then recruited to form the 80 S and translate mRNAs into proteins. The initiation factor eIF6 located on the 60 S represses its association with the 40 S. RACK1 has been shown to recruit PKC on the ribosome to phosphorylate eIF6 and allows its dissociation from the 60 S to let the 80 S formation (**Fig. 14, bottom C**) (Ceci et al., 2003).

RACK1 senses stalling ribosomes and regulate abberant mRNAs and nascent chains

Stalled ribosomes occur when the ribosome block at specific sequences of the mRNA, especially at polyA tracts coding for poly-lysine. It is the coincidence of polyA in the mRNA and poly-lysine in the nascent chain that slows down the ribosome until its stalling (Yip and Shao, 2021). Polysomes have multiple ribosomes translating the same mRNA. Therefore, if a ribosome stall at one point, the following one will collide, in particular at the 40 S part which is sensed by RACK1 (**Fig. 14, bottom D**) (Yip and Shao, 2021). In particular, RACK1 mediates the Ribosome Quality Control (RQC) to ubiquitinylate the stalled ribosome to be adressed to the proteasome (Sundaramoorthy et al., 2017). RACK1 othologous in yeast, Asc1, has been shown to facilitate the degradation of the aberrant mRNA (Ikeuchi and Inada, 2016) as well as the elimination of the premature nascent chain by ubiquitin ligase (Matsuda et al., 2014). However, stalled ribosomes can also have physiological roles such as the targeting to the ER by ufmylation by recruiting UFL1 (Xu and Barna, 2020). One can hypothesize also that stalled ribosomes can be a mean to pause translation to be transported along the cell processes even though the full 80 S ribosome has not been seen present in RNA granules.

Finally, in response to stress, RACK1 mediates the degradation of misfolded nascent chains by recruitment another partner at the ribosome, JNK, a kinase that phosphorylate an elongation factor eEF1A2 to promote the polypeptide proteasome-mediated degradation (**Fig. 14, bottom B**) (Gandin et al., 2013).

RACK1 interacts with RBP to translate specific mRNAs

In the previous section we showed that the regulation of translation could involve RNA-binding proteins (RBP) carrying specific subsets of RNAs. RACK1 has been shown to interact and recruit RBPs at the ribosome along with kinases to mediate the phosphorylation of RBP and regulate translation of RBP-specific mRNAs (**Fig. 14, bottom E**). For instance, RACK1 interacts with ZBP1 in neurons. RACK1, located at the 40 S surface, recruits ZBP1 with its *β-actin* mRNA and recruits the Src kinase. Src phosphorylates ZBP1, which releases its mRNA in the ribosome to be translated. In physiology, BDNF triggers Src activation to translate β-actin via RACK1 (Ceci et al., 2012). TDP43, another RBP involved in RNA granule transport and translation, has been shown to be recruited at the ribosome by RACK1 in neuronal cultures (Russo et al., 2017). This interaction represses global translation and a ribosomal loss of RACK1 revert the phenomenom. In ALS, the recruitment of TDP43 by RACK1 could lead to cytoplasmic inclusions deleterious for the cell. Plasminogen activator inhibitor 1 RNA-binding protein (SERBP1) has been shown to interact with RACK1 by yeast 2-hybrid (Bolger, 2017). SERBP1 and Vigilin, 2 RBPs, associate with the dengue virus genome and with RACK1 from the host cell to facilitate the viral replication (Brugier et al., 2022). La-related protein 4B (LARP4B) and poly(A) binding protein 1 (PABPC1) have been shown to co-immunoprecipitate with RACK1 and to stimulate global mRNA synthesis (Schäffler et al., 2010). Finally, KSRP interacts with RACK1 in a cancer paradigm although not in the context of translation (Bae et al., 2021). Interestingly, SERBP1, TDP43, LARP4B and KSRP are expressed in astrocytes. The association between RACK1 and these RBPs could play a role in this cell.

RACK1 regulates translation of IRES-containing mRNAs

As shown in the previous section, the specificity of RACK1 translation regulation comes also from its capacity to be involved in IRES-mediated translation (**Fig. 14, bottom A**). IRES-containing mRNAs are often found in viruses (hepatitis, poliovirus, dengue virus for instance) that hijack RACK1 for their own replication. However, IRES are not only in viral RNAs but also in mammalian mRNAs translated in a 5’ cap-independent manner and might also confer a RACK1-sensitivity.

RACK1 regulates translation with miRNAs

RACK1 has been reported to interact with the miRNA biogenesis machinery in particular with the previously mentioned KSRP. RACK1 interacts also with the Argonaute (AGO) protein carrying the miRNA in the RISC complex (Speth and Laubinger, 2014). RACK1 could recruit the RISC complex to the ribosomes and promote the mRNA degradation. Interestingly, the lab of Joseph D. Dougherty recently hypothesized a role for miRNAs and RBPs interactions in the regulation of translation in neurons and glia (Koester and Dougherty, 2022). Since AGO proteins are expressed in neurons and

astrocytes, RACK1 could interact with the RISC machinery locally and regulate mRNA stability by modulating miRNA activity. RACK1 could be a link between environmental cues where a receptor is activated and trasduces the miRNA pathway at the translational machinery by interacting with RBP, AGO and the 40 S.

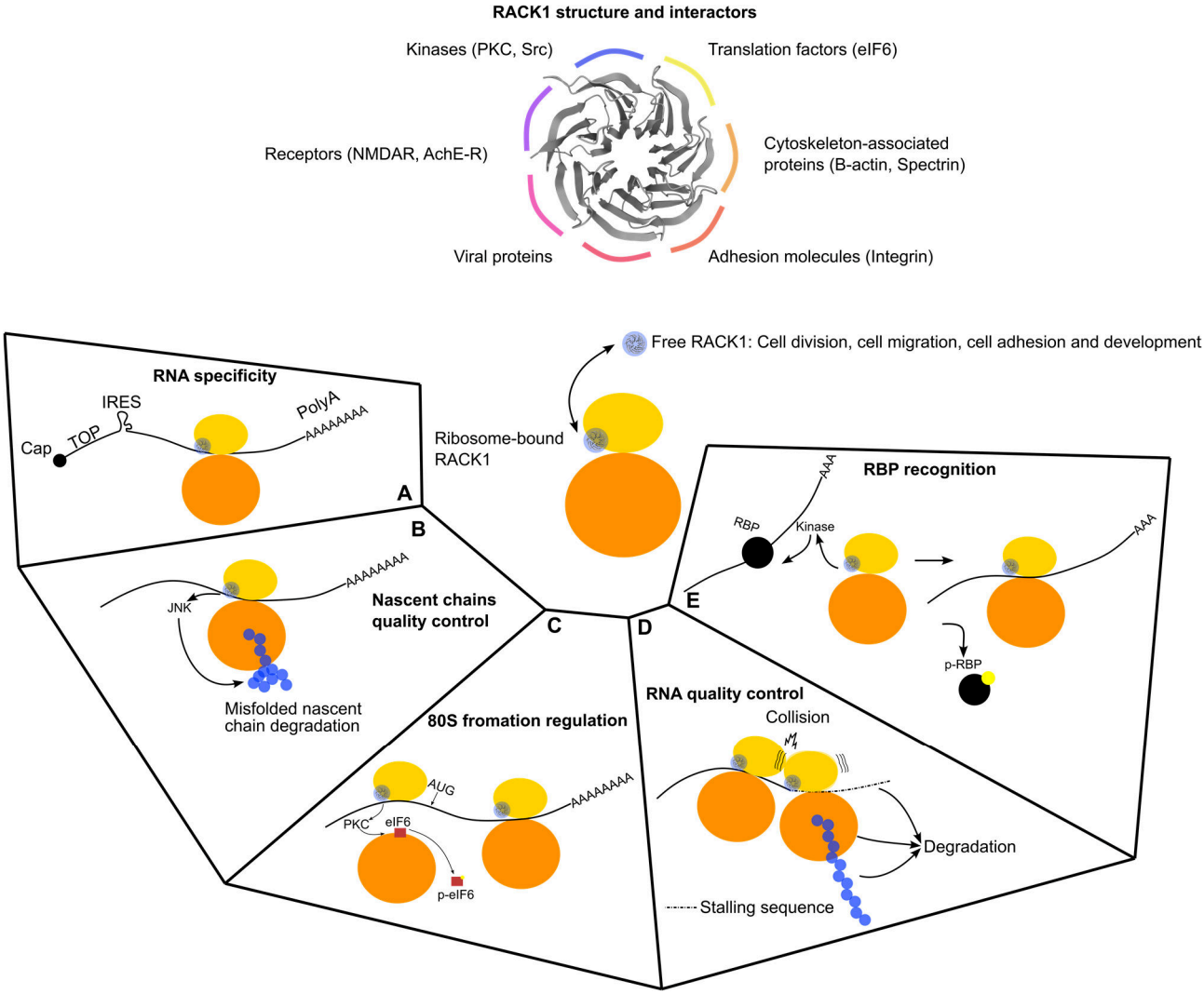

Figure 14. ***RACK1 structure allows multiples partners and has free and ribosome-bound functions.*** ***(Top)*** *Representation of RACK1 structure with its 7 blades which are interactions domains for kinases, translation factors, receptors, cytoskeleton-associated proteins, viral proteins and adhesion molecules.* ***(Bottom)*** *Free and ribosome-bound roles of RACK1. RACK1 can go on and off the ribosome. At the ribosome level, RACK1 regulates translation: (A) RACK1 has association preferences with capped, TOP, IRES, polyA mRNAs. (B) RACK1 recruits JNK kinase to mediate misfolding protein degradation. (C) RACK1 recruits PKC to phosphorylate eIF6 and promote the 80S formation. (D) RACK1 senses ribosome collision mediated by stalling sequences. RNA, ribosome and nascent chains are degraded. (E) RACK1 recognizes specific RBPs and recruits kinases to mediate RNA translation.*

IV.c) RACK1 in the CNS participates in development and synaptic plasticity

RACK1 is expressed throughout all the brain with slight higher levels in the hippocampus, the cortex and the cerebellum in the mouse (Ashique et al., 2006).

RACK1 has been shown to mediate calcium signaling by interacting with IP3R and enhancing its binding with IP3 in HEK cells (Patterson et al., 2004). Calcium signaling determines crucial functions in neurons for instance in synaptic plasticity. Recent findings showed the interaction between RACK1 and a neuronal calcium channel Cav3.2 to regulate calcium entry via PKC (Gandini et al., 2021).

The N-methyl-D-aspartate receptor (NMDAR) is a glutamate receptor found in post-synaptic compartments of neurons. When glutamate from the synaptic cleft binds NMDAR, it opens to let Ca^{2+} entry and to depolarize the cell. NMDAR is a heterotetramer with 2 NR1B and 2 NR2B subunits. RACK1 has been shown to bind the 2 NR2B subunits along with the Fyn kinase (**Fig. 15, left**). When in the RACK1/NR2B/Fyn complex, the NMDAR is not phosphorylated and Ca^{2+} current is limited. However, when a stimulus, such as cAMP/protein kinase A (Yaka et al., 2003), triggers the release of Fyn by RACK1, Fyn can phosphorylate NR2B to potentiate NMDAR-mediated Ca^{2+} currents involved in synaptic physiology (Yaka et al., 2002). Astrocytes do express also NMDAR and could be regulated by RACK1 the same way.

RACK1 has been implicated recently in the development of the brain. The previously mentioned Focal Adhesion Kinase (FAK) is associated with RACK1 at focal adhesion to promote cell adhesion and migration. Neurite outgrowth occurs in the developing CNS and requires FAK activity. In neuronal culture, a team showed that RACK1 recruits AGAP2, a GTPase-activating protein, in growth cones to regulate FAK (Dwane et al., 2014). Indeed, when RACK1 is knocked-down, neurons have decreased neurite outgrowth. In addition, another team found RACK1 in association with point contacts, cytoskeleton anchor on the ECM, in growth cones of cultured neurons (**Fig. 15, right**) (Kershner and Welshhans, 2017a). They previously showed the regulation of the *β-actin* mRNA translation by RACK1 with ZBP1 (Ceci et al., 2012). Here, they showed the stimulation of point contacts, β-actin and RACK1 association in BDNF-stimulated growth cones. The right level of RACK1 was necessary for proper point contacts to function as either RACK1 knockdown and RACK1 overexpression lead to axon growth cone defects (Kershner and Welshhans, 2017a, 2017b). In a preprint, they pushed their investigations to demonstrate the role of RACK1 in axon guidance by the regulation of point contacts and translation of β-actin in growth cones after BDNF treatment (Kershner et al., 2019). Interestingly, RACK1 has been shown to regulate the cerebellar development. Using mouse cerebellum sections, authors showed that RACK1 decreased the Wnt/β-catenin

signaling pathway in Neural Stem Cells (NSCs) and increased Sonic hedgehog (Shh) pathway in Granule Neural Progenitors (GNPs) to control their proliferation and migration (Yang et al., 2019a). Indeed, in conditional RACK1 knock-out in NSC and GNP, the cerebellum architecture was disrupted, the Purkinje Cells (PC), a main type of neuron in the cerebellum, were misplaced and the Bergmann Glia (BG), a specialized astrocyte in the cerebellum, harbored process malformations. In addition, the mice had difficulty in movement control and died 3 weeks after birth. Curiously, a RACK1 knock-out specifically in BG did not disrupt the cerebellum development accounting for an earlier role of RACK1 in NSCs and GNP and a defect in BG morphology by non-cell-autonomous mechanisms. They further demonstrated that deletion of RACK1 in PC altered synaptogenesis and altered synaptic plasticity at the synapse between parallel fibers coming from granules cells and PC (Yang et al., 2019b). Corticogenesis is also regulated by RACK1. Indeed, RACK1 represses p21-mediated NSC senescence by interacting with the Smad signaling pathway mediated by TGFβ (Zhu et al., 2021).

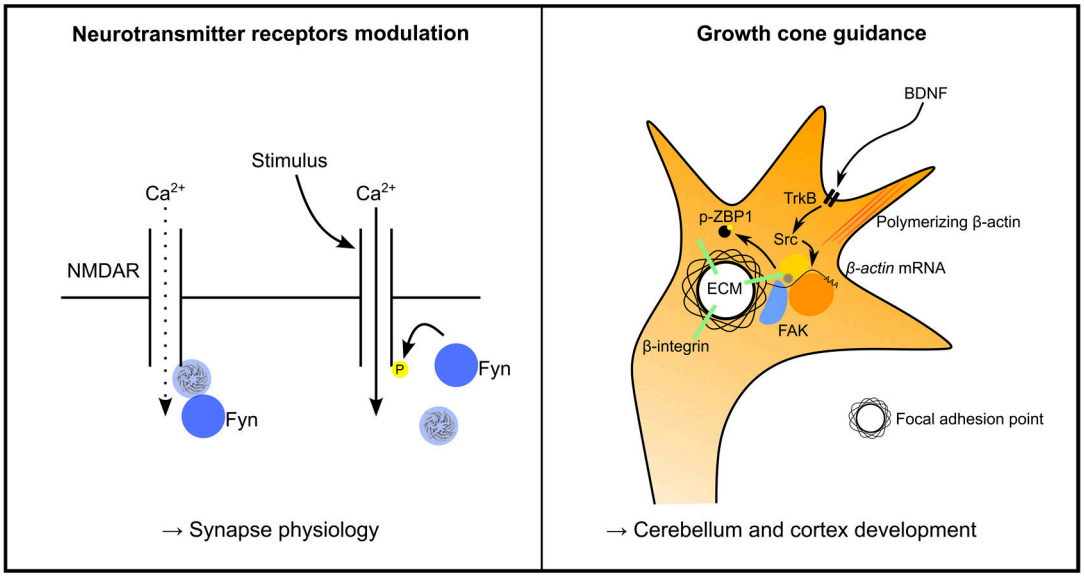

Figure 15. ***RACK1 participates in neuronal functions and CNS development. (Left)*** *RACK1 binds NMDAR and Fyn kinase in a basal state where calcium entry is limited. When stimulated, RACK1 releases Fyn to phosphorylate NMDAR and allow more calcium to enter the cell regulating synapse physiology.* ***(Right)*** *Ribosome-bound RACK1 is recruited at focal adhesion point in neuronal growth cone by FAK and integrins making the link between the extracellular matrix (ECM) and the cytosplam. BDNF, a guidance molecule, binds to its receptor TrkB triggering Src kinase activation. Src is recruited by RACK1 on the ribosome along with the RBP ZBP1 and its β-actin mRNA. SRC phosphorylates ZBP1 to release the mRNA in the ribosome and allow actin translation promoting axonal wiring and brain development.*

IV.d) RACK1 expression is modified in diseases

IV.d.i. Expression of RACK1 is altered in cancers

RACK1 is involved in cell cycle progression, cell migration and adhesion. Therefore, a deregulated expression of RACK1 would alter these properties and lead in cell invasion and over proliferation. Furthermore, RACK1 is also upregulated during angiogenesis. Indeed, RACK1 has been associated with different types of cancers.

Box 5: Role of free or ribosome-bound RACK1?

Since RACK1 has free and ribosome-bound roles it is difficult to discriminate which one is at play in a specific condition. For instance, RACK1 brings ribosomes at the focal adhesion points to regulate cell migration. In cancers, this feature could be used to create metastasis and regulate the translation of cytoskeleton proteins at invading points. In the CNS development, the ribosome-bound RACK1 could regulate the brain cells migration.
To decipher these 2 functions, the use of the mutated RACK1 unable to fix the ribosome would be of importance.

RACK1 is either overexpressed or downregulated depending on the type of cancer and even within the same type. For instance, RACK1 is increased in melanoma, a skin cancer, and accelerate cancer progression by augmentation of JNK and ERK kinases (Campagne et al., 2017). A knock-down of RACK1 in mouse melanoma cells reduced their invasion capacity. In hepatocelular carcinomas, an epithelial cells cancer, RACK1 increased Nanog expression to promote self-renewal of cancer stem cells (Cao et al., 2019). In lung squamous cell carcinoma, overexpressed RACK1 interacts with FGFR and MDM2, a ubiquitin ligase, to degrade the tumor suppressor p53 and to inhibit cancer cell apoptosis (Chen et al., 2021). As shown previously, RACK1 induces Shh signaling in GNP. In brain tumor medulloblastoma, increased RACK1 overactivated Shh to promote cancer (Liu et al., 2021). RACK1 has been proposed to be a therapeutic target by finding a molecule decreasing its expression (Langeswaran et al., 2019).

On the contrary, RACK1 expression is decreased in gastric cancer where a virus, *Helicobacter pylori*, inhibits RACK1 inducing the integrin β1 increase and the subsequent NfκB signaling to promote carcinogenesis (Hu et al., 2019). RACK1 is also downregulated in pancreatic cancer (Zhang et al., 2019a).

RACK1 has also been well studied in the context of breast cancers. For instance, the increase of glucocorticoid receptors in this pathology increases RACK1 transcription to induce cell migration and invasion (Buoso et al., 2019). However, expression in breast cancer is variable (either higher or

lower) (Buoso et al., 2020). Interestingly the authors hypothesized a link between cancer cells, RACK1 and ribosomes where RACK1 would bring ribosomes at adhesion focal points to promote translation of pro-invasive molecules. In addition, cells during stress, especially during tumorigenesis, translate more mRNAs with IRES which, as shown previously, is regulated by RACK1.

The difficulty of RACK1 studies in cancers is that it interacts with so many partners that it could do something and its contrary. RACK1 can be pro- and anti-apoptose, pro- and anti-proliferation, pro- and anti-migration (Einhorn, 2013; Li and Xie, 2015). To be a good cancer biomarker, further investigations need to be performed in elucidating RACK1 roles in different scenarios.

IV.d.ii. RACK1 is involved in neurological disorders

Although RACK1 mutations are not known to induce diseases because it is too important for the cell, RACK1 has been correlated with several neurological disorders when up- or down-regulated. For instance, an increased interaction of RACK1 with activated PKC has been detected in postmortem cortex of bipolar patients (Wang and Friedman, 2001). Curiously, this article shows RACK1 association with PKC only in the membrane fraction although it should be everywhere. RACK1 has also been shown to be downregulated in Down Syndrome (Peyrl et al., 2002). These data suggest alteration of neuronal migration or synaptogenesis in these pathologies related to RACK1 alteration. In Alzheimer's disease, inhibitory currents induced by GABAergic transmission is altered and is PKC dependent. Treatment of neuronal cultures with Aβ oligomers reduced RACK1 expression causing this inhibitory transmission alteration (Liu et al., 2011). Overexpression of RACK1 *in vivo* restored neuronal functions of Aβ-injected brains. Neuropathic pain is a disease where pain is felt in a chronic manner without painful stimuli due to a nerve crush for instance. A team has shown that RACK1 was upregulated in a neuropathic pain model in dorsal root ganglia neurons in the spinal cord (Lu et al., 2019). Interestingly, they injected a RACK1 siRNA directly in the cerebral spinal fluid in the spinal cord of a neuropathic pain rat model. They observed a decrease of RACK1 by western blot at levels of the Sham rats and an attenuation of neuropathic pain. Huntington's disease is a neurodegenerative disease characterized by aggregation of Huntingtin protein in neurons due to a polyglutamine expansion. Using a drosophila model, a team showed recently RACK1 in interaction with a ubiquitin ligase, Purity Of Essence (POE), to degrade ERK and induce polyglutamine-induced neurodegeneration (Xie et al., 2021).

Finally, RACK1 has been involved in epilepsy. In a mouse model of chronic epilepsy RACK1 expression was altered (over- and down-regulated depending on the brain region) (do Canto et al., 2020) as well as in humans where RACK1 was found increased (Xu et al., 2015). In addition, RACK1 has been shown to negatively regulate transcription of the voltage-gated sodium channel α subunit type 1 (Nav1.1) which downregulation has been associated with epilepsy (Dong et al., 2014).

According to the pre-cited articles, RACK1 increase in epilepsy would downregulate Nav1.1 and induce epilepsy.

With RACK1 involved in cancers and several neurological disorders, one could think it could be a perfect target for therapeutical assays. However, no compound has yet been developed to target specifically RACK1. But even if it was the case, RACK1 has such diverse roles, alteration of its expression would compromise other functions unless the molecule is cell-specific or target a specific domain of RACK1 (phosphorylation, ribosome-binding) or if it targets a specific downstream pathway of RACK1 action through its interaction with a kinase or a receptor for instance.

PART IV summary :

- RACK1 structure allows multiple protein interactions
- RACK1 is bound to the 40 S subunit of ribosomes and also has free roles
- RACK1 regulates translation by associating with specific RNAs, mediating RNA and nascent chain quality control and recruiting RBPs
- RACK1 participates in synaptic physiology and brain development
- RACK1 is altered in diseases including neurological disorders but no therapeutics have been developed
- RACK1 has never been addressed in astrocytes

Objectives

The main objective of my PhD was to decipher translation regulatory mechanisms in astrocytes and assess their physiological consequences. I divided my work in 2 aims:

Aim 1: Characterizing and quantifying RNA distribution in astrocytes in healthy and pathological contexts (Alzheimer's disease)

RNA distribution in neuronal processes has already been investigated but has been neglected in astrocytes. Former studies have identified pools of RNA in astrocyte processes but no tool was available to characterize and quantify the distribution of targeted mRNAs in this cell type. We developed *AstroDot*, a tool to visualize and quantify the distribution of virtually any RNA in astrocytes in mouse brain slices. For these purposes, we optimized a RNAscope FISH-based technique and we created an image analysis plugin on ImageJ to quantify FISH dots in 3D in hippocampal astrocytes based on their localization on astrocytic-specific intermediate filament GFAP. Importantly, we also wanted to explore if distal RNA distribution also occurred in microglia. The results of this study have been published in the *Journal of Cell Science* in 2020 (Oudart et al., 2020).

Aim 2: Characterizing translation mechanisms in astrocytes and in PAPs

The mechanisms regulating translation in astrocytes have been poorly investigated. We hypothesized that the regulation of astrocytic translation could regulate important brain functions. As shown in the introduction, translation can be regulated by proteins such as RBP, cytoskeleton or translation factors for instance. Here, we immunoprecipitated polysomes from astrocytes and identified the proteins associated by mass spectrometry. For the first time, we had access to the proteome associated with polyribosomes in astrocytes. The role of this proteome was assessed by focusing on one member, the ribosomal protein RACK1, known to regulate translation and local translation. We explored RACK1's roles in astrocytes and its physiological contributions. The corresponding manuscript is currently under review and published as a preprint in *BioRxiv* (Oudart et al., 2022).

In summary, my PhD provided, for the first time, tools, datasets and mechanistic views of the translation regulation in astrocytes in particular through the study of RACK1. This work offers new understandings for astrocytes physiology in the brain.

Experimental results

I. AstroDot – a new method for studying the spatial distribution of mRNAs in astrocytes

Summary

RNA transport along the cell processes has been studied in neurons to feed local translation in dendrites and axons. Local translation has also been shown in astrocytes PAPs and PvAPs. However, the RNA distribution in astrocytic processes is relatively misunderstood. Here, we developed a method called *AstroDot* to visualize RNAs in astrocytes in fixed brain slices with an optimized RNAscope FISH technique and to quantify their distribution in the cell in 3D with an ImageJ plugin developed in the lab. The plugin is using the co-immunostaining of the astrocytic-specific intermediate filament GFAP to attribute FISH dots in the astrocyte soma (nucleus + 2 µm), large processes (>0.3 µm), fine processes (<0.3 µm) or not in on GFAP processes (GFAP negative). The plugin has an option to study astrocyte specific RNAs in which all RNAs will be attributed to the cell. With AstroDot, we were able to quantify the distribution of 2 *Gfap* mRNA isoforms, *Gfap alpha* and *Gfap delta*. Our results, corroborated by qPCR studies, show that *Gfap alpha* RNAs are more abundant than *delta* and located more distally in hippocampal astrocytes. Next we were wondering if *Gfap* RNA distribution was altered in pathologies. Thus, we used *AstroDot* on an Alzheimer's mouse model. We found, first, that RNA density was increased in the pathology and more dramatically when the astrocyte was close to an amyloid beta plaque. Second, the distributions were changed as RNAs were shifted toward fine processes, with stronger effects for *Gfap alpha* in astrocytes near plaques. Finally, we demonstrated for the first time, the presence of RNAs, here *Rpl4*, in microglial processes.

This work has been published in *Journal of Cell Science* in 2020. I am co-first author with Romain Tortuyaux and Philippe Mailly.

In this work, I contributed in the optimization of the FISH technique with Romain Tortuyaux, in the development of the *AstroDot* plugin with Romain Tortuyaux and Philippe Mailly and in the analysis of the Alzheimer's study with Romain Tortuyaux. I also accomplished the reviews and built the figures. I helped writing the article with Martine Cohen-Salmon.

© 2020. Published by The Company of Biologists Ltd | Journal of Cell Science (2020) 133, jcs239756. doi:10.1242/jcs.239756

TOOLS AND RESOURCES

AstroDot – a new method for studying the spatial distribution of mRNA in astrocytes

Marc Oudart[1,2,*], Romain Tortuyaux[1,2,*], Philippe Mailly[2,3,*], Noémie Mazaré[1,2], Anne-Cécile Boulay[1,2] and Martine Cohen-Salmon[1,2,‡]

ABSTRACT

Astrocytes are morphologically complex and use local translation to regulate distal functions. To study the distribution of mRNA in astrocytes, we combined mRNA detection via *in situ* hybridization with immunostaining of the astrocyte-specific intermediate filament glial fibrillary acidic protein (GFAP). mRNAs at the level of GFAP-immunolabelled astrocyte somata, and large and fine processes were analysed using AstroDot, an ImageJ plug-in and the R package AstroStat. Taking the characterization of mRNAs encoding GFAP-α and GFAP-δ isoforms as a proof of concept, we showed that they mainly localized on GFAP processes. In the APPswe/PS1dE9 mouse model of Alzheimer's disease, the density and distribution of both α and δ forms of *Gfap* mRNA changed as a function of the region of the hippocampus and the astrocyte's proximity to amyloid plaques. To validate our method, we confirmed that the ubiquitous *Rpl4* (large subunit ribosomal protein 4) mRNA was present in astrocyte processes as well as in microglia processes immunolabelled for ionized calcium binding adaptor molecule 1 (Iba1; also known as IAF1). In summary, this novel set of tools allows the characterization of mRNA distribution in astrocytes and microglia in physiological or pathological settings.

KEY WORDS: Astrocytes, Microglia, Hippocampus, mRNA, *In situ* hybridization, Immunofluorescence, ImageJ, APPswe/PS1dE9 mouse, Alzheimer's disease, GFAP

INTRODUCTION

Astrocytes are the most abundant glial cells in the brain. Although astrocyte characteristics vary from one region of the brain to another, they all have a large number of processes that ramify into branches and then secondary branchlets. Hence, protoplasmic astrocytes are large, bushy-shaped cells with diameters of ∼40–60 µm and volumes of ∼10^4 µm^3. Each astrocyte covers a unique domain, and (in humans) contacts up to 2 million synapses (Ogata and Kosaka, 2002). At the synaptic interface, perisynaptic astrocyte processes (PAPs) sense the extracellular interstitial fluid, take up neurotransmitters and ions (Dallérac et al., 2018), and release neuroactive factors (Chever et al., 2014; Sultan et al., 2015). Astrocytes are also in contact with blood vessels; indeed, the latter are entirely sheathed in perivascular astrocyte processes (PvAPs) (Mathiisen et al., 2010). The astrocytes at this interface modulate the integrity and functions of the blood–brain barrier, neuroinflammation (Alvarez et al., 2013; Boulay et al., 2016), cerebral blood flow (Iadecola, 2017) and interstitial fluid drainage (Aspelund et al., 2015). The mechanisms underlying the synaptic and vascular influence of astrocytes are critically important, and have attracted much research interest. Indeed, dysregulation of astrocyte functions and their interplay with neurons and the vascular system contributes to the development and progression of most neurological diseases (Dossi et al., 2018; Iadecola, 2017; Verkhratsky et al., 2015).

Recent studies of astrocyte functional polarity have suggested that mRNA distribution and local translation regulates protein delivery in space and time. In a previous study, we showed that local translation is determined in PvAPs and we characterized the locally translated molecular repertoire (Boulay et al., 2017). Local translation has also been observed in the radial glia during brain development (Pilaz et al., 2016) and in PAPs in the adult cortex (Sakers et al., 2017). Interestingly, these studies showed that some mRNAs were specifically present in low or high levels in the astrocyte soma or processes; hence, mRNA distribution appears to follow specific rules and meet specific needs, and may help to regulate distal perivascular and perisynaptic functions.

To further characterize the mRNA distribution in astrocytes, we developed a new three-dimensional *in situ* method for identifying astrocyte mRNAs localized at the level of GFAP-immunolabelled processes and quantifying them with dedicated bioinformatics tools. More precisely, we studied the distribution of mRNAs encoding the astrocyte-specific GFAP-α and GFAP-δ isoforms (generated by alternative splicing) in the CA1 and CA3 regions of the hippocampus in wild-type (WT) mice and in the APPswe/PS1dE9 mouse model of Alzheimer's disease (AD). We further showed that our approach can be applied to microglia immunolabelled for ionized calcium binding adaptor molecule 1 (Iba1; also known as IAF1) and to all types of mRNA.

RESULTS

Gfapα and *Gfapδ* mRNAs are distributed in PAPs

Gfap mRNAs have been detected in distal perivascular (Boulay et al., 2017) and perisynaptic processes (Sakers et al., 2017) of astrocytes suggesting that local GFAP translation regulates distal intermediate filament assembly. Although previous research focused on the canonical isoform GFAP-α, at least 10 GFAP isoforms (generated by alterative mRNA splicing and polyadenylation signal selection) have been described (Hol and Pekny, 2015; Kamphuis et al., 2012; Middeldorp and Hol, 2011;

[1]Physiology and Physiopathology of the Gliovascular Unit Research Group, Center for Interdisciplinary Research in Biology (CIRB), College de France, CNRS Unité Mixte de Recherche 724, INSERM Unité 1050, Labex Memolife, PSL Research University, Paris 75005, France. [2]Center for Interdisciplinary Research in Biology (CIRB), College de France, Unité Mixte de Recherche 7241 CNRS, Unité1050 INSERM, PSL Research University, Paris 75005, France. [3]Orion Imaging Facility, Center for Interdisciplinary Research in Biology (CIRB), College de France, CNRS Unité Mixte de Recherche 724, INSERM Unité 1050, Labex Memolife, PSL Research University, Paris 75005, France.
*These authors contributed equally to this work

‡Author for correspondence (martine.cohen-salmon@college-de-france.fr)

R.T., 0000-0002-4182-6023; N.M., 0000-0003-4073-8811; A.-C.B., 0000-0001-5620-6209; M.C.-S., 0000-0002-5312-8476

Received 27 September 2019; Accepted 9 February 2020

Journal of Cell Science (2020) 133, jcs239756. doi:10.1242/jcs.239756

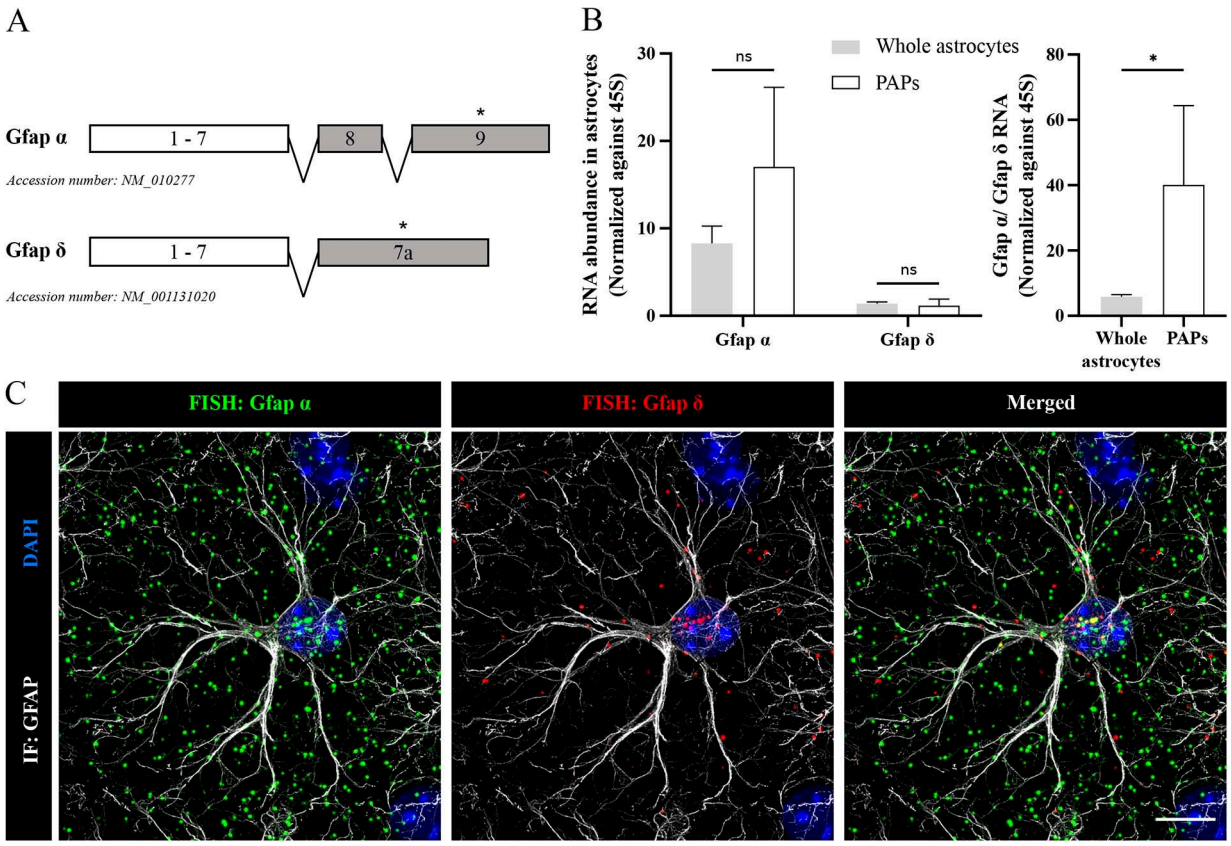

Fig. 1. Detection of *Gfapα* and *Gfapδ* mRNAs in hippocampal astrocytes. (A) Schematic representation of mouse GFAP-α and GFAP-δ isoforms. The positions of the qPCR and FISH probes are indicated with an asterisk. (B) Polysomal *Gfapα* and *Gfapδ* mRNA levels in hippocampal astrocytes and perisynaptic astrocyte processes (PAPs), determined by qPCR and normalized against 45S RNA. Statistical significance was determined in a one-way unpaired Mann–Whitney test; n=3; *P<0.05; ns, not significant. Error bars represent s.e.m. (C) Merged and separated images of a deconvoluted confocal z-stack of a CA1 astrocyte, with FISH detection of *Gfapα* (in green) and *Gfapδ* (in red) mRNAs and co-immunofluorescence detection (IF) of GFAP (in grey). The nucleus was stained with DAPI (in blue). Note the abundance of *Gfapα* mRNA FISH dots (relative to *Gfapδ*) in distal areas of the astrocyte. Scale bar: 10 µm.

Moeton et al., 2016). GFAP-δ is encoded by the same first 7 exons as GFAP-α but has a different C-terminus (Fig. 1A). This isoform has received special interest because it is associated with neurogenic niches (van den Berge et al., 2010) and is expressed in glioma. The GFAP-δ/GFAP-α ratio correlates with the malignancy grade (Brehar et al., 2015; Choi et al., 2009; Heo et al., 2012). In fact, GFAP-δ does not form intermediate filaments alone but integrates the intermediate filament network only if GFAP-α and/or vimentin are present and aggregates or collapses the network when highly expressed in cells (Moeton et al., 2016; Perng et al., 2008). Here, we first looked for *Gfapα* and *Gfapδ* mRNAs in PAPs. Polysomal mRNAs were extracted by translating ribosome affinity purification (TRAP) from adult Aldh1L1:l10a-eGFP mice, which express the chimeric ribosomal protein Rpl10a-eGFP specifically in astrocytes (Heiman et al., 2014). Extractions were performed either from hippocampus (for whole-astrocyte polysomal mRNAs) or synaptogliosome preparations (consisting of apposed pre- and post-synaptic membranes and astrocyte PAPs), in order to extract polysomal mRNAs contained in PAPs (Carney et al., 2014; Sakers et al., 2017). Quantitative qPCR amplification of *Gfapα* and *Gfapδ* mRNA was performed using specific primers (Fig. 1B). Both isoforms were detected in whole astrocytes (mean±s.e.m.: 8.28±1.99 arbitrary units for *Gfapα* and 1.38±0.20 for *Gfapδ*) and in the perisynaptic processes (17.04±9.09 for *Gfapα* and 1.16±0.76 for *Gfapδ*). For polysomal mRNAs, the *Gfapα*/*Gfapδ* ratio was significantly higher in PAPs (40.09±24.27; n=3; P=0.05) than in whole astrocytes (5.81±0.67), suggesting the predominance of Gfapα in PAPs (Fig. 1B).

We next sought to visualize *Gfapα* and *Gfapδ* mRNAs in hippocampal astrocytes. Fluorescent *in situ* hybridization (FISH) was performed on 30-µm-thick free-floating adult mouse brain sections, using specific fluorophore-coupled RNAscope® probes against *Gfapα* exon 9 and *Gfapδ* exon 7a (Fig. 1C). Next, the astrocyte somata and processes were labelled by GFAP immunostaining (Fig. 1C). Importantly, the co-immunofluorescence detection of proteins depends on the preservation of their epitopes during the protease digestion step preceding FISH. We observed dense, continuous, GFAP-labelled arborizations indistinguishable from GFAP immunolabelling obtained without protease treatment (Fig. S1), which indicated that our protocol preserved the GFAP epitopes. In line with the qPCR results presented above, *Gfapα* and *Gfapδ* mRNA FISH signals were detected as discrete dots in the soma and in distal astrocyte areas; *Gfapα* mRNA (Fig. 1B) was more abundant than *Gfapδ*, which was mainly present in the somata (Fig. 1C).

AstroDot and AstroStat: bioinformatics tools for analyzing the mRNA distribution in astrocytes

In order to analyse the distribution of *Gfapα* and *Gfapδ* mRNAs in astrocytes, we developed AstroDot, a dedicated ImageJ plug-in. We had two main objectives: (i) to detect mRNA FISH dots that localized on GFAP-immunostained astrocyte processes; and (ii) to quantify these dots and analyse their distribution in the astrocytes.

Journal of Cell Science (2020) 133, jcs239756. doi:10.1242/jcs.239756

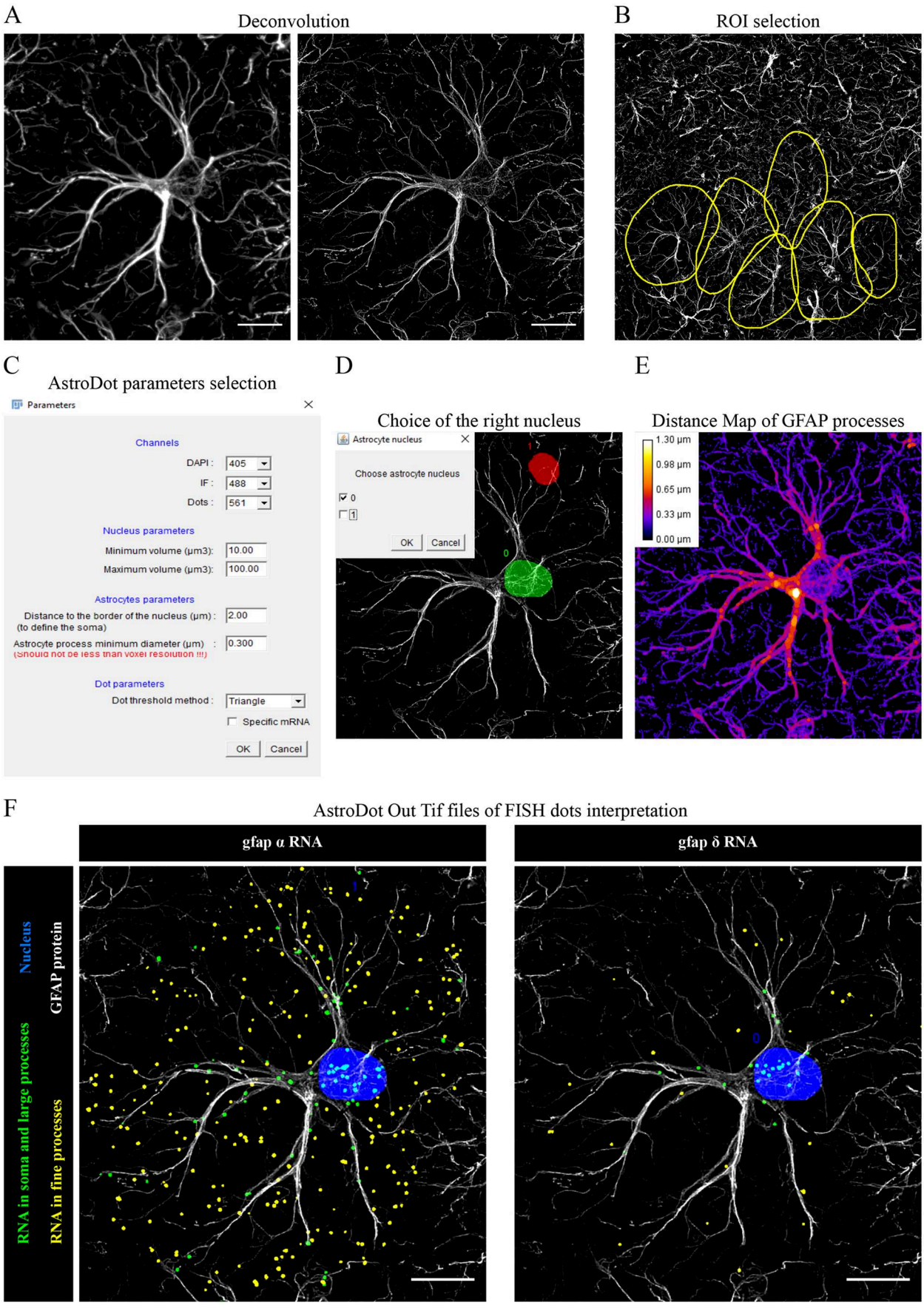

Fig. 2. See next page for legend.

Journal of Cell Science (2020) 133, jcs239756. doi:10.1242/jcs.239756

Fig. 2. AstroDot image processing. All images correspond to a single confocal *z*-stack for a CA1 astrocyte. (A) Effect of deconvolution on GFAP immunofluorescence. Left panel: raw confocal image; right panel: deconvoluted images. (B) Selection of regions of interest (ROIs; yellow circles). (C) AstroDot dialogue box for the definition of fluorescence channels, the nucleus and astrocyte parameters, the threshold method for FISH dots and the choice of the 'Specific mRNA' option. (D) Detection of the astrocyte nucleus (in green) and other nuclei (in red). (E) Heat map of GFAP immunofluorescence, used to calculate the process diameter. (F) AstroDot interpretation of the results for *Gfapα* and *Gfapδ* mRNAs, with the 'Specific mRNA' option active. Green dots are located in the soma or large GFAP-labelled processes. Yellow dots are located in fine processes. Scale bars: 10 µm.

Confocal images of the CA1 and CA3 regions of the hippocampus were acquired and then deconvoluted, so as to eliminate the inherent fluorescence blurring [the point spread function (PSF)] and noise, and to increase the resolution (Fig. 2A). Astrocytes define individual domains, and GFAP processes do not intermingle (Bushong et al., 2002). Using this property, regions of interest (ROIs, i.e. the soma and processes) corresponding to individual astrocytes were selected manually by assessing the GFAP (intermediate filaments) and DAPI (nuclei) staining on the *Z*-projection of image stacks and by defining the stack of confocal planes for each ROI (Fig. 2B). AstroDot opens with a dialogue box (Fig. 2C) that enables the operator to attribute: (1) a specific purpose for each of the three fluorescence channels, e.g. 'DAPI' for nuclear staining, 'IF' for GFAP immunofluorescence, and 'Dots' for FISH dot thresholding and detection; (2) a minimum and maximum nucleus volume; (3) a distance from the DAPI staining to define the somatic domains; (4) a minimum astrocyte process diameter. This value should not be less than the Voxel resolution. This dialogue box also contains a 'Specific mRNA' option, which can be selected when the studied mRNA is expressed only in the cell-type of interest as is the case here for *Gfap* in astrocytes. In such situations, all mRNA FISH dots are considered to belong to this cell type. The first step in the analysis was calculation of the mean GFAP immunofluorescence background, i.e. the value above which the signal was considered to be positive. Importantly, to verify the background homogeneity, this value was calculated on whole images as well as on individual ROIs. In the second step, each astrocyte nucleus was defined; given that astrocytes interact with other brain cell types, some ROIs can contain more than one nucleus. AstroDot was designed to optimize the recognition of astrocyte nuclei on the basis on the GFAP immunostaining. The putative astrocyte nucleus appears in green, and any other nuclei appears red. A second dialogue box allows the operator to confirm or modify AstroDot's automatic selection by clicking on the correct nucleus (Fig. 2D). AstroDot then starts to detect astrocyte mRNAs, based on their localization at the level of the GFAP immunostaining. A distance map is used to calculate the diameter of each GFAP-immunolabelled process. Processes with a diameter greater than the minimum distance between two confocal planes (0.3 µm, in the present case), are defined as 'large', and those with a smaller diameter as 'fine' (Fig. 2E). The DAPI staining and the surrounding 2 µm space corresponded here to the somatic domain of each astrocyte. A TIF image was generated for each ROI (Fig. 2F). The mRNA FISH dots are red if they were outside astrocytes, green if they localize on astrocyte large processes and somata, or yellow if they localize on astrocyte fine processes (Fig. 2F). All the results were automatically entered on a table with the following items for each ROI: (1) image name; (2) ROI name; (3) background intensity; (4) astrocyte volume; (5) dot density in astrocytes; (6) percentage of dots not in astrocytes; (7) percentage of dots in astrocyte somata; (8) percentage of dots in astrocyte fine processes; (9) percentage of dots in astrocyte large processes; (10) mean astrocyte process diameter. To facilitate the statistical analysis of AstroDot data, we developed an optional R package named AstroStat; it automatically calculates and compares the mean±s.d. values, and produces a summary report of the results.

Characterization of *Gfapα* and *Gfapδ* mRNAs in CA1 and CA3 hippocampal astrocytes from WT mice and the APPswe/PS1dE9 mouse model of AD

We analysed the density and distribution of *Gfapα* and *Gfapδ* mRNAs in CA1 and CA3 hippocampal adult astrocytes in WT adult mice by using the AstroDot 'Specific mRNA' option (Fig. 3 and Tables S2–S5). Comparison of the astrocytes in CA1 versus CA3 indicated that CA1 astrocytes had a slightly greater overall volume but displayed processes with the same mean diameter (Fig. 3A). The *Gfapα*/*Gfapδ* mRNA ratio was the same in the two regions (Fig. 3B). Overall, and in line with our initial qPCR analysis (Fig. 1B), *Gfapα* was 5.2 times more abundant than *Gfapδ* in both CA1 and CA3 (Fig. 3C). Both mRNAs were more abundant in the processes (*Gfapα*, 88.5±6.7% in CA1 and 86.7±8.1% in CA3; *Gfapδ*, 73.4±11.3% in CA1 and 71.5±16.4% in CA3; mean±s.d.) than in the soma. *Gfapδ* was more abundant than *Gfapα* in the soma and in large processes (Fig. 3D). We next analysed the data without considering the astrocytic-specific expression of GFAP, unselecting the 'Specific mRNAs' option of AstroDot (Fig. 3E). In this case, both *Gfapα* and *Gfapδ* mRNAs were localized on GFAP-labelled intermediate filaments in CA1 (mean±s.d.: 59.5±9.0 for *Gfapα* and 74.4±11.0 for *Gfapδ*) and CA3 (62.2±10.1 for *Gfapα* and 74.7±12.4 for *Gfapδ*), suggesting that the majority of *Gfap* RNAs are associated with intermediate filaments (Fig. 3E).

Astrocytes are involved in neuroinflammation, and become reactive in virtually all pathological situations in the brain. Astrocyte reactivity is characterized by GFAP overexpression and morphological changes, such as process hypertrophy and remodelling (Hol and Pekny, 2015). Hence, we next sought to study *Gfapα* and *Gfapδ* mRNAs in reactive astrocytes. We chose the example of AD, in which astrocytes undergo drastic morphological and molecular changes that perturb their physiology (Ben Haim et al., 2015; Burda and Sofroniew, 2014). Using the method described above, *Gfapα* and *Gfapδ* mRNA FISH dots were detected on GFAP-immunolabelled sections of CA1 and CA3 hippocampus from 9-month-old APPswe/PS1dE9 mice (Fig. 4). We quantified astrocytes associated with a beta-amyloid plaque (Aβ, labelled with DAPI) or more than 30 µm from an Aβ plaque (Fig. 5 and Tables S2–S5). As reported in the literature, CA1 and CA3 astrocytes from APP/PS1dE9 mice were larger than those from WT mice (Fig. 5A) but had a slightly smaller process diameter (Fig. 5A). In astrocytes not associated with Aβ, the *Gfapα*/*Gfapδ* ratio was slightly but significantly higher (by a factor of 1.3) in CA1 and CA3 (Fig. 5B), with a higher *Gfapα* mRNA level in fine processes only (Figs 4A and 5F). In contrast, the *Gfapδ* mRNA density was the same as in WT mice in CA1 and CA3 (Fig. 5C). However, the distribution of this mRNA within the astrocytes differed; levels in large processes were lower (relative to the WT) in CA1 and CA3 (Fig. 5E), and levels in fine processes were higher in CA3 only (Fig. 5F). The relative differences in mRNA levels were greater in Aβ-associated astrocytes (Fig. 4B); the density of *Gfapα* mRNAs was significantly higher than in WT cells (5.0-fold for CA1, and 4.7-fold in CA3) or in astrocytes not associated with Aβ (3.8-fold for CA1, and 3.7-fold in CA3) (Fig. 5C). The distribution of *Gfapα* mRNA also differed, with lower

Journal of Cell Science (2020) 133, jcs239756. doi:10.1242/jcs.239756

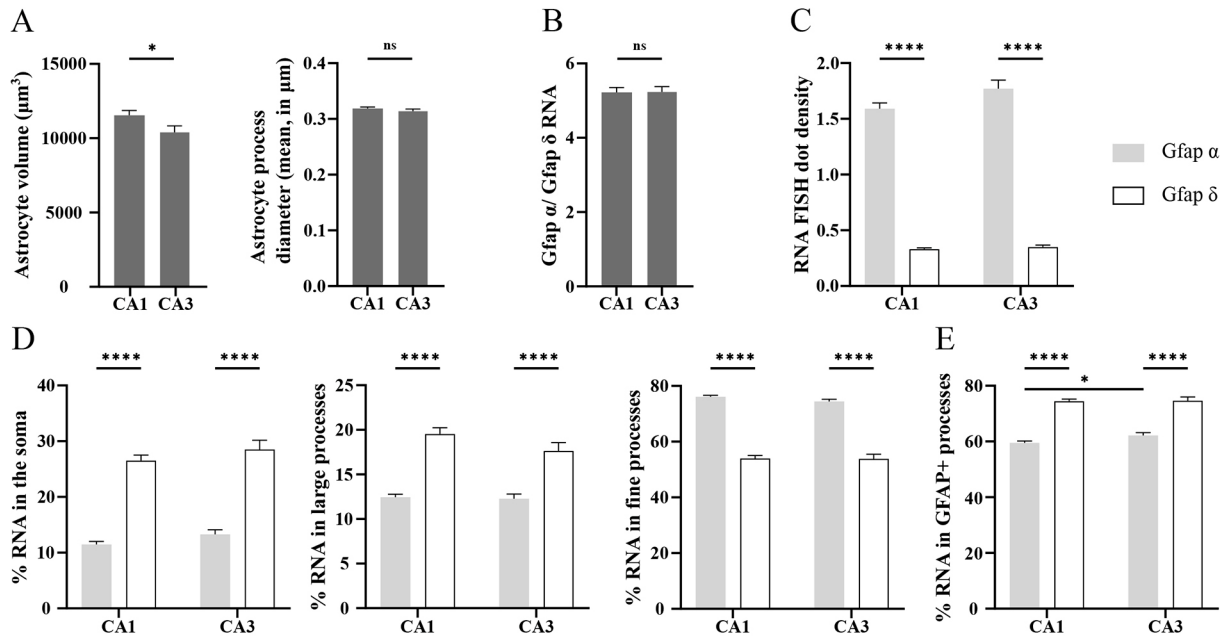

Fig. 3. Distribution of *Gfapα* and *Gfapδ* mRNAs in CA1 and CA3 hippocampal astrocytes. (A) Astrocyte volume, and process diameter. (B) The *Gfapα*/*Gfapδ* mRNA ratio. (C) Total mRNA density: number of RNA FISH dots/µm^3×100. (D) Percentages of *Gfapα* and *Gfapδ* mRNAs in astrocyte somata, fine processes and large processes. (E) Percentages *Gfapα* and *Gfapδ* mRNA dots localized on GFAP when the 'Specific mRNA' option was not applied. In total, 175 CA1 and 94 CA3 astrocytes from 3 mice and 5 slices per mouse were analysed (values are presented in Tables S2–S5). Statistical significance was determined in two-way unpaired Student's *t*-tests. *P<0.05; ****P<0.0001; ns, not significant. Error bars represent the s.e.m.

levels (relative to the WT) in the soma (Fig. 5D) and in large processes (only in CA1) (Fig. 5E) and higher levels in fine processes in CA1 and CA3 (Fig. 5F). The same effect was observed for the *Gfapδ* mRNA, with a greater abundance in Aβ-associated astrocytes than in WT samples (3.6-fold for CA1, and 3.5-fold in CA3) or in astrocytes far from plaques (3.3-fold for CA1, and 3.4-fold in CA3) (Fig. 5C). The redistribution was most prominent in fine processes in CA1 and CA3 (Fig. 5F). These results show that the density and distribution of *Gfapα* and *Gfapδ* mRNAs vary markedly as a function of the astrocyte's reactivity status, the brain area and the proximity of Aβ deposits.

Application of AstroDot and AstroStat to the analysis of ubiquitous mRNAs in astrocytes and microglia

To further validate our approach, we studied the distribution of *Rpl4* mRNA (a ubiquitously expressed mRNA encoding the large subunit ribosomal protein 4) in CA1 (Fig. 6A). Interestingly, 62.52±11.77% of the *Rpl4* mRNA FISH dots were localized in astrocytes (n=67). Of these, 83.33±5.41% were present in fine GFAP-immunolabelled processes, with 9.59±3.45% in large GFAP-immunolabelled processes, and 7.09±4.14% in somata (all values are mean±s.d.). This result was unexpected because Rpl4 integrates into the 60S ribosome subunit in the nucleus (Huber and Hoelz, 2017), but was corroborated by a qPCR analysis (performed as described above) of polysomal mRNAs extracted by TRAP from adult Aldh1L1:l10a-eGFP mouse hippocampus or PAPs; in the latter, Rpl4 was enriched 120-fold (P=0.05, n=3) (Fig. 6B). To study the distribution of non-astrocyte *Rpl4* mRNA FISH dots, we performed additional, independent experiments by immunostaining neuronal and microglial specific markers. Immunostaining of the neuronal-specific cytoskeletal high and medium chains of the neurofilament protein (NF-H and NF-M), the microtubule-associated protein 2 (MAP2) and the hippocampal immature neuron protein doublecortin (DCX) was however not preserved enough even after a mild FISH protease pre-treatment (Fig. S2). In contrast, as with the GFAP immunofluorescence experiments, our FISH protocol was compatible with the detection of the microglial-specific Iba1 protein, which was detected and remained homogeneous throughout the somata and processes (Fig. 6C). Our analysis of the distribution of *Rpl4* mRNA in microglia (n=28) indicated that 16.07±4.47% of the *Rpl4* mRNA FISH dots were localized in microglial processes. Of these, 37.72±9.24% were localized in fine processes, with 27.06±10.78% in large processes and 35.22±10.13% in somata (means±s.d.). In conclusion, this novel set of tools allows the characterization of mRNA distribution in astrocytes and microglia.

DISCUSSION

Although local translation has been recently described in astrocyte processes, tools for studying the distribution of astrocyte mRNAs were not previously available. Accordingly, we developed a co-labelling method that combined mRNA *in situ* hybridization, the immunofluorescence detection of GFAP-containing intermediate filaments on brain slices, confocal imaging and a bioinformatics analysis of mRNA density and distribution in astrocytes.

A key technical obstacle to the implementation of this approach was the risk of protein epitope degradation during the protease digestion step that precedes *in situ* RNA hybridization. Our previous tests on transgenic hGfap-eGFP mouse brain sections (in which eGFP fills the astrocyte cytoplasm; Nolte et al., 2001) indicated that these adaptations were not sufficient to preserve eGFP (data not shown) and thus precluded the use of this reporter mouse strain to detect astrocytes in parallel with *in situ* hybridization. In contrast to previous reports (Boulay et al., 2017; Pilaz et al., 2016), however, our protocol preserved GFAP and enabled us to perform parallel *in situ* hybridization and GFAP immunodetection. Interestingly, these conditions also allowed us to immunodetect the microglia-specific

Journal of Cell Science (2020) 133, jcs239756. doi:10.1242/jcs.239756

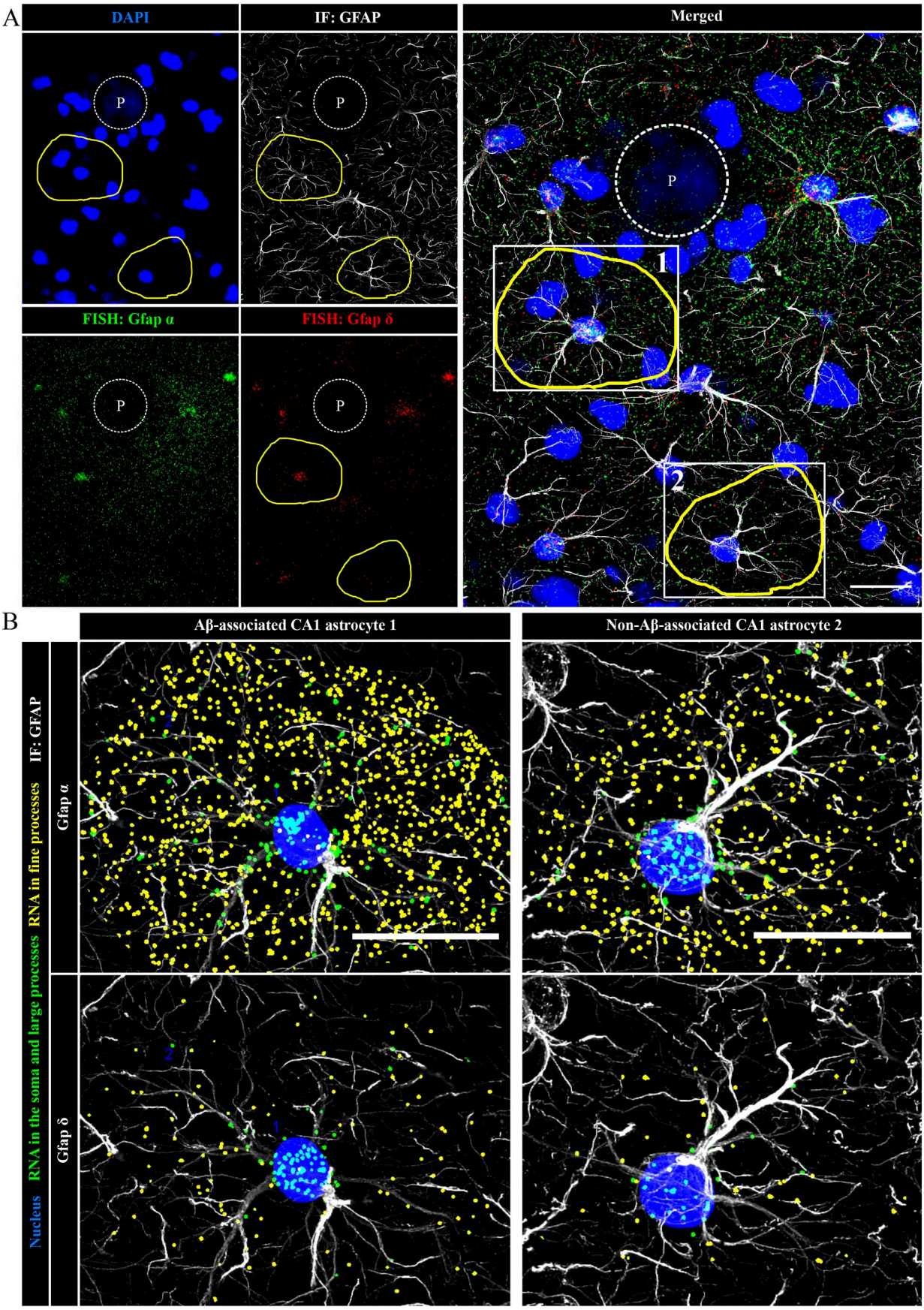

Fig. 4. See next page for legend.

Journal of Cell Science (2020) 133, jcs239756. doi:10.1242/jcs.239756

Fig. 4. Detection of *Gfapα* and *Gfapδ* mRNAs in CA1 hippocampal APPswe/PS1dE9 astrocytes. (A) Merged and separated images of a deconvoluted confocal *z*-stack of APPswe/PS1dE9 CA1 astrocytes, with FISH detection of *Gfapα* mRNA (in green) and *Gfapδ* mRNA (in red) and co-immunofluorescence detection of GFAP (in grey). The nucleus and an amyloid deposit (dotted circle labelled 'P') are stained with DAPI (in blue). ROI #1 (yellow circle) is an astrocyte close to an Aβ deposit. ROI #2 is located more than 60 µm from an Aβ plaque. (B) TIF images of ROI1 and ROI2 for *Gfapα* and *Gfapδ* mRNA, as analysed with AstroDot using the 'Specific mRNA' option. Green dots belong to the soma and large GFAP-labelled immunofluorescent processes. Yellow dots belong to fine processes. Scale bars: 20 µm.

Iba1. In contrast to glial cells, we could not find any neuronal immunolabelling preserved after the FISH pre-treatment. Further efforts are therefore needed to eventually find compatible markers.

It is noteworthy that GFAP is not expressed uniformly in the brain, and so GFAP immunolabelling is somewhat limited by its lack of applicability to all brain regions. Nevertheless, our optimization of the GFAP immunolabelling makes it possible to distinguish between labelled astrocyte processes and their secondary extensions in regions where GFAP is highly expressed (e.g. the hippocampus, olfactory bulbs, cerebellum and hypothalamus). Another advantage of immunolabelling GFAP and Iba1 relates to the fact that both proteins are standard markers of glial reactivity – a process initiated in response to immune attack, chronic neurodegenerative disease or acute trauma (Liddelow and Barres, 2017). Hence, GFAP and Iba1 co-immunolabelling could therefore be used to address possible changes in mRNA distribution in reactive astrocytes and microglia, as demonstrated here in APPswe/PS1dE9 mice.

It was previously determined that GFAP immunolabelling delineates only 15% of the total astrocyte volume (Bushong et al., 2002). Nevertheless, we found that the majority of the *Gfapα* and *Gfapδ* mRNA dots were attributed to GFAP processes. The mRNA dots not detected in GFAP intermediate filaments probably belonged to fine distal astrocyte processes where GFAP is less present (e.g. PAPs). These observations suggest that the majority of *Gfap* mRNAs are bound to intermediate filaments, and are consistent with previous reports of colocalization between mRNAs encoding collagens (Challa and Stefanovic, 2011) and alkaline phosphatase (Schmidt et al., 2015) on one hand and vimentin (another intermediate filament protein) on the other. Taken as a whole, these findings suggest that intermediate filaments may have crucial roles in the distal distribution of mRNAs. Consequently, it is conceivable that GFAP alterations, deficiency or upregulation (one or the other of which occurs in most neuropathological conditions; Hol and Pekny, 2015) might greatly modify the distribution of astrocyte mRNAs and their local translation. In turn, these changes might alter the astrocyte functions, particularly at their synaptic and vascular interfaces.

In order to demonstrate the applicability of our approach, we first focused on mRNAs encoding (i) the canonical α isoform of GFAP and (ii) the δ Cter variant, the assembly of which with GFAP-α promotes intermediate filament aggregation and dynamic changes (Moeton et al., 2016; Perng et al., 2008). Interestingly, the results of our experiments in WT mice showed that *Gfapδ* mRNA was more likely than *Gfapα* mRNA to be found in the astrocyte soma. This finding corroborated the results of a previous *in vitro* study in which the proportion of mRNA in primary astrocyte protrusions was higher

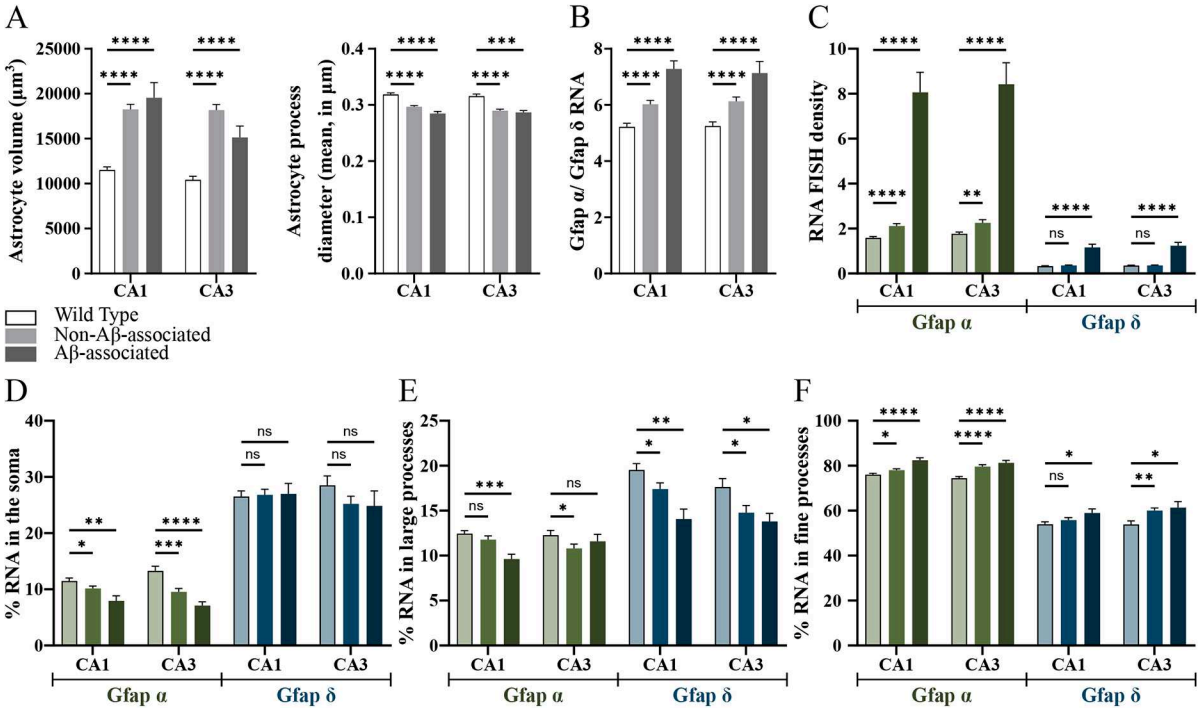

Fig. 5. Comparison of *Gfapα* and *Gfapδ* mRNA densities and distributions in CA1 and CA3 hippocampal astrocytes from WT and APPswe/PS1dE9 mice. (A) Astrocyte volume and process diameter. (B) The *Gfapα*/*Gfapδ* mRNA ratio. (C) Total mRNA density: number of RNA FISH dots/µm^3×100. (D-F) Percentages of *Gfapα* and *Gfapδ* mRNA dots localized on GFAP immunostaining in astrocyte somata (D), fine processes (E) and large processes (F). Analyses were performed on 175 CA1 WT astrocytes, 94 CA3 WT astrocytes, 127 APPswe/PS1dE9 CA1 astrocytes not associated with plaques, 78 APPswe/PS1dE9 CA3 astrocytes not associated with plaques, 27 plaque-associated CA1 APPswe/PS1dE9 astrocytes, and 28 plaque-associated CA3 APPswe/PS1dE9 astrocytes. 3 mice per genotype and 5 slices per mouse were analysed (values are presented in Tables S2–S5). Statistical significance was determined using two-way unpaired Student's *t*-tests. **P*<0.05; ***P*<0.001; ****P*<0.001; *****P*<0.0001; ns: not significant. Error bars represent s.e.m.

Journal of Cell Science (2020) 133, jcs239756. doi:10.1242/jcs.239756

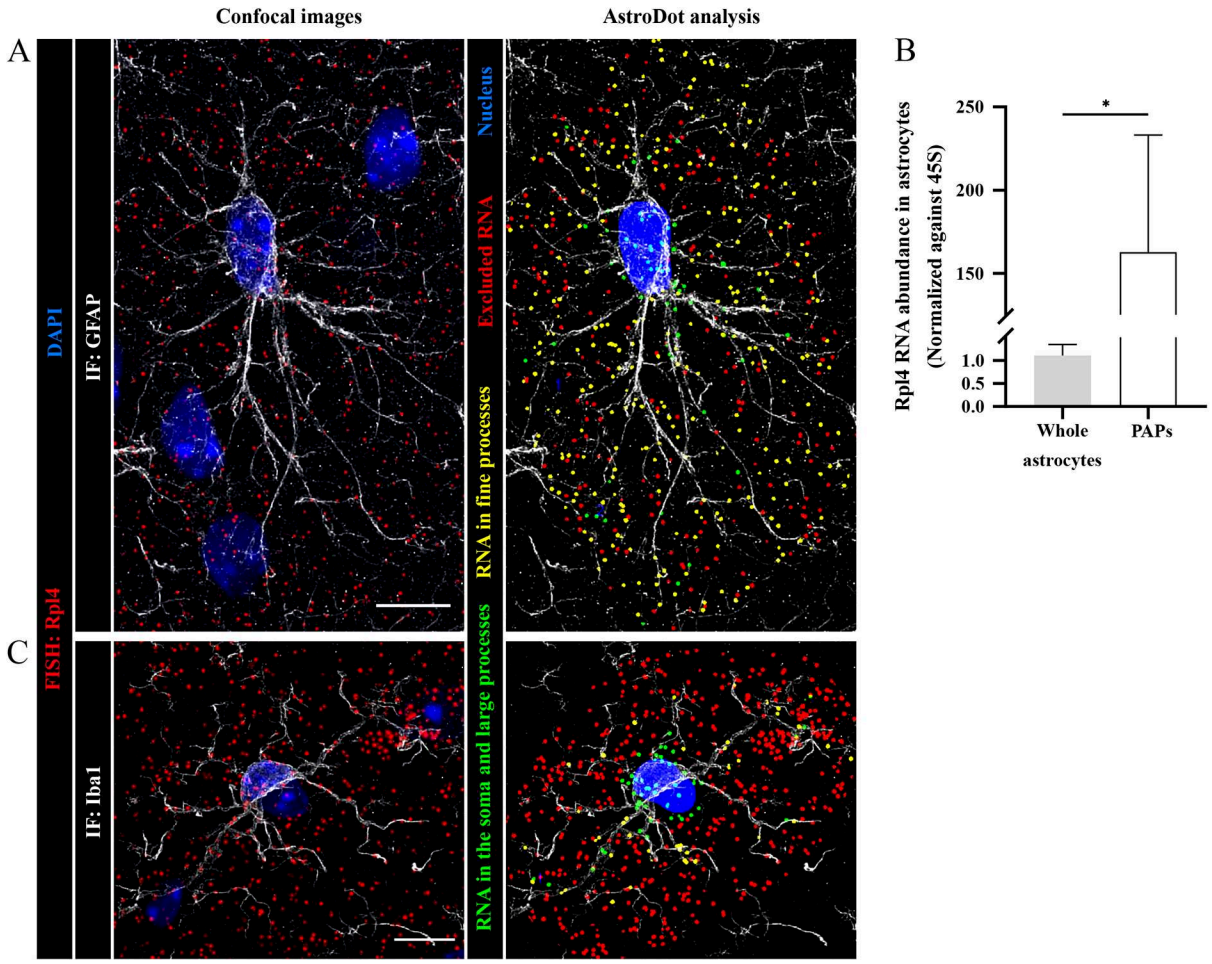

Fig. 6. Detection and characterization of *Rpl4* mRNA distribution in CA1 hippocampal astrocytes, microglia. (A) Left: Confocal *z*-stack of a CA1 astrocyte with FISH detection of *Rpl4* mRNA (in red) and co-immunofluorescence GFAP detection (in grey). The nucleus is stained with DAPI (in blue). Right: AstroDot analysis. Green dots are located in the soma or in GFAP-immunolabelled large processes; yellow dots are located in GFAP-immunolabelled fine processes; red dots are not localized on GFAP immunostaining (i.e. excluded RNAs). (B) The polysomal *Rpl4* RNA level in hippocampal astrocytes and PAPs, determined by qPCR and normalized against 45S RNA. Statistical significance was determined in a one-way unpaired Mann–Whitney's test; $n=3$; *$P<0.05$. Error bars represent s.e.m. (C) Left: confocal *z*-stack of a CA1 microglial cell with FISH detection of *Rpl4* mRNA (in red) and co-immunofluorescent Iba1 (in grey). The nucleus was stained with DAPI (in blue). Right: AstroDot analysis. Green dots are located in the soma or Iba1-immunolabelled large processes; yellow dots are located in Iba1-immunolabelled fine processes; red dots do not localize on Iba1 immunostaining (i.e. excluded RNAs). Scale bars: 10 µm.

for *Gfapα* than for *Gfapδ* (Thomsen et al., 2013). The high *Gfapα* and *Gfapδ* mRNA density observed in amyloid plaque-associated astrocytes was also consistent with previous qPCR-based assays of mRNA in the cortex of APPswe/PS1dE9 mice (Kamphuis et al., 2012). Interestingly, levels of human GFAP-α and GFAP-δ isoforms are elevated in plaque-associated astrocytes in the CA1-3 region (Kamphuis et al., 2014). Although RNA density in fine processes could also be secondary to the increase in GFAP filament density linked to astrocyte reactivity, our observations of elevated mRNA density and distribution in the fine processes of plaque-associated astrocytes suggest that local translation of *Gfapα* and *Gfapδ* mRNA might be a critical mechanism for regulating intermediate filament dynamics in distal astrocyte processes during the progression of AD. Given that the GFAP-α/GFAP-δ isoform ratio is known to strongly influence astrocyte proliferation and malignancy (Stassen et al., 2017; van Bodegraven et al., 2019), our approach might constitute a valuable tool for accurately assessing the differentiation state of astrocytomas in preclinical and clinical settings.

Lastly, we demonstrated that our approach is applicable to any type of mRNA and can also be used in microglia. In fact, the present study is the first to have demonstrated that mRNAs are distributed across microglial processes; this is an important observation in view of the microglia's complex morphology and motility, and its roles in immune surveillance and synaptic remodelling in the brain (Squarzoni et al., 2014). Our results strongly suggest that mRNA distribution and local translation are of physiological significance in this important neural cell type. In conclusion, our new semi-automated *in situ* histological method is the first to have characterized mRNA distribution in astrocytes and microglia.

MATERIALS AND METHODS

Mice

Aldh1L1:l10a-eGFP mice (Heiman et al., 2014) and C57BL6 WT mice were housed under pathogen-free conditions in the animal facility at the Centre Interdisciplinaire de Recherche en Biologie (CIRB, Collège de France, Paris, France). The APPswe/PS1dE9 (Borchelt et al., 1997) mice were housed in the MIRCen animal facility (CEA, Fontenay-aux-Roses, France). All analyses were performed on 3 mice (males) per genotype.

Ethical approval

All experiments were approved by the French Ministry of Research and Higher Education, and conducted in accordance with the host institution's ethical standards (Collège de France, Paris, France).

Journal of Cell Science (2020) 133, jcs239756. doi:10.1242/jcs.239756

Aldh1L1:l10a-eGFP TRAP from whole astrocytes and PAPs, and qPCR

Two hippocampi from 5-month-old mice were used for each whole-astrocyte polysome extraction. Each synaptosome preparation was done on four hippocampi as described in Carney et al. (2014) for perisynaptic astrocyte extraction. Polysomes were extracted using the method described in Boulay et al. (2019). Three independent samples were prepared for qPCR analysis. Messenger RNAs were purified using the RNeasy Lipid tissue kit (Qiagen). cDNA was synthesized from 100 ng of whole-astrocyte RNA or PAP mRNA using a Reverse Transcriptase Superscript III kit (Invitrogen) with random primers, and stored at −20°C. Next, 1 µl of cDNA suspension was pre-amplified using SoAmp reagent (Bio-Rad), and droplet qPCR was performed using a QX200™ Droplet Digital™ PCR System (Bio-Rad). The cDNA content was normalized against 45S RNA. TaqMan probes and primer references are listed in Table S1. The data were analysed by applying a one-way unpaired Mann–Whitney test. The threshold for statistical significance was set to $P<0.05$.

Brain slice preparation

Nine-month-old mice were anaesthetized with a mix of ketamine and xylazine (0.1 ml/mg) and killed by transcardiac perfusion with 1× phosphate-buffered saline (PBS) with 4% paraformaldehyde (PFA). The brain was removed and immersed in 4% PFA overnight at 4°C. The PFA solution was replaced with 15% sucrose for 24 h at 4°C and, lastly, by 30% sucrose for 24 h at 4°C. The brains were cut into 30-µm-thick coronal sections using a Leitz microtome (1400). Sections were stored at −20°C in a cryoprotectant solution (30% glycerol and 30% ethylene glycol in 1× PBS).

Fluorescent *in situ* hybridization and immunostaining

Slices were carefully washed three times with 1× PBS in a 24-well plate. For the last wash, the 1× PBS was replaced with 7 drops of RNAscope® hydrogen peroxide solution (Advanced Cell Diagnostics Inc.) for 10 min at room temperature (RT); this blocked endogenous peroxidase activity, and resulted in the formation of small bubbles. The slices were washed in Tris-buffered saline with Tween® (50 mM Tris-Cl, pH 7.6; 150 mM NaCl, 0.1% Tween® 20) at RT, and mounted on Super Frost+®-treated glass slides using a paintbrush. Slices were dried at RT for 1 h in the dark, quickly (in less than 3 s) immersed in deionized water in a glass chamber, dried again for 1 h at RT in the dark, incubated for 1 h at 60°C in a dry oven, and dried again at RT overnight in the dark.

The slices were rehydrated by rapid immersion (for less than 3 s) in deionized water at RT. Excess liquid was removed with an absorbent paper, and a hydrophobic barrier was drawn. A drop of pure ethanol was applied on the slice for less than 3 s and removed using an absorbing paper. The slides were incubated at 100°C in a steamer, while ensuring that condensation did not fall back on them. A drop of preheated RNAscope® 1× Target Retrieval Reagent (Advanced Cell Diagnostics Inc.) was added to the steamer, and the slides were left for 15 min. Next, the slides were washed three times in deionized water at RT, and excess liquid was removed with absorbent paper. A drop of 100% ethanol was applied for 3 min, and excess liquid was then removed. A drop of RNAscope® Protease+ solution (Advanced Cell Diagnostics Inc.) was applied and slices were incubated at 40°C in a humid box for 30 min. Target retrieval treatment and RNAscope® Protease+ treatment were used to unmask the mRNAs. Lastly, the slides were washed three times with deionized water at RT. For neuronal assays (Fig. S2), several pre-treatment conditions were tested: no protease, Protease 3, Protease 4 and Protease+ of the RNAscope® Multiplex Fluorescent Reagent Kit v2 (Advanced Cell Diagnostics Inc.) during 10, 20, or 30 min.

FISH was performed using the RNAscope® Multiplex Fluorescent Reagent Kit v2 (Advanced Cell Diagnostics Inc.) and specific probes (Table S1; Fig. S3), according to the manufacturer's instructions. Following the FISH procedure, slides were incubated with a blocking solution (0.2% normal goat serum, 0.375% Triton X-100 and 1 mg ml^{-1} bovine serum albumin in 1× PBS) for 1 h at RT, incubated with the primary antibody overnight at 4°C (Table S1), rinsed three times with 1× PBS, and incubated with the secondary antibody (Table S1) for 2 h at RT. Lastly, the slides were washed three times in 1× PBS and mounted in Fluoromount-G® and DAPI (Southern Biotech).

Imaging

Images were acquired using a Yokogawa W1 Spinning Disk confocal microscope (Zeiss) with a 63× oil objective (1.4 numerical aperture). The imaging conditions and acquisition parameters were the same for all slides. The experimental PSF was obtained using carboxylate microsphere beads (diameter: 170 nm; Invitrogen/ThermoFisher Corp.). Except for DAPI, all channels were deconvoluted with Huygens Essential software (version 19.04, Scientific Volume Imaging, The Netherlands; http://svi.nl), using the classic maximum likelihood estimation algorithm and a signal-to-noise ratio of 50 (for the immunofluorescence channel) or 20 (for the FISH channel), a quality change threshold of 0.01, and 150 iterations at most.

AstroDot and AstroStat

As shown in the Results section, AstroDot can be used to study mRNA density and distribution not only in astrocytes but also in microglia immunolabelled for Iba1. In addition to FISH signals, AstroDot can be used to quantify any type of dot-shaped fluorescence signal. AstroStat was used to analyse the AstroDot results table, using an R script. The programs can be downloaded free of charge from https://github.com/pmailly/Astrocyte_RNA_Analyze and https://github.com/rtortuyaux/astroStat, respectively.

For AstroDot, an image analysis plug-in was developed for the ImageJ/Fiji software (Schindelin et al., 2012; Schneider et al., 2012), using Bio-Format (openmicroscopy.org), mcib3D (Ollion et al., 2013), GDSC (https://github.com) and local thickness (https://imagej.net/Local_Thickness) libraries.

ROIs enclosing each astrocyte were drawn by hand, using the Fiji polygon tool on the *Z*-projection of the stack, and using the ImageJ option 'Max intensity'. In the ROI Manager, the ROI names were coded as (roi_number-z_top-z_bottom) and saved in a zip file.

AstroDot processing

The plug-in was designed to process all images in a specific folder containing MetaMorph .nd files, and to read metadata images (channel name, z step, etc.), deconvoluted image channels (except for DAPI), and ROI zip files. Steps followed were as below:

1. AstroDot's parameters (the image folder, the channel order, the threshold method, etc.) were displayed in a dialogue box (see Fig. 2C).
2. The immunofluorescence background was estimated on whole images using a 0.5 median filter, a binary mask (using Li's threshold method), and an inversion of the binary mask (Li and Lee, 1993; Li and Tam, 1998). The immunofluorescence value was multiplied by the inverted mask and then divided by 255. The background value (bgThreshold) was defined as the mean intensity of all voxels other than those with a value of zero. To ascertain the background homogeneity, we also recommend this calculation is performed on individual ROIs to check that values are comparable.
3. For each ROI, a substack corresponding to zTop and zBottom (defined in the ROI name) was created for all channels.
4. For semi-automatic determination of the astrocyte or microglial cell nucleus, DAPI fluorescence was processed by removing DAPI potential background with a 'remove outliers size=15'. DAPI fluorescence was next segmented with the nuclei outline plugin from GSD. A binary mask and a three-dimensional watershed were finally generated to separate nucleus clusters (Otsu, 1979). An astrocyte nucleus was selected on the basis of its high GFAP immunofluorescence intensity, and was displayed in green. All other detected nuclei were displayed in red. A dialogue box enabled the user to confirm or correct the software's choice of nuclei.
5. The GFAP immunofluorescence was processed using a 0.5 median filter and a binary mask, using Li's threshold method (Li and Lee, 1993). The three-dimensional local thickness of the processes was used to generate a distance map and calculate the local process diameters.
6. For FISH dot channel processing, a value of 500 (a manual estimation of the background after deconvolution) was subtracted from each voxel. A difference of Gaussian filter (kernel: 3–1) and a binary mask were applied, using the threshold method defined in the "parameters"

dialogue box. The mean dot size volume was computed after the exclusion of dot clusters (volume >2 µm^3). For dot clusters (which arise when mRNAs are strongly expressed), the dot number was calculated by dividing the cluster by the previously determined mean dot size volume. For each dot, the mean intensity in the GFAP immunofluorescence channel and the distance map value (the process diameter) was calculated.

7. FISH dots were classified into one of three categories: (a) Dot 0 (in red) was a dot in the immunofluorescence background (without using the 'Specific mRNA' option only): mean GFAP immunofluorescence intensity ≤bgThreshold; distance to the boundary of the nucleus >2 µm. (b) Dot 1 (in yellow) was a dot in a fine process: mean GFAP immunofluorescence intensity >bgThreshold; distance to the boundary of the nucleus >2 µm; astrocyte process diameter <step in the z calibration (0.3 µm). (c) Dot 2 (green) was a dot in a large process: mean GFAP immunofluorescence intensity >bgThreshold; distance to the boundary of the nucleus >2 µm; astrocyte process diameter >step in the z calibration (0.3 µm); or a dot in the soma if the distance to the boundary of the nucleus ≤2 µm. Hence, Dots 1 and 2 were inside astrocytes, and Dots 0 were outside astrocytes.
8. For each image and for each computed ROI, a .csv output table was generated with the following headers: Image name; ROI name; Background intensity; Astrocyte volume; Dot density inside astrocytes (number of dots 1+number of dots 2)/astrocyte volume); Percentage of dots outside the astrocyte (number of dots 0/total dot number); Percentage of dots in astrocyte somata (number of dots less than 2 µm from the boundary of the nucleus/number of dots in astrocytes); Percentage of dots in fine processes (number of dots 1/number of dots in astrocytes); Percentage of dots in large processes [(number of dots 2–number of dots in somata)/number of astrocyte dots]; Mean astrocyte diameter. For each image and each ROI, the selected nucleus, astrocyte channel and classified dot populations were saved as .TIF images.

Astrostat

AstroStat was designed to: (i) define the template analysis using a checkbox (working directory, conditions to be compared, paired or unpaired analysis, or data normality plot); (ii) pool data appropriately for each mouse; (iii) test the normality of the data distribution of each group (using Shapiro's test). If there were more than 30 cells in each group, the central limit theorem was applied; (iv) test the equality of variances (using Fisher's test) for an unpaired analysis; and (v) compare the means using an unpaired or paired analysis. Student's *t*-test was used for normally distributed data and equal variances; Welch-Satterthwaite's test for a normal data distribution and unequal variances; Wilcoxon's test for non-normally distributed data; for paired analyses, a paired Student's *t*-test was used for normally distributed data; Wilcoxon signed rank test for non-normally distributed data. The threshold for statistical significance was set to $P<0.05$.

Acknowledgements

We thank Carole Escartin for the gift of APPswe/PS1dE9 mouse brain slices, and all members of the Orion imaging facility for their high-quality technical support.

Competing interests

The authors declare no competing or financial interests.

Author contributions

Conceptualization: M.O., R.T., P.M., M.C.-S.; Methodology: M.O., R.T., P.M., M.C.-S.; Software: M.O., R.T., P.M.; Validation: M.O., R.T., P.M., N.M., A.-C.B., M.C.-S.; Formal analysis: M.O., R.T., P.M., M.C.-S.; Investigation: M.O., R.T., P.M., N.M., A.-C.B., M.C.-S.; Resources: M.C.-S.; Data curation: M.C.-S.; Writing - original draft: M.C.-S.; Writing - review & editing: M.O., M.C.-S.; Visualization: M.O., M.C.-S.; Supervision: M.C.-S.; Project administration: M.C.-S.; Funding acquisition: M.C.-S.

Funding

This work was funded by the Fondation pour la Recherche Médicale (AJE20171039094; FDT201904008077 to N.M.). R.T. received a grant from the Journées de Neurologie de Langue Francaise. The creation of the Center for Interdisciplinary Research in Biology (CIRB) was funded by the Fondation Bettencourt Schueller.

Supplementary information

Supplementary information available online at
http://jcs.biologists.org/lookup/doi/10.1242/jcs.239756.supplemental

Peer review history

The peer review history is available online at
https://jcs.biologists.org/lookup/doi/10.1242/jcs.239756.reviewer-comments.pdf

References

Alvarez, J. I., Katayama, T. and Prat, A. (2013). Glial influence on the blood brain barrier. *Glia* **61**, 1939-1958. doi:10.1002/glia.22575

Aspelund, A., Antila, S., Proulx, S. T., Karlsen, T. V., Karaman, S., Detmar, M., Wiig, H. and Alitalo, K. (2015). A dural lymphatic vascular system that drains brain interstitial fluid and macromolecules. *J. Exp. Med.* **212**, 991-999. doi:10.1084/jem.20142290

Ben Haim, L., Carrillo-de Sauvage, M. A., Ceyzériat, K. and Escartin, C. (2015). Elusive roles for reactive astrocytes in neurodegenerative diseases. *Front. Cell. Neurosci.* **9**, 278. doi:10.3389/fncel.2015.00278

Borchelt, D. R., Ratovitski, T., van Lare, J., Lee, M. K., Gonzales, V., Jenkins, N. A., Copeland, N. G., Price, D. L. and Sisodia, S. S. (1997). Accelerated amyloid deposition in the brains of transgenic mice coexpressing mutant presenilin 1 and amyloid precursor proteins. *Neuron* **19**, 939-945. doi:10.1016/S0896-6273(00)80974-5

Boulay, A. C., Cisternino, S. and Cohen-Salmon, M. (2016). Immunoregulation at the gliovascular unit in the healthy brain: a focus on Connexin 43. *Brain Behav. Immun.* **56**, 1-9. doi:10.1016/j.bbi.2015.11.017

Boulay, A.-C., Saubaméa, B., Adam, N., Chasseigneaux, S., Mazaré, N., Gilbert, A., Bahin, M., Bastianelli, L., Blugeon, C., Perrin, S. et al. (2017). Translation in astrocyte distal processes sets molecular heterogeneity at the gliovascular interface. *Cell Discov.* **3**, 17005. doi:10.1038/celldisc.2017.5

Boulay, A.-C., Mazare, N., Saubaméa, B. and Cohen-Salmon, M. (2019). Preparing the astrocyte perivascular endfeet transcriptome to investigate astrocyte molecular regulations at the brain–vascular interface. *Methods Mol. Biol.* **1938**, 105-116. doi:10.1007/978-1-4939-9068-9_8

Brehar, F. M., Arsene, D., Brinduse, L. A. and Gorgan, M. R. (2015). Immunohistochemical analysis of GFAP-delta and nestin in cerebral astrocytomas. *Brain Tumor Pathol.* **32**, 90-98. doi:10.1007/s10014-014-0199-8

Burda, J. E. and Sofroniew, M. V. (2014). Reactive gliosis and the multicellular response to CNS damage and disease. *Neuron* **81**, 229-248. doi:10.1016/j.neuron.2013.12.034

Bushong, E. A., Martone, M. E., Jones, Y. Z. and Ellisman, M. H. (2002). Protoplasmic astrocytes in CA1 stratum radiatum occupy separate anatomical domains. *J. Neurosci.* **22**, 183-192. doi:10.1523/JNEUROSCI.22-01-00183.2002

Carney, K. E., Milanese, M., van Nierop, P., Li, K. W., Oliet, S. H., Smit, A. B., Bonanno, G. and Verheijen, M. H. (2014). Proteomic analysis of gliosomes from mouse brain: identification and investigation of glial membrane proteins. *J. Proteome Res.* **13**, 5918-5927. doi:10.1021/pr500829z

Challa, A. A. and Stefanovic, B. (2011). A novel role of vimentin filaments: binding and stabilization of collagen mRNAs. *Mol. Cell. Biol.* **31**, 3773-3789. doi:10.1128/MCB.05263-11

Chever, O., Lee, C. Y. and Rouach, N. (2014). Astroglial connexin43 hemichannels tune Basal excitatory synaptic transmission. *J. Neurosci.* **34**, 11228-11232. doi:10.1523/JNEUROSCI.0015-14.2014

Choi, K. C., Kwak, S. E., Kim, J. E., Sheen, S. H. and Kang, T. C. (2009). Enhanced glial fibrillary acidic protein-delta expression in human astrocytic tumor. *Neurosci. Lett.* **463**, 182-187. doi:10.1016/j.neulet.2009.07.076

Dallérac, G., Zapata, J. and Rouach, N. (2018). Versatile control of synaptic circuits by astrocytes: where, when and how? *Nat. Rev. Neurosci.* **19**, 729-743. doi:10.1038/s41583-018-0080-6

Dossi, E., Vasile, F. and Rouach, N. (2018). Human astrocytes in the diseased brain. *Brain Res. Bull.* **136**, 139-156. doi:10.1016/j.brainresbull.2017.02.001

Heiman, M., Kulicke, R., Fenster, R. J., Greengard, P. and Heintz, N. (2014). Cell type-specific mRNA purification by translating ribosome affinity purification (TRAP). *Nat. Protoc.* **9**, 1282-1291. doi:10.1038/nprot.2014.085

Heo, D. H., Kim, S. H., Yang, K. M., Cho, Y. J., Kim, K. N., Yoon, D. H. and Kang, T. C. (2012). A histopathological diagnostic marker for human spinal astrocytoma: expression of glial fibrillary acidic protein-delta. *J. Neurooncol.* **108**, 45-52. doi:10.1007/s11060-012-0801-z

Hol, E. M. and Pekny, M. (2015). Glial fibrillary acidic protein (GFAP) and the astrocyte intermediate filament system in diseases of the central nervous system. *Curr. Opin. Cell Biol.* **32**, 121-130. doi:10.1016/j.ceb.2015.02.004

Huber, F. M. and Hoelz, A. (2017). Molecular basis for protection of ribosomal protein L4 from cellular degradation. *Nat. Commun.* **8**, 14354. doi:10.1038/ncomms14354

Iadecola, C. (2017). The neurovascular unit coming of age: a journey through neurovascular coupling in health and disease. *Neuron* **96**, 17-42. doi:10.1016/j.neuron.2017.07.030

Kamphuis, W., Mamber, C., Moeton, M., Kooijman, L., Sluijs, J. A., Jansen, A. H. P., Verveer, M., de Groot, L. R., Smith, V. D., Rangarajan, S. et al. (2012).

GFAP isoforms in adult mouse brain with a focus on neurogenic astrocytes and reactive astrogliosis in mouse models of Alzheimer disease. *PLoS ONE* **7**, e42823. doi:10.1371/journal.pone.0042823

Kamphuis, W., Middeldorp, J., Kooijman, L., Sluijs, J. A., Kooi, E. J., Moeton, M., Freriks, M., Mizee, M. R. and Hol, E. M. (2014). Glial fibrillary acidic protein isoform expression in plaque related astrogliosis in Alzheimer's disease. *Neurobiol. Aging* **35**, 492-510. doi:10.1016/j.neurobiolaging.2013.09.035

Li, C. H. and Lee, C. K. (1993). Minimum cross entropy thresholding. *Pattern Recogn.* **26**, 617-625. doi:10.1016/0031-3203(93)90115-D

Li, C. H. and Tam, P. K. S. (1998). An iterative algorithm for minimum cross entropy thresholding. *Pattern Recognit. Lett.* **18**, 771-776.

Liddelow, S. A. and Barres, B. A. (2017). Reactive astrocytes: production, function, and therapeutic potential. *Immunity* **46**, 957-967. doi:10.1016/j.immuni.2017.06.006

Mathiisen, T. M., Lehre, K. P., Danbolt, N. C. and Ottersen, O. P. (2010). The perivascular astroglial sheath provides a complete covering of the brain microvessels: an electron microscopic 3D reconstruction. *Glia* **58**, 1094-1103. doi:10.1002/glia.20990

Middeldorp, J. and Hol, E. M. (2011). GFAP in health and disease. *Prog. Neurobiol.* **93**, 421-443. doi:10.1016/j.pneurobio.2011.01.005

Moeton, M., Stassen, O. M., Sluijs, J. A., van der Meer, V. W., Kluivers, L. J., van Hoorn, H., Schmidt, T., Reits, E. A., van Strien, M. E. and Hol, E. M. (2016). GFAP isoforms control intermediate filament network dynamics, cell morphology, and focal adhesions. *Cell. Mol. Life Sci.* **73**, 4101-4120. doi:10.1007/s00018-016-2239-5

Nolte, C., Matyash, M., Pivneva, T., Schipke, C. G., Ohlemeyer, C., Hanisch, U. K., Kirchhoff, F. and Kettenmann, H. (2001). GFAP promoter-controlled EGFP-expressing transgenic mice: a tool to visualize astrocytes and astrogliosis in living brain tissue. *Glia* **33**, 72-86. doi:10.1002/1098-1136(20010101)33:1<72::AID-GLIA1007>3.0.CO;2-A

Ogata, K. and Kosaka, T. (2002). Structural and quantitative analysis of astrocytes in the mouse hippocampus. *Neuroscience* **113**, 221-233. doi:10.1016/S0306-4522(02)00041-6

Ollion, J., Cochennec, J., Loll, F., Escudé, C. and Boudier, T. (2013). TANGO: a generic tool for high-throughput 3D image analysis for studying nuclear organization. *Bioinformatics* **29**, 1840-1841. doi:10.1093/bioinformatics/btt276

Otsu, N. (1979). A threshold selection method from gray-level histograms. *IEEE Trans. Sys. Man. Cyber* **9**, 62-66. doi:10.1109/TSMC.1979.4310076

Perng, M. D., Wen, S. F., Gibbon, T., Middeldorp, J., Sluijs, J., Hol, E. M. and Quinlan, R. A. (2008). Glial fibrillary acidic protein filaments can tolerate the incorporation of assembly-compromised GFAP-delta, but with consequences for filament organization and alphaB-crystallin association. *Mol. Biol. Cell* **19**, 4521-4533. doi:10.1091/mbc.e08-03-0284

Pilaz, L. J., Lennox, A. L., Rouanet, J. P. and Silver, D. L. (2016). Dynamic mRNA transport and local translation in radial glial progenitors of the developing brain. *Curr. Biol.* **26**, 3383-3392. doi:10.1016/j.cub.2016.10.040

Sakers, K., Lake, A. M., Khazanchi, R., Ouwenga, R., Vasek, M. J., Dani, A. and Dougherty, J. D. (2017). Astrocytes locally translate transcripts in their peripheral processes. *Proc. Natl. Acad. Sci. USA* **114**, E3830-E3838. doi:10.1073/pnas.1617782114

Schindelin, J., Arganda-Carreras, I., Frise, E., Kaynig, V., Longair, M., Pietzsch, T., Preibisch, S., Rueden, C., Saalfeld, S., Schmid, B. et al. (2012). Fiji: an open-source platform for biological-image analysis. *Nat. Methods* **9**, 676-682. doi:10.1038/nmeth.2019

Schmidt, Y., Biniossek, M., Stark, G. B., Finkenzeller, G. and Simunovic, F. (2015). Osteoblastic alkaline phosphatase mRNA is stabilized by binding to vimentin intermediary filaments. *Biol. Chem.* **396**, 253-260. doi:10.1515/hsz-2014-0274

Schneider, C. A., Rasband, W. S. and Eliceiri, K. W. (2012). NIH Image to ImageJ: 25 years of image analysis. *Nat. Methods* **9**, 671-675. doi:10.1038/nmeth.2089

Squarzoni, P., Oller, G., Hoeffel, G., Pont-Lezica, L., Rostaing, P., Low, D., Bessis, A., Ginhoux, F. and Garel, S. (2014). Microglia modulate wiring of the embryonic forebrain. *Cell Rep.* **8**, 1271-1279. doi:10.1016/j.celrep.2014.07.042

Stassen, O., van Bodegraven, E. J., Giuliani, F., Moeton, M., Kanski, R., Sluijs, J. A., van Strien, M. E., Kamphuis, W., Robe, P. A. J. and Hol, E. M. (2017). GFAPdelta/GFAPalpha ratio directs astrocytoma gene expression towards a more malignant profile. *Oncotarget* **8**, 88104-88121. doi:10.18632/oncotarget.21540

Sultan, S., Li, L., Moss, J., Petrelli, F., Cassé, F., Gebara, E., Lopatar, J., Pfrieger, F. W., Bezzi, P., Bischofberger, J. et al. (2015). Synaptic integration of adult-born hippocampal neurons is locally controlled by astrocytes. *Neuron* **88**, 957-972. doi:10.1016/j.neuron.2015.10.037

Thomsen, R., Daugaard, T. F., Holm, I. E. and Nielsen, A. L. (2013). Alternative mRNA splicing from the glial fibrillary acidic protein (GFAP) gene generates isoforms with distinct subcellular mRNA localization patterns in astrocytes. *PLoS ONE* **8**, e72110. doi:10.1371/journal.pone.0072110

van Bodegraven, E. J., van Asperen, J. V., Robe, P. A. J. and Hol, E. M. (2019). Importance of GFAP isoform-specific analyses in astrocytoma. *Glia* **67**, 1417-1433. doi:10.1002/glia.23594

van den Berge, S. A., Middeldorp, J., Zhang, C. E., Curtis, M. A., Leonard, B. W., Mastroeni, D., Voorn, P., van de Berg, W. D., Huitinga, I. and Hol, E. M. (2010). Longterm quiescent cells in the aged human subventricular neurogenic system specifically express GFAP-delta. *Aging Cell* **9**, 313-326. doi:10.1111/j.1474-9726.2010.00556.x

Verkhratsky, A., Nedergaard, M. and Hertz, L. (2015). Why are astrocytes important? *Neurochem. Res.* **40**, 389-401. doi:10.1007/s11064-014-1403-2

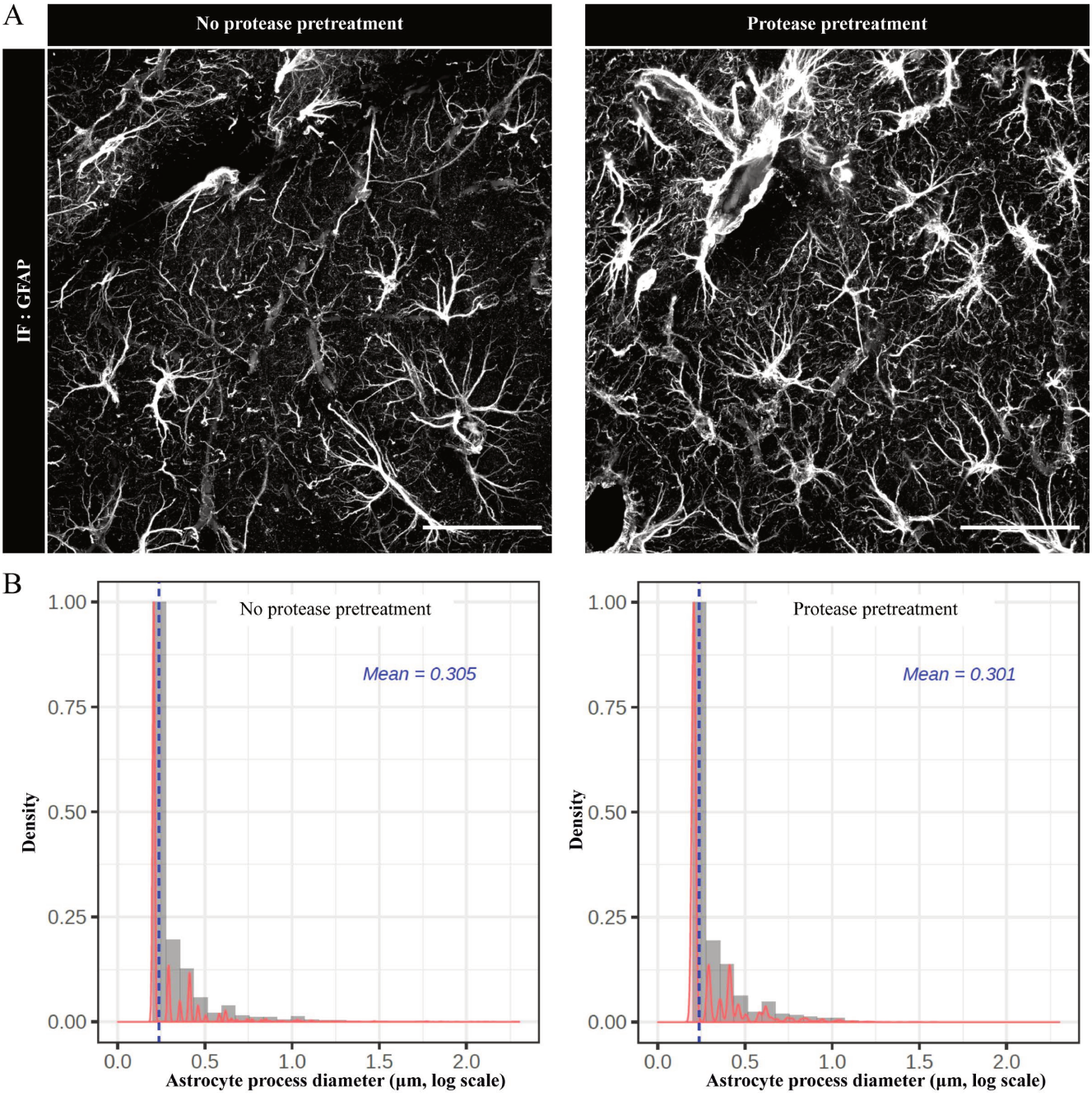

Figure S1: Comparison of GFAP immunolabelling in untreated and protease-treated brain sections. A. Confocal image projections of GFAP immunofluorescent detection in hippocampal sections untreated, or pre-treated with proteases. B. ImageJ analysis of the GFAP-immunolabeled process diameter using the ImageJ plugin *Astro_FineProcess*: For each ROIs, a substack corresponding to the zTop and zBottom was created for all channels. Images were filtered and

thresholded with same parameters as for AstroDot : Astrocyte GFAP channel was processed using a 0.5 median filter size and a binary mask using “Li” threshold method. 3D local thickness calculation was converted into an astrocyte distance map to access the local diameter of astrocyte processes. A skeleton was generated from the binary image mask and for each points, the diameter was extracted from the distance map image. Plots distributions of process diameters were generated in R. The grey bars represent the histograms of the diameter distribution (Gaussian curves in pink). The blue dotted line indicates the mean value of the diameter distribution. 52 astrocytes were analyzed for the untreated condition and 49 for the protease-treated. Scale bars: 50 µm.

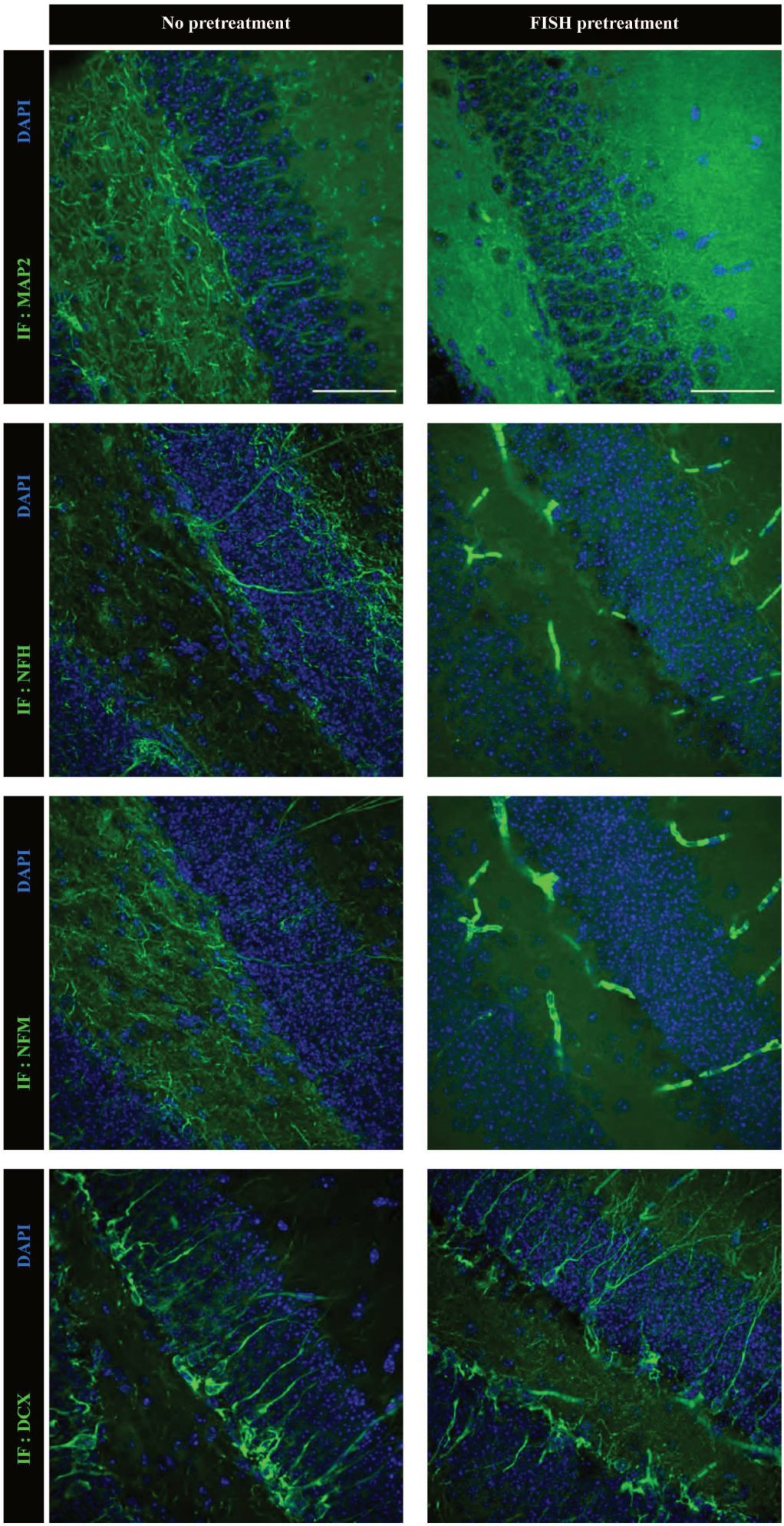
No pretreatment
FISH pretreatment
IF : MAP2
DAPI
IF : NFH
DAPI
IF : NFM
DAPI
IF : DCX
DAPI

Figure S2: Immunolabelling of the neurofilament medium (NF-M) and high (NF-H) chains, the microtubule-associated protein 2 (MAP2) and Doublecortin (DCX) in untreated and protease-treated brain sections. Projection confocal images. NFH and NFM were immunolabeled on the same brain section. In contrast to GFAP and Iba1, the recommended protease treatment used to unmask the mRNAs leads to the degradation of these neuronal epitopes. Scale bars: 50 µm.

Figure S3: FISH target sequences of Gfap α and Gfap δ

Target sequence for GFAP alpha exon 9 probes: Mus musculus glial fibrillary acidic protein (Gfap), transcript variant 2, mRNA NCBI Reference Sequence: NM_010277.3 (copied from emsembl.org)

TCATTAAGGACTCGAAGCAGGAGCACAAGGACGTGGTGATGTGAGGTGTGCCCACCTGG
TGGCCCTTGCCATGCAGTGTGAGGGCCCAAAGCTTATCCTCAAATAGTCCTGTTTGCCAG
GCTCAGTTCCCACCCACACCAGCACTTCCCTTCCTTCTGGTTTTCTGCCTGTGTGCTGCC
CAAGGCTCAATCAGTGCTAAGCTTCATAGATGGCATATACCCTTCACCTTCAACTAACAG
GATACTCACCCCAAAGGCGCAGTCAGGAGGGGAGGGAACCCCAGCTGGGTTAGAATTGGA
AGGGAAGAGGAAAGATGAGCAGAGTAGAGAGATTTAACAAATCACTTCCTTCATCCTTGT
TGTTATGGAAACCGTTGCCAGAGCTGGAAGTTTCCACAGGCTGCTGGAGCTAGACAACAA
TTCAGACAGAAAGGGAAAGTCCCTGAGGCAAAGTCTCTCTAGCCAGAGACCTATGCATCC
CGAATGGCCACTAAGGCAGTCCTGAAGGGCCCTCCAGGGTGATGACTCCAGTGTGTCAGC
CCCACTGAGCAGCTATGCAGGTTGACTGCCCACAGGCATGTGGAAACTTGGTTCTCAGCA
CTTGGCAGGATCTATGGCATAAGTGGAGAGGGAAGGTGTACTGGACGGCGGAGAGGAGGG
CTCCCTGGCCCCTAAGTGTGGATGCAGAGAGGTGGAGCCCAGGAAGGGTCTCTGCTTAGG
CTGCAGGGGTGCCAATGGCAGAGGCACTGGTAGAGATCATTTGGACACTGGAGTTGAAAG
TTACAGGCAATCTGTTACACTTGGCTCTGAATCCTATGAATCAAGGAAATAACCCGTTCT
CTGGAAGACACTGAAACAGGAGAGAGGGACTTCCGTCCACTGGGCAGGGTACAGATGTGT
CTCAGTTGTGAAGGTCTATTCCTGGCTGCACAGTCCCCATCCGCTCAGTCATCTTACCCT
GTGACTGCTCTCAGCCCTGAAGAATCCACAACCATCCTTCCAAGGTTCTCCATCCCCACA
ATGACTAGCTGTTGCTCTCCAAGCTAAGGGACCATTCCCTGTCTTATGCATATACGTAAT
GTCACCTATTTAGGTATCATCCTATTTGAGAGTTTGAGGAACTGAAACGTGTTGTGTTCA
AGCAGCCTGGTGGCTAGTGCCTTCATATTAGAGCACCTTCTCTGAGGCTGATTGGTGGGC
AGGTAGGGAAGACATTGAGCAGACAGTGTCCGCTCAGTTGTCCTTCCCTCCCTTCCAAGG
TCCCTCCCTCTTTCCAGGACATCGCCCCCCACACCCCACCCCTCCTTTCCACCTCCGCTAA
CCTCCAGAGCAGTACTGTCACCTTTACTCACTGGGCAGAAATAAAGACATGTGCCATAGA
CTTCCA

Target sequence for GFAP delta exon 8 probes: Mus musculus glial fibrillary acidic protein (Gfap), transcript variant 1, mRNA NCBI Reference Sequence: NM_001131020.1 (copied from emsembl.org)

GGGCAAAAGCACCAAAGAAGGGGAAGGCCAAAAAGTCACAAGACCTCTCAAAAGGCTCA
CAATACAAGTTGTCCCAATACAGGCTCACCAGATTGAAAATGGAGCCCTGCCAGCTCTCC
CTTAGATAGATTGCGTGCTCCAGCTCTCCCTTAGATAGAGGCGTGCTCCAGCTCTCCCTTA
GATAGAGGCGTGCTCCAGCTCTCCCTTAGATAGAGGCGTGCTCCAGCTCTCCCTTAGATA
GAGGCGTGCTCCAGCTCTCCCTTAGATAGAGGCGTGCTCCAGCTCTCCCTTAGATAGATG
CGCGCATTTCAGCCACACCTTTCCAGCTTGTCTTCTTCCTCCCAGGCCTCCTCTAAGGGA
CTGAACCATGTCCTTTGTCTAGAAGCTTCCAGGCCCACCCTAGGTCCTGGCTCTGTGTAA
TTAGGTTATACCGATAGAGCTAGCCTATGCTAAAGGTTAGGTTGTACTAACAGAGCTAGC
CTATGCTAAAGGTTAGGTTGTACTAATTAGAGCTAGTCTTATGCTAAAGGTTAGGTTGTAT
TAACAGAGCTAGCCTATGCTAAAGGTTAGGTTGTACTAACAGAGCTAGTCATGTTAAGTT
AGGTTGTACTAACAGAGCTAGCTTATGCTAAAGTTAGGTTGTACTAACATAGCTAGCCTA
TGCTAAAGGTTTGGTTGTACTAACAGAGCTGGCCTATGTTAAAGGTTAGGTTGTACTAAT
AGAGCTAGTCTTATGCTAAAGGTTAGGTTGTATTAACAGAGCTAACCTATGCTAAAGGTT
AGGTTGTACTAACAGAGCTGGCCTATGTTAAAGGTTAGGTTGTACTAATAGAGCTAGCCT
ATGCTAAAGGTTAGGTTGTACTAACAGAGCTGGCCTATGTTAAAGGTTAGGTTTTACTAA
TAGAGCTAGTCTTATGCTAAAGGTTAGGTTGTACTAACAGAGCGAGCCTATGCTAAAGAT
TAGGTTATATTAACAGAGCTAGCCTATGCTAAAGGTTAGGTTGTACTAATAGAGCTAGCC
TATGCTAAAGGTTAGGTTGTACTAATAGAGCTAGCCTATGCTAAAGGTTAGGTTGTATTA
ACAGAGCTAGCCAATGTTAAAGGCAGCAAGTCCCTGGGAGCTCCAAGGAGATACTCTGAA
CCCTCTGAGCAAATGCCTCCGGCTCACCAGTTTCTGTCGCTAGGTGGTCCCCTTGGGTCT
TGCAGTGCCTGTGGGCAGGCTCTGTGTTTGATTCATGTGTCCCCAGAGTTCTATTGCTTC
ACTTCAGTGCTGATTCAGCCCAGAGGGTTAGTTAGTTCCCTCTGGACGGCTGCTCTTGTA
GTGAATAAAGCTTTATGCTCCCTGCTCTTCATTTT

Table S1: Antibodies, qPCR and FISH probes and reagents

qPCR probes		
Gene name	**Supplier**	**Reference**
Gfap α RNA (mouse)	BioRad	10042961 (HEX) dMmuCNS635118061
Gfap δ RNA (mouse)	BioRad	10042958 (FAM) dMmuCNS795284650
Rpl4 RNA (mouse)	ThermoFisher Scientific	4331182 (FAM) Mm00834993_g1
45S RNA (mouse)	ThermoFisher Scientific	4426961 (FAM) Mm03985792_s1

FISH reagents		
Name	**Supplier**	**Reference**
RNAscope® Multiplex Fluorescent detection reagent V2	Advanced Cell Diagnostic	323110
RNAscope® H_2O_2 and Protease	Advanced Cell Diagnostic	322381
Fluoromount-G®	Southern Biotech	0100-01
Coverglass 0.13 – 0.17mm thick	Immuno Cell	65.300.13
SuperFrost® Plus slides	VWR	631-0108
Hydrophobic immunostaining pen	Vector laboratories	H-4000

FISH RNA probes			
Gene name	**Probe**	**Reference and supplier**	**Dilution**
Gfap α RNA	RNAscope® Probe – Mm-Gfap-O2-C2	557051-C2 Advanced Cell Diagnostic	1:1[e]
Gfap δ RNA	RNAscope® Probe – Mm-Gfap-03	557061 Advanced Cell Diagnostic	1:1[e]
Rpl4 RNA	RNAscope® Probe – Mm-Rpl4	535821 Advanced Cell Diagnostic	1:1[e]
FISH Fluorophore			
Name		**Reference and supplier**	**Dilution**
Opal 570		FP14488A Perkin Elmer	1:1500[e]
Opal 650		FP1496A Perkin Elmer	1:1500[e]

Antibodies		
Name	**Reference and supplier**	**Dilution**
Rabbit anti-Glial Fibrillary Acidic Protein (GFAP) antibody	G9269 Sigma	1:500[e]
Rabbit anti-Iba1	W1w019-19741 Sobioda	1:500[e]
Mouse anti-Neurofilament medium polypeptide (NFM)	Given by Dr. Beat M. RIEDERER, University of Lausanne, Switzerland	1:10[e]
Chicken anti-Neurofilament heavy polypeptide (NFH)	Ab4680 Abcam	1:500[e]
Rabbit anti-Doublecortin (DCX)	4604S Cell signaling	1:500[e]
Mouse anti-MAP2	M4403 Sigma-Aldrich	1:500[e]
Goat anti-Rabbit IgG (H+L) Highly Cross-Adsorbed Secondary Antibody, Alexa Fluor 488	A11034 Invitrogen	1:1000[e]
Goat anti-Rabbit IgG (H+L), Superclonal™ Recombinant Secondary Antibody, Alexa Fluor 647	A27040 Invitrogen	1:1000[e]

Table S2: Astrodot and Astrostat raw data for Gfap α and Gfap δ mRNAs in CA1 and CA3 hippocampal astrocytes from WT and APPswe/PS1dE9 mice
SD, standard deviation; N, number of cells analyzed

		Gfap α WT	SD	N	Non-Aβ-associated	SD	N	AB-associated	SD	N
RNA FISH density	*CA1*	1,59	0,7	175	2,11	1,21	127	8,06	4,66	27
	CA3	1,77	0,75	94	2,25	1,3	78	8,42	5,07	28
% RNA in the soma	*CA1*	11,49	6,77	175	10,16	4,91	127	7,96	4,6	27
	CA3	13,27	8,15	94	9,56	5,12	78	7,1	3,69	28
% RNA in large processes	*CA1*	12,44	4,42	175	11,79	4,54	127	9,61	2,88	27
	CA3	12,29	4,91	94	10,8	4,19	78	11,6	4,09	28
% RNA in fine processes	*CA1*	76,07	7,56	175	78,05	6,46	127	82,43	5,85	27
	CA3	74,45	7,61	94	79,64	7,04	78	81,3	5,6	28
% RNA in GFAP+ processes	*CA1*	59,48	9,04	175	59,29	7,8	127	60,07	7,71	27
	CA3	62,16	10,05	94	56,38	6,52	78	59,35	8,29	28
		Gfap δ WT	**SD**	**N**	**Non-Aβ-associated**	**SD**	**N**	**AB-associated**	**SD**	**N**
RNA FISH density	*CA1*	0,33	0,17	175	0,36	0,18	127	1,16	0,76	27
	CA3	0,35	0,17	94	0,36	0,18	78	1,24	0,77	28
% RNA in the soma	*CA1*	26,51	13,52	175	26,81	11,38	127	26,98	9,66	27
	CA3	28,5	16,39	94	25,2	12,1	78	24,85	14,09	28
% RNA in large processes	*CA1*	19,54	9,19	175	17,4	7,73	127	14,08	5,73	27
	CA3	17,64	9	94	14,79	6,84	78	13,81	4,73	28
% RNA in fine processes	*CA1*	53,95	14,67	175	55,79	11,21	127	58,94	9,47	27
	CA3	53,86	15,74	94	60,02	10,64	78	61,34	14,5	28
% RNA in GFAP+ processes	*CA1*	74,41	11	175	73,91	7,73	127	75,63	7,57	27
	CA3	74,66	12,41	94	69,01	8,43	78	73,66	8,75	28
		WT	**SD**	**N**	**Non-Aβ-associated**	**SD**	**N**	**AB-associated**	**SD**	**N**
Astrocyte volume (µm^3)	*CA1*	11541,3	4277,5	175	18264,9	6355	127	19550,01	8747,7	27
	CA3	10430,5	3842,5	94	18181,5	5395	78	15144,21	6640,6	28
Astrocyte process diameter (mean, in µm)	*CA1*	0,32	0,03	175	0,3	0,02	127	0,26	0,02	27
	CA3	0,32	0,04	94	0,29	0,02	78	0,29	0,02	28
Gfap α/ Gfap δ RNA	*CA1*	5,22	1,7	175	6,02	1,62	127	7,29	1,48	27
	CA3	5,25	1,42	94	6,13	1,38	78	7,14	2,19	28

Table S3: Comparison of AstroDot data for Gfap α and Gfap δ mRNAs between CA1 and CA3 hippocampal astrocytes in WT and APPswe/PS1dE9

SD, standard deviation; N, number of cells analyzed

CA1 versus CA3

		WT	Non-Aβ-associated	AB-associated
Astrocyte volume (µm³)	***Fold Change***	1,11	1,00	1,29
	p-value	3.57E-02 (*)	9.23E-01 (NS)	6.01E-02 (NS)
Mean astrocyte process diameter (µm)	***Fold Change***	1,00	1,03	0,90
	p-value	3.91E-01 (NS)	2.61E-02 (*)	5.87E-01 (NS)
Ratio Gfap α/ Gfap δ RNA	***Fold Change***	0,99	0,98	1,02
	p-value	9.08E-01 (NS)	6.27E-01 (NS)	7.67E-01 (NS)

		Gfap α			Gfap δ		
		WT	**Non-Aβ-associated**	**AB-associated**	**WT**	**AB-not associated**	**AB-associated**
RNA FISH density	***Fold Change***	0,90	0,94	0,96	0,94	1,00	0,94
	p-value	5.26E-02 (NS)	4.55E-01 (NS)	8.61E-01 (NS)	2.21E-01 (NS)	7.49E-01 (NS)	6.46E-01 (NS)
% RNA in the soma	***Fold Change***	0,87	1,06	1,12	0,93	1,06	1,09
	p-value	7.15E-02 (NS)	4.05E-01 (NS)	5.99E-01 (NS)	3.16E-01 (NS)	3.37E-01 (NS)	5.18E-01 (NS)
% RNA in large processes	***Fold Change***	1,01	1,09	0,83	1,11	1,18	1,02
	p-value	7.95E-01 (NS)	1.21E-01 (NS)	1.12E-01 (NS)	1.04E-01 (NS)	1.50E-02 (*)	1.00E00 (NS)
% RNA in fine processes	***Fold Change***	1,02	0,98	1,01	1,00	0,93	0,96
	p-value	9.36E-02 (NS)	1.01E-01 (NS)	4.67E-01 (NS)	9.65E-01 (NS)	8.13E-03 (**)	4.70E-01 (NS)
% RNA in GFAP+ processes	***Fold Change***	0,96	1,05	1,01	1,00	1,07	1,03
	p-value	2.60E-02 (*)	6.36E-03 (**)	7.39E-01 (NS)	8.67E-01 (NS)	3.20E-05 (****)	2.89E-01 (NS)

Table S4: Comparison of AstroDot data for Gfap α and Gfap δ mRNAs between WT and APPswe/PS1dE9 hippocampal astrocytes

SD, standard deviation; N, number of cells analyzed

APP/PS1dE9 versus WT						
			Not-Aβ-associated / WT	Aβ-associated / WT		
Astrocyte volume (µm^3)	CA1	*Fold Change*	1,58	1,69		
		p-value	1.80E-20 (****)	3.91E-06 (****)		
	CA3	*Fold Change*	1,74	1,45		
		p-value	1.22E-19 (****)	7.95E-06 (****)		
Astrocyte process diameter (mean, in µm)	CA1	*Fold Change*	0,94	0,81		
		p-value	3.16E-13 (****)	3.23E-08 (****)		
	CA3	*Fold Change*	0,91	0,91		
		p-value	3.21E-08 (****)	1.04E-04 (***)		
Gfap α/ Gfap δ RNA	CA1	*Fold Change*	1,15	1,40		
		p-value	5.05E-05 (****)	2.05E-08 (****)		
	CA3	*Fold Change*	1,17	1,36		
		p-value	6.12E-05 (****)	1.34E-04 (***)		
			Gfap α		Gfap δ	
			Not-Aβ-associated / WT	Aβ-associated / WT	Not-Aβ-associated/ WT	Aβ-associated / WT
RNA FISH density	CA1	*Fold Change*	1,33	5,07	1,09	3,52
		p-value	2.27E-05 (****)	3.66E-16 (****)	1.50E-01 (NS)	8.00E-14 (****)
	CA3	*Fold Change*	1,27	4,76	1,03	3,54
		p-value	4.81E-03 (**)	3.77E-12 (****)	6.85E-01 (NS)	7.94E-10 (****)
% RNA in the soma	CA1	*Fold Change*	0,88	0,69	1,01	1,02
		p-value	4.93E-02 (*)	3.86E-03 (**)	8.35E-01 (NS)	8.27E-01 (NS)
	CA3	*Fold Change*	0,72	0,54	0,88	0,87
		p-value	3.67E-04 (***)	5.53E-05 (****)	1.31E-01 (NS)	3.99E-01 (NS)
% RNA in large processes	CA1	*Fold Change*	0,95	0,77	0,89	0,72
		p-value	2.10E-01 (NS)	9.07E-04 (***)	2.92E-02 (*)	1.34E-03 (**)
	CA3	*Fold Change*	0,88	0,94	0,84	0,78
		p-value	3.53E-02 (*)	4.42E-01 (NS)	1.95E-02 (*)	1.71E-02 (*)
% RNA in fine processes	CA1	*Fold Change*	1,03	1,08	1,03	1,09
		p-value	1.76E-02 (*)	1.27E-05 (****)	2.18E-01 (NS)	2.83E-02 (*)
	CA3	*Fold Change*	1,07	1,09	1,11	1,14
		p-value	7.53E-06 (****)	1.24E-05 (****)	2.73E-03 (**)	2.67E-02 (*)
% RNA in GFAP+ processes	CA1	*Fold Change*	1,00	1,01	0,99	1,02
		p-value	8.54E-01 (NS)	7.46E-01 (NS)	6.42E-01 (NS)	5.16E-01 (NS)
	CA3	*Fold Change*	0,91	0,95	0,92	0,99
		p-value	1.02E-05 (****)	1.80E-01 (NS)	5.30E-04 (***)	4.30E-01 (NS)

Supplementary tables are available on BioRxiv

Table S5: Number of astrocytes analyzed per mouse and hippocampal regions

Number of astrocytes per mice				
Brain region	**Genotype**	**Mice identification number**	**Number of astrocytes analyzed**	**Total**
CA1	WT	009	51	
		013	70	
		017	54	175
CA3	WT	009	29	
		013	29	
		017	36	94
CA1	APPswe/PS1dE9 / not-Aβ associated	008	56	
		010	38	
		014	33	127
CA3	APPswe/PS1dE9 / not-Aβ associated	008	33	
		010	14	
		014	31	78
CA1	APPswe/PS1dE9/ Aβ associated	008	11	
		010	5	
		014	11	27
CA3	APPswe/PS1dE9/ Aβ associated	008	7	
		010	5	
		014	16	28

Journal of Cell Science • Supplementary information

II. Translational regulation by RACK1 in astrocytes represses KIR4.1 expression and regulates neuronal activity

Summary

Translation regulation in neurons has been shown to be performed by RNA-binding proteins (RBPs), cytoskeleton and ribosome associated proteins among others. These molecules regulate crucial neuronal functions as well as the brain physiology. However, these mechanisms are unknown in astrocytes. To tackle this question, we identified the proteins associated with astrocytic polyribosomes by Translating Ribosome Affinity Purification (TRAP) from Aldh1l1-eGFP/Rpl10a (BacTRAP) mice in which GFP fused ribosomes are found only in astrocytes, followed by mass spectrometry (MS). This approach led us to identify 249 candidate proteins corresponding mainly to ribosomal proteins, ribosome-associated proteins and cytoskeleton-associated proteins. In this proteome, we further focused on RACK1. RACK1 is a scaffolding protein involved in several cellular functions including regulation of translation by its association with the 40S subunit of ribosomes. We first showed that RACK1 was expressed in astrocytes by FISH and immunostaining. To understand its role in astrocytes, we investigated its association with a restricted panel of astrocytic specific RNAs. We found that *Kcnj10* coding for KIR4.1 and *Slc1a2* coding for GLT1 were the most associated with RACK1 in the whole astrocyte and in perisynaptic astrocytic processes (PAPs). To further deepen our knowledge for RACK1's function in astrocytes, we developed a mouse model in which RACK1 is deleted in astrocytes in the adult mouse (RACK1 cKO). We found that KIR4.1 was increased in both whole astrocyte and PAPs in the hippocampus while GLT1 levels remained unchanged. In RACK1 KO HEK cells, we found that this KIR4.1 increase was related to a translational regulation mediated by sequences of the 2nd half of *Kcnj10* 5'UTR. Since KIR4.1 regulates ion homeostasis, water exchange could be at play regulating the cell volume. In the mouse, we found that RACK1 cKO astrocytes were bigger and had more processes. Finally, KIR4.1 regulates K^+, a crucial synaptic function regulator and we found that RACK1 regulate neuronal transmission. Indeed, in RACK1 cKO mice, the depression of local field potentials of neurons due to high frequency stimulation in the hippocampus was less dramatic than in the control. This was not the case in low frequency stimulation or in the presence of a KIR4.1 specific inhibitor. In a multi electrode array experiment where hippocampal neurons were recorded as a network in pro epileptic conditions, RACK1 cKO neurons fired less frequently but with longer bursts.

This study is under review in *Cell reports*. I am first author.

In this work, I performed the TRAP and extracts for the mass spectrometry platform. I studied the analysed proteome and I performed the gene ontology analysis. I performed the FISH, immunostainings and western blots on the different astrocytic compartments. I did the RACK1 IP and TRAP and qPCR assays with the help of my students. I developed and bred the RACK1 cKO model. Clément Chapat and Clara Moch performed all *in vitro* studies. I helped Anne-Cécile Boulay injecting the viruses for the study of astrocyte morphology. I perfused the mice. I supervised Mathis Gaudey for the imaging, reconstruction and analysis of the astrocyte volumes. I helped Elena Dossi and Giampaolo Milior for electrohysiologycal experiments. Elena Dossi and Giampaolo Milior performed the local field potential experiments. Elena Dossi analysed the electrophysiology data. I helped writing the paper with Martine Cohen-Salmon and I built the figures.

Supplementary tables are available on BioRxiv

Translational regulation by RACK1 in astrocytes represses KIR4.1 expression and regulates neuronal activity

Marc Oudart [1], Katia Avila-Gutierrez [1], Clara Moch [2], Elena Dossi [1], Giampaolo Milior [1], Anne-Cécile Boulay[1], Mathis Gaudey [1], Julien Moulard [1], Bérangère Lombard [3], Damarys Loew [3], Alexis-Pierre Bemelmans [4], Nathalie Rouach [1], Clément Chapat [2], Martine Cohen-Salmon[1]

[1] Center for Interdisciplinary Research in Biology (CIRB), College de France, CNRS, INSERM, Université PSL, Paris, France.

[2] Laboratoire de Biochimie, Ecole polytechnique, CNRS, Université Paris-Saclay, Palaiseau, France.

[3] CurieCoreTech Spectrométrie de Masse Protéomique, Institut Curie, University PSL, Paris, France.

[4] CEA, Institut de Biologie François Jacob, Molecular Imaging Research Center (MIRCen), Fontenay-aux-Roses, France; CNRS, CEA, Université Paris-Sud, Université Paris-Saclay, Fontenay-aux-Roses, France.

Correspondence: martine.cohen-salmon@college-de-france.fr

Summary

The regulation of translation in astrocytes, the main glial cells in the brain, remains poorly characterized. We developed a high-throughput proteomic screen for polysome-associated proteins in astrocytes and focused on the ribosomal protein receptor of activated protein C kinase 1 (RACK1), a critical factor in translational regulation. In astrocyte somata and perisynaptic astrocytic processes (PAPs), RACK1 preferentially bound to a number of mRNAs, including *Kcnj10*, encoding the inward rectifying potassium (K^+) channel KIR4.1, a critical astrocytic regulator of neurotransmission. By developing an astrocyte-specific, conditional RACK1 knock-out mouse model, we showed that RACK1 repressed the production of KIR4.1 in hippocampal astrocytes and PAPs. Reporter-based assays revealed that RACK1 controlled *Kcnj10* translation through the transcript's 5' untranslated region. Upregulation of KIR4.1 in the absence of RACK1 modified the astrocyte territory volume and neuronal activity attenuatin burst frequency and duration in the hippocampus. Hence, astrocytic RACK1 represses KIR4.1 translation and influences neuronal activity.

Keywords: Astrocytes; RACK1; Translation; KIR4.1

Introduction

Astrocytes, the main glial cells in the brain, are large and highly ramified. They project long processes to neurons (perisynaptic astrocytic processes, PAPs) and brain blood vessels (perivascular astrocytic processes, PvAPs) and dynamically regulate synaptic and vascular functions through the expression of specific, polarized molecular repertoires (Cohen-Salmon et al., 2021; Dallerac et al., 2018). There are few data on the mechanisms that regulate translation in astrocytes. Translation is known to be mediated by cis-acting elements, including RNA motifs and secondary structures that influence the binding of trans-acting proteins (also known as RNA-binding proteins, RBPs) (Harvey et al., 2018). A few RBPs have been identified and studied in astrocytes (Blanco-Urrejola et al., 2021; Mazare et al., 2021). For example, *fragile-X* mental retardation protein (FMRP) has been shown to bind and transport mRNAs encoding autism-related signaling proteins and cytoskeletal regulators in radial glial cells (Pilaz et al., 2016). The selective loss of FMRP in astrocytes was shown to dysregulate protein synthesis in general and expression of the glutamate transporter GLT1 in particular (Higashimori et al., 2016). In the mouse, the expression of a pathological form of FMRP (linked to late-onset fragile X syndrome/ataxia syndrome) in astrocytes was found to impair motor performance (Wenzel et al., 2019). More recently, mRNAs enriched in PAPs were shown to contain a larger number of Quaking-binding motifs (Sakers et al., 2021), and inactivation of the cytoplasmic Quaking isoform QKI-6 in astrocytes altered the binding of a subset of mRNAs to ribosomes (Sakers et al., 2021). *Quaking* was also shown to regulate the differentiation of neural stem cells into glial precursor cells by upregulating several genes involved in gliogenesis (Takeuchi et al., 2020). Another general parameter of importance in the regulation of translation is the composition of the translation machinery itself, including ribosomal RNAs (rRNA) and proteins (Gay et al., 2022; Mauro and Matsuda, 2016). This aspect had not previously been studied in astrocytes. Lastly, RNA distribution and local translation are important, highly conserved mechanisms for translational regulation in most morphologically complex cells (Besse and Ephrussi, 2008). We and others have demonstrated that local translation occurs in astrocyte PvAPs and PAPs; this translation might sustain the cells' molecular and functional polarity (Boulay et al., 2017; Mazare et al., 2020b; Sakers et al., 2017).

To advance our understanding of translation mechanisms in astrocytes, we identified a pool of polysome-associated proteins in astrocytes by combining translating ribosome affinity purification (TRAP) (Mazare et al., 2020a) with mass spectrometry (TRAP-MS). We then focused on receptor of activated protein C kinase 1 (RACK1), a highly conserved eukaryotic protein that is involved in several aspects of translation. RACK1 is positioned at the head of the 40S subunit in the vicinity of the mRNA exit channel (Gallo and Manfrini, 2015; Nilsson et al., 2004). It regulates not only ribosome activities (such as frameshifting and quality-control responses) but also polysome localization and mRNA stability (Ikeuchi and Inada, 2016; Juszkiewicz et al., 2020). In the brain, RACK1 has been mainly described in neurons (Kershner and Welshhans, 2017b) and is involved in local translation and axonal guidance and growth (Kershner and Welshhans, 2017a). The changes in RACK1 expression observed in several neuropathological contexts (such as bipolar disorder (Wang and Friedman, 2001), Alzheimer's disease (Battaini and Pascale, 2005; Battaini et al., 1999), epilepsy (do Canto et al., 2020; Xu et al., 2015), addiction (McGough et al., 2004), amyotrophic lateral sclerosis (Russo et al., 2017), and Huntington's disease (Culver et al., 2012)) indicate the importance of the protein's physiological role in the brain.

In the present study, we demonstrate that RACK1 associates with specific mRNAs, represses the translation of *Kcnj10* mRNA (encoding the inward rectifying K^+ channel KIR4.1), and regulates neuronal activity.

Results

Identification of polysome-associated proteins in astrocytes

We used TRAP-MS to identify polysome-associated proteins in astrocytes **(Fig. 1A)**. Enhanced green fluorescent protein (eGFP)-tagged polysomal complexes were immunopurified from whole brain cytosolic extracts prepared from 2-month-old Aldh1l1:L10a-eGFP transgenic BacTRAP (BT) mice. These animals express the eGFP-tagged ribosomal protein RPL10a specifically in astrocytes (Heiman et al., 2008) **(Fig 1A)**. The same experiment was performed on brain samples from C57/BL6 (wild type) mice, as a control **(Fig 1A)**. A Western blot analysis of immunoprecipitated proteins showed that RPL10a-GFP and the ribosomal protein S6 (RPS6, a component of the 40S ribosomal subunit) were present in BT immunoprecipitates only – demonstrating the efficiency and specificity of TRAP-MS **(Fig. 1B)**. Extracted proteins were characterized using proteomics and quantitative label-free tandem MS (LC-MS-MS) **(Fig 1A, C)**.Three proteins were found only in WT extracts and 139 were found only in BT extracts (fold changes (FC): – or +∞), 61 proteins were enriched in WT extracts (p-value < 0.05; Log2 FC < -1), 106 proteins were detected in both WT and BT extracts (p-value < 0.05; -1 < Log2 FC < 1), and 110 proteins were enriched in BT extracts (p-value < 0.05; Log2 FC > 1) **(Fig. 1C; Table 1; Table S1).** A Gene Ontology (GO) analysis of the 249 proteins enriched or specifically identified in BT immunoprecipitates indicated that most were ribosomal proteins (26%) or RBPs (39.1%) involved in ribosome biogenesis (22.7%) and gene expression (30.9%) (**Fig. 1D)**. We were able to identify a set of polysome-associated proteins in astrocytes.

RACK1 associates with polysomes in astrocytes

Among the ribosome-associated proteins preferentially extracted with TRAP-MS, we focused on RACK1. This protein binds to the small ribosomal subunit 40S and has a key role in the translation of capped, polyadenylated mRNAs (Johnson et al., 2019) (**Fig. 2A**). RACK1's role in astrocytes had not been assessed previously. However, we recently identified *Gnb2l1* mRNA (encoding RACK1) as one of the most highly enriched, translated mRNAs in PAPs; this finding suggested that RACK1 has an important role at this cellular interface (Mazare et al., 2020b); A Western blot analysis of TRAP-MS

immunoprecipitated proteins showed that RACK1 was specifically detected in the BT condition and thus confirmed the co-immunoprecipitation of RACK1 with astrocytic polysomes (**Fig. 2B**). We next characterized RACK1 expression in astrocytes, with a focus on samples from hippocampus. We used fluorescent *in situ* hybridization (FISH) to detect *Gnb2l1* mRNAs in astrocytes **(Fig. 2C)**. Since *Gnb2l1* is ubiquitous, we immunolabeled astrocytes for GFAP. The *Gnb2l1* FISH dots localized on GFAP processes were identified using our recently developed *Astrodot* protocol (Oudart et al., 2020). In line with our previous results, *Gnb2l1* mRNAs were detected somewhat in astrocyte somata but mainly in astrocytic processes (Mazare et al., 2020b) **(Fig. 2C)**. We next performed immunofluorescence imaging of RACK1 on hippocampal sections **(Fig. 2D)**. RACK1 was clearly detected in neurons and GFAP-immunolabeled astrocytic soma and processes (**Fig. 2D**). These results suggested that RACK1 is expressed in astrocytes and associates with astrocytic polysomes.

RACK1 associates with specific mRNAs in astrocytes and in PAPs

We next determined which mRNAs were associated with RACK1 in astrocytes via mRNA immunoprecipitation (using a RACK1-specific antibody) of whole brain astrocytic cytoplasmic extracts prepared from 2-month-old mice. We first checked the efficiency of RACK1 immunoprecipitation on Western blots. Increasing levels of anti-RACK1 antibody indeed immunoprecipitated higher levels of RACK1 and the small subunit ribosomal protein RPS6 (**Fig. 3A**). We then repeated the experiment with the optimal quantity of RACK1 antibody, extracted the immunoprecipitated mRNAs, and analyzed them with qPCRs (**Fig. 3B**). Nonspecific mouse immunoglobulins G (IgG) were used as a negative control (**Fig. 3B**). Extracts prepared from whole brain were immunoprecipitated (**Fig. 3C**). RACK1 was present in astrocyte processes (**Fig. 2D**) and was preferentially translated in hippocampal PAPs (Mazare et al., 2020b). We therefore also immunoprecipitated RACK1 in synaptogliosome preparations consisting of PAPs attached to synaptic neuronal membranes (Carney et al., 2014) (**Fig. 3C'**). Since RACK1 is ubiquitously expressed in the brain, we limited our analysis on a selection of astrocyte-specific mRNAs and focused on those detected previously in PAPs (Mazare et al., 2020b), such as *Kcnj10*, encoding the inward rectifying K^+ channel KIR4.1, *Slc1a2*, encoding the glutamate transporter GLT1, *Aqp4*, encoding the water channel aquaporin 4, *Slc1a3*, encoding the glutamate transporter GLAST, and *Gja1* and *Gjb6*,

encoding the gap junction proteins connexin 43 and 30, respectively. With the exception of *Gjb6,* all the tested mRNAs were immunoprecipitated more significantly by RACK1 than by IgG in whole brain (**Fig. 3C)** and synaptogliosome extracts (**Fig. 3C'**). These results were probably influenced by the level of polysomal mRNAs in astrocytes and PAPs. We therefore determined the level of each polysomal mRNA in astrocytes and PAPs by performing TRAP and qPCRs on whole-brain extracts from 2-month-old BT mice (**Fig. 3D, E**) or on synaptogliosome extracts (**Fig. 3D, E'**). The mean value for each mRNA was then used to normalize the quantity of RACK1-immunoprecipitated mRNA (**Fig. 3F)** in whole brain (**Fig. 3G**) and in synaptogliosomes (**Fig. 3G'**). The results of these experiments suggested that *Slc1a2* and *Kcnj10* were preferentially associated with RACK1 in astrocytes (**Fig 3G**) and in PAPs (**Fig. 3G'**).

Taken as a whole, these results suggested that RACK1 associates preferentially with specific mRNAs in astrocytes and in PAPs.

RACK1 represses the expression of *Kcnj10* in astrocytes

To gain insights into RACK1's function in astrocytes, we generated a RACK1 conditional knock-out mouse model (RACK1 cKO) by crossing RACK1 fl/fl mice with Aldh1L1-CreERT2 mice (**Fig. 4A**). Two month-old Aldh1L-CreERT2: RACK1 fl/fl mice were injected with tamoxifen, to induce RACK1 KO in astrocytes (**Fig 4A**). *Gnb2l1* KO in astrocytes was confirmed by PCRs on DNA extracted from whole brain (**Fig. 4B**) and by immunofluorescence assays of hippocampal sections (**Fig. 4C**). In the cKO mice, RACK1 was detected in pyramidal layer neurons but not in astrocytes immunolabelled for GFAP (**Fig. 4C**). We next sought to determine the impact of RACK1 KO in astrocytes on the level of GLT1 and KIR4.1 in whole hippocampus or hippocampal synaptogliosome protein extracts from RACK1 fl/fl and RACK1 cKO mice (**Fig. 4D**). Interestingly, the various extracts did not differ significantly with regard to the level of GLT1 but the level of KIR4.1 was significantly higher in the two extracts from RACK1 cKO mice (**Fig. 4D**).

These results demonstrated that RACK1 deficiency in astrocytes led to a higher level of KIR4.1 in whole astrocytes and in PAPs.

In cellulo* translational control by RACK1 depends on the 5' untranslated region (5'UTR) of *Kcnj10

RACK1 is an essential factor in translation and in ribosome quality control. It senses ribosome stalling on rare codons (such as CGA, coding for arginine, and AAA, coding for lysine) and can cause translation elongation to pause or abort. The absence of RACK1 results in the more frequent translation of mRNAs with stalling sequences and eventually the accumulation of peptides with frameshifts (Juszkiewicz et al., 2020). Since we observed RACK1-dependent downregulation of *Kcnj10*, we first hypothesized that the *Kcnj10* gene's coding sequence (CDS) is subject to a stalling event that can only be resolved by RACK1. To test this hypothesis, we generated Human Embryonic Kidney 293T (HEK293T) cells in which RACK1 expression was disrupted through a CRISPR/Cas9-based strategy ($RACK1^{KO}$ cells; **Fig. 5A**). We then designed a dual fluorescence reporter system in which GFP and mCherry fluorescent proteins were expressed in-frame from a single mRNA and were separated by the *Kcnj10* CDS (**Fig. 5B**). The *Kcnj10* CDS was insulated with viral P2A sequences, at which ribosomes skip the formation of a peptide bond without interrupting elongation (Lin et al., 2013). Complete translation of this cassette generates three proteins (GFP, mKIR4.1, and mCherry), and the presence of any stall-inducing sequences in *Kcnj10* CDS would modify the translation rate prior to mCherry synthesis and would thus result in a sub-stoichiometric mCherry:GFP ratio. A reporter without *Kcnj10* CDS served as a negative control. The positive control was a reporter in which *Kcnj10* CDS had been replaced by a sequence containing a stretch of consecutive lysine AAA codons (termed K20) and that was known to induce ribosome stalling (**Fig.S1A**) (Juszkiewicz and Hegde, 2017). These reporters were expressed in WT and $RACK1^{KO}$ cells, and the mCherry:GFP ratio was measured at the single-cell level using fluorescence-activated cell sorting (**Fig. 5C, Fig. S1B**). We found that $RACK1^{KO}$ cells displayed a robust elevation of the mCherry level expressed downstream of the K20 sequence, confirming that loss of RACK1 impairs ribosome stalling (**Fig. S1B, C**). In contrast, the absence of RACK1 did not modify the mCherry/GFP ratio of the reporter cassette containing *Kcnj10* CDS, when compared with WT cells (**Fig. 5C, D**). Taken as a whole, these data indicate that the sensitivity of the *Kcnj10* mRNA with regard to RACK1 is not mediated by a RACK1-modulated ribosomal event involving its CDS.

We next sought to determine whether *Kcnj10*'s sensitivity to RACK1 was conferred by its 5'UTR. Two distinct 5'UTRs have been reported for *Kcnj10* in the mouse (NM_001039484.1 and AB039879.1, hereafter referred to respectively as 5'UTR#1 and 5'UTR#2). 5'UTR#1 is composed of a G/C-rich first half (region 1-104, not found in other mammalian *Kcnj10* orthologs) and a highly conserved second half (the 147-242 region which is shared with 5'UTR#2) (**Fig. S2A, Fig. 5E**). 5'UTR#1 and 5'UTR#2 were inserted in the psiCHECK-2 luciferase reporter vector downstream of the *Renilla* luciferase (RLuc) CDS (**Fig. 5E**). A reporter harboring the 3'UTR of *Kcnj10* upstream of RLuc was also constructed as a control. These reporters were transfected into WT and RACK1^{KO} HEK293T cells, and the effect of RACK1 loss on RLuc activity for each UTR construct was calculated relative to an empty psiCHECK2 reporter level (control RLuc). RLuc activity was normalized against the activity of the co-expressed FLuc (**Fig. 5F**). We detected significantly greater RLuc activity when the RLuc reporters harboring *Kcnj10* 5'UTRs were expressed in RACK1^{KO} cells (relative to expression in WT cells) (**Fig. 5F**). In contrast, no difference between WT and RACK1^{KO} cells was observed for the RLuc-Kcnj10 3'UTR construct – indicating that translational control by RACK1 is mediated by *Kcnj10* 5'UTRs (**Fig. 5F**). A qPCR analysis did not show significant differences in RLuc mRNA levels under any conditions, which confirmed that the *Kcnj10* 5'UTR-mediated effect on RLuc activity was post-transcriptional (**Fig. S3A,B**). Since 5'UTR#1 and 5'UTR#2 share a common 96-nucleotide region (**Fig. S2B**), we hypothesized that this sequence confers RACK1-dependent translation control. To test this hypothesis, we truncated the 242-nucleotide-long *Kcnj10* 5'UTR#1 into five overlapping fragments, which were inserted upstream of the RLuc sequence and expressed in WT and RACK1^{KO} cells (**Fig. 5G**). We found that both the 127-242 region and the shorter 181-242 region were sufficient to increase the RLuc activity in RACK1^{KO} cells (relative to WT cells), whereas the first half (region 1-146) did not confer RACK1 sensitivity (**Fig. 5G, H**).

Taken as a whole, these data demonstrate that RACK1's control over the translation of *Kcnj10* mRNA depends on the *Kcnj10* 5'UTR rather than its CDS or 3'UTR.

RACK1 regulates astrocyte volume

KIR4.1 is a weakly inwardly rectifying K^+ channel that confers astrocytes with high K^+ conductance. K^+ influx into astrocytes is thought to be coupled to water intake, leading to transient or prolonged swelling (MacVicar et al., 2002; Risher et al., 2009). Thus, elevation of KIR4.1 levels in RACK1 cKO might be associated with a greater hippocampal astrocyte volume. We used an adeno-associated virus (AAV) bearing the gfaABC1D synthetic promoter (derived from Gfap; (Lee et al., 2008)) to drive the expression of the fluorescent protein tdTomato in astrocytes. AAVs were injected into the CA1 region of the dorsal hippocampus of adult mice (**Fig. 6A**). A three-dimensional (3D) analysis was performed on sparse labelled CA1 hippocampal astrocytes from 2-month-old WT and RACK1 cKO mice (**Fig. 6B-F**). RACK1 cKO astrocytes had a larger territory volume (**Fig. 6D**) and longer distal processes **(Fig. 6F)** than RACK1 fl/fl astrocytes.

These results indicated that astroglial RACK1 is required for a correct hippocampal astrocyte territory volume.

RACK1 regulates neuronal activity

During their activity, neurons release large amounts of K^+ at the synapses. The K^+ is rapidly taken up by astrocytic KIR4.1 and is redistributed across the astrocytic network. This astrocytic K^+ clearance mechanism maintains perisynaptic homeostasis and prevents neuronal hyperexcitability. Since we had shown that RACK1 cKO astrocytes contained high levels of KIR4.1, we sought to determine whether this change alters basal excitatory synaptic transmission. To this end, we stimulated CA1 Schaffer collateral (SC) synapses in acute hippocampal slices and thus evoked α-amino-3-hydroxy-5-methyl-4-isoxazolepropionic acid receptor (AMPAR)-mediated field excitatory postsynaptic potentials (fEPSPs) (**Fig. 7A**). The size of the presynaptic fiber volley (the input) was compared with the slope of the fEPSP (the output). RACK1 cKO mice and control RACK1 fl/fl mice did not differ with regard to basal synaptic transmission (**Fig. 7B**). We next investigated the effect of the KIR4.1 K^+ channel blocker VU0134992 (30 μM) and found a similar overall decrease in excitatory synaptic transmission in both RACK1 fl/fl and RACK1 cKO animals after 20 minutes of application (**Fig. 7B**). These results indicate that the elevated expression of astrocytic KIR4.1 K^+ channels in RACK1 cKO mice does not modify hippocampal basal excitatory synaptic transmission evoked in the hippocampal CA1 region.

We reasoned that the elevated expression of KIR4.1 K^+ channels in RACK1 cKO astrocytes and the consequent enhancement in K^+ buffering capacity might have major roles during intense neuronal activity. To test this hypothesis, we repeatedly stimulated SCs (10 Hz, 30 s) and analyzed the fEPSPs in CA1 region of the hippocampus. This stimulation induced rapid synaptic facilitation and then depression (**Fig. 7C**), which results from depletion of the presynaptic glutamate pool. Facilitation was greater and depression was slower in RACK1 cKO slices than in RACK1 fl/fl slices (**Fig. 7D**). This finding indicates that the elevated expression of KIR4.1 K^+ channels in RACK1 cKO mice sustains repetitive excitatory synaptic activity. Accordingly, KIR4.1 K^+ channel inhibition by VU0134992 (30 μM, for 20 min) had more of an effect on synaptic facilitation and depression in RACK1 cKO mice than in RACK1 fl/fl mice (**Fig. 7D**). Indeed, in the presence of VU0134992, repetitive stimulation-induced facilitation and subsequent depression were similar in RACK1 fl/fl and RACK1 cKO mice (**Fig. 7D**). These results indicate that astrocytic RACK1 regulates neuronal activity in response to repetitive stimulation by controlling the expression of KIR4.1 K^+ channel.

We next tested the impact of RACK1 on recurrent burst activity. This was induced in hippocampal slices by incubation in a pro-epileptic artificial cerebrospinal fluid (ACSF) (Mg^{2+}-free with 6 mM KCl (0Mg6K ACSF)). We recorded neuronal bursts in all hippocampal regions by using the multi-electrode array (MEA) technique (**Fig. 7E**). We found that bursts were less frequent and last for longer in RACK1 cKO mice than in RACK1 fl/fl mice (**Fig. 7F, G**). Hence, the burst rate under pro-epileptic conditions appeared to be better controlled in astrocytic RACK1 cKO mice than in RACK1 fl/fl mice. To check whether this was due to more efficient buffering of extracellular K^+ released during sustained activity, we recorded burst activity in RACK1 fl/fl and RACK1 cKO slices in the presence of VU0134992 (30 μM). In RACK1 fl/fl mice, 15-25 min of inhibition of the KIR4.1 K^+ channel by VU0134992 was associated with a transient increase in burst frequency that was likely due to the neuronal depolarization caused by extracellular K^+ accumulation. This was followed (after >30 min of VU0134992 exposure) by a long-lasting decrease in burst frequency, which probably resulted from the accumulation of excess extracellular K^+ (**Fig. 7H, top, left**). There was no effect on burst duration (**Fig. 7H, bottom, left**). Interestingly, this dual regulation of burst frequency was not observed in RACK1

cKO mice (**Fig. 7H, top, right**), which showed only a decrease in burst duration after >30 min treatment with VU0134992 (**Fig. 7H, bottom, right**). These results indicate that by controlling KIR4.1 expression and the associated K^+ buffering capacity in astrocytes, RACK1 helps to modulate the firing rate when neuronal activity is sustained.

Collectively, our results show that RACK1 associates with specific mRNAs in astrocytes and, in particular, represses the translation of *Kcnj10* mRNA. This translational effect is mediated by the *Kcnj10* gene's 5'UTR. RACK1 cKO in astrocytes is associated with higher KIR4.1 levels overall and in PAPs; in turn, this affects astrocyte volume and attenuates recurrent neuronal burst activity.

Discussion

The objective of the present study was to investigate the molecular mechanisms that regulate translation in astrocytes. We developed a TRAP method for purifying polysome-associated proteins in astrocytes and focused on the 40S-associated protein RACK1, a critical factor in translational regulation (Gallo and Manfrini, 2015; Nielsen et al., 2017). We demonstrated that RACK1 interacts with specific mRNAs in astrocytes and PAPs, represses the translation of *Kcnj10* (encoding KIR4.1), and thus impacts astrocyte volume and neurotransmission.

The TRAP technique that we used to purify astrocyte polysomes was originally developed for the analysis of polysomal mRNAs (Doyle et al., 2008). Here, we demonstrated that TRAP was compatible with MS. As expected, the most abundant immunopurified proteins were ribosomal or translation complex-associated proteins, although other proteins were also identified. The most highly represented cytoskeletal associated proteins in our screen included Ckap4 (CLIMP63), an endoplasmic reticulum (ER) integral membrane protein that binds to microtubules and promotes ER tubule elongation (Vedrenne et al., 2005). Interestingly, Ckap4 has a crucial role in the dendritic organization of the ER in neurons (Cui-Wang et al., 2012). The cytoplasmic linker associated protein CLASP2 mediates asymmetric microtubule nucleation in the Golgi apparatus and is crucial for establishing the latter's continuity and shape (Miller et al., 2009). CLASP2 cytoskeleton-related mechanisms have been shown to underlie microtubule stabilization, neuronal polarity and synapse formation and activity (Beffert et al., 2012). These proteins might be candidates for the regulation of translation in astrocytes. In contrast, our experiments did not pinpoint all the known RBPs in astrocytes; for instance, we did not detect Qki, which was recently shown to regulate translation in astrocytes (Radomska et al., 2013; Sakers et al., 2021). Thus, the TRAP-MS technique probably does not give a comprehensive view of the ribosome-associated proteome in the astrocyte. However, it is cell-specific and so might be a powerful approach for identifying some of the key post-transcriptional regulators in astrocytes.

Among the astrocytic ribosome-associated proteins identified in our screen, we focused on the highly enriched RACK1. Interestingly, use of a selection of astrocyte-specific mRNAs enabled us to determine the preferential association of RACK1 with *Kcnj10* and *Slc1a2* mRNAs. This finding

indicated that RACK1-containing ribosomes associate with specific mRNAs in astrocytes and probably confer specific translational properties on the ribosomes. Along the same lines, it has been shown that ribosomes with different stoichiometries of RACK1 translate different subsets of mRNAs (Coyle et al., 2009). RACK1 was also recently described as one of the ribosomal proteins translated in neurites and able to rapidly go on and off the ribosomes in neurons – suggesting strongly that RACK1-containing ribosomes have specific functions (Fusco et al., 2021). Taken as a whole, these data suggest that RACK1 is involved in ribosome filtering mechanisms (Mauro and Matsuda, 2016). It remains to be seen how the interaction between RACK1-containing ribosomes and specific mRNAs is achieved but various elements might be involved in this process. RACK1 has been shown to discriminate between mRNAs according to their length and to promote the translation of mRNAs with a short open reading frame (Thompson et al., 2016). In viruses, RACK1 might mediate the translation of mRNAs with an internal ribosome entry site (Majzoub et al., 2014). Other studies have demonstrated that RACK1 controls translation by sensing 5'UTR sequences and structures (Gallo et al., 2018).

Here, we showed that cell-selective RACK1 KO led to higher levels of KIR4.1 in astrocytes and in PAPs, indicating that RACK1 represses *Kcnj10* translation. RACK1 has been shown to control important aspects of ribosome quality control by sensing stalled ribosomes on polyarginine or proline codons and contributing to the degradation of nascent protein chains on stalled ribosomes (Juszkiewicz et al., 2020; Kuroha et al., 2010; Sitron et al., 2017; Sundaramoorthy et al., 2017). We further confirmed this effect on a lysine AAA sequence. However, we showed that this type of mechanism does not operate on the *Kcnj10* CDS – indicating that the increase in KIR4.1 seen after RACK1 KO is not related to a ribosomal readthrough mechanism. In contrast, we showed that the RACK1-mediated control of *Kcnj10* relied on specific 5'UTR sequences. It now remains to be determined how this regulatory mechanism operates. With regard to RACK1's mRNA selectivity, this question reamins extremely complex because several mechanisms might be involved. RACK1 recruits and controls the activity of translation factors like the elongation factor eIF6 (Rollins et al., 2019). RACK1 is known to interact with components of the microRNA-induced gene silencing complex. This interaction recruits the complex to the translation site and facilitates gene repression (Jannot et al., 2011). Baum et al. suggested that recruitment of the mRNA-binding protein Scp160 to the yeast homolog (Asc1p) of RACK1 may influence the translation

of specific mRNAs (Baum et al., 2004). On the same lines, changes to the translation machinery recruited on the *Kcnj10* 5'UTR might occur in the absence of RACK1, which would change the ribosomal translational efficiency.

In previous research, we demonstrated that the RACK1-encoding gene *Gnb2l1* is preferentially translated in PAPs. This suggests that RACK1-ribosome composition in astrocytes is not homogenous and that RACK1 exerts its translational control preferentially in PAPs (Mazare et al., 2020b). We also determined that *Kcnj10* polysomal mRNAs are present in PAPs (Mazare et al., 2020b). In neuronal processes, the plasticity of ribosomal protein composition involves RACK1 (Fusco et al., 2021). Here, we found that RACK1 was associated with *Kcnj10* mRNAs in astrocytes in general but also in PAPs in particular. Moreover, we found that PAP levels of KIR4.1 were lower in the absence of RACK1. Taken as a whole, these data indicate that RACK1 regulates KIR4.1 translation not only in astrocytes in general but also locally in PAPs.

KIR4.1 is a weakly inwardly rectifying K^+ channel; in astrocytes, it helps to maintain the resting membrane potential, high K^+ conductance, volume regulation, and glutamate uptake (Chever et al., 2010; Djukic et al., 2007; Juszkiewicz and Hegde, 2017; Kucheryavykh et al., 2007; Olsen and Sontheimer, 2008; Seifert et al., 2009; Sibille et al., 2015). During neuronal activity, neurons release large amounts of K^+ at the synapse. This K^+ is rapidly taken up by astrocytic KIR4.1 and is then transported through the astrocytic network to regions with lower K^+ levels. This astrocytic K^+ clearance mechanism (known as "spatial K^+ buffering" is vital for the maintenance of K^+ homeostasis and the prevention of neuronal hyperexcitability. Defects in KIR4.1 expression or function are associated with various brain pathologies and with epilepsy in particular (Nwaobi et al., 2016). In mice, KIR4.1 inactivation or reduced expression of KIR4.1 in astrocytes affects neuronal function (as indicated by a reduction in hippocampal short-term plasticity) and leads to ataxic seizures and early death (Sibille et al., 2014).

Here, we showed that KIR4.1 overexpression did not modify basal excitatory synaptic transmission but was critical during sustained activity (10 Hz stimulation and recurrent bursts). Indeed, we observed greater facilitation and slower depression (compared with control mice) after repetitive stimulation in

RACK1 cKO mice. This effect was abolished upon addition of a specific KIR4.1 blocker, thus demonstrating that the greater facilitation and slower depression observed in RACK1 cKO were related to the upregulation of KIR4.1. These results are consistent with previous reports of a role for KIR4.1 in the 3-10 Hz frequency band but not in the baseline activity (0.1 Hz) (Chever et al., 2010; Sibille et al., 2015). Regarding the neuronal network burst activity under pro-epileptic conditions (with 0Mg6K ACSF), the burst frequency was lower in RACK1 cKO than in RACK1 fl/fl mice. This finding suggests that the astrocytes were better able to buffer extracellular K^+ through higher levels of KIR4.1, which enhanced the RACK1 cKO mice's ability to control extracellular K^+ levels and the firing rate. Taken as a whole, these data thus indicate that by modulating KIR4.1 expression, RACK1 regulates neurotransmission. Interestingly, a relationship between RACK1 and epilepsy has been reported previously, albeit without a focus on astrocytes. RACK1 was shown to repress the transcription of the voltage-gated sodium channel α subunit type I (SCN1A) mRNA, the downregulation of which is associated with epilepsy (Dong et al., 2014). In the lithium-pilocarpine rat model, RACK1 levels in the hippocampus are elevated after epileptic episodes (Xu et al., 2015). Furthermore, in a rat model of mesial temporal lobe epilepsy, RACK1 was upregulated in the granular layer dorsal dentate gyrus and downregulated in the ventral dentate gyrus (do Canto et al., 2020). These literature data and our present results suggest that RACK1 is an important factor in the regulation of neurotransmission.

The present study focused on mechanisms of translation in astrocytes. We found that in astrocytes, RACK1 is a ribosomal associated protein able to interact selectively with mRNAs. We showed that RACK1 represses the synthesis of KIR4.1, which has a critical role in maintaining extracellular K^+ levels in the brain. Dysfunction of KIR4.1 in rodents and humans evokes seizures and chronic epilepsy. Thus, through the regulation of KIR4.1 levels, RACK1 might be a therapeutic target in epilepsy.

Acknowledgements

We are grateful to the donors who support the charities and charitable foundations cited below. This work was funded by a grant from the *Fondation pour la Recherche Médicale* (FRM, grant reference AJE20171039094) to M. C.-S., and by the European Research Council (Consolidator grant #683154) to N.R.. The creation of the Center for Interdisciplinary Research in Biology (CIRB) was funded by the Fondation Bettencourt Schueller. We thank Robin Rondon and Ines Masurel for their help with RNA immunoprecipitation experiments. Lastly, we thank Julien Dumont and Philippe Mailly (Orion CIRB imaging platform) for help with imaging and analysis. The pSpCas9(BB)-2A-Puro vector (Addgene plasmid 62988) was a gift from Feng Zhang (https://zlab.bio/), and pmGFP-P2A-K0-P2A-RFP and pmGFP-P2A-K(AAA)20-P2A-RFP (Addgene plasmids 105686 and 105688) were gifts from Ramanujan Hegde (MRC Laboratory of Molecular Biology). The flow cytometry experiments were performed at the Imagerie-Gif core facility, which is funded by the French Agence Nationale de la Recherche (ANR-11-EQPX-0029/Morphoscope, ANR-10-INBS-04/FranceBioImaging; ANR-11-IDEX-0003-02/ Saclay Plant Sciences). Copy-editing assistance was provided by Biotech Communication SARL (Ploudalmézeau, France).

Figure legends

Figure 1: Identification of polysome-associated proteins in astrocytes

A. Flowchart of the TRAP-MS analysis on whole brain extracts. Proteins extracted from whole brain in C57/Bl6 WT mice or Aldh1l1:L10a-eGFP (BT) mice were immunoprecipitated by TRAP and analyzed by LC-MS/MS. **B.** Western blot detection of Rpl10a-eGFP and RPS6 in whole brain extracts or TRAP immunoprecipitated proteins (IP-GFP). WT extracts were used as negative controls. **C.** Volcano plot of the TRAP-MS results. Each protein is represented by a dot. The dot size is proportional to the number of peptides identified by LC-MS/MS. Dots for proteins specific to or enriched in BT mice are represented with a color code: ribosomal proteins are given in light blue, with ribosome-associated proteins in red, RNA-binding proteins in purple, cytoskeleton-associated proteins in green, vesicles-ER-Golgi-lysosome-associated proteins in orange, and other proteins in black. Five independent replicates were analyzed (one brain per sample). The protein distribution is represented as the Log2 FC of the BT/WT (x-axis) versus -Log10 adjusted p-value (y axis): Proteins identified only in WT extracts (3 proteins) or only in BT extracts (139 proteins) (FC: – or +∞); Proteins enriched in WT or BT extracts. The threshold for the enrichment in WT or BT extracts is p-value < 0.05 (red line) and Log2 FC > 1 or < -1 (green lines). 61 proteins were enriched in WT extracts (p-value < 0.05; Log2 FC < -1), 106 proteins were detected with a similar abundance in WT and BT extracts (p-value < 0.05, -1 < Log2 FC < 1) and 110 proteins were enriched in BT extracts (p-value < 0.05; Log2 FC > 1). **D.** A GO analysis of the 249 proteins enriched or detected solely in BT extracts (p-value < 0.05; Log2 FC > 1) for biological processes (left) and molecular functions (right). The raw data are given in **Table S1**.

Figure 2: RACK1 is associated with ribosomes in astrocytes

A. Representation of the human 80S ribosome, generated with PyMol software (https://pymol.org/2/, PyMol version 2.3.4, Python 3.7) on the basis of the high-resolution cryo-EM structure (Natchiar et al., 2017). RPL10a is shown in green, and RACK1 is shown in black. **B.** Western blot detection of RACK1 and RPl10a-GFP in whole brain protein extracts and in TRAP-MS extracts (IP

GFP) in BT conditions. WT extracts were used as negative controls. **C.** FISH detection of *Gnb2l1* mRNAs encoding RACK1 in hippocampal astrocytes immunolabeled for GFAP. **From left to right:** Confocal microscopy image of a GFAP-immunolabeled astrocyte (in green); FISH detection of *Gnb2l1* mRNAs (red dots); merged image; *AstroDot* analysis of *Gnb2l1* mRNA located on GFAP-positive processes. The green dots are located in the soma or in GFAP-immunolabeled large processes; the yellow dots are located in GFAP-immunolabeled fine processes. **D.** Confocal images of RACK1 immunofluorescence detection (in red) in the hippocampus. Astrocytes (*) are co-immunolabeled for GFAP (in green). A neuron (°) is also labelled for RACK1. Scale bar: 20 µm.

Figure 3: RACK1 associates with specific mRNAs in astrocytes and PAPs

A. Western blot analysis of RACK1 immunoprecipitation in whole brain extracts from 2-month-old mice. Increasing quantities of RACK1 antibodies (0, 2, and 5 µg) were used. *Lower panel:* RPS6 is also detected in RACK1-immunoprecipitated proteins. **B.** Flowchart of RNA immunoprecipitation using anti-RACK1 antibodies (in red) on whole brain extracts (**C**) or synaptogliosome extracts (**C'**) prepared from 2-month-old WT mice. Red dots on ribosomes represent RACK1. Immunoprecipitated RNAs were purified and screened (in qPCR assays) for a selection of astrocyte-specific mRNAs. IgG-subtracted signals were normalized against rRNA *18S.* The data are quoted as the mean ± SD (N=5 or 6 samples; 1 mouse brain per sample); one-sample t-test vs. 0 (except for *Gjb6* whole brain experiment, One-sample Wilcoxon test). **D.** Flowchart of polysomal immunoprecipitation (TRAP) using anti GFP antibodies (in green) on whole brain (**E**) or synaptogliosomes extracts (**E'**) prepared from 2-month-old BT mice. Immunoprecipitated RNAs are purified and analyzed by qPCR for a selection of astrocyte specific mRNAs. Signals were normalized against rRNA *18S.* The data are quoted as the mean ± SD (N=4 samples; 1 mouse brain per sample). **F.** Flowchart of the normalization of the RACK1 immunoprecipitation against mean TRAP values. Ratios were calculated for experiments on whole brain (**G**) or synaptogliosomes (**G'**). The data are quoted as the mean ± SD (N=5 or 6 samples; 1 mouse brain per sample). P values are indicated in green when *Kncj10* results was the reference and in red when *Slc1a2* results was the reference. Two-tailed unpaired t-test or a two-tailed Mann-Whitney test. ns, not

significant (p>0.05); *, p<0.05; **, p<0.01; ***, p<0.001; ****, p<0.0001. The raw data are presented in **Table S2**.

Figure 4: RACK1 KO in astrocytes leads to higher levels of KIR4.1 in astrocyte somata and PAPs

A. Generation of a mouse line with RACK1 knocked out in astrocytes. Schematic representation of the RACK1 fl/fl and Aldh1l1-Cre/ERT2 alleles. Deletion of exon 2 in *Gnb2l1* (the gene coding for RACK1) is induced in astrocytes by tamoxifen injection; this results in a frameshift and the premature termination of *Gnb2l1* translation. **B.** PCR assays for *Gnb2l1* KO in brain DNA from RACK1 fl/fl or Aldh1L-CreERT2/ RACK1 fl/fl tamixofen-injected mice (RACK1 cKO). Primers are indicated in (**A**) by red arrows. The 898 base-pair (bp) band corresponds to the floxed allele. The 672 bp band corresponds to the exon2-deleted allele**. C.** Confocal images of RACK1 immunofluorescence detection (in red) in the hippocampus in RACK1 fl/fl and RACK1 cKO mice. Astrocytes are co-immunolabeled for GFAP (in green). The lower panel gives a higher magnification view of the boxed area in the RACK1 cKO images, which shows that RACK1 is specifically depleted in astrocytes (*) and is still expressed by neurons (°). **D.** Western blot detection and analysis of KIR4.1 and GLT-1 in protein extracts from whole hippocampus or synaptogliosomes purified from RACK1 fl/fl or RACK1 cKO mice. The data are quoted as the mean ± SD (N=5 samples per genotype; 1 mouse per sample); two-tailed unpaired t-test. ns, not significant, p-value>0.05; *, p<0.05; **, p<0.01; ***, p<0.001; ****, p<0.0001. The raw data are presented in **Table S2**.

Figure 5: The 5'UTR of *Kcnj10* confers RACK1 sensitivity *in vitro*

A. CRISPR/CAS9-based KO of RACK1 in HEK293T cells. The Western blot for the indicated proteins was performed using WT and $RACK1^{KO}$ cell extracts. **B.** Topology of the reporters for flow cytometry analysis of *Kcnj10* mRNA translation. The constructs contain GFP and mCherry separated by a multiple cloning site (into which the *Kcnj10* CDS had been inserted) and two viral 2A sequences (at which ribosomes skip formation of a peptide bond, without interrupting chain elongation). **C.** Representative flow-cytometry-based assay of the fluorescence ratio in WT or $RACK1^{KO}$ HEK293T cells transfected by the constructs described in (**B**). **D.** A histogram of the data, presented as the mean ±

SD (N = 3); Two-tailed t-test with Welch's correction. **E**. Schematic representation of the *Renilla* luciferase (RLuc) reporter constructs harboring the 5'UTR and/or 3'UTR of mouse *Kcnj10* mRNA. These sequences were inserted in the psiCHECK2 vector, which also encodes the Firefly luciferase (Fluc). The "control" RLuc was generated by transfecting the empty psiCHECK2 vector. **F**. WT and RACK1^{KO} HEK293T cells were transfected with the reporters described in (**E**). Luciferase activity was measured 24 h after transfection. RLuc values were normalized against FLuc levels, and a ratio was calculated for each *Kcnj10* reporter relative to the empty psiCHECK2 reporter (value set to 1) for each population. **F.** A histogram of the data, presented as the mean ± SD (N = 4); unpaired Mann-Whitney test or unpaired t-test. **G.** Schematic representation of the truncated versions of the *Kcnj10* 5'UTR inserted in the RLuc reporter. Blue boxes indicated GC-rich regions (see **Fig.** S**2B**). Plasmids were transfected in WT and RACK1^{KO} HEK293T cells. For each experiment, the ratio was calculated for each *Kcnj10* reporter relative to the empty psiCHECK2 reporter (value set to 1). **H**. A histogram of the data, presented as the mean ± SD (N = 4); unpaired Mann-Whitney test. ns, not significant, p-value>0.05; *, p<0.05; **, p<0.01; ***, p<0.001; ****, p<0.0001. The raw data are presented in **Table** S**2**.

Figure 6: RACK1 regulates astrocyte volume

A. Raw confocal image of an isolated CA1 astrocyte expressing tdTomato. **B-F**. Imaris analysis: filament tracing (**B**); convex hull volume (**C**); a 3D Sholl analysis (**E**). **D.** Mean territory volume and filament length of RACK1 fl/fl and RACK1 cKO astrocytes. A histogram of the data, presented as the mean ± SD (N = 4 mice per genotype; 45 astrocytes); two-tailed *t-test*. **F.** A Sholl analysis of the ramification complexity of RACK1 fl/fl and RACK1 cKO astrocytes. Two-way analysis of variance. *, p<0.05; **, p<0.01. The raw data are presented in **Table** S**2**.

Figure 7: RACK1 KO in astrocytes does not affect basal excitatory synaptic transmission but does alter network population activity and neuronal responses to intense stimulation

A. Schematic representation of electrode positions used to record field excitatory postsynaptic potentials (fEPSP) evoked by Schaffer collateral (SC) stimulation in the CA1 region of hippocampal

slices. **B.** Input-output curves for basal synaptic transmission. Left, representative recordings in RACK1 fl/fl mice (black) and RACK1 cKO mice before (pink) and after (blue) application of a Kir 4.1 antagonist (VU0134992). Scale bars: 10 ms, 0.5 mV. Right, quantification of the fEPSP slope for different fiber volley amplitudes after SC stimulation. (RACK1 fl/fl: n=5 slices from 4 mice; p=0.0087; RACK1 cKO: n=5 slices from 5 mice; repeated measures two-way ANOVA with Sidak's correction for multiple comparisons). **C.** Top: a representative recording of fEPSPs evoked by repetitive stimulation (10 Hz, 30 s) of CA1 SCs in RACK1 fl/fl mice under control conditions. Scale bars: 5 s, 0.2 mV. Bottom: enlarged view of fEPSPs evoked by the first 10 stimuli. Scale bars: 200 ms, 0.2 mV. **D.** Quantification of changes in the fEPSP slope induced by 10 Hz stimulation relative to responses measured before the onset of stimulation (baseline responses) in RACK1 fl/fl mice (white filled dots) and in RACK1 cKO mice (pink-filled dots) before (black) and after (blue) application of VU0134992 (RACK1 fl/fl: n=5 from 5 mice; RACK1 cKO: n = 6 slices from 4 mice; repeated measures two-way ANOVA with Sidak's correction for multiple comparisons). **E.** Schematic representation (left) and picture (right) of a hippocampal slice placed on a multielectrode array (MEA). Scale bar: 200 µm. **F.** Representative MEA recordings of burst activity induced in hippocampal slices of RACK1 fl/fl (black) and RACK1 cKO (pink) mice by incubation in Mg^{2+}-free ACSF containing 6 mM KCl. The expanded recordings of the bursts (surrounded by grey rectangles) are shown on the right. Scale bars: 10 s (left)/200 ms (right), 50 µV. **G.** Quantification of burst frequency (top) and burst duration (bottom) in RACK1 fl/fl (white) and RACK1 cKO (pink) hippocampal slices (n=15 slices from 5 mice for RACK1 fl/fl, and n=18 slices from 6 mice for RACK1 cKO; unpaired t-test). **H.** Quantification of VU0134992's effect on burst frequency (top) and duration (bottom) in RACK1 fl/fl (white) and RACK1 cKO (pink) hippocampal slices (RACK1 fl/fl: n=15 slices from 5 mice for burst frequency and duration, respectively; RACK1 cKO: n=18 slices from 6 mice for burst frequency and duration; repeated measures one-way ANOVA with Tukey's multiple comparison test). The raw data are presented in **Table S2**.

Table 1: The most abundant polysome-associated proteins in astrocytes, identified using TRAP-MS

The raw TRAP-MS data for a selection of the most specific (+∞) or enriched (p-value < 0.05; Log2 FC > 1) abundant immunoprecipitated proteins in the BT condition. FC, fold-change. The first six proteins in each GO “molecular function” term are listed.

Methods

Animal care and ethical approval

Tg (Aldh1l1-eGFP/Rpl10a) JD130Htz (MGI: 5496674) (bacTRAP, **BT**) mice were obtained from Nathaniel Heintz's laboratory (Rockefeller University, New York City, NY) and kept under pathogen-free conditions (Heiman et al., 2014). The genotyping protocol is described on the bacTRAP project's website (www.bactrap.org). Tg(Aldh1l1-cre/ERT2)1Khakh (MGI:5806568) (Aldh1l1-Cre/ERT2) mice (Srinivasan et al., 2016) were obtained from the Jackson laboratory (https://www.jax.org/) and B6J.Cg-Rack1$^{tm1.1Cart}$/Mmucd (RACK1 fl/fl) (MMRRC 044021-UCD) from the mutant mouse resource and research center (MMRRC) (https://www.mmrrc.org/)(Cheng and Cartwright, 2018). C57BL6 WT mice were purchased from Janvier Labs (Le Genest-Saint-Isle, France). Mice were maintained on a C57BL6 genetic background. All experiments were performed on 2-month-old mice. Both sexes were used for all experiments.

Mice were kept in pathogen-free conditions. All animal experiments were carried out in compliance with (i) the European Directive 2010/63/EU on the protection of animals used for scientific purposes and (ii) the guidelines issued by the French National Animal Care and Use Committee (reference: 2013/118). The study was also approved by the French Ministry for Research and Higher Education's institutional review board (reference 21817).

Tamoxifen induction of RACK1 inactivation

Two-month-old mice received a daily intraperitoneal injection of 100 mg/kg tamoxifen solution in corn oil (10 mg/ml dissolved extemporaneously for 6-8h at 37°C) for 5 consecutive days and were analyzed 3 weeks later. For controls, RACK1 fl/fl received corn oil only (immunofluorescence; Western blot; qPCR), or tamoxifen (astrocyte volume study; electrophysiology)

TRAP-MS

Whole brain homogenates (one brain per sample) from 2-month-old C57Bl/6 mice (WT, negative control) and BT mice were submitted to TRAP by immunoprecipitating GFP-fused astrocytic

polyribosomes with anti-GFP antibodies and protein-G-coupled magnetic beads, as described elsewhere (Mazare et al., 2020a), except that 1 mg of proteins were used for the immunoprecipitation on 25 μL G-protein-coupled magnetic Dynabeads coated with anti-GFP antibodies at 4°C. At the end of the procedure, immunoprecipitated proteins were eluted by boiling the beads in 20 µL of 0.35 M KCl buffer with 5X Laemmli buffer for 5 min. Samples were run on SDS-PAGE gels (Invitrogen) without separation as a clean-up step and then stained with colloidal blue staining (LabSafe GEL Blue^{TM} G Biosciences). Gel slices were excised, and proteins were reduced with 10 mM DTT prior to alkylation with 55 mM iodoacetamide. After washing and shrinking the gel pieces with 100% acetonitrile, in-gel digestion was performed using 0.10 µg trypsin/Lys-C (Promega) overnight in 25 mM NH_4HCO_3 at 30 °C. Peptides were then extracted (using 60/35/5 acetonitrile/H_2O/HCOOH) and vacuum concentrated to dryness. Peptides were reconstituted in injection buffer (0.3% TFA) before LC-MS/MS analysis. Five replicates per conditions were prepared.

LC-MS/MS analysis: Online chromatography was performed with an RSLCnano system (Ultimate 3000, Thermo Scientific) coupled to a Q Exactive HF-X. Peptides were first trapped onto a C18 column (75 µm inner diameter × 2 cm; nanoViper Acclaim PepMapTM 100, Thermo Scientific) with buffer A (0.1% formic acid) at a flow rate of 2.5 µL/min over 4 min. The peptides were separated on a 50 cm x 75 µm C18 column (nanoViper C18, 3 µm, 100 Å, Acclaim PepMap^{TM} RSLC, Thermo Scientific) at 50°C, with a linear gradient from 2% to 30% buffer B (100% acetonitrile, 0.1% formic acid) at a flow rate of 300 nL/min over 91 min. Full MS scans were performed with the ultrahigh-field Orbitrap mass analyzer in the range m/z 375–1500, with a resolution of 120,000 at m/z 200. The top 20 intense ions were subjected to Orbitrap for further fragmentation via high energy collision dissociation activation and a resolution of 15,000, with the intensity threshold kept at 1.3×10^5. We selected ions with a charge from 2+ to 6+ for screening. The normalized collision energy was set to 27 and the dynamic exclusion was set to 40 s.

Data analysis: Data were searched against the *Mus musculus* UniProt canonical database (downloaded in August 2017 and containing 16888 sequences) using Sequest HT via proteome discoverer (version 2.0). The enzyme specificity was set to trypsin, and a maximum of two missed cleavage sites was allowed. Oxidized methionine, carbamidomethyled cysteine, and N-terminal

acetylation were set as variable modifications. The maximum allowed mass deviation was set to 10 ppm for monoisotopic precursor ions and to 0.02 Da for MS/MS peaks. The resulting files were further processed using myProMS (Poullet et al., 2007) version 3.9.3 (https://github.com/bioinfo-pf-curie/myproms). The false-discovery rate (FDR) was calculated using Percolator (The et al., 2016) and was set to 1% at the peptide level for the whole study. Label-free quantification was performed using peptide extracted ion chromatograms (XICs) computed with MassChroQ (Valot et al., 2011) v.2.2.1. For protein quantification, XICs from proteotypic peptides shared between compared conditions (TopN matching) with two-missed cleavages were used. Median and scale normalization at the peptide level was applied to the total signal, in order to correct the XICs in each biological replicate. To estimate the significance of the change in protein abundance, a linear model (adjusted for peptides and biological replicates) was used, and p-values were adjusted using the Benjamini–Hochberg FDR procedure. Proteins with at least three total peptides in all replicates, a two-fold enrichment and an adjusted p-value ≤ 0.05 were considered to be significantly enriched in sample comparisons. Proteins only found in one condition were also considered if they matched the peptide criteria. Proteins selected with these criteria were further analyzed and subjected to a GO functional enrichment analysis. The raw MS proteomics data have been deposited to the ProteomeXchange Consortium via the PRIDE (Perez-Riverol et al., 2019) partner repository (http://www.ebi.ac.uk/pride), with the dataset identifier PXD033121.

GO analysis

A GO analysis was performed for proteins with at least three peptides read by LC-MS/MS and found to be enriched in BT extracts (p-value < 0.05 and Log2 FC > 1), using UniProt bank annotations for the mouse (UniProt-GOA Mouse - *Mus musculus*). GO-term-associated p-values were computed with the GOTermFinder module of myProMS (Poullet et al., 2007). We analyzed biological processes and molecular functions (p-value threshold: 0.05). For each family, GO terms were classified manually according to the GO hierarchy, taking into account the number of genes from the study included in the highest GO. For instance, the in the "Gene Expression" category were included in the highest GO "Metabolic process", and the proteins in the 'Ribosomal proteins' category were included in "Structural molecule activity". The number of proteins in each category was expressed as a percentage of the total

number of proteins. These data should be taken as illustrative because some proteins have more than one role and so the categories overlap.

RACK1 immunoprecipitation (IP)

IP was performed according to the TRAP-MS protocol (i.e. using an anti-RACK1 antibody) but with some changes, as follows. Columns (bead volumes: 100μL for the precleaning column, 25μL for precleaning + IgG column, 25 μL for IP column) were prepared the day before. The IP column was first blocked 1 h with 2% bovine serum albumin and 0.1 mg/100 µL beads of yeast tRNA in 0.15 M KCl buffer, rinsed with 0.15 M KCl three times and coated with 5 μg of anti-RACK1 antibodies or 5 μg of non-specific immunoglobulins IgG (negative control). 500 μg of protein extract was used. The precleaning steps have been described elsewhere (Mazare et al., 2020a). The precleaned extract was incubated with IP columns for 30 min at 4°C. The beads were rinsed three times with 0.35 M KCl and RNA were eluted in 300 μL RLT buffer (Qiagen, Hilden, Germany) for 5 min at room temperature (RT) and kept at -80°C until extraction.

Quantitative RT-PCR

RNA was extracted using the Rneasy kit (Qiagen, Hilden, Germany). cDNA was then generated using the Superscript™ III Reverse Transcriptase kit (ThermoFisher). Differential levels of cDNA expression were measured using the droplet digital PCR (ddPCR) system (Bio-Rad) and TaqMan® copy number assay probes or primers (**Key resource table**). Briefly, cDNA and 6-carboxyfluorescein probes or primers were distributed into 10,000–20,000 droplets. The nucleic acids were then PCR-amplified in a thermal cycler and read (as the number of positive and negative droplets) with a QX200 ddPCR system. The results were normalized as follows: the IgG IP results were subtracted from the RACK1 RNA IP results for each gene. The results were then normalized against 18S rRNA gene expression. For GFP RNA IP (TRAP), results were normalized against the 18S rRNA.

Brain slices for FISH and immunofluorescence

Mice were anesthetized with a mix of ketamine/xylazine (80/100 mg/kg i.p.) and killed by transcardiac perfusion with PBS/PFA 4%. The brain was removed, incubated in 30% sucrose overnight, and cut into 40-µm-thick sections using a cryomicrotome (HM 450, Thermo Scientific). For long-term storage, slices were kept at -20°C in a cryoprotectant solution (30% ethylene glycol, 30% glycerol, 40% PBS).

High-resolution FISH and GFAP co-immunofluorescent detection and analysis

FISH was performed using the v2 Multiplex RNAscope technique (Advanced Cell Diagnostics, Inc., Newark, CA, USA). After the FISH procedure, GFAP was detected via immunofluorescence. Astrocyte-specific FISH dots were identified from their position on the GFAP immunolabeling image, using the *AstroDot* ImageJ plug-in. This method has been described in detail elsewhere (Oudart et al., 2020).

Immunohistochemical labeling and confocal imaging

Immunohistochemical labeling was performed on frozen brain sections (see above) rinsed in PBS and incubated for 2 h at RT in blocking solution (5% normal goat serum, 0.5% Triton X-100 in PBS). Sections were incubated with primary antibodies diluted in the blocking solution overnight at 4°C, rinsed for 5 min in PBS three times, incubated with secondary antibodies diluted in blocking solution for 2 h at RT, rinsed for 5 min in PBS three times, and mounted in Fluoromount (Southern Biotech, Birmingham, AL). Brain sections were imaged on X1 or W1 spinning-disk confocal microscopes (Yokogawa). Images were acquired with a 40X oil immersion objective (Zeiss). For the astrocyte morphology study, a LSM 980 confocal (Zeiss) and a 63X oil immersion objective (Zeiss) were used. The antibodies used in the present study are listed in **Key resource table**.

Preparation of synaptogliosomes

Synaptosomes were prepared as described elsewhere (Mazare et al., 2020a). All steps were performed at 4°C. Hippocampi (two per extract; 1 mouse) were dissected and homogenized with a tight glass homogenizer (20 strokes) in buffer solution (0.32 M sucrose and 10 mM HEPES in DNAse/RNAse-free water, with 0.5 mM DTT, protease inhibitors (cOmplete^{TM}, EDTA free, 1 minitablet/10 mL), ribonuclease inhibitor (1 µL/mL, cycloheximide (CHX) 100 µg/mL freshly prepared). The homogenate was centrifuged at 900 g for 15 min. The pellet was discarded, and the supernatant was centrifuged at 16,000 g for 15 min. The new supernatant was discarded, and the pellet (containing synaptogliosomes) was diluted in 600 µl of buffer solution and centrifuged again at 16,000 g for 15 min. The final pellet contained the synaptogliosomes.

Western blots

Whole hippocampi were crushed with a pestle and a mortar at -80°C. Proteins were extracted from the tissue powder or synaptogliosome pellets in 2% SDS (500 µl or 200 µl per sample, respectively) with EDTA-free Complete Protease Inhibitor (Roche), sonicated twice for 5 min or once for 5 min, respectively (Bioruptor UCD 200, diagenode), and centrifuged at 20,000 g for 20 min at 4°C. Supernatants were heated at 56°C in Laemmli loading buffer for 5 min. Protein content was measured using the Pierce 660 nm protein assay reagent (Thermo Scientific) and the Multiskan™ FC spectrophotometer (Thermo Scientific). Equal amounts of protein (whole immunoprecipitation extracts: 10 to 20 µg for hippocampus and synaptogliosomes) were separated by denaturing electrophoresis in Mini-Protean TGX stain-free gels (Biorad) and then electrotransferred to nitrocellulose membranes using the Trans-blot Turbo Transfer System (Biorad). Membranes were hybridized as described previously (Ezan et al., 2012). The antibodies used in this study are listed in **Key resource table**. Horseradish peroxidase activity was visualized by enhanced chemiluminescence in a Western Lightning Plus system (Perkin Elmer, Waltham, MA, USA). Chemiluminescent imaging was performed on a

Fusion FX system (Vilber). The chemiluminescence signal intensity for each antibody was normalized against that of stain-free membranes.

Representative structure of the human 80S ribosome

The human 80S ribosome's representative structure was depicted using the PyMol software (version 2.3.4, python 3.7, https://pymol.org/2/). A high-resolution cryo-electron microscopy (EM) structure of the human 80S ribosome (Natchiar et. al., 2017) was obtained from the Protein Data Bank in Europe (code 6EK0) because the mouse 80S ribosome is not available. The chain codes can be found on the Protein Data Bank in Europe website. The Lz chain for RPL10a and the Sg chain for RACK1 were selected.

Cell lines and culture conditions

HEK293T (Thermo Fisher Scientific, Waltham, MA) cells were cultured in DMEM supplemented with 10% fetal bovine serum (FBS) and 1% penicillin/streptomycin (P/S) (Wisent Technologies). Control and RACK1 KO HEK293 cells were maintained in DMEM supplemented with 10% FBS, 1% P/S, 100 µg/mL zeocin (Thermo Fisher Scientific, R25001), and 15 µg/mL blasticidin (Thermo Fisher Scientific, R210-01). All cells were cultured at 37°C, in a humidified atmosphere with 5% CO_2.

Plasmid constructs

To generate the *Kcnj10* CDS containing a fluorescent reporter, a control cassette was first created by replacing the BspEI/KpnI segment of the pmGFP-P2A-K0-P2A-RFP (Addgene plasmids 105686) with a linker containing a P2A site, a Flag coding sequence, and the EcoRI and NotI restriction sites. A gene block (Integrated DNA Technologies) encoding mKIR4.1 (AAI41089.1) without a stop codon was then inserted at the EcoRI/NotI sites of this control cassette in frame with both the GFP and mCherry coding sequences. The psiCHECK-2 vector (Promega, C8021) was used to build the dual

luciferase reporters with *Kcnj10* UTRs. The UTR sequences of mouse *Kcnj10* mRNA (NM_001039484.1 and AB039879.1) were synthesized as gBlocks and inserted at the NheI site of the psiCHECK-2 vector. The 3'UTR of the *Kcnj10* mRNA (AB039879.1) was inserted as a gBlock into the XhoI and NotI restriction sites in the psiCHECK-2 vector downstream of the *Renilla* luciferase reporter gene. The truncated versions of the *Kcnj10* 5′ UTR (1-146; 127-242; 95-242; 95-191; 1-191; 181-242) were inserted as NheI/NheI PCR fragments into the psiCHECK-2 vector at the 5′ end of the *Renilla* luciferase gene. The sequences of the primers and gBlocks used for subcloning are listed in **Key resource table**.

Flow cytometry analysis

Transient transfection of fluorescent reporter constructs was performed using Lipofectamine 2000 (Thermo Fisher Scientific), according to manufacturer's instructions. In all experiments, WT and RACK1^{KO} HEK293T cells were plated in 6-well plates at a concentration of 500,000 cells per well, and transfected with 10 ng of plasmids on the following day. The cells were then trypsinized, washed once with PBS and pelleted at RT at 500 g for 5 min. The cells were resuspended in 500 µl PBS containing 10% FBS, passed through a 40 µm filter, and analyzed with a CytoFlex flow cytometer (Beckman Coulter). 10,000 fluorescent cells were selected for the analysis of GFP and mCherry signals. The data were analyzed using FlowJo software.

CRISPR/cas9-mediated genome editing

CRISPR-Cas9-mediated genome editing of HEK293 cells was performed according to the method described by Ran *et al.* (Ran et al., 2013). The DNA oligonucleotides (encoding a small guide RNAs (sgRNAs) cognate to the coding region of human *Rack1*/*Gnb2l1* gene) are detailed in **Key resource table**. These oligos contained BbsI restriction sites and were annealed to create overhangs for cloning of the guide sequence oligos into pSpCas9(BB)-2A-Puro (PX459) V2.0 (Addgene plasmid 62988) by BbsI digestion. To generate KO HEK293T cells, we transfected 500,000 cells with the guide sequence containing the pSpCas9(BB)−2A-puro plasmid. Twenty-four hours after transfection,

puromycin was added to the cell medium. After 72 h, puromycin-resistant cells were isolated in 96-well plates and cultured until monoclonal colonies were obtained. Clonal cell populations were analyzed for protein depletion in Western blots.

Dual luciferase reporter assays

WT or RACK1^{KO} HEK293T cells were transfected with 20 ng per well of each psiCHECK2 construct or the empty psiCHECK2 in a 24-well plate by using Lipofectamine 2000 (Thermo Scientific, 11668019), according to the manufacturer's instructions. Cells were lysed 24 h after transfection, and luciferase activities were measured with the Dual-Luciferase Reporter Assay System (Promega) in a GloMax 20/20 luminometer (Promega). The RLuc activity was normalized against the activity of co-expressed FLuc, and the normalized RLuc values were quoted relative to the corresponding control.

Viral vectors and stereotaxic injection

Two-month-old mice were anesthetized with a mixture of ketamine (95 mg/kg; Merial) and xylazine (10 mg/kg; Bayer) in 0.9% NaCl and placed on a stereotaxic frame with constant body temperature monitoring. AAVs were diluted in PBS with 0.01% Pluronic F-68 at a concentration of $9x10^{12}$ vg/ml and 1 µl of virus was injected bilaterally into the hippocampus at a rate of 0.1 µl/min, using a 29-gauge blunt-tip needle linked to a 2 µl Hamilton syringe (Phymep). The stereotaxic coordinates relative to the bregma were as follows: anteroposterior, ±2 mm; mediolateral: +1.5 mm; dorsoventral, -1.5 mm. The needle was left in place for 5 min and then removed slowly. The skin was glued back in place, and the animals' recovery was checked regularly for the next 24 h. After 11 days, the mice were sacrificed and the tissues were processed for immunofluorescence assays.

Measurement of astrocyte volume

To drive expression in astrocytes, the transgene encoding cytosolic red fluorescent protein Td tomato was inserted under the control of the gfaABC1D (Lee et al., 2008) into an AAV shuttle plasmid

containing the inverted terminal repeats of AAV2. Pseudotyped serotype 9 AAV particles were produced by transient co-transfection of HEK-293T cells, as described previously (Fol et al., 2016). Viral titers were determined by quantitative PCR amplification of the inverted terminal repeats on DNase-resistant particles and were expressed in vg per ml.

Astrocytes on 100 µm brain sections were reconstructed in 3D, using IMARIS software (Oxford Instruments, version 9.7.2). Filaments were created with a unique starting point in the astrocyte soma and with seeds defined with a manual threshold, according to the fluorescence intensity. Filaments outside the astrocyte were removed manually. An envelope of the astrocyte territory was created using the convex hull plugin (Matlab). The following variables were computed and exported for analysis: astrocyte volume (corresponding to the envelope volume), the sum of the filament length and data for a 3D Sholl analysis (5 µm steps).

Electrophysiology

Electrophysiological recordings were performed in the hippocampus of 3-month-old RACK1 fl/fl (Control) and RACK1 cKO mice 3 weeks after tamoxifen injection, using ACSF in the presence or absence of a Kir4.1 blocker (30 µM VU0134992, Tocris, Biotechne) (Kharade et al., 2018).

Acute hippocampal slice preparation: Acute transverse hippocampal slices (400 µm) were prepared as described previously (Chever et al., 2016) from 3-month-old RACK1 fl/fl or astrocytic RACK1 cKO mice. Briefly, slices were cut at low speed (0.04 mm/s) and at a vibration frequency of 70 Hz in ice-cold oxygenated ACSF supplemented with sucrose (in mM: 87 NaCl, 2.5 KCl, 2.5 $CaCl_2$, 7 $MgCl_2$, 1 NaH_2PO_4, 25 $NaHCO_3$ and 10 glucose, saturated with 95% O_2 and 5% CO_2). Slices were then maintained at 32°C in a storage chamber containing standard ACSF (in mM: 119 NaCl, 2.5 KCl, 2.5 $CaCl_2$, 1.3 $MgSO_4$, 1 NaH2PO_4, 26.2 $NaHCO_3$ and 11 glucose, saturated with 95% O_2 and 5% CO_2), for at least 1 h prior to recording.

Field recordings: Slices were transferred to a submerged recording chamber mounted on an Olympus BX51WI microscope equipped for infrared-differential interference microscopy and were

perfused with standard ACSF at a rate of 1-2 ml/min at 32°C. Extracellular field recordings were performed with glass pipettes (2–5 MΩ) filled with ACSF and placed in the stratum radiatum. Stimulus artifacts were blanked in sample recordings. Basal excitatory synaptic transmission (input/output curves) was evaluated in presence of picrotoxin (100 μM), and the tissue was cut between CA1 and CA3 to prevent the propagation of epileptiform activity. Evoked postsynaptic responses were induced by stimulating SCs at 0.1 Hz in the CA1 *stratum radiatum*. Slices underwent prolonged, repetitive stimulation at 10 Hz for 30 s. Responses (neuronal fEPSP slope) were binned (bin size: 1.2 s) and normalized against the mean baseline response measured at 0.1 Hz prior to repetitive stimulation. Both basal excitatory synaptic transmission and responses to repetitive stimulation were evaluated before and after treatment with VU0134992. Field potentials were acquired with Axopatch-1D amplifiers (Molecular Devices), digitized at 10 kHz, filtered at 2 kHz, and stored and analyzed on a computer using pCLAMP9 and Clampfit10 software (Molecular Devices).

MEA recordings: MEA recordings were performed as described previously (Chever et al., 2016). After a 20 min incubation in standard ACSF at 32°C, slices were stored for at least 1 h before recording in magnesium-free ACSF containing 6 mM KCl (0Mg6K ACSF) at 32°C. Hippocampal slices were then transferred onto planar MEA petri dishes (200-30 indium tin oxide electrodes, organized in a 12×12 matrix, with an internal reference, 30 μm diameter and 200 μm inter-electrode distance; Multichannel Systems), kept in place with a small platinum anchor, and continuously perfused at 1-2 ml/min with 0Mg6K ACSF at 32°C. Pictures of cortical slices on MEAs were acquired with a video microscope table (MEA-VMT1; Multichannel Systems). MEA_Monitor software (Multichannel Systems) was used to identify the location of the electrodes relative to the various regions of the hippocampal. Data were sampled at 10 kHz, and the slice activity was recorded at 32°C using a MEA2100-120 system (bandwidth: 1-3000 Hz; gain: 5x; Multichannel Systems) and MC_Rack 4.5.1 software (Multichannel Systems). The slices' activity was recorded in 0Mg6K ACSF before and after treatment with 30 μM VU0134992. Raw data on 0Mg6K ACSF-induced network burst activity was analyzed with MC Rack software (Multichannel Systems). Bursts were detected with the Spike Sorter algorithm, which sets a threshold based on multiples of the standard deviation of the noise calculated

over the first 500 ms of recording free of electrical activity. A 5-fold standard deviation threshold was used to automatically detect each event. If required (after a visual check), each event could be modified in real-time by the operator. Bursts were defined arbitrarily as discharges lasting less than 5 s. The bursts were characterized by fast voltage oscillations and then slow oscillations or negative shifts. The burst duration was measured using Neuroexplorer software (version 4.109, Nex Technologies, USA).

Statistics

All statistical analyses were performed using GraphPad Prism software (version 8.0.2, GraphPad Software, Inc.). The statistical tests are listed in **Table S2** and in the figure legends. For the analysis of qPCR and Western blot data, a t-test was applied if the data were normally distributed (according to the Kolmogorov-Smirnov test) and the variances were equal (according to Fisher's test); if not, a Mann-Whitney test was applied. For *in cellulo* studies, a t-test was used with Welch's correction if the variances were equal; if not, a Mann-Whitney test was used.

Supplementary Informations

Figure S1: RACK1's stalling effect on a reporter sequence

A. Schematic representation of the reporter constructs used to quantify ribosome stalling. The reporter contains GFP and mCherry separated by a sequence either lacking or containing 20 AAA lysine codons (K_0 and K_{20}, respectively) and surrounded by viral 2A sequences. **B.** A representative experiment monitoring the fluorescence protein ratio in WT or $RACK1^{KO}$ HEK293T cells transfected with the K_0 and K_{20} reporters. **C.** A histogram of the data, presented as the mean ± SD (N = 3); an unpaired Mann-Whitney test and a two-tailed t-test with Welch's correction. ns, not significant, p-value>0.05; ***, p<0.001. The raw data are presented in **Table S2**.

Figure S2: Alignment of the 5'UTR sequences of *Kcnj10*

A. The sequences were aligned using Clustal Omega and default parameters, and colored in Jalview by identity. **B.** Plot showing the GC content in the 5'UTR sequence of murine *Kcnj10* mRNA. The schematic representation shows two GC-rich regions (blue boxes).

Figure S3: RACK1's sensitivity to Kcnj10 5'UTR is not mediated by an effect on mRNA levels

A. Schematic representation of the *Renilla* luciferase (RLuc) reporter constructs harboring the 5'UTR of mouse *Kcnj10* mRNA. These sequences were inserted in the psiCHECK2 vector, which also encodes the Firefly luciferase (Fluc). The "control" RLuc was generated by transfecting the empty psiCHECK2 vector. **B.** The qPCR ratio of *Renilla* luciferase (RLuc) to firefly luciferase (Fluc) mRNA levels in WT and $RACK1^{KO}$ HEK293T cells transfected with constructs empty of harboring the 5'UTR #1 or 2 of mouse *Kcnj10* mRNA.

Table S1: The raw data for TRAP-MS and GO analyses

1. Parameters used for the LC-MS-MS study. **2.** Comparison of immunoprecipitation data in WT vs. BT extracts. **3.** FC, fold change. GO analysis of biological processes. **4.** GO analysis of molecular functions

Table S2: Datasets

References

Battaini, F., and Pascale, A. (2005). Protein kinase C signal transduction regulation in physiological and pathological aging. Ann N Y Acad Sci *1057*, 177-192.

Battaini, F., Pascale, A., Lucchi, L., Pasinetti, G.M., and Govoni, S. (1999). Protein kinase C anchoring deficit in postmortem brains of Alzheimer's disease patients. Exp Neurol *159*, 559-564.

Baum, S., Bittins, M., Frey, S., and Seedorf, M. (2004). Asc1p, a WD40-domain containing adaptor protein, is required for the interaction of the RNA-binding protein Scp160p with polysomes. Biochem J *380*, 823-830.

Beffert, U., Dillon, G.M., Sullivan, J.M., Stuart, C.E., Gilbert, J.P., Kambouris, J.A., and Ho, A. (2012). Microtubule plus-end tracking protein CLASP2 regulates neuronal polarity and synaptic function. J Neurosci *32*, 13906-13916.

Besse, F., and Ephrussi, A. (2008). Translational control of localized mRNAs: restricting protein synthesis in space and time. Nat Rev Mol Cell Biol *9*, 971-980.

Blanco-Urrejola, M., Gaminde-Blasco, A., Gamarra, M., de la Cruz, A., Vecino, E., Alberdi, E., and Baleriola, J. (2021). RNA Localization and Local Translation in Glia in Neurological and Neurodegenerative Diseases: Lessons from Neurons. Cells *10*.

Boulay, A.C., Saubaméa, B., Adam, N., Chasseigneaux, S., Mazaré, N., Gilbert, A., Bahin, M., Bastianelli, L., Blugeon, C., Perrin, S., *et al*. (2017). Translation in astrocyte distal processes sets molecular heterogeneity at the gliovascular interface. Cell Discovery *3*, 17005.

Carney, K.E., Milanese, M., van Nierop, P., Li, K.W., Oliet, S.H., Smit, A.B., Bonanno, G., and Verheijen, M.H. (2014). Proteomic analysis of gliosomes from mouse brain: identification and investigation of glial membrane proteins. J Proteome Res *13*, 5918-5927.

Cheng, Z.F., and Cartwright, C.A. (2018). Rack1 maintains intestinal homeostasis by protecting the integrity of the epithelial barrier. Am J Physiol Gastrointest Liver Physiol *314*, G263-G274.

Chever, O., Djukic, B., McCarthy, K.D., and Amzica, F. (2010). Implication of Kir4.1 channel in excess potassium clearance: an in vivo study on anesthetized glial-conditional Kir4.1 knock-out mice. J Neurosci *30*, 15769-15777.

Chever, O., Dossi, E., Pannasch, U., Derangeon, M., and Rouach, N. (2016). Astroglial networks promote neuronal coordination. Sci Signal *9*, ra6.

Cohen-Salmon, M., Slaoui, L., Mazare, N., Gilbert, A., Oudart, M., Alvear-Perez, R., Elorza-Vidal, X., Chever, O., and Boulay, A.C. (2021). Astrocytes in the regulation of cerebrovascular functions. Glia *69*, 817-841.

Coyle, S.M., Gilbert, W.V., and Doudna, J.A. (2009). Direct link between RACK1 function and localization at the ribosome in vivo. Mol Cell Biol *29*, 1626-1634.

Cui-Wang, T., Hanus, C., Cui, T., Helton, T., Bourne, J., Watson, D., Harris, K.M., and Ehlers, M.D. (2012). Local zones of endoplasmic reticulum complexity confine cargo in neuronal dendrites. Cell *148*, 309-321.

Culver, B.P., Savas, J.N., Park, S.K., Choi, J.H., Zheng, S., Zeitlin, S.O., Yates, J.R., 3rd, and Tanese, N. (2012). Proteomic analysis of wild-type and mutant huntingtin-associated proteins in mouse brains identifies unique interactions and involvement in protein synthesis. J Biol Chem *287*, 21599-21614.

Dallerac, G., Zapata, J., and Rouach, N. (2018). Versatile control of synaptic circuits by astrocytes: where, when and how? Nat Rev Neurosci *19*, 729-743.

Djukic, B., Casper, K.B., Philpot, B.D., Chin, L.S., and McCarthy, K.D. (2007). Conditional knock-out of Kir4.1 leads to glial membrane depolarization, inhibition of potassium and glutamate uptake, and enhanced short-term synaptic potentiation. J Neurosci *27*, 11354-11365.

do Canto, A.M., Vieira, A.S., A, H.B.M., Carvalho, B.S., Henning, B., Norwood, B.A., Bauer, S., Rosenow, F., Gilioli, R., Cendes, F., *et al*. (2020). Laser microdissection-based microproteomics of the hippocampus of a rat epilepsy model reveals regional differences in protein abundances. Sci Rep *10*, 4412.

Dong, Z.F., Tang, L.J., Deng, G.F., Zeng, T., Liu, S.J., Wan, R.P., Liu, T., Zhao, Q.H., Yi, Y.H., Liao, W.P., *et al*. (2014). Transcription of the human sodium channel SCN1A gene is repressed by a scaffolding protein RACK1. Mol Neurobiol *50*, 438-448.

Doyle, J.P., Dougherty, J.D., Heiman, M., Schmidt, E.F., Stevens, T.R., Ma, G., Bupp, S., Shrestha, P., Shah, R.D., Doughty, M.L., *et al*. (2008). Application of a translational profiling approach for the comparative analysis of CNS cell types. Cell *135*, 749-762.

Ezan, P., Andre, P., Cisternino, S., Saubamea, B., Boulay, A.C., Doutremer, S., Thomas, M.A., Quenech'du, N., Giaume, C., and Cohen-Salmon, M. (2012). Deletion of astroglial connexins weakens the blood-brain barrier. J Cereb Blood Flow Metab *32*, 1457-1467.

Fol, R., Braudeau, J., Ludewig, S., Abel, T., Weyer, S.W., Roederer, J.P., Brod, F., Audrain, M., Bemelmans, A.P., Buchholz, C.J., *et al.* (2016). Viral gene transfer of APPsalpha rescues synaptic failure in an Alzheimer's disease mouse model. Acta Neuropathol *131*, 247-266.

Fusco, C.M., Desch, K., Dorrbaum, A.R., Wang, M., Staab, A., Chan, I.C.W., Vail, E., Villeri, V., Langer, J.D., and Schuman, E.M. (2021). Neuronal ribosomes exhibit dynamic and context-dependent exchange of ribosomal proteins. Nat Commun *12*, 6127.

Gallo, S., and Manfrini, N. (2015). Working hard at the nexus between cell signaling and the ribosomal machinery: An insight into the roles of RACK1 in translational regulation. Translation (Austin) *3*, e1120382.

Gallo, S., Ricciardi, S., Manfrini, N., Pesce, E., Oliveto, S., Calamita, P., Mancino, M., Maffioli, E., Moro, M., Crosti, M., *et al.* (2018). RACK1 Specifically Regulates Translation through Its Binding to Ribosomes. Mol Cell Biol *38*.

Gay, D.M., Lund, A.H., and Jansson, M.D. (2022). Translational control through ribosome heterogeneity and functional specialization. Trends Biochem Sci *47*, 66-81.

Harvey, R.F., Smith, T.S., Mulroney, T., Queiroz, R.M.L., Pizzinga, M., Dezi, V., Villenueva, E., Ramakrishna, M., Lilley, K.S., and Willis, A.E. (2018). Trans-acting translational regulatory RNA binding proteins. Wiley Interdiscip Rev RNA *9*, e1465.

Heiman, M., Kulicke, R., Fenster, R.J., Greengard, P., and Heintz, N. (2014). Cell type-specific mRNA purification by translating ribosome affinity purification (TRAP). Nat Protoc *9*, 1282-1291.

Heiman, M., Schaefer, A., Gong, S., Peterson, J.D., Day, M., Ramsey, K.E., Suarez-Farinas, M., Schwarz, C., Stephan, D.A., Surmeier, D.J., *et al.* (2008). A translational profiling approach for the molecular characterization of CNS cell types. Cell *135*, 738-748.

Higashimori, H., Schin, C.S., Chiang, M.S., Morel, L., Shoneye, T.A., Nelson, D.L., and Yang, Y. (2016). Selective Deletion of Astroglial FMRP Dysregulates Glutamate Transporter GLT1 and Contributes to Fragile X Syndrome Phenotypes In Vivo. J Neurosci *36*, 7079-7094.

Ikeuchi, K., and Inada, T. (2016). Ribosome-associated Asc1/RACK1 is required for endonucleolytic cleavage induced by stalled ribosome at the 3' end of nonstop mRNA. Sci Rep *6*, 28234.

Jannot, G., Bajan, S., Giguere, N.J., Bouasker, S., Banville, I.H., Piquet, S., Hutvagner, G., and Simard, M.J. (2011). The ribosomal protein RACK1 is required for microRNA function in both C. elegans and humans. EMBO Rep *12*, 581-586.

Johnson, A.G., Lapointe, C.P., Wang, J., Corsepius, N.C., Choi, J., Fuchs, G., and Puglisi, J.D. (2019). RACK1 on and off the ribosome. RNA *25*, 881-895.

Juszkiewicz, S., and Hegde, R.S. (2017). Initiation of Quality Control during Poly(A) Translation Requires Site-Specific Ribosome Ubiquitination. Mol Cell *65*, 743-750 e744.

Juszkiewicz, S., Speldewinde, S.H., Wan, L., Svejstrup, J.Q., and Hegde, R.S. (2020). The ASC-1 Complex Disassembles Collided Ribosomes. Mol Cell *79*, 603-614 e608.

Kershner, L., and Welshhans, K. (2017a). RACK1 is necessary for the formation of point contacts and regulates axon growth. Dev Neurobiol *77*, 1038-1056.

Kershner, L., and Welshhans, K. (2017b). RACK1 regulates neural development. Neural Regen Res *12*, 1036-1039.

Kharade, S.V., Kurata, H., Bender, A.M., Blobaum, A.L., Figueroa, E.E., Duran, A., Kramer, M., Days, E., Vinson, P., Flores, D., *et al.* (2018). Discovery, Characterization, and Effects on Renal Fluid and Electrolyte Excretion of the Kir4.1 Potassium Channel Pore Blocker, VU0134992. Mol Pharmacol *94*, 926-937.

Kucheryavykh, Y.V., Kucheryavykh, L.Y., Nichols, C.G., Maldonado, H.M., Baksi, K., Reichenbach, A., Skatchkov, S.N., and Eaton, M.J. (2007). Downregulation of Kir4.1 inward rectifying potassium channel subunits by RNAi impairs potassium transfer and glutamate uptake by cultured cortical astrocytes. Glia *55*, 274-281.

Kuroha, K., Akamatsu, M., Dimitrova, L., Ito, T., Kato, Y., Shirahige, K., and Inada, T. (2010). Receptor for activated C kinase 1 stimulates nascent polypeptide-dependent translation arrest. EMBO Rep *11*, 956-961.

Lee, Y., Messing, A., Su, M., and Brenner, M. (2008). GFAP promoter elements required for region-specific and astrocyte-specific expression. Glia *56*, 481-493.

Lin, Y.J., Huang, L.H., and Huang, C.T. (2013). Enhancement of heterologous gene expression in Flammulina velutipes using polycistronic vectors containing a viral 2A cleavage sequence. PLoS One *8*, e59099.

MacVicar, B.A., Feighan, D., Brown, A., and Ransom, B. (2002). Intrinsic optical signals in the rat optic nerve: role for K(+) uptake via NKCC1 and swelling of astrocytes. Glia *37*, 114-123.

Majzoub, K., Hafirassou, M.L., Meignin, C., Goto, A., Marzi, S., Fedorova, A., Verdier, Y., Vinh, J., Hoffmann, J.A., Martin, F.*, et al*. (2014). RACK1 controls IRES-mediated translation of viruses. Cell *159*, 1086-1095.

Mauro, V.P., and Matsuda, D. (2016). Translation regulation by ribosomes: Increased complexity and expanded scope. RNA Biol *13*, 748-755.

Mazare, N., Oudart, M., Cheung, G., Boulay, A.C., and Cohen-Salmon, M. (2020a). Immunoprecipitation of Ribosome-Bound mRNAs from Astrocytic Perisynaptic Processes of the Mouse Hippocampus. STAR Protoc *1*, 100198.

Mazare, N., Oudart, M., and Cohen-Salmon, M. (2021). Local translation in perisynaptic and perivascular astrocytic processes - a means to ensure astrocyte molecular and functional polarity? J Cell Sci *134*.

Mazare, N., Oudart, M., Moulard, J., Cheung, G., Tortuyaux, R., Mailly, P., Mazaud, D., Bemelmans, A.P., Boulay, A.C., Blugeon, C.*, et al*. (2020b). Local Translation in Perisynaptic Astrocytic Processes Is Specific and Changes after Fear Conditioning. Cell Rep *32*, 108076.

McGough, N.N., He, D.Y., Logrip, M.L., Jeanblanc, J., Phamluong, K., Luong, K., Kharazia, V., Janak, P.H., and Ron, D. (2004). RACK1 and brain-derived neurotrophic factor: a homeostatic pathway that regulates alcohol addiction. J Neurosci *24*, 10542-10552.

Miller, P.M., Folkmann, A.W., Maia, A.R., Efimova, N., Efimov, A., and Kaverina, I. (2009). Golgi-derived CLASP-dependent microtubules control Golgi organization and polarized trafficking in motile cells. Nat Cell Biol *11*, 1069-1080.

Natchiar, S.K., Myasnikov, A.G., Kratzat, H., Hazemann, I., and Klaholz, B.P. (2017). Visualization of chemical modifications in the human 80S ribosome structure. Nature *551*, 472-477.

Nielsen, M.H., Flygaard, R.K., and Jenner, L.B. (2017). Structural analysis of ribosomal RACK1 and its role in translational control. Cell Signal *35*, 272-281.

Nilsson, J., Sengupta, J., Frank, J., and Nissen, P. (2004). Regulation of eukaryotic translation by the RACK1 protein: a platform for signalling molecules on the ribosome. EMBO Rep *5*, 1137-1141.

Nwaobi, S.E., Cuddapah, V.A., Patterson, K.C., Randolph, A.C., and Olsen, M.L. (2016). The role of glial-specific Kir4.1 in normal and pathological states of the CNS. Acta Neuropathol *132*, 1-21.

Olsen, M.L., and Sontheimer, H. (2008). Functional implications for Kir4.1 channels in glial biology: from K+ buffering to cell differentiation. J Neurochem *107*, 589-601.

Oudart, M., Tortuyaux, R., Mailly, P., Mazare, N., Boulay, A.C., and Cohen-Salmon, M. (2020). AstroDot - a new method for studying the spatial distribution of mRNA in astrocytes. J Cell Sci *133*.

Perez-Riverol, Y., Csordas, A., Bai, J., Bernal-Llinares, M., Hewapathirana, S., Kundu, D.J., Inuganti, A., Griss, J., Mayer, G., Eisenacher, M., *et al.* (2019). The PRIDE database and related tools and resources in 2019: improving support for quantification data. Nucleic Acids Res *47*, D442-D450.

Pilaz, L.J., Lennox, A.L., Rouanet, J.P., and Silver, D.L. (2016). Dynamic mRNA Transport and Local Translation in Radial Glial Progenitors of the Developing Brain. Curr Biol *26*, 3383-3392.

Poullet, P., Carpentier, S., and Barillot, E. (2007). myProMS, a web server for management and validation of mass spectrometry-based proteomic data. Proteomics *7*, 2553-2556.

Radomska, K.J., Halvardson, J., Reinius, B., Lindholm Carlstrom, E., Emilsson, L., Feuk, L., and Jazin, E. (2013). RNA-binding protein QKI regulates Glial fibrillary acidic protein expression in human astrocytes. Hum Mol Genet *22*, 1373-1382.

Ran, F.A., Hsu, P.D., Wright, J., Agarwala, V., Scott, D.A., and Zhang, F. (2013). Genome engineering using the CRISPR-Cas9 system. Nat Protoc *8*, 2281-2308.

Risher, W.C., Andrew, R.D., and Kirov, S.A. (2009). Real-time passive volume responses of astrocytes to acute osmotic and ischemic stress in cortical slices and in vivo revealed by two-photon microscopy. Glia *57*, 207-221.

Rollins, M.G., Jha, S., Bartom, E.T., and Walsh, D. (2019). RACK1 evolved species-specific multifunctionality in translational control through sequence plasticity within a loop domain. J Cell Sci *132*.

Russo, A., Scardigli, R., La Regina, F., Murray, M.E., Romano, N., Dickson, D.W., Wolozin, B., Cattaneo, A., and Ceci, M. (2017). Increased cytoplasmic TDP-43 reduces global protein synthesis by interacting with RACK1 on polyribosomes. Hum Mol Genet *26*, 1407-1418.

Sakers, K., Lake, A.M., Khazanchi, R., Ouwenga, R., Vasek, M.J., Dani, A., and Dougherty, J.D. (2017). Astrocytes locally translate transcripts in their peripheral processes. Proc Natl Acad Sci U S A *114*, E3830-E3838.

Sakers, K., Liu, Y., Llaci, L., Lee, S.M., Vasek, M.J., Rieger, M.A., Brophy, S., Tycksen, E., Lewis, R., Maloney, S.E., *et al*. (2021). Loss of Quaking RNA binding protein disrupts the expression of genes associated with astrocyte maturation in mouse brain. Nat Commun *12*, 1537.

Seifert, G., Huttmann, K., Binder, D.K., Hartmann, C., Wyczynski, A., Neusch, C., and Steinhauser, C. (2009). Analysis of astroglial K+ channel expression in the developing hippocampus reveals a predominant role of the Kir4.1 subunit. J Neurosci *29*, 7474-7488.

Sibille, J., Dao Duc, K., Holcman, D., and Rouach, N. (2015). The neuroglial potassium cycle during neurotransmission: role of Kir4.1 channels. PLoS Comput Biol *11*, e1004137.

Sibille, J., Pannasch, U., and Rouach, N. (2014). Astroglial potassium clearance contributes to short-term plasticity of synaptically evoked currents at the tripartite synapse. J Physiol *592*, 87-102.

Sitron, C.S., Park, J.H., and Brandman, O. (2017). Asc1, Hel2, and Slh1 couple translation arrest to nascent chain degradation. RNA *23*, 798-810.

Srinivasan, R., Lu, T.Y., Chai, H., Xu, J., Huang, B.S., Golshani, P., Coppola, G., and Khakh, B.S. (2016). New Transgenic Mouse Lines for Selectively Targeting Astrocytes and Studying Calcium Signals in Astrocyte Processes In Situ and In Vivo. Neuron *92*, 1181-1195.

Sundaramoorthy, E., Leonard, M., Mak, R., Liao, J., Fulzele, A., and Bennett, E.J. (2017). ZNF598 and RACK1 Regulate Mammalian Ribosome-Associated Quality Control Function by Mediating Regulatory 40S Ribosomal Ubiquitylation. Mol Cell *65*, 751-760 e754.

Takeuchi, A., Takahashi, Y., Iida, K., Hosokawa, M., Irie, K., Ito, M., Brown, J.B., Ohno, K., Nakashima, K., and Hagiwara, M. (2020). Identification of Qk as a Glial Precursor Cell Marker that Governs the Fate Specification of Neural Stem Cells to a Glial Cell Lineage. Stem Cell Reports.

The, M., MacCoss, M.J., Noble, W.S., and Kall, L. (2016). Fast and Accurate Protein False Discovery Rates on Large-Scale Proteomics Data Sets with Percolator 3.0. J Am Soc Mass Spectrom *27*, 1719-1727.

Thompson, M.K., Rojas-Duran, M.F., Gangaramani, P., and Gilbert, W.V. (2016). The ribosomal protein Asc1/RACK1 is required for efficient translation of short mRNAs. Elife *5*.

Valot, B., Langella, O., Nano, E., and Zivy, M. (2011). MassChroQ: a versatile tool for mass spectrometry quantification. Proteomics *11*, 3572-3577.

Vedrenne, C., Klopfenstein, D.R., and Hauri, H.P. (2005). Phosphorylation controls CLIMP-63-mediated anchoring of the endoplasmic reticulum to microtubules. Mol Biol Cell *16*, 1928-1937.

Wang, H., and Friedman, E. (2001). Increased association of brain protein kinase C with the receptor for activated C kinase-1 (RACK1) in bipolar affective disorder. Biol Psychiatry *50*, 364-370.

Wenzel, H.J., Murray, K.D., Haify, S.N., Hunsaker, M.R., Schwartzer, J.J., Kim, K., La Spada, A.R., Sopher, B.L., Hagerman, P.J., Raske, C., *et al*. (2019). Astroglial-targeted expression of the fragile X CGG repeat premutation in mice yields RAN translation, motor deficits and possible evidence for cell-to-cell propagation of FXTAS pathology. Acta Neuropathol Commun *7*, 27.

Xu, X., Yang, X., Xiong, Y., Gu, J., He, C., Hu, Y., Xiao, F., Chen, G., and Wang, X. (2015). Increased expression of receptor for activated C kinase 1 in temporal lobe epilepsy. J Neurochem *133*, 134-143.

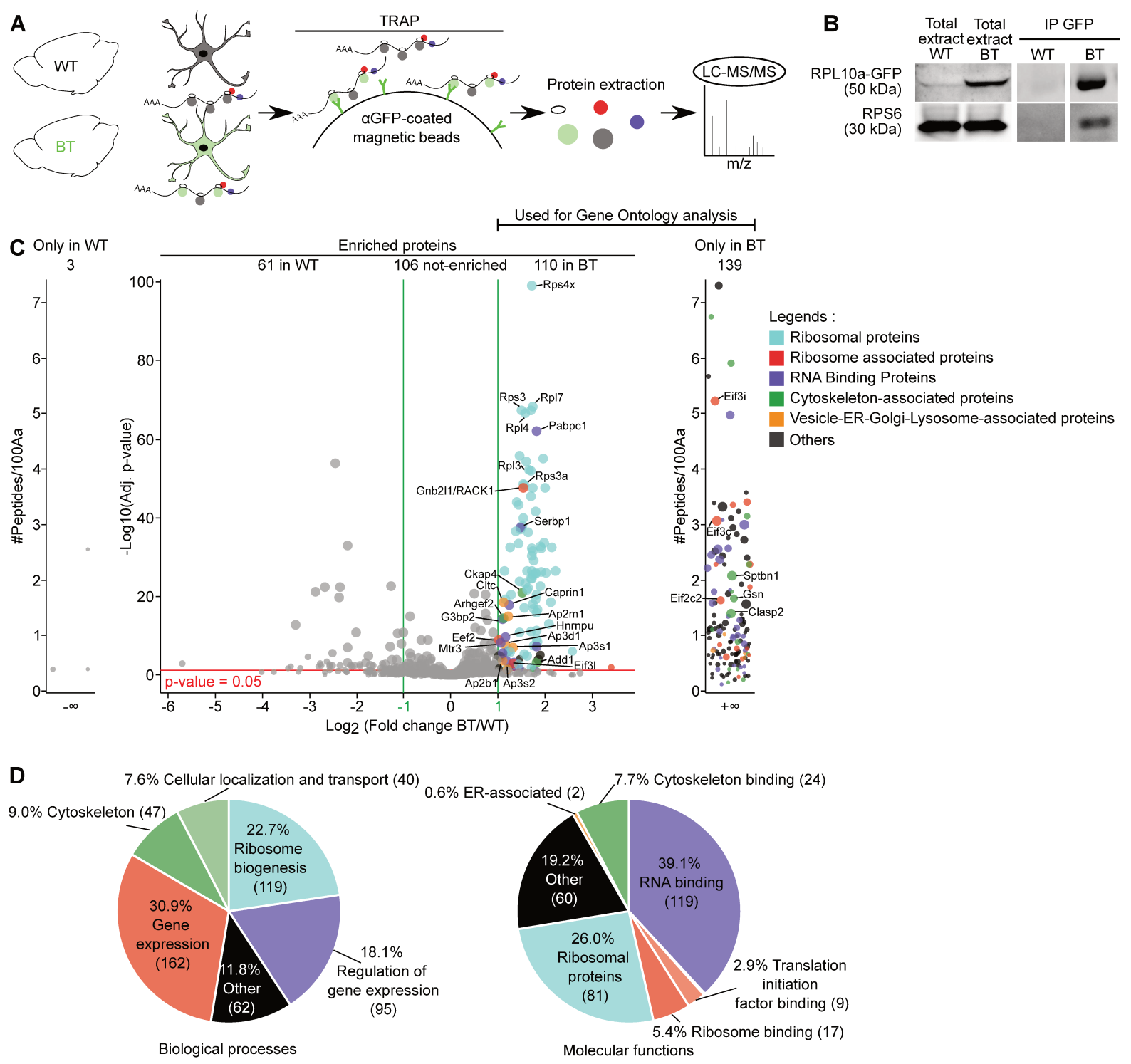
A
WT
BT
TRAP
αGFP-coated
magnetic beads
Protein extraction
LC-MS/MS
m/z
B
Total extract WT
Total extract BT
IP GFP
WT
BT
RPL10a-GFP (50 kDa)
RPS6 (30 kDa)
C
Only in WT
3
Enriched proteins
61 in WT
106 not-enriched
110 in BT
Only in BT
139
Used for Gene Ontology analysis
#Peptides/100Aa
-Log10(Adj. p-value)
p-value = 0.05
Log2 (Fold change BT/WT)
Rps4x
Rps3
Rpl7
Rpl4
Pabpc1
Rpl3
Rps3a
Gnb2l1/RACK1
Serbp1
Ckap4
Cltc
Caprin1
Arhgef2
G3bp2
Ap2m1
Hnrnpu
Eef2
Ap3d1
Mtr3
Ap3s1
Add1
Eif3l
Ap2b1
Ap3s2
Eif3i
Eif3c
Eif2c2
Sptbn1
Gsn
Clasp2
Legends :
Ribosomal proteins
Ribosome associated proteins
RNA Binding Proteins
Cytoskeleton-associated proteins
Vesicle-ER-Golgi-Lysosome-associated proteins
Others
D
7.6% Cellular localization and transport (40)
9.0% Cytoskeleton (47)
22.7% Ribosome biogenesis (119)
30.9% Gene expression (162)
11.8% Other (62)
18.1% Regulation of gene expression (95)
Biological processes
0.6% ER-associated (2)
7.7% Cytoskeleton binding (24)
19.2% Other (60)
39.1% RNA binding (119)
26.0% Ribosomal proteins (81)
2.9% Translation initiation factor binding (9)
5.4% Ribosome binding (17)
Molecular functions

Figure 1

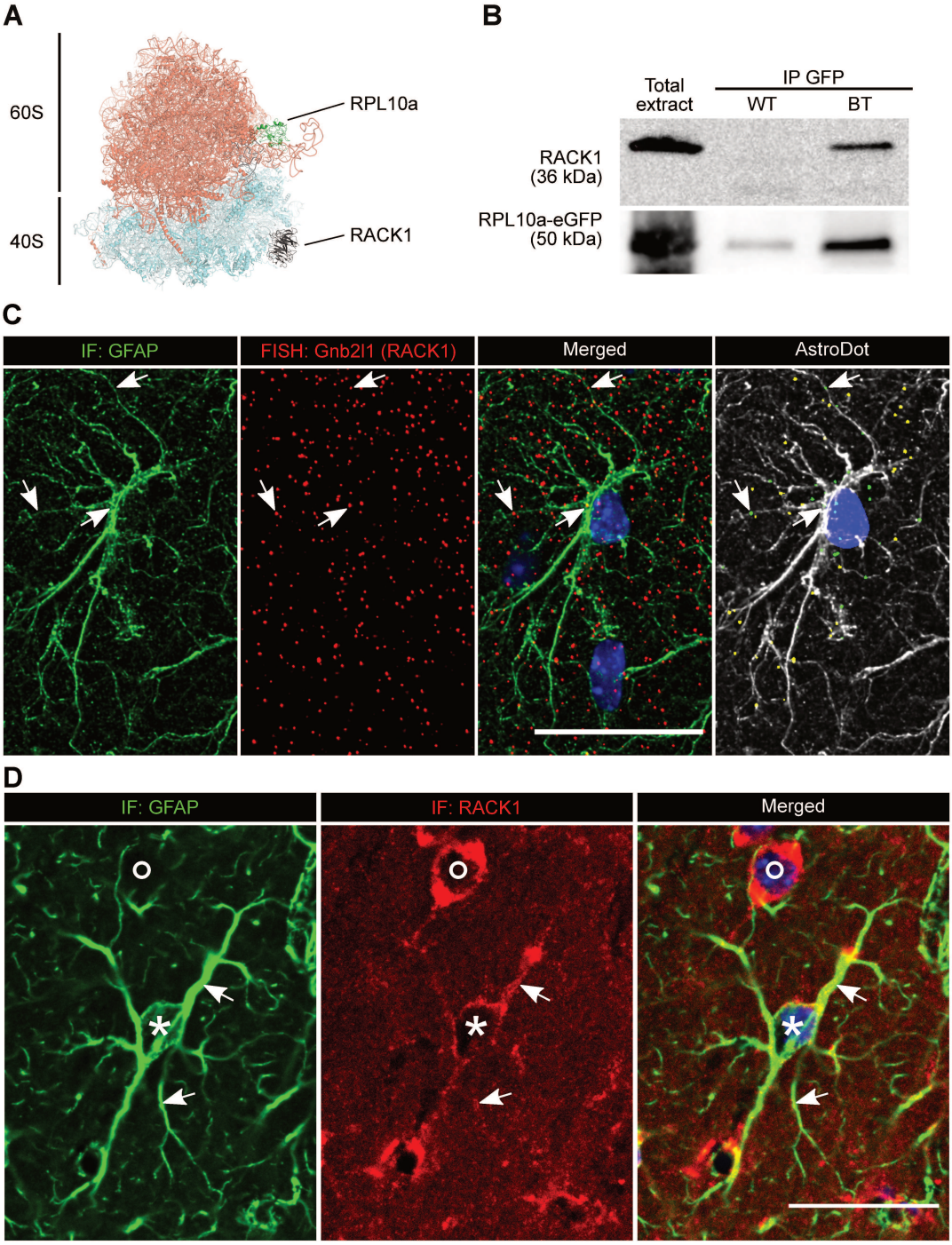
A
60S
40S
RPL10a
RACK1
B
Total extract
IP GFP
WT
BT
RACK1 (36 kDa)
RPL10a-eGFP (50 kDa)
C
IF: GFAP
FISH: Gnb2l1 (RACK1)
Merged
AstroDot
D
IF: GFAP
IF: RACK1
Merged

Figure 2

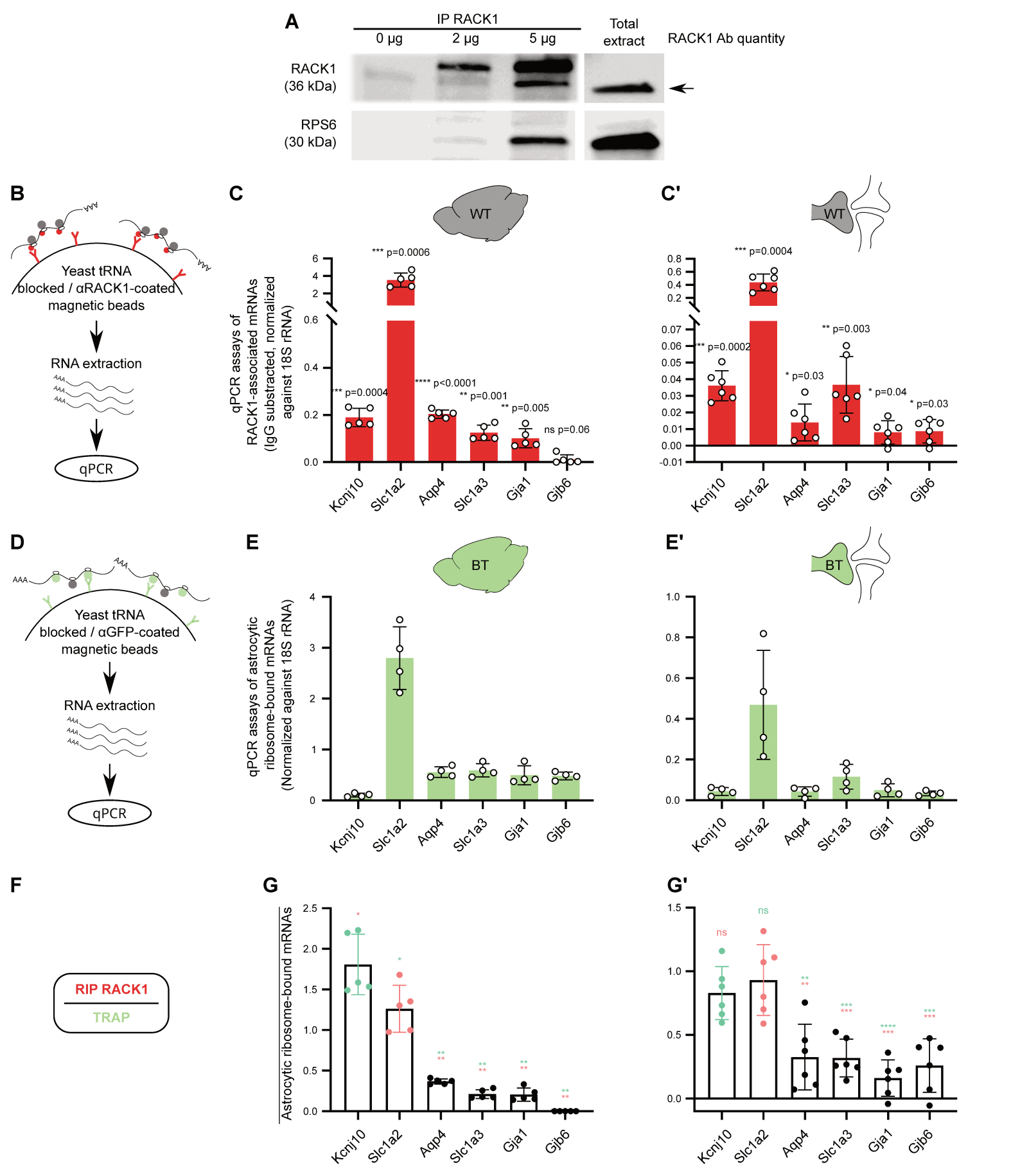
A
IP RACK1
0 µg
2 µg
5 µg
Total extract
RACK1 Ab quantity
RACK1 (36 kDa)
RPS6 (30 kDa)
B
Yeast tRNA blocked / αRACK1-coated magnetic beads
RNA extraction
qPCR
C
WT
qPCR assays of RACK1-associated mRNAs (IgG substracted, normalized against 18S rRNA)
*** p=0.0006
** p=0.0004
**** p<0.0001
** p=0.001
** p=0.005
ns p=0.06
Kcnj10
Slc1a2
Aqp4
Slc1a3
Gja1
Gjb6
C'
WT
*** p=0.0004
*** p=0.0002
* p=0.03
** p=0.003
* p=0.04
* p=0.03
D
Yeast tRNA blocked / αGFP-coated magnetic beads
RNA extraction
qPCR
E
BT
qPCR assays of astrocytic ribosome-bound mRNAs (Normalized against 18S rRNA)
E'
BT
F
RIP RACK1
TRAP
G
Astrocytic ribosome-bound mRNAs
G'
ns

Figure 3

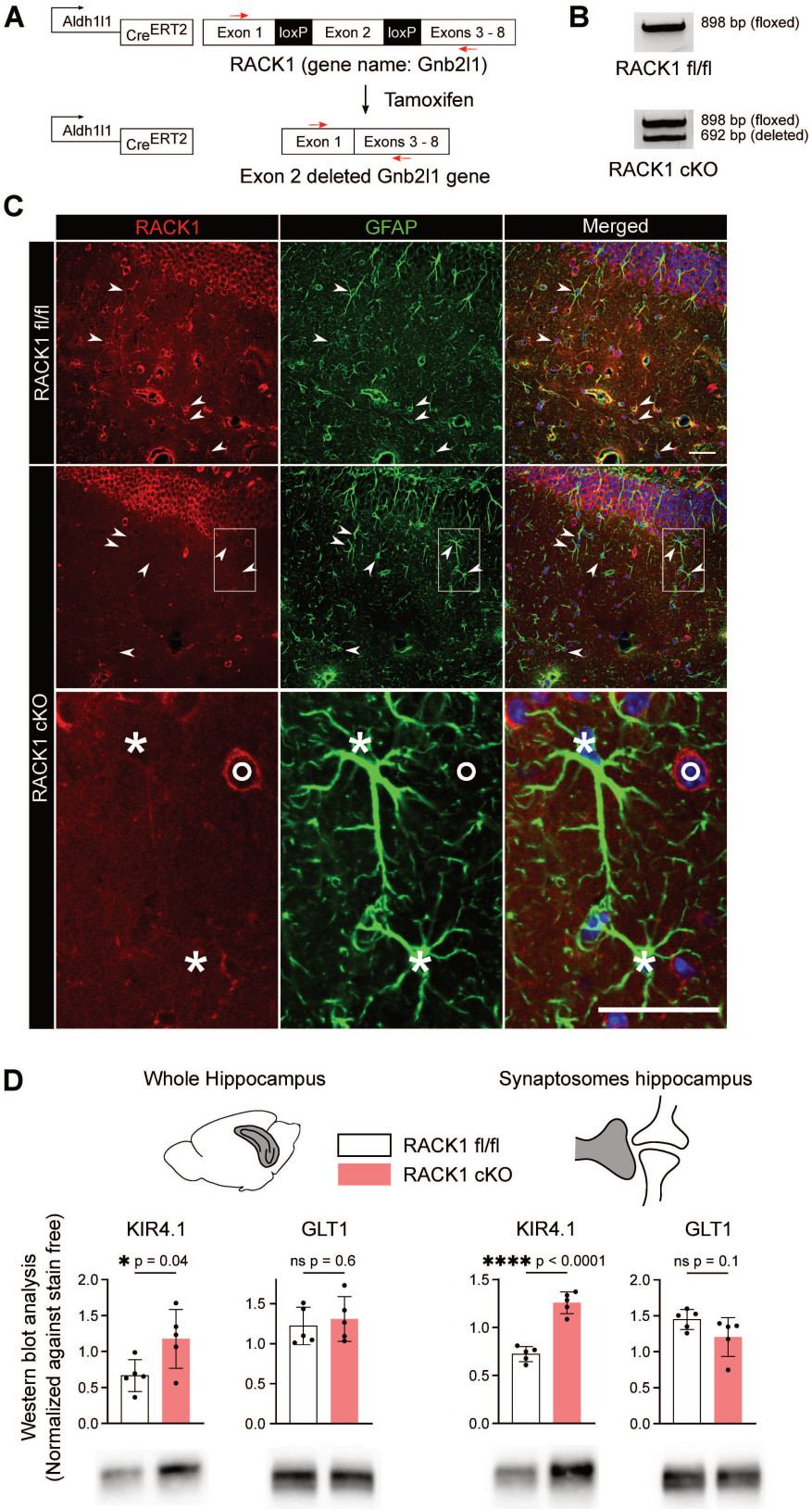
A
Aldh1l1
CreERT2
Exon 1
loxP
Exon 2
loxP
Exons 3 - 8
RACK1 (gene name: Gnb2l1)
Tamoxifen
Exon 1
Exons 3 - 8
Exon 2 deleted Gnb2l1 gene
B
898 bp (floxed)
RACK1 fl/fl
898 bp (floxed)
692 bp (deleted)
RACK1 cKO
C
RACK1
GFAP
Merged
RACK1 fl/fl
RACK1 cKO
D
Whole Hippocampus
Synaptosomes hippocampus
RACK1 fl/fl
RACK1 cKO
Western blot analysis
(Normalized against stain free)
KIR4.1
* p = 0.04
GLT1
ns p = 0.6
KIR4.1
**** p < 0.0001
GLT1
ns p = 0.1

Figure 4

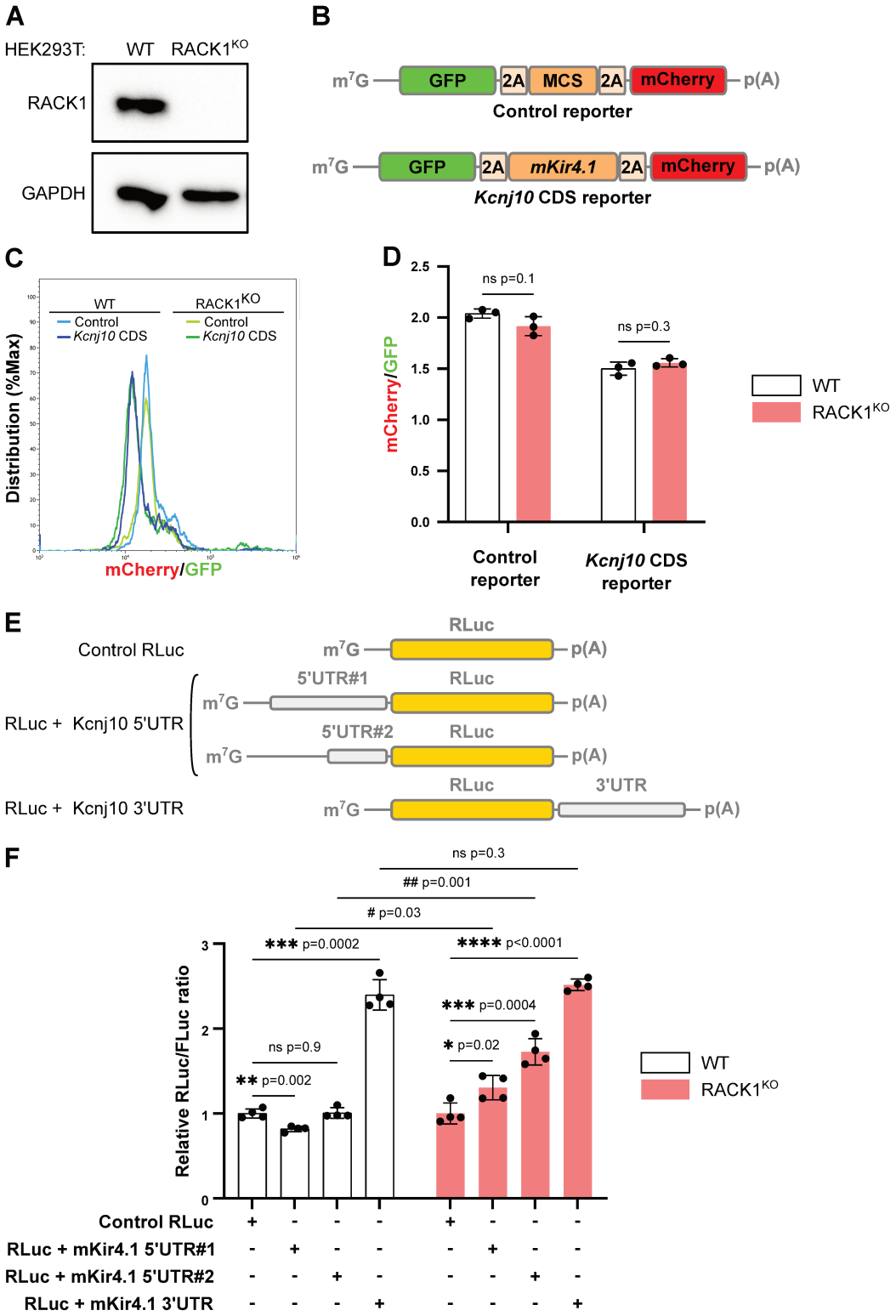
A
HEK293T:
WT
RACK1KO
RACK1
GAPDH
B
m7G
GFP
2A
MCS
2A
mCherry
p(A)
Control reporter
mKir4.1
Kcnj10 CDS reporter
C
Control
Kcnj10 CDS
Distribution (%Max)
mCherry/GFP
D
ns p=0.1
ns p=0.3
mCherry/GFP
Control reporter
Kcnj10 CDS reporter
WT
RACK1KO
E
Control RLuc
RLuc
5'UTR#1
5'UTR#2
RLuc + Kcnj10 5'UTR
RLuc + Kcnj10 3'UTR
3'UTR
F
ns p=0.3
p=0.001
p=0.03
*** p=0.0002
**** p<0.0001
*** p=0.0004
* p=0.02
ns p=0.9
** p=0.002
Relative RLuc/FLuc ratio
Control RLuc
RLuc + mKir4.1 5'UTR#1
RLuc + mKir4.1 5'UTR#2
RLuc + mKir4.1 3'UTR
G
Kcnj10 5'UTR#1
1
242
95
191
127
181
H
RLuc/FLuc ratio (relative to control RLuc)
* p=0.03
ns p=0.3
Kcnj10 5'UTR#1:
FL
1-146
95-242
95-191
127-242
181-242

Figure 5

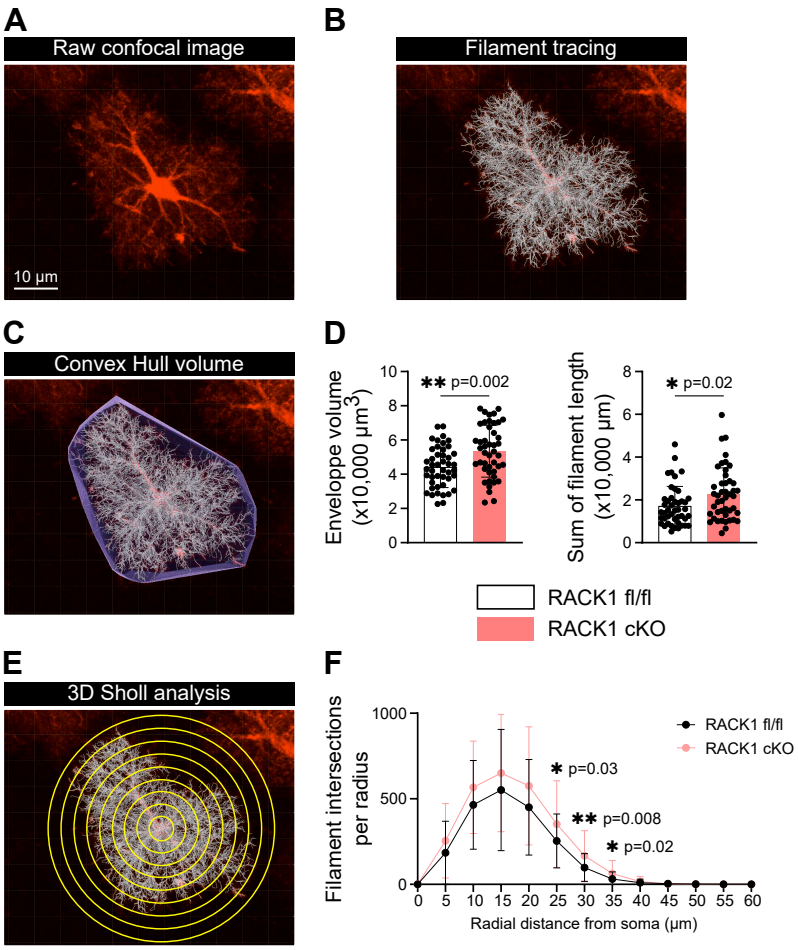
A
Raw confocal image
10 µm
B
Filament tracing
C
Convex Hull volume
D
Enveloppe volume (x10,000 µm3)
** p=0.002
Sum of filament length (x10,000 µm)
* p=0.02
RACK1 fl/fl
RACK1 cKO
E
3D Sholl analysis
F
Filament intersections per radius
* p=0.03
** p=0.008
* p=0.02
Radial distance from soma (µm)

Figure 6

Figure 7

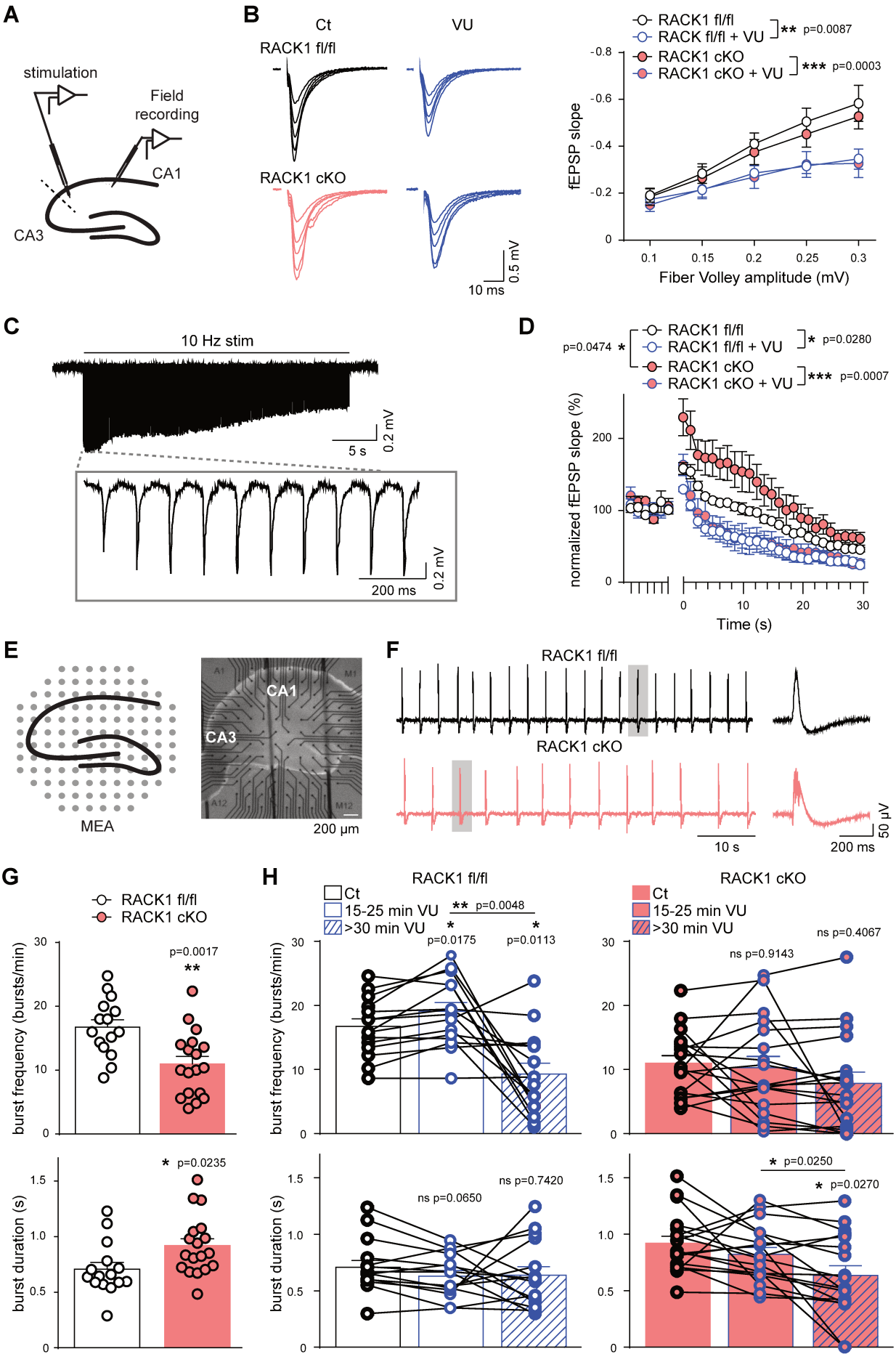
A
stimulation
Field recording
CA1
CA3
B
Ct
VU
RACK1 fl/fl
RACK1 cKO
0.5 mV
10 ms
RACK1 fl/fl
RACK fl/fl + VU
** p=0.0087
RACK1 cKO
RACK1 cKO + VU
*** p=0.0003
fEPSP slope
Fiber Volley amplitude (mV)
C
10 Hz stim
0.2 mV
5 s
200 ms
D
p=0.0474 *
RACK1 fl/fl
RACK1 fl/fl + VU
* p=0.0280
RACK1 cKO
RACK1 cKO + VU
*** p=0.0007
normalized fEPSP slope (%)
Time (s)
E
MEA
CA1
CA3
200 µm
F
RACK1 fl/fl
RACK1 cKO
10 s
200 ms
50 µV
G
RACK1 fl/fl
RACK1 cKO
burst frequency (bursts/min)
p=0.0017
**
burst duration (s)
* p=0.0235
H
RACK1 fl/fl
Ct
15-25 min VU
>30 min VU
** p=0.0048
p=0.0175
p=0.0113
ns p=0.0650
ns p=0.7420
RACK1 cKO
ns p=0.9143
ns p=0.4067
* p=0.0250
* p=0.0270

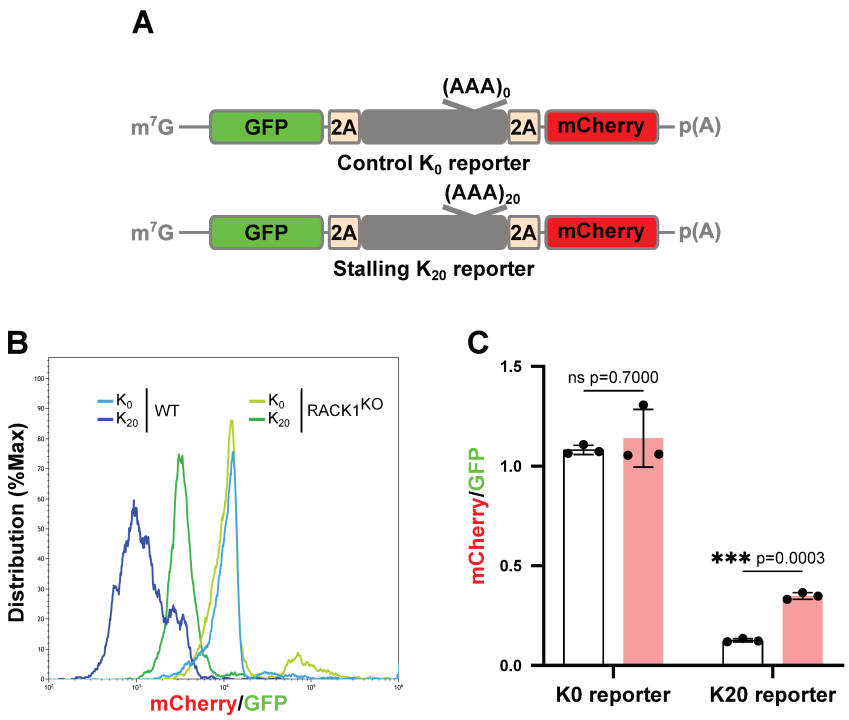
A
(AAA)0
m7G
GFP
2A
2A
mCherry
p(A)
Control K0 reporter
(AAA)20
m7G
GFP
2A
2A
mCherry
p(A)
Stalling K20 reporter
B
K0
K20
WT
K0
K20
RACK1KO
Distribution (%Max)
mCherry/GFP
C
ns p=0.7000
*** p=0.0003
mCherry/GFP
1.5
1.0
0.5
0.0
K0 reporter
K20 reporter

Figure S1

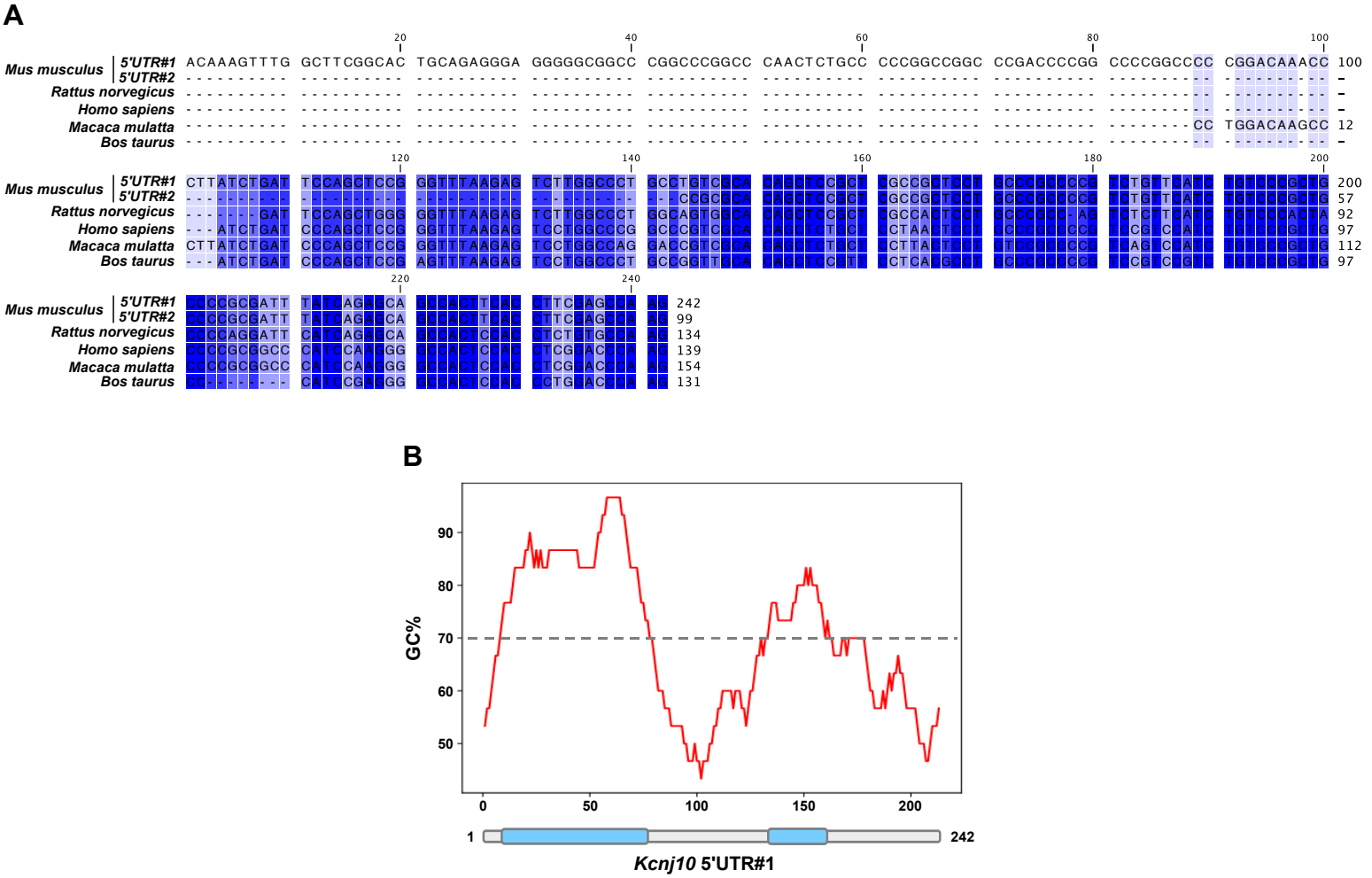
A
Mus musculus
5'UTR#1
5'UTR#2
Rattus norvegicus
Homo sapiens
Macaca mulatta
Bos taurus
B
GC%
Kcnj10 5'UTR#1

Figure S2

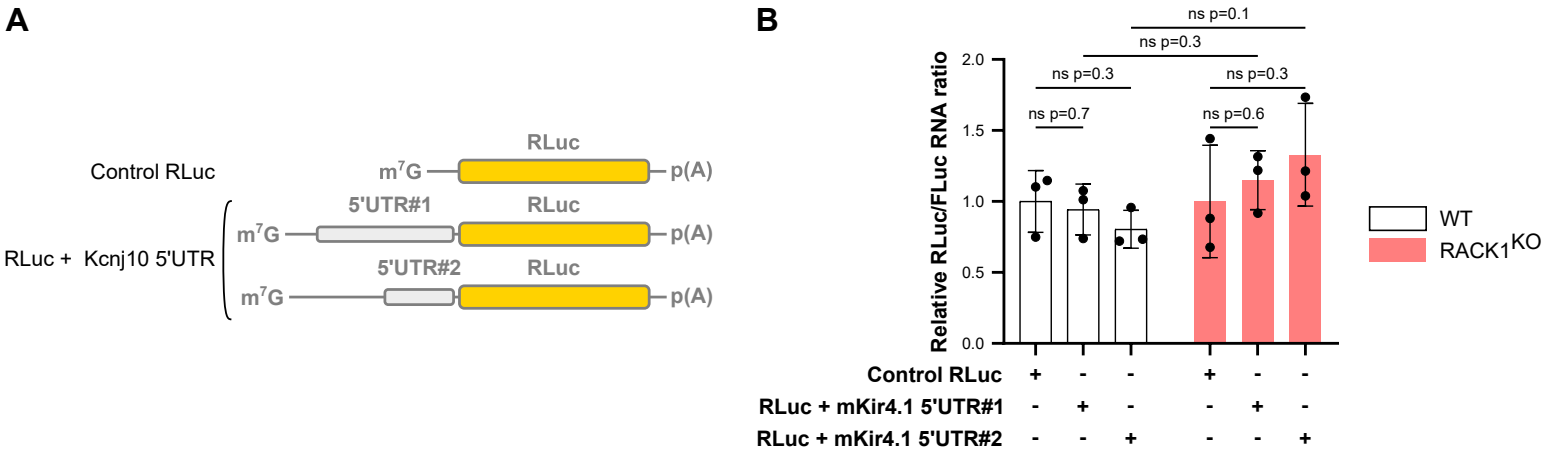
A
Control RLuc
RLuc
m7G
p(A)
RLuc + Kcnj10 5'UTR
5'UTR#1
5'UTR#2
B
Relative RLuc/FLuc RNA ratio
2.0
1.5
1.0
0.5
0.0
ns p=0.1
ns p=0.3
ns p=0.3
ns p=0.3
ns p=0.7
ns p=0.6
WT
RACK1KO
Control RLuc + - - + - -
RLuc + mKir4.1 5'UTR#1 - + - - + -
RLuc + mKir4.1 5'UTR#2 - - + - - +

Figure S3

Uniprot Accesion number	Gene name	Protein description	Log_2 FC (BT/WT)	p-value	Peptides used	MW (kDa)
		Ribosomal proteins (75)				
P62702	Rps4x	40S ribosomal protein S4, X isoform	1,72	6,99E-100	305	29,6
Q9D8E6	Rpl4	60S ribosomal protein L4	1,57	2,66E-67	286	47,2
P27659	Rpl3	60S ribosomal protein L3	1,65	5,67E-53	253	46,1
P62908	Rps3	40S ribosomal protein S3	1,51	3,98E-68	243	26,7
P97351	Rps3a	40S ribosomal protein S3a	1,55	3,20E-49	240	29,9
P14148	Rpl7	60S ribosomal protein L7	1,74	5,02E-69	224	31,4
		Ribosome-associated proteins (19)				
P68040	Gnb2l1	Receptor of activated protein C kinase 1	1,54	2,43E-48	205	35,1
P58252	Eef2	Elongation factor 2	1,02	1,24E-09	91	95,3
Q8R1B4	Eif3c	Eukaryotic translation initiation factor 3 subunit C	+∞	NA	28	105,5
Q8QZY1	Eif3l	Eukaryotic translation initiation factor 3 subunit L	1,31	1,24E-03	19	66,6
Q9QZD9	Eif3i	Eukaryotic translation initiation factor 3 subunit I	+∞	NA	17	36,5
Q8CJG0	Eif2c2	Protein argonaute-2	+∞	NA	14	97,3
		RNA binding proteins (43)				
P29341	Pabpc1	Polyadenylate-binding protein 1	1,83	1,08E-62	226	70,7
Q9CY58	Serbp1	Plasminogen activator inhibitor 1 RNA-binding protein	1,49	2,36E-38	127	44,7
Q60865	Caprin1	Caprin-1	1,24	1,13E-18	78	78,2
P97379	G3bp2	Ras GTPase-activating protein-binding protein 2	1,10	5,44E-15	76	54,1
Q8K310	Matr3	Matrin-3	1,05	5,50E-09	47	94,6
Q8VEK3	Hnrnpu	Heterogeneous nuclear ribonucleoprotein U	1,17	2,04E-10	46	87,9
		Cytoskeleton-associated proteins (20)				
Q60875	Arhgef2	Rho guanine nucleotide exchange factor 2	1,12	2,96E-15	88	112,0
Q8BMK4	Ckap4	Cytoskeleton-associated protein 4	1,52	8,75E-22	85	63,7
Q62261	Sptbn1	Spectrin beta chain, non-erythrocytic 1	+∞	NA	49	274,2
Q9QYC0	Add1	Alpha-adducin	1,82	7,42E-04	25	80,6
Q8BRT1	Clasp2	CLIP-associating protein 2	+∞	NA	18	140,7
P13020	Gsn	Gelsolin	+∞	NA	13	85,9
		Vesicles - ER - Golgi - Lysosomes-associated proteins (10)				
Q68FD5	Cltc	Clathrin heavy chain 1	1,11	2,28E-19	269	191,6
O54774	Ap3d1	AP-3 complex subunit delta-1	1,16	2,17E-08	125	135,1
P84091	Ap2m1	AP-2 complex subunit mu	1,23	1,36E-15	79	49,7
Q9DBG3	Ap2b1	AP-2 complex subunit beta	1,09	1,60E-04	39	104,6
Q9DCR2	Ap3s1	AP-3 complex subunit sigma-1	1,31	7,88E-08	32	21,7
Q8BSZ2	Ap3s2	AP-3 complex subunit sigma-2	1,19	3,34E-02	19	22,0

Table 1

Supplementary results

I. RACK1 in astrocytes is not involved in pentylenetetrazol (PTZ)-induced acute epilepsy

Introduction

KIR4.1 mediates potassium homeostasis at the synapse. We have shown that in the RACK1 cKO model, in which RACK1 is deleted in the astrocytes, KIR4.1 was increased in astrocytes and in PAPs. This augmentation was accompanied by an overall decrease in neuronal network burst frequency and increase in burst duration in pro-epileptic conditions (0 Mg 6 mM K+ aCSF) *ex vivo* in the hippocampus. We wondered next if RACK1 could have a role in pro-epileptic conditions *in vivo*. In collaboration with Key-Obs (Orléans), a preclinical Contract Research Organisation (CRO), we performed a PTZ-induced seizure behavioral test consisting in infusing PTZ in the mouse blood stream and record seizure susceptibility. PTZ acts as an inhibitor of GABA-A receptor therefore reducing inhibitory inputs and increasing neuronal excitation. We hypothesized that KIR4.1 increased in the RACK1 cKO mice would protect from epilepsy by increasing the dose necessary for seizure induction because of a higher potassium buffering in the synapse.

Materials and methods

All the experiments were conducted at Key-Obs laboratory by authorized technicians, engineers or researchers regularly employed by the company. They were directed by a researcher of Key-Obs. Manipulations of animals were conducted carefully in order to reduce stress to a minimum. All the experiments were performed in compliance with the guidelines of the French Ministry of Agriculture for experiments with laboratory animals (law 2013-118). The experimental protocols have been approved by the internal Ethical Committee of Key-Obs SAS N° 27, registered at the French ministry of research. Experiments were conducted during the light phase, in standard conditions (T°= 22.0 ± 1.5°C), with artificial light in quiet conditions (no noise except those generated by ventilation and by the apparatus used for experiments). Experiments were conducted blindly. The animals have not been subjected to other experiments before the study.

12 adult males RACK1 cKO mice and 12 adult males RACK1 fl/fl were used.

The animal is placed in a plastic cylinder (length 12 cm, diameter 3.5 cm) where only limited movement is possible and leaving the tail of the mouse outside the cylinder. A needle is inserted into the lateral tail vein, fixed to the vein by a piece of adhesive. PTZ (pentylenetetrazole, Sigma-Aldrich, France, ref p6500) solution (10 mg/ml in 0.9% NaCl) is infused using a syringe pump at a concentration rate of 0.25 ml/min (**Fig. 1A**). The following parameters were measured: dose before tonic seizure (body tremor), tonic-clonic seizure (extension of hind-paws) and death.

Results and discussion

Results show no significant difference in all measured parameters between RACK1 cKO and RACK1 fl/fl mice (**Fig. 1B**). PTZ acts on inhibitory networks via GABA-A receptor. We could hypothesized that potassium homeostasis does not regulate synaptic activity similarly between inhibitory and excitatory synapses. To tackle this question, another seizure-induced test targeting excitatory synapses could be used such as the pilocarpine molecule, an agonist of muscarinic acetylcholine receptor or kainate, a glutamate-like molecule agonist of NMDA and AMPA receptors. In addition, in *ex vivo* experiments and in the literature (Cui et al., 2018), KIR4.1 increase reduces neuronal bursting frequency but also changes the bursting pattern and increase the burst duration. Therefore, these activity changes may not be sufficient to protect against seizures in epilepsy.

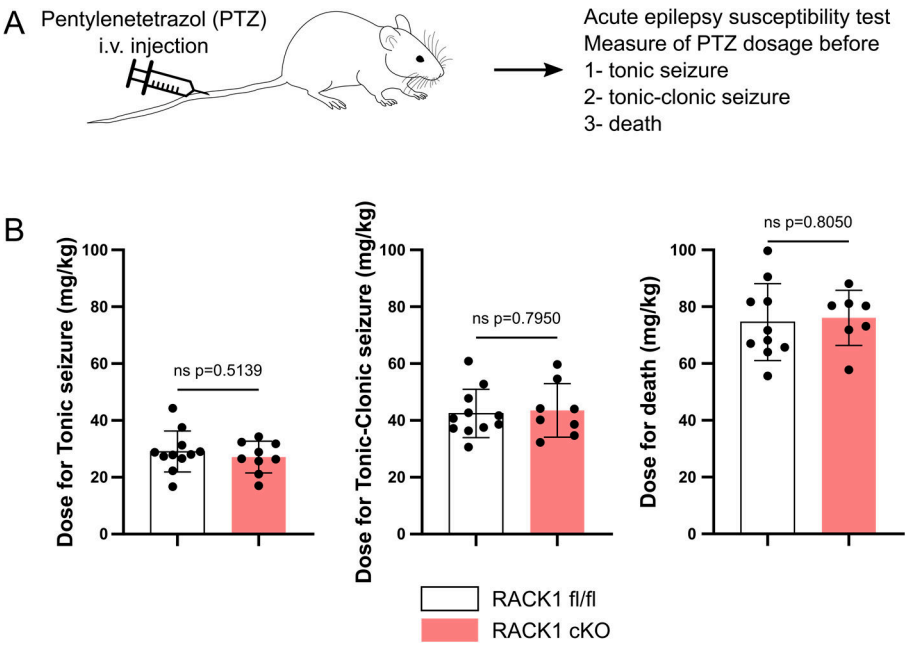

Figure 16. ***RACK1 in astrocytes is not involved in pentylenetetrazol (PTZ)-induced acute epilepsy.*** ***(A)*** *Schematic representation of intravenous (i.v.) injection of PTZ in the mouse tail. Increase dose of PTZ was injected and following parameters were recorded: dose before tonic seizure (body tremor), tonic-clonic seizure (hind-paws extension) and death.* ***(B)*** *Quantifications of the doses necessary for the 3 parameters between RACK1 fl/fl (control) and RACK1 cKO mice. Mean ± standard deviation (SD). ns, p>0.05.*

II. RACK1 is not involved in depressive-like behavior tested with the forced-swimming test

Introduction

In congenic depressive rats, KIR4.1 is increased in the lateral habenula (Cui et al., 2018) which is sufficient to generate a depressive-like behavior. KIR4.1 is also increased in post-mortem tissues of depressive patients (Della Vecchia et al., 2021). Therefore, we tested depression-like behavior in our RACK1 cKO model in which KIR4.1 is upregulated. A forced-swimming test related to depressive-like phenotypes was performed at Key-Obs. A depressive behavior is represented as an increase in immobility time (giving up) and reduced swimming and climbing time.

Materials and methods

Experimental conditions are described in the previous chapter.

12 adult males RACK1 cKO mice and 12 adult males RACK1 fl/fl were used.

The experiment is carried out in glass cylinders (36 cm high, 24 cm diameter) filled with 20 cm 25°C water. The experiment is recorded with a camcorder, placed in front of the glass cylinders.

Animals are placed individually in a glass cylinder containing water (**Fig. 2A**). They are subjected to a 6-min swimming test session. The behavior of the mouse is measured on each 1-min period on the test.

Behavior is classified as one of three categories:

- Immobility: defined as floating in the water without struggling and using only small movements to keep the head above water.
- Swimming: defined as moving limbs in an active manner, more than required to keep the head above water and causing movement among quadrants of the cylinder.
- Climbing: defined as making active movements with forepaws moving in and out of the water, usually directed against the side of the cylinder.

The behavior is recorded on a camcorder and is scored at a later time by an experimenter blind to the treatments.

Results and discussion

All parameters had a high heterogeneity and no changes were statistically significant between RACK1 fl/fl and RACK1 cKO mice (**Fig. 2B, C**). Therefore, RACK1 does not seem to be involved in depressive-like behavior through KIR4.1 increased expression. However we performed only one behavioral test for depression and others exist such as the sucrose preference (depressive-like mice will not prefer sweet over normal water) or the learned helplessness tests (depressive-like mice will

not try to avoid repetitive aversive stimuli). We only tested KIR4.1 expression in hippocampus and whole brain and not in the lateral habenula specifically which is the area linked with negative emotion and is hyper functional in depression. Although some studies have linked the hippocampus to depression (Campbell and MacQueen, 2004), post-mortem investigations have found a decreased level of KIR4.1 in the hippocampus in depressive patients (Della Vecchia et al., 2021).

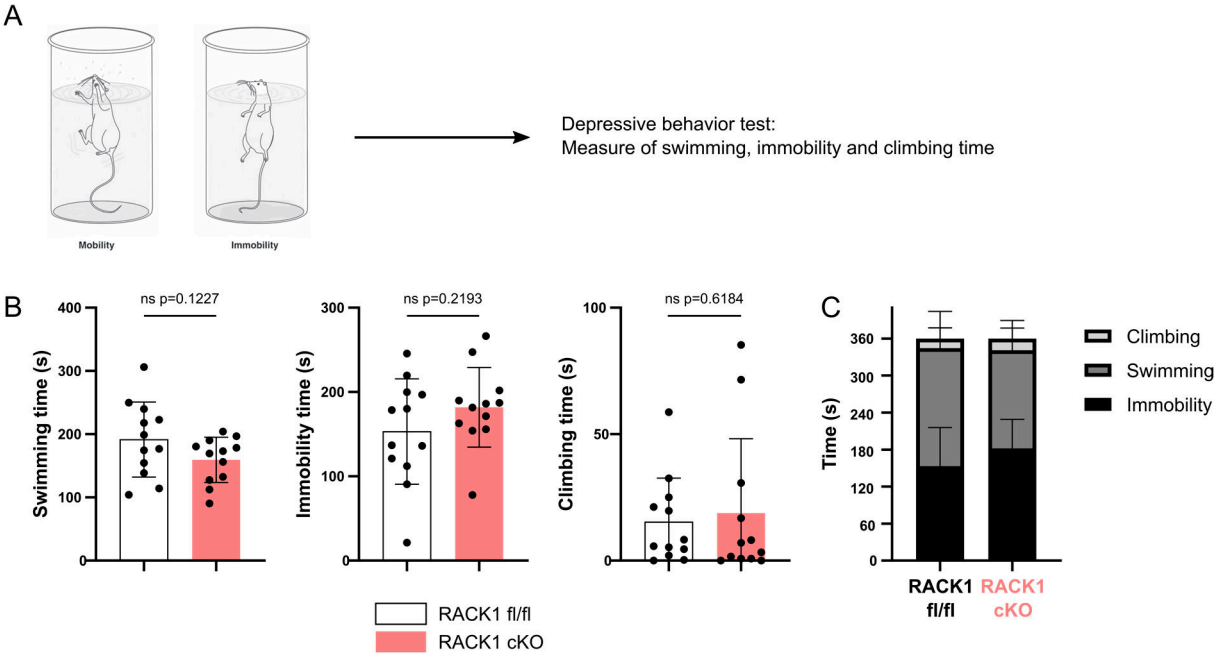

Figure 2. ***RACK1 is not involved in a depressive-like behavior. (A)*** *Schematic representation of the forced-swimming test. Measured parameters include swimming, wall climbing and immobility time. Adapted from (Abelaira et al., 2013).* ***(B)*** *Quantifications of the 3 parameters in RACK1 fl/fl (control) and RACK1 cKO mice. Mean ± SD. ns, p>0.05.* ***(C)*** *Representation of the time superposition over the 6 minutes experiment of the 3 measured parameters between the 2 mice groups.*

III. A model for RACK1 translation regulation on *Kcnj10* mRNA 5'UTR

Introduction

We showed that *Kcnj10* 5'UTR (and not the 3'UTR) was sensitive to RACK1 in a model of RACK1 KO HEK cells. By cutting the 5'UTR into smaller pieces, we demonstrated that the regulation was mostly due to its 2nd part from 127 to 242 nucleotides (nt). However, it remains elusive how RACK1 regulates *Kcnj10* translation through this particular sequence. RACK1 has been shown in the literature to co-immunoprecipitate with some known RBPs: PABPC1, LARP4B, TARDBP (TDP43), EIF3H, SERBP1, KHSRP and ZBP1 (IGF2BP1). For instance, RACK1 has been shown to recruit

ZBP1 with its mRNA *β-actin* and the kinase Src at the ribosome. Src phosphorylates ZBP1 to release its mRNA in the ribosome and activate translation. We hypothesized that RACK1 regulates Kcnj10 translation through the interaction of RNA-binding proteins (RBP). To test this hypothesis, we used *RBPsuite* to predict the interaction sites between several RBPs and *kcnj10* mRNA. Then we used *POSTAR3* to search for RBP – *kcnj10* interaction in Cross Linking ImmunoPrecipitation (CLIP)-sequencing data. Finally, we compiled the *RBPsuite*, POSTAR3 and literature data to draw an interaction map with *STRING* between RACK1 (Gnb2l1) and the RBP that were shown or predicted to interact with the 5'UTR of Kcnj10.

Materials and methods

RBP-Kcnj10 predicted interaction sites using RBPsuite

RBPsuite (http://www.csbio.sjtu.edu.cn/bioinf/RBPsuite/) (Pan et al., 2020) is a webserver using deep learning from the *ENCODE* eCLIP-seq database of 154 RBP and scoring, using *iDeepS* algorithm (Pan et al., 2018), the prediction of the RBP binding on a given linear RNA based on its sequence and secondary structure. We fed *RBPsuite* with the FASTA sequence of *Kcnj10 Mus musculus* mRNA and searched interactions among all 154 RBPs (general model). We only present here 14 RBPs involved in the CNS with key physiological functions: EIF3H, EWSR1, FMR1, FUS, FXR2, G3BP1, LARP4, MATR3, SERBP1, STAU2, YBX3, ZBP1, KHSRP and TARDBP (references in the result section).

RBP-Kcnj10 experimental interactions using POSTAR3

POSTAR3 (http://111.198.139.65/index.html) (Zhao et al., 2022) is a database for exploring post-transcriptional regulation based on sequencing data. We used the module RBP Binding Sites (http://111.198.139.65/RBS.html) to search for known interactions in CLIP-seq data between RBPs and the mouse *Kcnj10* mRNA. We selected the CLIP-seq data and peak calling method where *Kcnj10* interacts with previously encountered RBP from the *RBPsuite* study: HITS-CLIP with CIMS and Piranha peak calling methods and iCLIP with CITS peak calling method. Peak calling is a computational method used to identify the sequences in an mRNA that have been enriched with aligned reads from CLIP-seq experiments.

Interaction map between RACK1 and selected RBP using STRING

STRING (https://string-db.org/cgi/input?sessionId=bpg0I7L963iY&input_page_active_form=multiple_identifiers) is a database allowing the representation of protein-protein interactions from experimental and prediction data. *STRING* was fed with the 14 previously investigated RBPs in addition to RACK1 and PABPC1, a RBP known to interact with RACK1, which is not available in *RBPsuite*. Mouse database was selected. The interaction map was generated with confidence view for only experimental interactions with confidence score of 0.4 (medium).

Results and discussion

We used the webserver *RBPsuite* to predict RBP interactions sites on *kcnj10* mRNA (**Fig. 3A**). Among the 154 available RBPs, we selected 14 that we considered relevant because of their known roles in the CNS and in crucial physiological functions: EIF3H has been reported to control zebrafish development by regulating the translation of specific mRNAs (Choudhuri et al., 2013); EWSR1, FUS, MATR3 and TARDBP have been associated with Amyotrophic Lateral Sclerosis (ALS) (Barton et al., 2019); FMR1 and FXR2 have been associated with the Fragile X Syndrome (FXS) (Zhang et al., 2009); G3BP1 is concentrated in stress granules and has been associated with TARDBP (Sidibé et al., 2021); LARP4 and SERBP1 have been associated with brain cancer (Blagden et al., 2016; Kosti et al., 2020); STAU2 is required for dendritic spine morphology (Goetze et al., 2006); YBX3 is a known RBP to regulate subsets of RNAs (Cooke et al., 2019); ZBP1 is involved in growth cone orientation in the CNS (Lin and Holt, 2007) and KHSRP mediates neuronal development (Olguin et al., 2022). We showed previously that the regulation of *Kcnj10* by RACK1 occurs on its 5'UTR. In **Figure 3A**, 12 RBPs have a high score of predicted interaction at least in 1 of the 3 first bins (corresponding to 5'UTR of *Kcnj10*). For instance, FMR1 or FMRP is predicted to interact on all the 3 first bins and LARP4 only on the 2nd bin. Of note, several interactions have been predicted for each RBP including in the CDS and the 3'UTR. We showed previously that only the 2nd half, 127 – 242 nt, of *kcnj10* was sensitive to RACK1 corresponding to the 2nd and 3rd bins. Therefore, SERBP1 and ZBP1, having a high score in only the first bin on the 5'UTR, do not seem to be good candidates for the RACK1-mediated *kcnj10* regulation. In addition, KHSRP and TARDBP are predicted to only interact with kcnj10 at its 3'UTR.

We next searched for known interactors of *Kcnj10* by interrogating the POSTAR3 CLIP-seq database (**Fig. 3B**). We selected CLIP technologies and peak calling methods displaying previously investigated RBPs. Results show that FMR1 (Darnell et al., 2011), TARDBP (Lagier-Tourenne et al., 2012) and FUS (Lagier-Tourenne et al., 2012) have already been shown to interact experimentally with *Kcnj10* mRNA by CLIP. No indications on the targeted sequence are given, but considering the RBPsuite study, FMR1 and FUS are predicted to bind the 5'UTR of *Kcnj10*.

To link these RBPs with RACK1, we used the STRING database to draw the interaction map between RACK1 and the 14 RBPs previously investigated plus PABPC1, an RBP known to interact with RACK1 (**Fig. 3C**). The map shows the physical and functional interactions known to have been described in experiments and displayed as confidence view (the thicker the line, the more confident the interaction). Dotted lines have been added to describe the interactions known in the literature. Results show a direct link with PABPC1, LARP4B, TARDBP, EIF3H, SERBP1, KHSRP and ZBP1 and indirect interaction with FUS, EWSR1, FMR1, FXR2 and G3BP1. No interactions have been described between RACK1 and YBX3, STAU2 and MATR3.

The summary of these 3 studies, RBPsuite, POSTAR3 and STRING, are presented in **Table 1**. Among the 12 RBPs predicted to bind Kcnj10 5'UTR, only 2 have been shown to be in CLIP-seq data, FMR1 and FUS, and only 4 have been shown to interact with RACK1 : LARP4B, ZBP1, SERBP1, EIF3H. ZBP1 and SERBP1 are only predicted to interact with the first half of *Kcnj10* 5'UTR which is not sensitive to RACK1. FMR1 and FUS have not been shown to interact with RACK1 but it could be because it was not investigated. Interestingly, FMR1 or FMRP has been found in the whole brain TRAP-MS study (RACK1 article) with 20 peptides and a BT/WT ratio of 2.5 (**Table 1**). FUS is not present in this study. LARP4B is also interesting because it has been shown to co-immunoprecipitate with RACK1 and is present in the TRAP-MS specifically in the BT condition with 19 peptides (**Table 1**). Finally, PABPC1, as a polyA binding protein, is known to interact with the translation machinery including RACK1 but is not included in the RBPsuite study. FMRP is expressed in astrocytes and LARP4B in gliomas.

These data allow to propose a model of *kcnj10* translation regulation by RACK1 with an intermediate RBP. RACK1 in astrocytes could recruit FMRP or LARP4B bound to *kcnj10* mRNA. To address this hypothesis, we could perform RACK1 immunoprecipitation (IP) followed by western blot against FMRP or LARP4B; or followed by mass spectrometry. However, this approach would not be astrocyte specific unless using a mouse expressing a GFP-tagged RACK1 specifically in astrocytes. This model of regulation could not be the only one as RACK1 can regulate mRNA expression with microRNAs as well or with RNA specific sequences.

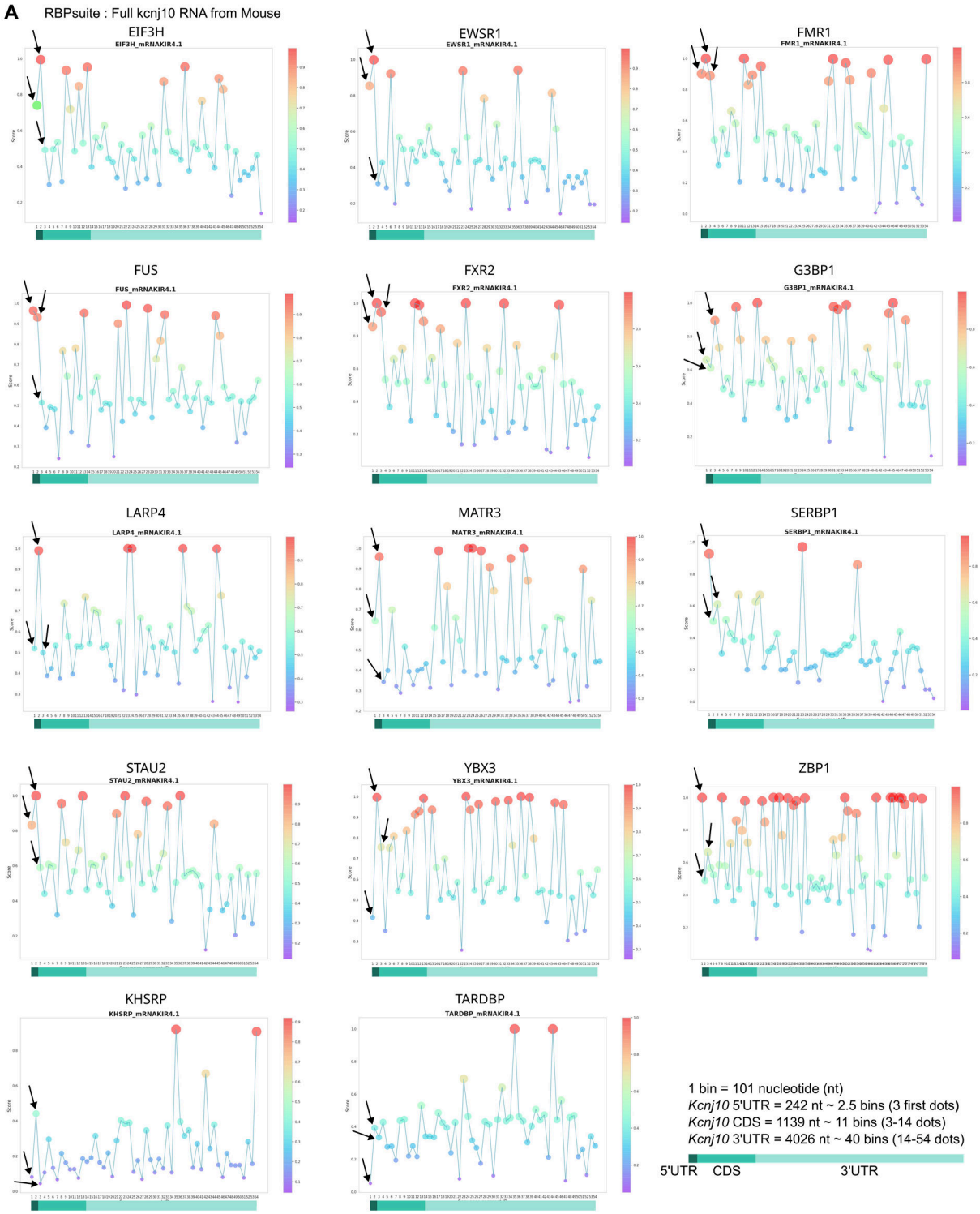

Figure 3 continues next page.

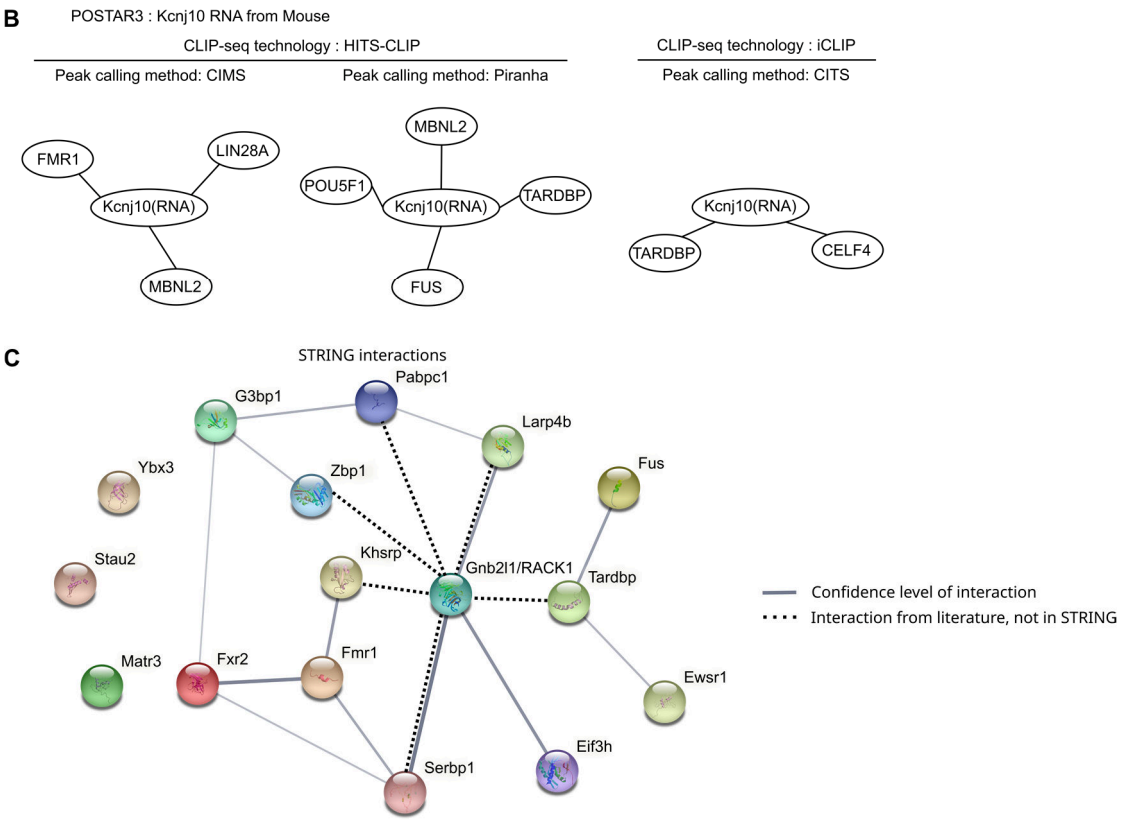

Figure 3. ***Kcnj10 5'UTR is predicted to be recruited by RNA binding proteins (RBP) and RACK1 binds to some of them. A.*** *List of RBPs predicted to bind mouse kcnj10 mRNA. Predicted score of RBP binding along the Kcnj10 mRNA. Arrows indicate the predicted score for the 5'UTR. The score is represented along the y-axis and as colors (from purple, low score, to red, high score). The Kcnj10 mRNA sequence on the x-axis is divided into bins (1 to 54) of 101 nucleotides (nt) each. The 5'UTR of Kcnj10, 242 nt, is represented in the 3 first bins (see arrows). The prediction was realized with RBPsuite website with the Mus musculus Kcnj10 mRNA.* ***B.*** *Interaction map of RBP associated with Kcnj10 mRNA from CLIP seq data either by HITS-CLIP (left) or iCLIP (right). For HITS-CLIP, 2 discovery methods have been used: CIMS and Piranha. Of note, FMR1, FUS and TARDBP have been shown to bind Kcnj10 experimentally. Data mining using POSTAR3 website.* ***C.*** *STRING interaction map between RACK1 (Gnb2l1) and RBP predicted to bind the 5'UTR of Kcnj10 and RBP known to interact with RACK1 in the literature. Confidence view, experiments interaction only and 0.4 interaction score. Interactions from literature was added in dashed lines.*

Table 1. ***List of candidate RBPs interacting with RACK1 of Kcnj10.*** *Expression in astrocyte data are available at the barres lab website (Zhang et al., 2014). FPKM: fragments per kilobase per million*

RBP name	Gene name	Expression in astrocytes in FPKM (Sequencing data)	Present in the astrocyte TRAP-MS?	Associated with RACK1 in the literature?	Predicted as associated with 5'UTR of kcnj10?	From CLIP experiments with Kcnj10?
EIF3H	Eif3h	24	Yes BT specific, 12 peptides	No	Yes	No
EWSR1	Ewsr1	33	No	No	Yes	No
FMRP	Fmr1	29	Yes, ratio 2.5, 20 peptides	No	Yes	Yes
FUS	Fus	54	No	No	Yes	Yes
FXR2	Fxr2	19	Yes BT specific, 5 peptides	No	Yes	No
G3BP1	G3bp1	10	Yes BT specific, 12 peptides	No	Yes	No
LARP4B	Larp4b	10	Yes BT specific, 19 peptides	Yes	Yes	No
MATR3	Matr3	34	Yes, ratio 2.08, 53 peptides	No	Yes	No
SERBP1	Serbp1 (pairbp1)	17	Yes, ratio 2.8, 127 peptides	Yes	Yes	No
STAU2	Stau2	6	No	No	Yes	No
YBX3	Ybx3	NA	No	No	Yes	No
ZBP1	Igf2bp1	0.1	No	Yes	Yes	No
KHSRP	Khsrp	14	No	Yes	No	No
TDP43	Tardbp	27	No	Yes	No	Yes
PABPC1	Pabpc1	28	Yes, ratio 3.5, 226 peptides	Yes	NA	No

IV. Western blot analyses of astrocytic-specific proteins in RACK1 cKO mice versus RACK1 fl/fl control mice in different brain areas and astrocytic compartments

Introduction

Among the panel of astrocyte-specific mRNAs tested in our study, we showed that RACK1 preferentially associates with *Kcnj10* and Slc1a2. We wondered if RACK1 could regulate the translation of other astrocyte-specific mRNAs also significantly associated with RACK1 (see **Fig. 3** of the RACK1 article). Since RACK1 is also associated with polysomes in PvAPs (see previous chapter), we also tested the impact of its absence in this specific compartment.

Materials and methods

Whole brains or hippocampi from adult RACK1 cKO and RACK1 fl/fl mice were collected for whole brain and whole hippocampus extracts or were subjected to synaptogliosome preparation described in the article or to brain microvessel isolation which allows the isolation of the PvAPs along with the

vessels. 1 brain per replicate has been used. Proteins were extracted in 2% SDS and Laemmli buffer at 56°C and subjected to western blot analyses using specific antibodies. The chemiluminescence signal of the targeted protein bands was normalized against the stain free staining except for the brain microvessels in which the normalization was performed against Histone3 as the stain free is unreliable for this compartment due to low protein quantities.

Results and discussion

We investigated by Western blot in RACK1 cKO and RACK1 fl/fl mice the levels of KIR4.1, a potassium channel; GLT1 and GLAST, two glutamate transporters; Cx43 and Cx30, two gap-junction proteins and Aqp4, a water channel; in whole brain, whole hippocampus, brain synaptogliosomes, hippocampus synaptogliosomes and whole brain microvessels. This study is not exhaustive and some proteins were not tested in all type of extracts (**Fig. 4**).

As shown in the article, KIR4.1 is increased in the hippocampus and its synaptosomes in RACK1 cKO condition. KIR4.1 is also increased in the whole brain and brain synaptosomes when RACK1 is deleted from astrocytes. Interestingly, KIR4.1 remains unchanged in brain microvessels, highlighting a potential different role of RACK1 in PvAPs. As shown in the article, GLT1 remained unchanged in all extracts as well as CX43 and AQP4. CX30 is increased in hippocampus and its synaptosomes but not in whole brain (although there is a tendency) and its synaptosomes. Either RACK1 functions are heterogenous among brain regions or this higher level of Cx30 specific to the hippocampus is related to an astrocytic adaptation linked to the increase of KIR4.1. First, RACK1 is poorly linked to Cx30 mRNAs (Fig. 3 of our article). Second, it has been previously shown that Cx30 regulates neurotransmission at the level of PAPs (Pannasch et al., 2014). Finally, GLAST is slightly increased in whole hippocampus.

Despite its ubiquitous presence and its light expression in astrocytes compared to neurons, RACK1 seems to regulate specifically the level of some proteins in astrocytes in the whole brain and hippocampus as well as in PAPs and PvAPs. Interestingly, in RACK1 cKO, KIR4.1 levels are higher in PAPs but not in PvAPs , while, as shown below, RACK1 is also associated with PvAP polysomes. It would be therefore interesting to further address these differences between astrocytic compartments. Of note, our study is limited to few proteins because of the ubiquitous presence of RACK1 and a complete view of RACK1 role could be achieved by proteomic studies on RACK1 cKO isolated astrocytes.

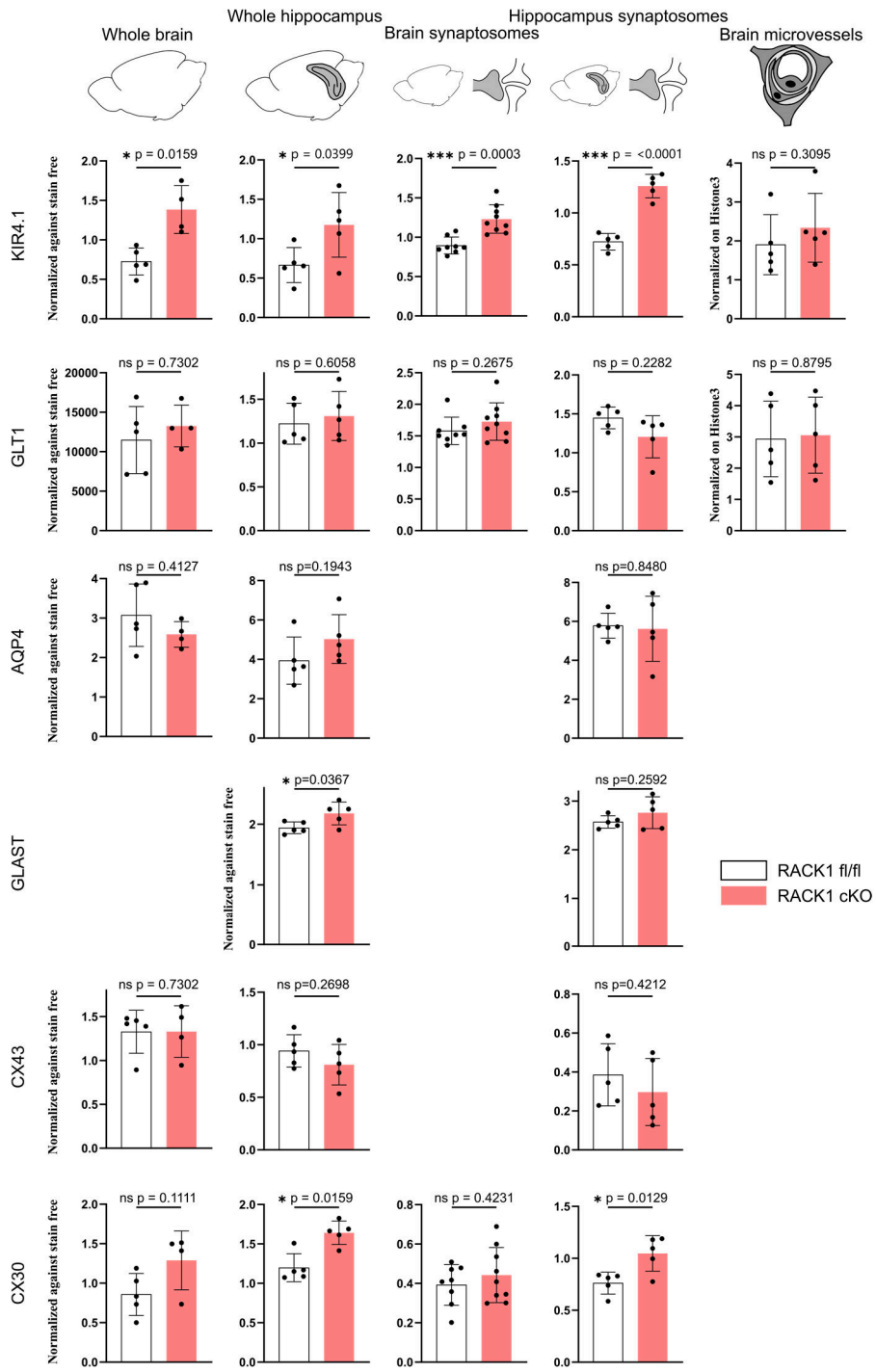

Figure 4. ***Western blot analyses of astrocytic-specific protein study in RACK1 cKO mice versus RACK1 fl/fl control mice in different compartments.*** *From left to right: whole brain, whole hippocampus, whole brain synaptosomes, whole hippocampus synaptosomes and brain microvessels. Studied proteins are KIR4.1, a potassium channel; GLT1, a glutamate transporter; AQP4, a water channel; GLAST, a glutamate transporter; CX43, a gap-junction protein and CX30, a gap-junction protein. KIR4.1 is increased in every extract except microvessels. CX30 is increased only in hippocampus and its synaptosomes and GLAST is slightly increased in hippocampus. Holes in the figure highlight the absence of data for specific extract and protein. Ns, not significant (p>0.05); *, p<0.05; ***, p<0.001.*

V. RACK1 associates differently with astrocytic mRNAs during development

Introduction

We showed that RACK1 associated preferentially with some astrocytic mRNAs in the adult mouse by RACK1 immunoprecipitation, especially *Kcnj10* and *Slc1a2*.

Astrocytes undergo morphological and molecular changes during development. In the mouse, astrocytes are generated before birth but mature during the early postnatal (P) days. Indeed, they proliferate between P0 and P7 in the cortex (Clavreul et al., 2019), undergo radical molecular changes between P10 and P30 and their morphology become more complex at the same time.

We wondered whether RACK1 could have a different role in astrocytes during development. We looked at the changes in astrocytic RNAs association with RACK1 during development in P5, P10, P30 and P60 (adult) mouse brains by RACK1 immunoprecipitation (RACK1 IP). As previously, we normalized the RACK1 IP by the levels of RNAs present in astrocyte ribosomes obtained by TRAP.

Materials and methods

Brains from WT P5, P10, P30 and P60 mice were collected to be subjected to RACK1 IP and TRAP followed by qPCR as previously described. RACK1 IP was IgG subtracted. RACK1 IP and TRAP were normalized on 18S.

Results and discussion

To investigate the role of RACK1 in astrocytes in development, we performed qPCR analyses of a restricted panel of astrocyte-specific markers after RACK1 IP and TRAP in P5, P10, P30 and P60 (adult) mice (**Fig. 5**). In RACK1 IP (**Fig. 5A and A'**), *Slc1a2* coding for GLT1 remained highly associated with RACK1 during development but limited at P5. Overall RNAs increased their association with RACK1 from P5 to P60. As previously, we thought that the relative association with RACK1 by RACK1 IP could depend on the level of the given RNA in the ribosome. We then performed TRAP (**Fig. 5B and B'**) to normalize the RACK1 IP over the astrocyte polyribosome RNA level. The results of the normalization are depicted in **Figure 5C and C'**. At P60, *kcnj10* is more associated with RACK1 than the other studied RNAs. At P30, it remains high but *Slc1a2* is the most associated. At P5, except for *Slc1a2* and *Aqp4*, the other RNAs have less affinity for RACK1. During development, *Kcnj10* increases its association with RACK1 whereas *Slc1a3* and *Gja1* ones remain stable. *Slc1a2* is quite unchanged except for an increase at P30. *Gjb6* does not seem to be associated with RACK1 except at P30.

RACK1 differential association with astrocytic RNAs during development could highlight a different regulatory mechanism at early stages. RACK1 association with *Kcnj10* at P5 is limited and RACK1

cKO brains at this stage could display no changes in KIR4.1 levels (Also because KIR4.1 expression is very limited at young stages). Is RACK1 involved in astrocyte maturation for the acquisition of its molecular signature remain unresolved. The study on synaptogliosomes during development has not been performed either. The deletion of RACK1 in early postnatal days could help answer to these questions.

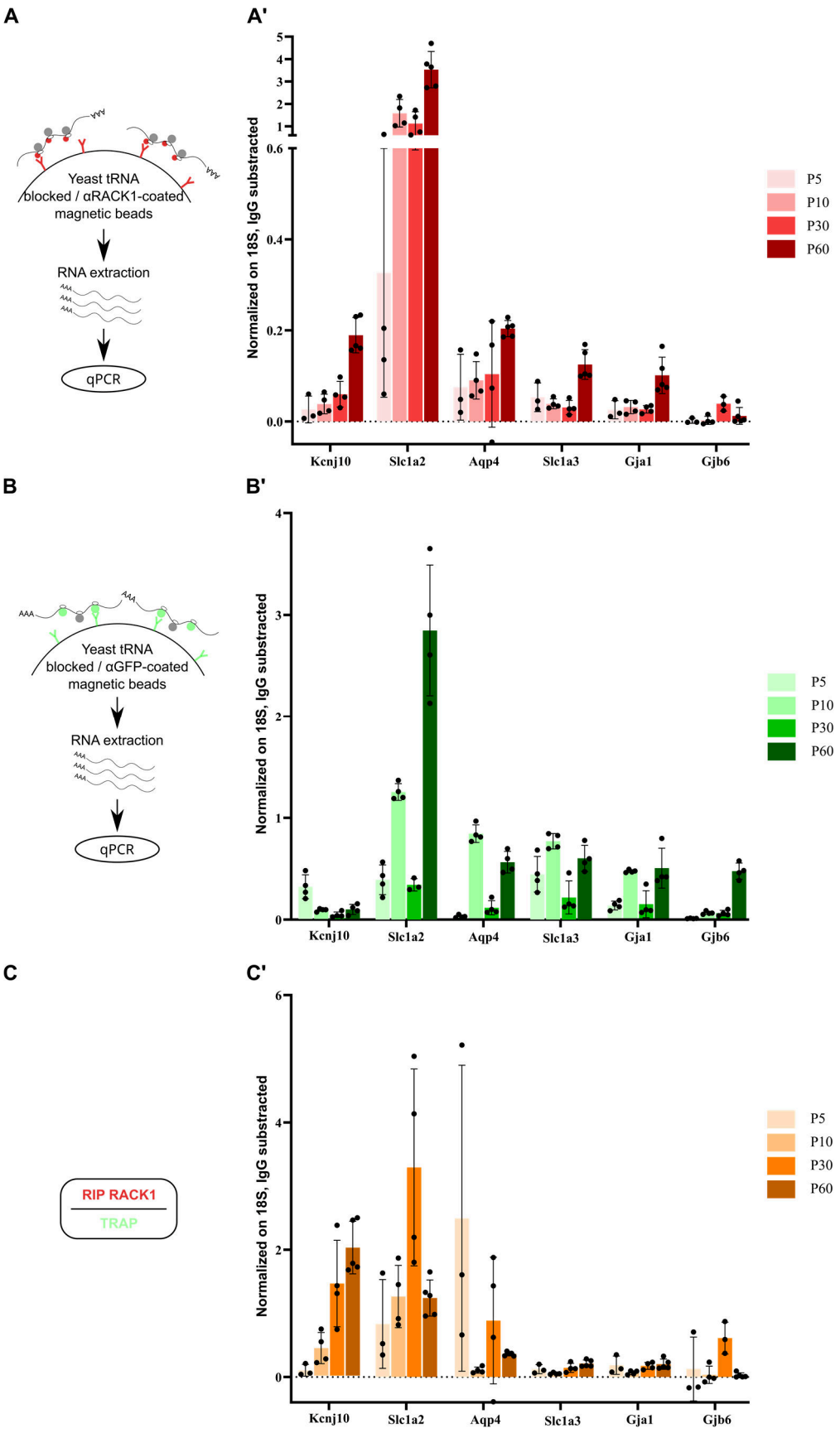
A
A'
Yeast tRNA
blocked / αRACK1-coated
magnetic beads
RNA extraction
qPCR
Normalized on 18S, IgG substracted
P5
P10
P30
P60
Kcnj10
Slc1a2
Aqp4
Slc1a3
Gja1
Gjb6
B
B'
Yeast tRNA
blocked / αGFP-coated
magnetic beads
RNA extraction
qPCR
C
C'
RIP RACK1
TRAP

Figure 5. ***RACK1 associates differently with astrocytic mRNAs during development. A.*** *Flowchart of RNA immunoprecipitation using anti-RACK1 antibodies (in red) on whole brain extracts prepared from Postnatal day 5 (P5), P10, P30 and P60 WT mice. Red dots on ribosomes represent RACK1.* ***A'****. Immunoprecipitated RNAs were purified and screened (in qPCR assays) for a selection of astrocyte-specific mRNAs. IgG-subtracted signals were normalized against rRNA 18S. The data are quoted as the mean ± SD (N=3 (P5), 4 (P15 and P30) and 5 (P60); 1 mouse brain per sample).* ***B****. Flowchart of polysomal immunoprecipitation (TRAP) using anti GFP antibodies (in green) on whole brain prepared from P5, P10, P30 and P60 BT mice.* ***B'****. Immunoprecipitated RNAs are purified and analyzed by qPCR for a selection of astrocyte specific mRNAs. Signals were normalized against rRNA 18S. The data are quoted as the mean ± SD (N=4 samples; 1 mouse brain per sample).* ***C and C'****. Flowchart of the normalization of the RACK1 immunoprecipitation against mean TRAP values. The data are quoted as the mean ± SD.*

VI. Identification of polysome binding proteins in PvAPs by TRAP MS

Introduction

Previous data from the laboratory have shown that local translation occurs in PvAPs (Boulay et al., 2017). To investigate translation regulatory mechanisms in PvAPs, we performed our previously optimized TRAP-MS technique on isolated gliovascular units (microvessels with associated PvAPs).

Materials and methods

Isolation of the gliovascular unit has been described previously and adapted by the lab (Boulay et al., 2015b). Briefly, the purification of brain microvessels allows the isolation of the PvAPs along with the vessels. In the BacTRAP mouse, GFP-polyribosomes of these extracts are present only in PvAPs. TRAP-MS, described in the article, was performed here on 3 replicates with 4 animals per replicate.

Results and discussion

We performed TRAP-MS on isolated GVU in which astrocytic endfeet (PvAP) remain attached to blood vessels detached from their soma (**Fig. 6A**). The **Figure 6B** presents the results and show 53 identified proteins only (compared to the whole astrocyte experiment) with more than 3 peptides and with p-value less than 0.05. Among them, 29 proteins were enriched or specific to the BT condition. We identified 23 ribosomal proteins, 1 ribosomal-associated protein (Gnb2l1/RACK1), 3

cytoskeleton proteins (GFAP, Myh9 and Myh11) and 2 immunoglobulins probably related to the antibodies used for the immunoprecipitation (**Fig. 6C**).

Despite the small size of PvAPs and the low amount of material when isolating brain microvessels, we were able to identify the proteome, or at least part of it, associated with PvAP polyribosomes. The majority of them are ribosomal proteins (RP) because they are the direct interactors of the immunoprecipitated RPL10a (although this RP has not been identified in the screen). Interestingly, RACK1 has also been identified and could highlight its potential local role in endfeet and its high abundance locally (see next chapter). GFAP, the astrocytic-specific intermediate filament (IF), was surprisingly present in this proteome. It was not present in the whole astrocyte study (not enriched or specific in the BT condition) and IF have never been described to bind polyribosomes contrary to microtubules or actin filaments. It could highlight a new translation regulation mechanism in astrocytes with RNA and polyribosomes transport via IF. GFAP is present in endfeet contrary to PAPs and it could act as a storage protein for RNA granules like actin in dendrites and neuronal spines. However, no molecular motors are known to bind intermediate filaments. The polyribosome interaction with GFAP remains to be elucidated. Finally, 2 myosins have been identified here, Myh11 and Myh9. Myosins are molecular motors acting on actin filaments. It has been shown in neurons that actin filaments are stocking RNA granules in spines waiting for a trigger before translation. The same phenomenom could take place in endfeet even if no actin proteins have been identified in this study.

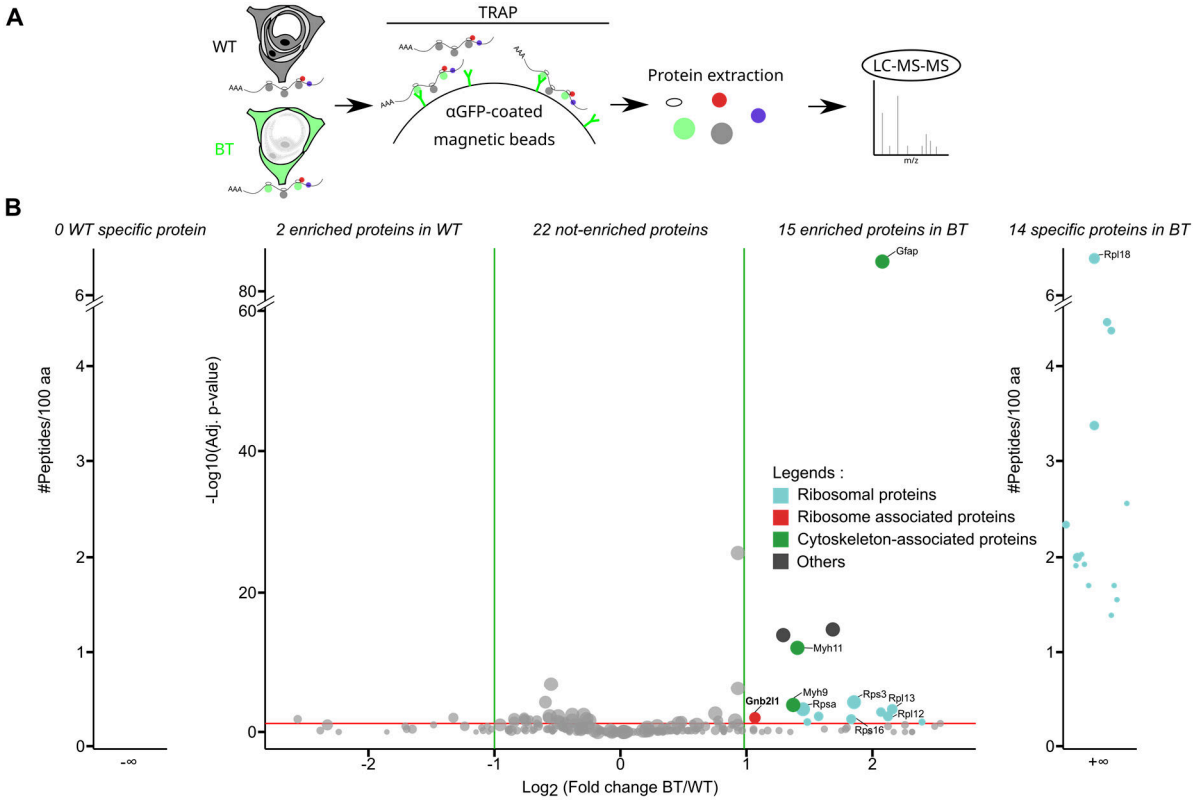

C

Uniprot accession number	Gene name	Protein description	Log_2 FC (BT/WT)	p-value	Peptides used	MW (kDa)
		Ribosomal proteins (23)				
P62908	Rps3	40S ribosomal protein S3	1,85	7,18E-05	19	26,7
P14206	Rpsa	40S ribosomal protein SA	1,45	5,31E-04	19	32,8
P35980	Rpl18	60S ribosomal protein L18	+∞	NA	12	21,6
P47963	Rpl13	60S ribosomal protein L13	2,16	6,88E-04	11	24,3
P35979	Rpl12	60S ribosomal protein L12	2,12	4,84E-03	10	17,8
P14131	Rps16	40S ribosomal protein S16	1,83	1,77E-02	10	16,4
P12970	Rpl7a	60S ribosomal protein L7a	+∞	NA	9	30,0
Q9CZM2	Rpl15	60S ribosomal protein L15	2,06	1,18E-03	9	24,1
Q9CZX8	Rps19	40S ribosomal protein S19	1,57	6,88E-03	9	16,1
P27659	Rpl3	60S ribosomal protein L3	+∞	NA	8	46,1
Q8BP67	Rpl24	60S ribosomal protein L24	+∞	NA	7	17,8
P41105	Rpl28	60S ribosomal protein L28	+∞	NA	6	15,7
P62918	Rpl8	60S ribosomal protein L8	+∞	NA	6	28,0
P63325	Rps10	40S ribosomal protein S10	1,48	3,19E-02	6	18,9
P62900	Rpl31	60S ribosomal protein L31	2,39	3,14E-02	5	14,5
P14115	Rpl27a	60S ribosomal protein L27a	+∞	NA	3	16,6
P62281	Rps11	40S ribosomal protein S11	+∞	NA	3	18,4
P62717	Rpl18a	60S ribosomal protein L18a	+∞	NA	3	20,7
P62751	Rpl23a	60S ribosomal protein L23a	+∞	NA	3	17,7
Q6ZWN5	Rps9	40S ribosomal protein S9	+∞	NA	3	22,6
Q9CR57	Rpl14	60S ribosomal protein L14	+∞	NA	3	23,6
Q9CXW4	Rpl11	60S ribosomal protein L11	+∞	NA	3	20,3
Q9D1R9	Rpl34	60S ribosomal protein L34	+∞	NA	3	13,3
		Ribosome-associated proteins (1)				
P68040	Gnb2l1	Receptor of activated protein C kinase 1	1,06	9,00E-03	13	35,1
		Cytoskeleton-associated proteins (3)				
P03995	Gfap	Glial fibrillary acidic protein	2,08	4,64E-85	290	49,9
O08638	Myh11	Myosin-11	1,40	8,73E-13	121	227,0
Q8VDD5	Myh9	Myosin-9	1,37	1,49E-04	20	226,4
		Others (2)				
P01867	Igh-3	Ig gamma-2B chain C region	1,29	1,16E-14	86	44,3
P03987	NA	Ig gamma-3 chain C region	1,68	2,18E-15	78	43,9

Figure 6. ***Identification of polysome binding proteins in PvAPs by TRAP MS. A.*** *Flowchart of the TRAP-MS analysis on isolated gliovascular units (GVU). Gliovascular units were isolated by microvessels purification in which PvAPs remain attached. Proteins extracted from isolated GVUs in*

C57/Bl6 WT mice or Aldh1l1:L10a-eGFP (BT) mice were immunoprecipitated by TRAP and analyzed by LC-MS/MS. ***B.*** *Volcano plot of the TRAP-MS on GVUs results. Each protein is represented by a dot. The dot size is proportional to the number of peptides identified by LC-MS/MS. Dots for proteins specific to or enriched in BT mice are represented with a color code: ribosomal proteins are given in light blue, ribosome-associated proteins in red, cytoskeleton-associated proteins in green and other proteins in black. Three independent replicates were analyzed (4 brains per sample). The protein distribution is represented as the Log2 FC of the BT/WT (x-axis) versus –Log10 adjusted p-value (y-axis). Proteins identified only in WT extracts (0 protein) or only in BT extracts (14 proteins) (FC: – or +∞). Proteins enriched in WT or BT extracts. The threshold for the enrichment in WT or BT extracts is p-value < 0.05 (red line) and Log2 FC > 1 or < -1 (green lines). 2 proteins were enriched in WT extracts (p-value < 0.05; Log2 FC < -1), 22 proteins were detected with a similar abundance in WT and BT extracts (p-value < 0.05, -1 < Log2 FC < 1) and 15 proteins were enriched in BT extracts (p-value < 0.05; Log2 FC > 1).* ***C.*** *Table of all the BT-enriched and BT-specific proteins identified in the TRAP-MS categorized as ribosomal proteins, ribosome-associated proteins, cytoskeleton-associated proteins and others.*

General discussion

I. RNAs are distributed in astrocytes and microglia (related to Article 1)

I.a) AstroDot enables RNA distribution studies in healthy and disease-related astrocytes

In the AstroDot article 1, we were able to quantify the distribution of 2 *Gfap* isoforms and *Rpl4* RNAs in astrocytes.

Theoretically, any RNA can be investigated with this method if the FISH probe is available or can be designed. *AstroDot* could also be used in spatial transcriptomics where FISH probes are set in arrays and the hybridization reaction takes place at a given location of the tissue so we can retrieve its coordinate and its fluorescence intensity. We could uncover the heterogeneity of RNA distribution between different astrocytes in different brain regions However, GFAP staining is not present in all brain regions, for instance in the cortex. Other proteins or immunostaining protocols should be used for astrocyte specific markers filling the astrocyte processes like aldh1l1 or glutamine synthetase (GS).

We were also able to find differences in RNA density and distribution of 2 *Gfap* RNA isoforms in a mouse model of Alzheimer's disease (AD). RNA transportation along cell processes is one of the translation regulation mechanisms. In AD, molecular motors could be altered leading to RNA distribution alteration. The amount of RNAs is also changed. The availability of RNA at a given place of the astrocyte is directly linked with translation efficiency. Local translation in astrocytes could then be perturbed in AD and in neuropathologies in general. Whether this could be a causative event of the pathology or could accelerate its development remains to be elucidated.

In several neurological disorders, astrocytes undergo reactivity. One hallmark of this reactivity is the hypertrophy of the cell by overexpression of GFAP. Because GFAP is the basis of RNA detection by AstroDot, its overexpression could bias the proportion of RNA detected in the cell. For instance, in the study of non-astrocytic-specific markers, GFAP overexpression in reactive astrocyte would extend in thinner processes compared to basal states and attribute an RNA at this place as in the cell in one condition and not the other. However, the comparison between RNAs remains valid. In addition, astrocyte reactivity may feature interconnection of domains (not in AD) that are normally well separated. It means that astrocytes territory definition, mandatory for the AstroDot analysis, would be complicated and one RNA could be attributed to a neighbor cell. Finally, fibrous astrocytes, located in the white matter, do not have such exclusive domains and it would be difficult to study RNA distribution in these cells for the previously mentioned reasons.

I.b) AstroDot enables RNA distribution studies in microglia

A big achievement of the AstroDot study was to study RNA distribution in microglia. Local translation had never been addressed in microglia until this study and the more recent preprint of the Joseph D. Dougherty lab (Vasek et al., 2021). We found that *Rpl4* mRNA was present in microglial processes based on the microglia-specific Iba1 staining.

Although we did not investigate local translation directly, we can draw a parallel with neurons and astrocytes. This study was possible because of the proteinase resistant property of Iba1. RNA distribution in this cell can now be studied for multiple RNAs and in pathological contexts. Translation regulation mechanisms are yet to be discovered in this cell but it could regulate important functions such as the brain immunity.

I.c) AstroDot is not suitable for RNA distribution in neurons

In our tests to implement AstroDot on neurons, we faced a problem with protease sensitive neuronal markers such as Microtubule Associated Protein 2 (MAP2), Neurofilament medium (NFM) and doublecortin (DCX). DCX was the most promising one because the staining could be visible. However, a high background noise was making AstroDot to attribute false positive RNAs. In addition, DCX only labels a sub population of neurons. Nonetheless, it exists now techniques to keep endogeneous protein intact during the FISH staining by performing immunolabelling before the protease treatment. It could be used for pan neuronal markers.

As mentioned above, cellular domains definition is mandatory for AstroDot implementation. Neurons do not have this property as their processes intersect to communicate through synapses. Therefore, AstroDot would have difficulties to attribute RNAs to the right cell. Nevertheless, we could imagine a sparse labeling of neurons with viral or genetic strategies where cells would be easily defined. Another problem we could encounter relates to the size of some neuronal processes that would be out of the slice. Our FISH technique works on 40 µm thick slices but has never been tested on thicker ones. Transparisation techniques could be helpful but has to be optimized for FISH.

I.d) Single RNA or RNA granules?

AstroDot is based on the detection of FISH dots. Is a FISH dot equivalent to 1 RNA as it is claimed by the RNAscope ACD company? I showed in the introduction that RNAs are transported along the cell processes in compact RNA granules. Is there only one RNA for each RNA species in the granules? Using molecular beacons to detect RNAs in live neurons, the team of Erin Schuman investigated the RNA spots intensity of 3 RNAs, *β-actin*, *psd95* and *camk2a* compared to a single fluorophore spot hypothesizing that the spot intensity was proportional to the number of beacons hybridized to its RNA

(Donlin-Asp et al., 2021). They concluded that spot intensity was heterogeneous with some granules containing one RNA whereas others had more. In addition, on average, *β-actin* had 1 RNA per spot whereas *psd95* and *camk2a* were found in multimeric copy number states.
In AstroDot, we compute the dot intensity parameter. It could be used in our studies to find if the granules have the same size in the soma or in processes; or if granules intensity change in pathological contexts.

II. Regulation of translation occurs in astrocytes (related to RACK1 Article 2)

II.a) Multiple protein partners are associated with astrocytic polyribosomes (related to figure 1)

For the first time, we identified the proteome associated with astrocyte polyribosomes. It was the first time to our knowledge that TRAP was followed by protein extraction and not RNA purification. We had to optimize the TRAP protocol to comply especially with mass spectrometry. For instance, we did not add detergents in our preparations that would affect the mass spectrometer tubing (although liquid chromatography is used beforehand). We optimized the antibody to magnetic beads ratio to have a maximum yield of ribosomal proteins. Finally, we did not block the beads with BSA and yeast tRNA that were used to avoid non-specific RNA interactions. However we kept the optimized steps of empty and non-specific IgG columns during the immunoprecipitation steps (Mazaré et al., 2020b). Indeed, the first checking points we addressed to know if we were in the optimized conditions were: the western blot showing no background in the Wild type condition, the presence of the GFP protein in the BT mass spectrometry replicates and the presence of the vast majority of ribosomal proteins (RP). For this latter point, we identified 95% of all known RPs (75 out of 79 RPs).
Whereas the choice of the 0.05 criterium for the p-value is accepted in the scientific community, the Log2 fold change set at 1 (fold change of 2) was arbitrary and decided with the mass spectrometry platform expertise. However, this fold change is considered stringent and given the fairly good number of identified proteins in the enriched and specific BT condition, we were confident in the identity of our proteome.
Mass spectrometry studies rely on protein extraction but lack the power of RNA sequencing that have an additive amplification step impossible with proteins. Therefore, proteome studies need a good starting material quantity. Thus, we started our TRAP-MS study from the whole brain (without cerebellum and olfactory bulb). However, astrocytes are heterogeneous in the brain and their translation regulation mechanisms could be different from one brain region to another. It could be

interesting to investigate this proteome heterogeneity by dissecting brain regions and, if the quantity of material is not sufficient, pool different animals. Here, we investigated the common regulation mechanisms performed by the average astrocyte.

As shown in the supplementary results, we performed the TRAP-MS protocol on isolated gliovascular units to investigate the proteome bound to perivascular astrocytic processes (PvAP) polyribosomes. But, the article on RACK1 studied the role of this protein in PAPs. Therefore, we could have performed the TRAP-MS on PAPs to see if known RBPs or translators regulators are also present at this interface.

When we started this study, we hypothesized to find astrocytic specific translation regulators that would be first, easy to study and second, able to explain the cellular differences with other cells such as neurons. However, and this is consistent with the literature, no such protein could be found. It means that cells have acquired conserved and common mechanisms to regulate their proteome. The cell specificities rely more on the identity and expression levels of the mRNAs.

II.b) Apart from RACK1, what other protein from the TRAP-MS screen could be investigated (related to figure 1)?

RACK1 has been chosen because it was present in the TRAP-MS studies from whole astrocytes and from PvAP. A previous study of the lab also determined that its RNA, *gnb2l1*, is more locally translated in PAPs than in the soma suggesting that it might regulate local translation in astrocytes. Finally, RACK1 is known in the literature to be an important regulator of translation.

However, our TRAP-MS study uncovered an interesting proteome worth studying:

- 43 RNA-binding proteins (RBPs) have been identified: Among them the well-known Fragile X Mental Retardation Protein (FMRP, FMR1) described in the introduction. FMRP is one of the best studied RBP and has been shown to promote GLT1 expression in astrocytes (Higashimori et al., 2016). In the supplementary results, FMRP has been hypothesized to work with RACK1 to control *Kcnj10* expression. FMRP has multiple partners that were identified in this study: Nuclear fragile X mental retardation-interacting protein 2 (Nufip2) and Fragile X mental retardation syndrome-related protein 2 (Fxr2), 2 other RBPs.

  Caprin1 or RNA granule protein 105 (RNG105) is an RBP present in RNA granules in neurons. Studies showed its role in memory formation as caprin1 KO mice have memory impairment due to disruption of mRNA transportation in neuronal dendrites, especially neurotransmitter receptor-coding mRNA (Nakayama et al., 2017). Interestingly, Caprin1 has been shown to interact with FMRP in neuronal granules (El Fatimy et al., 2012). Caprin1 has never been addressed in astrocytes.

Matrin 3 (MATR3) is a DNA and RNA binding protein present in neuronal nucleus. MATR3 is involved in Amyotrophic Lateral Sclerosis (ALS) and, in the pathology, can be found in cytoplasmic inclusions (TDP43 protein aggregations) in neurons. As suggested in a recent mini review (Barton et al., 2019), RBPs in astrocytes could also play a role in ALS and why not MATR3.

- 20 cytoskeleton-associated proteins have been identified: Spectrin beta chain (SPTBN1) is a scaffold protein linking the plasma membrane to the actin cytoskeleton. Spectrin has shown to interplay with actin in axons (Xu et al., 2013). Interestingly, in a preprint of the lab of Joseph D. Dougherty, they found that *Sptbn1* translation in astrocytes was increased upon seizure induction by PTZ (Sapkota et al., 2020). Spectrin could be of interest in storing RNA granules near membranes at local places.

  Tripartite Motif containing (TRIM) protein TRIM46 is a microtubule associated protein participating in the axonal specification during development and is associated with the axonal initiation segment in mature neurons (van Beuningen et al., 2015). Therefore, it regulates cell polarization through microtubule regulation. In astrocytes it could polarize polyribosome in astrocyte processes.

Because of the TRAP preparation, only cytoplasmic content can be identified. Indeed membranes are removed in the first steps of the preparations. Therefore, no membrane proteins have been identified although polyribosomes can be anchored by receptors or transmembrane proteins.

II.c) RACK1 is associated with polyribosomes and RNAs in astrocytes (related to figure 2 and 3)

In addition to the TRAP-MS study, FISH and immunostainings showed the expression of RACK1 in astrocytes at the RNA and protein levels. As shown by the immunofluorescence, RACK1 staining was difficult to achieve and a high background remains. Indeed, an antigen unmasking protocol with citrate buffer at 90°C was necessary. Therefore, a study to quantify RACK1 staining in astrocyte processes would be laborious. We can also observe that the staining is not the same between neurons and astrocytes. In neurons, it is strong in the soma and weak in processes whereas in astrocytes the staining is almost uniformly distributed between the soma and the processes. It could highlight differential RACK1 roles in both cells.

We have shown that RACK1-containing ribosomes are associated with some astrocytic-specific RNAs by qPCR on a restricted RNA panel. In this study, RACK1 was found to preferentially associates with *kcnj10* and *Slc1a2* compared to *Aqp4*, *Gja1*, *Slc1a3* and *Gjb6*. We showed that RACK1 had specific interactions, therefore probably specific regulations toward astrocytic RNAs.

Given the ubiquitous feature of RACK1, we could only investigate astrocyte-specific markers. In the future, designing a mouse strain transgenic for a GFP-fused RACK1 under the astrocytic-specific promoter Aldh1l1 and performing GFP immunoprecipitation and RNAseq could allow accessing the whole astrocytic transcriptome associated with RACK1.

We normalized the RACK1 immunoprecipitation by TRAP to have the ribosome occupancy of each RNA into account. Indeed, we thought that RACK1 associates with RNAs through the ribosome. Can we interpret the absolute value of the RACK1 IP/TRAP ratio? For instance, if the ratio is 1, does it mean that RACK1 is present in all ribosomes containing this RNA? Below 1, RACK1 would not be associated with all ribosomes with this RNA? However, we could find in the whole brain (**Fig. 4G**), ratios above 1. It would mean that RACK1 can associate with RNAs without the presence of ribosomes. Because RACK1 is unable to bind RNAs directly, it would act through an RBP or other translation-related proteins. Nevertheless, we wondered if these ratio values could really mean something by themselves. Indeed, RACK1 IP immunoprecipitates RACK1 from all cells of the tissue but TRAP is immunoprecipitating polysomes only from astrocytes. Therefore, the concentration of astrocytic RNAs is much higher in the TRAP extracts than in the RACK1 IP and we cannot compare them. In addition, we do not know if the polysome immunoprecipitation efficiency is the same between both antibodies. In summary, we can compare RNAs using this ratio but not take the absolute value into account.

Finally, *Gjb6* association with RACK1 seems peculiar as it is associated with it in PAPs but not in whole astrocytes. The regulation of this RNA by RACK1 could only occur in the PAPs. Curiously, in RACK1 cKO mice, CX30 (coded by *Gjb6*) is changed in hippocampus and hippocampus synaptosome and not in whole brain and brain synaptosome. We did not further investigate RACK1 association with RNAs in hippocampus but there could be a double regulation mechanism for this RNA: astrocyte compartment and the brain localization. Different RBPs could be at play in different compartment or brain regions and differently recruited by RACK1. Or, the sequence of *Gjb6* could undergo alternative splicing as we know that RACK1 is sensitive to some RNA features.

II.d) RACK1 cKO mouse is a good model to study impact of translation regulation on astrocyte physiology (related to figure 4)

We developed a mouse model in which RACK1 is deleted only in astrocytes in the adult mouse thanks to tamoxifen injection on Aldh1l1-creERT2;RACK1fl/fl mice. We found by PCR and by immunostaining a complete deletion of RACK1 from astrocytes only, 3 weeks after the first injection of tamoxifen although we did not quantify it. The Aldh1l1 promoter is also active in some neuronal

progenitors still present in the hippocampus in the adult. However, the proportion of such cells remains limited. Outside the brain, Aldh1l1 is also highly expressed in hepatocytes in the liver (human protein atlas source). We could not observe visible phenotypic alterations of our RACK1 cKO mice compared to RACK1 fl/fl: no more weight loss, no more anxiety, no less common mouse behaviors (grooming, walking by the walls, ...), no visible alterations although a thorough investigation with typical behavioral tests could help quantify these parameters.

The proteins we investigated in the RACK1 cKO mice were astrocytic-specific proteins especially the ones for which their RNA are more associated with RACK1: KIR4.1 and GLT1. We used a closed approach to target proteins with important functions and for which a change in expression level would influence the brain physiology. However, it does not reflect the whole changes occuring in RACK1 cKO mice. For this, we could have investigated the translatome of RACK1 cKO mouse brains by crossing the RACK1 mice (Aldh1l1-creERT2/RACK1fl/fl) and the bacTRAP mice (Aldh1l1-eGFP/RPl10a) and perform TRAP-seq. For the proteome, we could FACS sort astrocytes followed by mass spectrometry. Finally, we could also investigate the changes in the proteins bound to astrocytic polyribosomes by performing TRAP-MS on Bactrap-RACK1 cKO mice.

We characterized the increase of KIR4.1 in RACK1 cKO whole hippocampus and hippocampus synaptosomes by western blot. We wanted to add another method to quantify KIR4.1 increase such as immunofluorescence. Unfortunately, anti-KIR4.1 antibodies are giving bad stainings in immunofluorescence as we tested intracellular and extracellular-targeted antibodies and were not suitable to quantify any changes. In fact, we could not find good stainings in the literature and no quantifications. Super-resolution techniques as the Stimulated Emission Depletion (STED) could be used to quantify the increase of KIR4.1 near synapses, however we were advised by the microscopy platform that an increase of ~1.5-fold in expression would not be detectable by this technique.

II.e) RACK1 regulates Kcnj10 on its 5'UTR (related to figure 5)

As shown in the introduction, RACK1 is involved in ribosome stalling recognition to resolve blocked ribosomes. We first investigated this property to know if ribosomes could stall on *kcnj10* coding sequence *in vitro* in HEK cells. Although we demonstrated that RACK1 was indeed involved in stalling, it was not this mechanism involved in *kcnj10* regulation.

Nevertheless, we demonstrated with luciferase constructs that RACK1 was attenuating *kcnj10* translation by acting on its 5'UTR and more specifically on the 2nd part (127-242 nt) of the 5'UTR. Interestingly when we tried to go further, we could not find a shorter sequence regulated by RACK1 as the 95-191 nt and 181-242 nt constructs luciferase activity had also an increase in the absence of RACK1. Therefore, we wondered what could be the exact regulatory mechanism. As shown in the

supplementary results, we hypothesized that RACK1 binds to an RBP carrying *Kcnj10* mRNA and restrict its translation.

How to further investigate regulatory mechanisms? For the hypothesis in which RACK1 binds an intermediate factor, we could immunoprecipitate RACK1 and look by western blot proposed factors and RBPs. In addition, we could look for such changes in the above mentioned RACK1 cKO astrocytic translatome and proteome.

No specific motifs have been found in *kcnj10* mRNA but there could be the presence of secondary structures like loops or IRES recognized by RACK1 or associated RBPs. Algorithms for secondary structure prediction based on the mRNA sequence could be used.

II.f) RACK1 regulates astrocyte volume (related to figure 5)

We showed that in RACK1 cKO mice, astrocytes had a bigger volume, longer branches and more ramifications in distal parts of the cell. Thus, RACK1 regulates astrocyte volume and processes complexity. How? We hypothesized that it was related to KIR4.1 increase. Indeed, ion homeostasis is often related to water homeostasis to keep cell osmosis. Water flows in the astrocyte are mediated by AQP4 which has been shown to co-immunoprecipitate with KIR4.1 in Müller cells of the retina. However, this could be only the case in the retina, as AQP4 KO mice had no impact on KIR4.1 in the hippocampus where the astrocyte volume was investigated. Other proteins mediating fluid movement and controlling cell volume could be at play.

If astrocytes are bigger, and the brain is not, it directly impacts other volumes. It could reduce neuronal, oligodendrocyte or microglia volumes for instance. However the most probable is that extracellular space near astrocytes is reduced. This parameter could be assessed by Super-resolution shadow imaging (SUSHI) where cells are negatively labeled, highlighting the intercellular spaces. This reduction could alter interstitial fluid movement, extracellular ion concentrations and neuronal transmission.

II.g) RACK1 regulates neuronal transmission (related to figure 6)

Ex vivo, on hippocampal RACK1 fl/fl and RACK1 cKO slices, we showed by electrophysiological recordings that, in the absence of RACK1 in astrocytes, neuronal postsynaptic currents were higher in high frequency stimulations and that neuronal network bursts frequency was lower and bursts duration was longer in pro-epileptic conditions. Interestingly, in the 10 Hz stimulation experiment, the increase fEPSP slope in RACK1 cKO condition was erased when using a KIR4.1 specific blocker. Thus, we hypothesized that this neuronal changes were only mediated by KIR4.1.

Curiously, GLT1 expression was unchanged in RACK1 cKO mice despite KIR4.1 increase. Indeed, as shown in the introduction, KIR4.1 mediates the highly hyperpolarized resting membrane potential (RMP) of astrocytes allowing glutamate uptake by GLT1 because of the co-transport of Na+ in the cell. Does KIR4.1 increase changes the astrocytic RMP? In the lateral habenula, overexpressing KIR4.1 in astrocytes leads to an hyperpolarization of astrocytic RMP (Cui et al., 2018). Therefore, glutamate uptake would be increased in astrocytes with no change of GLT1 expression. Is it why neuronal transmission is changed in RACK1 cKO mice? To investigate RMP in our mouse model, whole cell patch clamp recording could be used. We could also measure extracellular potassium concentration with K+ probes. Interestingly, in CX30 KO mice, glutamate uptake was increased without changes in GLT1 but by a morphological invasion of PAPs in the synapse (Pannasch et al., 2014). We could investigate the PAP morphology in our RACK1 cKO mouse model by electron microscopy especially because we showed a morphological change of astrocytes in this model.

Another finding is that in basal states, meaning low frequency neuronal stimulation, KIR4.1 increase has no impact on synaptic transmission. It is consistent with previous models where KIR4.1 was predicted to only have a role when neurons were stimulated between 3 and 10 Hz and not at 0.1 and 1 Hz (Sibille et al., 2015). Therefore, when neuronal firing is low, the amount of synaptic K+ is increasing modestly requiring only modest buffering. However, when the firing is high, large amount of K+ is released in the synapse and KIR4.1 plays here an important role for its clearance.

The neuronal network, recorded in the MEA experiment in pro-epileptic conditions (0Mg/6K), of RACK1 cKO hippocampi, had less frequent but longer bursts. The 0 M Mg2+ in the aCSF alleviates the inhibitory clog of NMDAR receptors at post-synaptic terminals activating them and let Ca2+ entry to depolarize the cell. 6 mM K+ in the aCSF increases K+ concentration at the synaptic level, destabilizing the charge difference between inside and outside of the astrocyte unable to uptake glutamate efficiently. Glutamate stays in the synaptic cleft for longer time, activating post synaptic receptors for longer time leading to synchronous activity of neurons. In the case of KIR4.1 increase, synaptic K+ is taken up more efficiently as well as glutamate lowering burst frequency. Bursts duration is higher in RACK1 cKO. Maybe, if bursts are fewer, neurotransmitter vesicles have more time to recycle thus when neurons fire, a bigger amount of neurotransmitter is able to be released for longer time.

The blockage of KIR4.1 in the MEA experiment first increased then decreased bursts frequency in the control condition. At first, when KIR4.1 is blocked, even more glutamate stays in the synapse to trigger firing but then, neurotransmitter vesicles stock empty, unable to follow a high frequency firing. Burst duration in controls is not changed. However, in RACK1 cKO condition, in the presence of the KIR4.1 blocker, no changes in the burst frequency have been observed. We hypothesized that the KIR4.1 inhibition was not complete to cancel the increased KIR4.1 expression and that the remaining

active channels were sufficient to buffer K+ properly. Other experiments with an increased blocker concentration could be done. But, bursts duration was, this time, decreased in RACK1 cKO slices. After 30 min, burst duration reached the same levels as the control group. KIR4.1 blocker was indeed acting in RACK1 cKO condition but with actions difficult to interpret.

Neuronal transmission investigations were analyzed around KIR4.1 expression changes. Thus, what is the role of RACK1 in this physiology? RACK1 limits KIR4.1 expression in astrocytes. Therefore, RACK1 increases K+ concentration at the synapse when synaptic transmission is high. At the level of few neurons, RACK1 increases depression of post synaptic currents when stimulated at high frequency. At the level of the network level, RACK1 increases burst frequency and decreases burst duration in pro-epileptic conditions. If neuronal transmission is controlled by astrocytic RACK1, we could ask whether it has a role in synaptic plasticity and cognitive functions such as memory. LTP and LTD protocols in RACK1 cKO brain could be performed and memory tests such as the novel object recognition or the Morris water maze tests could be used. In the supplementary results we already showed that RACK1 was not involved in depression and PTZ-induced seizures.

III. RACK1 roles are quite specific

While conducting the western blot studies on RACK1 cKO brains, we were at first surprised by the little changes the inhibition of RACK1 induced in astrocytes. At least for the proteins we investigated. Despite RACK1's roles in several crucial functions in translation and other cell functions, its deletion in adult astrocytes did not induce a phenotype in the mouse, the astrocytes were not that changed and almost only KIR4.1 was increased by a ~1.5 fold. It first indicates that RACK1 plays specific roles in the cell, it is not just a passive ribosomal protein and that it can be considered as an adaptive and accessory protein for the ribosome. This statement is corroborated by the recent paper of the Erin Schuman's team in which they showed that RACK1 is incorporating the ribosome rapidly in neuronal processes as well as after oxydative stress.

Nonetheless, if RACK1 was deleted early on during development, it could have probably more impact on the brain physiology.

Apart from the depression model, no physiological conditions have been shown to increase KIR4.1 expression in the literature. Since KIR4.1 is crucial for synaptic transmission, the RACK1 cKO model is of great interest for neuronal physiology studies.

IV. In RACK1 cKO mice, other alterations could be considered

RACK1 integrates the pre-40S particle late in the maturation process of ribosomes subunits and its deletion *in vitro* does not change the 40S quantity (Cerezo et al., 2019). However, since RACK1 is regulating the 80S formation, it could alter the ribosome subunit/monosome/polysomes stoichiometry in astrocytes. We could use ribosome fractionation to investigate the relative changes in each fraction to see if there is a shift toward one fraction in RACK1 cKO mice. The RACK1 deletion is only in astrocytes and other cells could hide such changes. Thus fractionation could be performed on isolated sorted astrocytes which would be challenging to achieve.

As RACK1 has also non-ribosomal functions, they could be affected in RACK1 cKO brains. How to decipher the RACK1-free VS RACK1-ribosome bound roles? Some teams have mutated the residues by which RACK1 binds to the 40S of ribosomes (RACK1 R36D K38E) (Coyle et al., 2009). We could inject this construct by viral strategies for instance with an astrocytic-driven promoter in RACK1 cKO mice to rescue non ribosomal functions that could have been affected. In these mice, we would explore if the neuronal transmission is still affected.

V. What are the roles of local translation and translation regulation in astrocytes ?

Neuronal local translation is involved in synaptic plasticity, axonal wiring, spatial and temporal restriction of proteins among others. But what are the roles for local translation in astrocytes? Given the relatively recent findings of its occurrence in this cell, no answers have been brought yet. Nonetheless, it would be a hard question to tackle because the manipulation of local translation in astrocytes is not easy. Majority of studies in neurons have been done *in vitro* where neurons polarize with nice processes that can be targeted. Astrocytes *in vitro* do not polarize unless cocultured with neurons. Maybe, works can be achieved by laser dissecting astrocyte processes contacting neurons in cultures and apply different molecular stimuli or by electrically stimulating neurons nearby and investigating the isolated astrocyte process. However, astrocytes do not form PAPs *in vitro*. In addition, the vascular interface is not present. Attempts in reproducing PvAPs with blood vessel and mural cells in culture are in progress in the field. Microfluidic systems could be of use to investigate local translation in astrocyte processes. Boyden chambers with astrocytes on the membrane and neurons at the bottom could be used also where processes could be pealed off.

We now know the identity of locally translated RNAs in PAPs and PvAPs, thus we can guess local translation roles through these translatomes. In PAPs, it could regulate synaptic transmission through

the local translation of KIR4.1 for instance, or iron homeostasis through ferritins. In PvAPs, it could regulate water homeostasis with AQP4, or PvAP formation with MLC1 (Gilbert et al., 2021). To investigate local translation roles in astrocytes one strategy would consist to inhibit it. But how? To date, we do not know specific molecular motors or adaptor proteins that would be restricted in PAPs or PvAPs. Another strategy would consist in finding paradigms in which these local translations change. For instance, we used the fear-conditioning paradigm to test the role of local translation in memory formation in the dorsal hippocampus (Mazaré et al., 2020a). During exercise, the blood flow is increased in the brain. TRAP experiments on trained mice could reveal role of local translation in controlling blood flow. We could also place mice in rich environments to stimulate their brain and look if local translation in PAPs could regulate synaptic plasticity. Finally, the investigations of local translation in neuropathologies could also bring some answers for instance if the disease impact blood vessels or neurons such as in Alzheimer's disease.

These considerations are also valid for the translation regulation mechanisms. In the end, the proteins regulating local translation are the one regulating astrocytic functions at its interfaces, therefore regulating the brain physiology. Because the cells have to adapt constantly to their environment, the regulation of local translation is of crucial interest. Through RACK1, we found that it could regulate neuronal transmission. RACK1 or its partners could be modulated according to the firing state of neurons at a given moment. We could also ask what are the regulatory mechanisms in PvAPs or also in development where gene expression is drastically changed.

Finally, in our study of RACK1 roles in astrocytes, we did not investigate local translation regulation but global translation regulation as RACK1 KO is affecting the whole cell. The local part in our studies is tedious to address. We rely on interfaces isolation to study the impact locally. We rely also on enriched molecules in PAPs and PvAPs to hypothesize a local role. For instance, *Gnb2l1* coding for RACK1 has been shown by the lab to be much more translated in PAPs and PvAPs than in the soma of astrocytes. Therefore RACK1 could have a prominent role locally where ribosomes need to adapt by regulating their proteome.

VI. Are astrocytic local translation mechanisms heterogeneous?

As described in the introduction, astrocytes are heterogeneous across the brain and interact with structures molecularly heterogeneous as well. For instance, we have glimpses that the perivascular and the perisynaptic translatome are different. But we can also imagine that the processes contacting venules, arterioles or capillaries have different pools of mRNA since they contact interfaces molecularly different. On the synaptic level, PAPs contact excitatory and inhibitory synapses which

are themselves different depending on the nature of neurotransmitters. In addition, different neuronal networks are present in different brain regions. How to tackle this local translation heterogeneity question? First, we can dissect the different brain regions, for instance cortex, hippocampus, striatum and cerebellum, from BacTRAP mice and perform TRAP-seq on synaptosome preparations and microvessels purifications to target locally translated mRNAs. The excitatory and inhibitory synapses display differences in terms of proteins, especially neurotransmitters and membrane proteins as well as at the level of the PAP (Takano et al., 2020). TRAP on synaptosomes from BacTRAP mice would immunoprecipitate polyribosomes from both excitatory and inhibitory-associated PAPs. To investigate them separately, the BacTRAP mouse could be crossed either with a vGLUT1 (vesicular glutamate transporter, excitatory) or a vGAT (vesicular GABA transporter, inhibitory) fluorescent reporter mouse. This way, fluorescence activated synaptosome sorting (FASS) could be performed on both mice to either sort the excitatory or the inhibitory synapses (Hafner et al., 2019) along with their PAPs. TRAP could then be performed on these extracts to obtain the translatome of PAPs in either of these two conditions. The major issues would be first, the low material quantity after FASS to perform TRAP and second, the fact that maybe the PAPs do not stay along with the synapses during the sorting. Next, the translatome of 1 PAP of 1 astrocyte could not be the same as another PAP from the same astrocyte, for instance if it is associated with a different dendrite or if the neuronal activities are distinct. Single PAP translatome, if this technique would be invented, could reveal local translation heterogeneity within the same astrocyte in the future. Maybe, the PAP content could be aspirated by nano-pipettes for instance. Finally, we do not have, yet, techniques to isolate the other interfaces of the astrocyte such as the astrocyte-oligodendrocyte or the astrocyte-astrocyte interfaces.

VII. On the complexity of the proteome regulation

During this PhD, I realized how complex and with how much diversity, a cell can regulate its proteome. From the DNA to the protein, regulation steps are everywhere: regulation of transcription with transcription factors, epigenetic marks, histone condensation; then mRNA life with stabilization/degradation mechanisms, transport, miRNA, alternative splicing, shortening or lengthening; then regulation of translation with translation factors, RBPs, RNA motifs and secondary structures, m6A modifications, codon usage bias; and finally post translational modifications with Golgi apparatus, endoplasmic reticulum, glycosylation, sumoylation, multimere conformations.

When studying gene expression in a cell, we understand now how different a transcriptome, a translatome and a proteome can be because of all these regulatory mechanisms. Despite their powerful implications, transcriptome analyses should not be considered as granted as they do not reflect the

cell phenotype and even if an RNA is not in the top modified ones in a transcriptome comparing 2 conditions, it does not mean it does not have great implications in the physiology.

Appendix

© 2021. Published by The Company of Biologists Ltd | Journal of Cell Science (2021) 134, jcs251629. doi:10.1242/jcs.251629

REVIEW

Local translation in perisynaptic and perivascular astrocytic processes – a means to ensure astrocyte molecular and functional polarity?

Noémie Mazaré[1,2], Marc Oudart[1,2] and Martine Cohen-Salmon[1,2,*]

ABSTRACT

Together with the compartmentalization of mRNAs in distal regions of the cytoplasm, local translation constitutes a prominent and evolutionarily conserved mechanism mediating cellular polarization and the regulation of protein delivery in space and time. The translational regulation of gene expression enables a rapid response to stimuli or to a change in the environment, since the use of pre-existing mRNAs can bypass time-consuming nuclear control mechanisms. In the brain, the translation of distally localized mRNAs has been mainly studied in neurons, whose cytoplasmic protrusions may be more than 1000 times longer than the diameter of the cell body. Importantly, alterations in local translation in neurons have been implicated in several neurological diseases. Astrocytes, the most abundant glial cells in the brain, are voluminous, highly ramified cells that project long processes to neurons and brain vessels, and dynamically regulate distal synaptic and vascular functions. Recent research has demonstrated the presence of local translation at these astrocytic interfaces that might regulate the functional compartmentalization of astrocytes. In this Review, we summarize our current knowledge about the localization and local translation of mRNAs in the distal perisynaptic and perivascular processes of astrocytes, and discuss their possible contribution to the molecular and functional polarity of astrocytes.

KEY WORDS: Local translation, mRNA distribution, Astrocyte

Introduction

Although it was long thought that translation occurs in the vicinity of the nucleus, it is now known that mRNAs can also be transported to and translated in distal cell compartments as part of a process that helps to regulate protein delivery in space and time (Holt and Schuman, 2013). The first evidence for compartmentalized mRNA localization was published in 1983; it was found that actin mRNA was present in different regions of the ascidian egg (Jeffery et al., 1983). Since then, mRNA localization and local translation have been observed in a number of cell types, and particularly in cells with complex morphologies. The best-characterized example is the neuron, which can grow an axon of up to 1 m in length (Biever et al., 2019; Glock et al., 2017; Holt et al., 2019). mRNA localization and local translation has been observed at active synapses in neurons of the sea slug *Aplysia* and were shown to contribute to synaptic plasticity (Si et al., 2003). Local protein translation has also been observed in dissected squid giant axons (Mathur et al., 2018). In *Drosophila*, mRNA transport in synapses is linked to synaptic plasticity (Kuklin et al., 2017). In vertebrates, local translation was first described in isolated axons from rabbits and cats (Koenig, 1965a, b, 1967a,b), and has been intensively studied in recent years – notably after the development of a number of techniques for tracking local translation events *in vitro* and *in vivo* (Holt et al., 2019). Overall, the diversity observed in animal models suggests that local translation is an evolutionarily conserved mechanism for the functional polarization of cells.

In glial cells, mRNA localization was first observed in the 1980s; through *in situ* hybridization, the distal distribution of mRNAs coding for myelin-binding protein (which is crucial for building myelin sheaths) was observed in spinal cord sections from mice infected with a demyelinating virus (Kristensson et al., 1986). A later study demonstrated the presence of carbonic anhydrase II mRNA in the processes of primary cultured oligodendrocytes (Ghandour and Skoff, 1991). mRNA isoform transcripts encoding the amyloid precursor protein and Tau protein (both implicated in the pathology of Alzheimer's disease) have also been detected in primary oligodendrocyte processes (Garcia-Ladona et al., 1997; LoPresti et al., 1995). More recently, several research groups have demonstrated that mRNA localization and local translation also occur in astrocytes – the most abundant population of glial cells in the mammalian brain (Boulay et al., 2017; Sakers et al., 2017; Mazare et al., 2020a).

Astrocytes are voluminous, morphologically complex cells. They are highly ramified and polarized, and bear processes that form branches, secondary branches and terminations in contact with blood vessels and neurons (Fig. 1). In the CA1 region of the hippocampus, between 60% and 90% of the synapses are contacted by extremely thin (<50 nm) perisynaptic astrocytic processes (PAPs) (Reichenbach et al., 2010). The number of PAPs varies from one region of the brain to another (Ventura and Harris, 1999). At the synaptic interface, astrocytes regulate synaptic transmission (Dallerac et al., 2013; Ghezali et al., 2016). In fact, PAPs can sense changes in the composition of the perisynaptic extracellular space and thus can prevent prolonged neuronal activation and excitotoxicity by clearing ions and neurotransmitters that are released from the synapse (Dallerac et al., 2018). PAPs are equipped with transporters (such as glutamate transporters) and channels, which tightly control perisynaptic homeostasis (Murphy-Royal et al., 2017). PAPs also release neuroactive factors and influence synaptic functions by dynamically modulating synaptic coverage (Bernardinelli et al., 2014; Pannasch et al., 2011). Finally, PAPs orchestrate synaptogenesis during development and in the

[1]Physiology and Physiopathology of the Gliovascular Unit Research Group, Center for Interdisciplinary Research in Biology (CIRB), College de France, CNRS Unité Mixte de Recherche 724, INSERM Unité 1050, Labex Memolife, PSL Research University, F-75005 Paris, France. [2]École doctorale Cerveau Cognition Comportement 'ED3C' No. 158, Pierre and Marie Curie University, F-75005 Paris, France.

*Author for correspondence (martine.cohen-salmon@college-de-france.fr)

N.M., 0000-0003-4073-8811; M.O., 0000-0002-3933-9621; M.C.-S., 0000-0002-5312-8476

Journal of Cell Science (2021) 134, jcs251629. doi:10.1242/jcs.251629

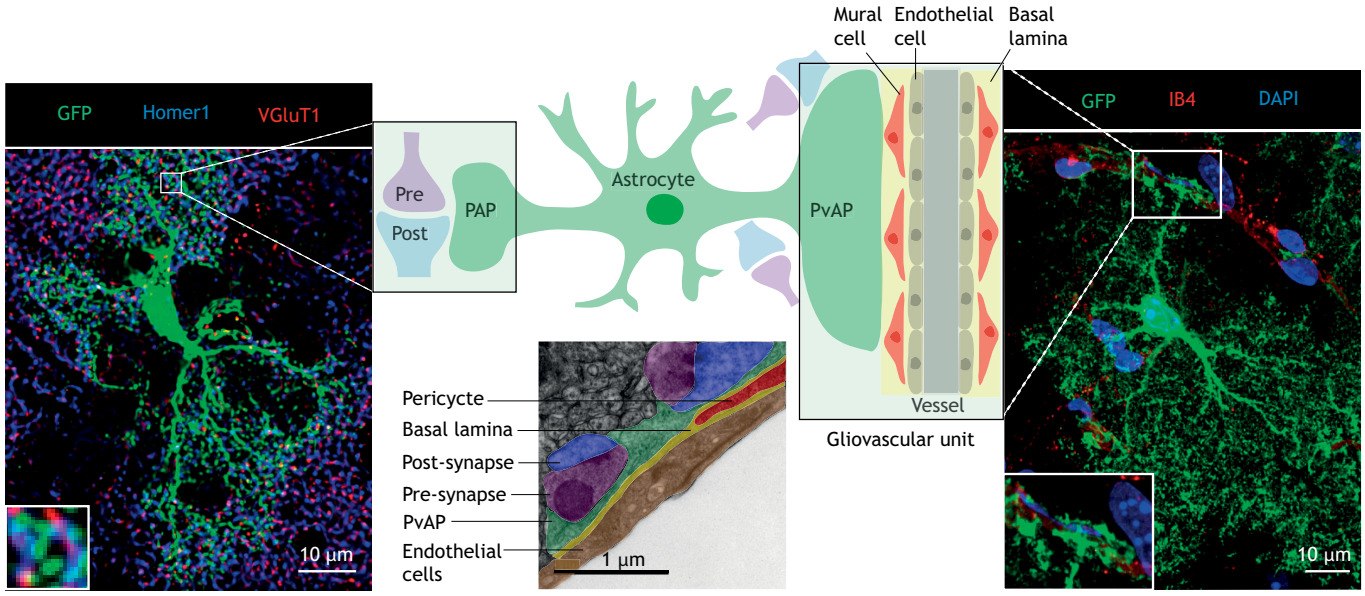

Fig. 1. Comparison of perivascular and perisynaptic astrocytic processes. Schematic representation of an astrocyte extending PAPs towards a synapse, comprising the pre- and the post-synapse. Astrocytes also send PvAPs towards blood vessels; together with mural cells, endothelial cells and the basal lamina, the PvAPs form the gliovascular unit. Synapses can be located adjacent to PvAPs (centre). A confocal microscopy image of an astrocyte filled with eGFP is shown on the left. The astrocyte comes from the pyramidal layer of the hippocampus in a transgenic mouse line expressing GFP under the control of the astrocyte-specific Gfap promoter. The synapses are labelled with the pre- and post-synaptic markers VGluT1 and Homer1. Scale bar: 10 µm. The inset shows PAPs in contact with synapses. On the right, a confocal microscopy image of a hippocampal astrocyte from a transgenic mouse expressing eGFP under the control of the Gfap promoter is shown. The astrocyte extends a PvAP (boxed area) that wraps around the blood vessel (labelled with isolectin B4; IB4). Scale bar: 10 µm. The inset highlights an astrocyte PvAP surrounding the blood vessel. The electron micrograph below the scheme shows a PvAP contiguous with PAPs: two synapses are abutting a PvAP around a blood vessel. Confocal images were taken by N.M.

mature brain (Allen and Eroglu, 2017; Chung et al., 2015; Stogsdill and Eroglu, 2017). At the vascular interface, perivascular astrocytic processes (PvAPs, often called endfeet) form a continuous layer around the brain vessels (Mathiisen et al., 2010; McCaslin et al., 2011). The dimensions of PvAPs vary greatly (from 8 to 198 µm^2) – even along the same vessel (Wang et al., 2020). On average, each astrocyte has 3.5 PvAPs (with a range from 1 to 7), which originate from one or more ramifications and that wrap around vessels (Bindocci et al., 2017). Via the PvAPs, astrocytes control several brain vascular functions, including the integrity of the blood–brain barrier, the homeostasis between the brain and the immune system, the transfer of metabolites and the regulation of cerebral blood flow (Alvarez et al., 2013; Cohen-Salmon et al., 2020). As in PAPs, most of the perivascular functions of astrocytes rely on a specific molecular repertoire that is enriched in PvAPs (Cohen-Salmon et al., 2020). For instance, the water channel aquaporin 4 (Aqp4) and the inward-rectifying K^+ channel Kir4.1 (encoded by *KCNJ10*) have critical roles in the regulation of perivascular homeostasis (Amiry-Moghaddam and Ottersen, 2003; Cohen-Salmon et al., 2020). Interestingly, PvAPs are sometimes contiguous with PAPs; this proximity might be critical for coupling the neuronal and vascular activities of astrocytes (Boulay et al., 2017) (Fig. 1).

The way astrocytes develop and maintain their high level of polarity has not been characterized. The recent discovery of local translation in the distal compartments of astrocytes strongly suggests that (as in neurons) this mechanism might underpin their functional polarity. Local translation requires mRNA transport, mRNA binding to the translation machinery and (for membrane and secreted proteins) proper folding and post-translational modifications. Here, we review the literature on RNA distribution, the detection of local translation in astrocytes, the subcellular organization of astrocytes at the perineuronal and perivascular interfaces, and the machinery for local translation. We conclude with a discussion on open questions in this new field of research.

Detection of mRNA in distal areas of the astrocyte

Several examples of local mRNA distribution in astrocytes had been described prior to the discovery of local translation. The analysis of protrusions obtained from primary cultures of astrocytes in a Boyden chamber (a cell culture device allowing cells to extend processes *in vitro*) provided an initial genome-wide assessment of mRNA localization in these structures (Thomsen et al., 2013a). *Glt1a* and *Glt1b* (also known as *Slc1a2a* and *Slc1a2b*) mRNAs were found to be differentially distributed; these mRNAs encode isoforms of the glutamate transporter 1 (GLT1), the most prominent glutamate transporter in astrocytes and which is responsible for glutamate uptake from the extracellular space in the brain (Murphy-Royal et al., 2017). Elevated amounts of *Glt1a* mRNA were found in the processes, whereas the *Glt1b* isoform was more restricted to the cell soma (Berger et al., 2005), suggesting that the composition and functions of GLT1 oligomers might differ in these two regions of the cell (Berger et al., 2005; Chen et al., 2004). A diurnal change in the distribution of fatty acid binding protein 7 (*Fabp7*) mRNA has been detected in mouse hippocampal PAPs, indicating that FABP7 might mediate diurnal changes in neuronal plasticity (Gerstner et al., 2012). mRNA encoding the glial fibrillary acidic protein (GFAP)-α isoform was preferentially detected in primary astrocyte protrusions, whereas mRNA encoding the GFAP-δ isoform was found in the soma (Thomsen et al., 2013b; Moeton et al., 2016). We recently confirmed these results in GFAP-immunolabelled hippocampal sections by combining mRNA detection (via *in situ* hybridization) with an *in silico* approach to quantify mRNAs in the somata, large processes and fine processes (Oudart et al., 2020). Changes in the distribution and density of *Gfap* mRNAs have also

been detected in a mouse model of Alzheimer's disease, suggesting that astrocyte mRNA transport is dysregulated in this pathology (Oudart et al., 2020). Interestingly, the assembly of GFAP-δ with GFAP-α promotes intermediate filament aggregation and dynamic changes (Moeton et al., 2016; Perng et al., 2008). Thus, the differential distribution of GFAP-α versus -δ-encoding mRNA might regulate intermediate filament dynamics in distal astrocyte processes.

The motility of mRNAs was recently assessed *in vivo* in radial glial cells (Pilaz et al., 2016). The latter are the progenitors of both neurons and astrocytes, and possess a basal process that emanates from the cell body, extends up to 450 µm away and terminates in an endfoot in contact with the meninges (Rakic, 2007). This basal process serves as a scaffold for the migration of excitatory neurons during early development (Nadarajah et al., 2001). The Ms2 system, which allows the movement of mRNA to be tracked *in vivo* (Bertrand et al., 1998), was used to study *Ccnd2* mRNA (encoding cyclin D2) in organotypic slices from embryonic mice (Pilaz et al., 2016). This work showed the active localization of the *Ccnd2* mRNA in the radial glia endfeet. Finally, three later studies used high-resolution *in situ* hybridization and RNA sequencing to demonstrate the presence of mRNAs in purified PvAPs (Boulay et al., 2017) and PAPs (Sakers et al., 2017; Mazare et al., 2020a) (see below).

Detection of local translation events in astrocytes

The localization of mRNAs in astrocytic distal processes raises the question of their translational status. To address this issue, Pilaz et al. linked a Dendra2 photoconvertible reporter to the *Ccnd2* 3′ untranslated region (UTR) and tracked the translation of this mRNA in radial glia endfoot preparations; green Dendra2 was irreversibly photoconverted to red, and time-lapse imaging over the following 45 min revealed a steady increase in green fluorescence recovery in the endfeet, suggesting *de novo* synthesis (Pilaz et al., 2016). Local translation of the *Gja1* mRNA, which encodes connexin 43 (Cx43; an astrocyte gap junction protein strongly expressed in PvAPs), has been measured in an *ex vivo* assay (Boulay et al., 2017). Cx43 is known to have a very dynamic life cycle, with a turnover time of 1.5 to 5 h (Fallon and Goodenough, 1981; Laird et al., 1995, 1991). Freshly isolated PvAPs attached to the surface of mechanically purified brain vessels (Boulay et al., 2015) were treated with cycloheximide (an inhibitor of protein synthesis) for 6 h. The level of Cx43 (assessed via western blots) was lower upon cycloheximide treatment than in untreated samples, indicating that Cx43 turnover in PvAPs relies on local translation (Boulay et al., 2017). Other recently developed techniques for visualizing local translation in astrocytes include the use of modified amino acid analogues, such as homopropargylglycine (HPG), or tRNA analogs (e.g. puromycin). The methionine analogue HPG inserts into the nascent protein chain and can be subsequently detected by a chemoselective ligation ('click') reaction with a fluorescent protein reporter (Horisawa, 2014). The aminoglycoside antibiotic puromycin, which can be detected by immunofluorescence, mimics tRNA-Tyr; it incorporates into the ribosome A binding site and induces the premature termination of translation by ribosome-catalysed covalent incorporation into the C-terminal of the nascent peptide (Schmidt et al., 2009; Pestka, 1971; Pestka and Brot, 1971). An HPG protein synthesis assay of freshly purified brain vessels gave a strong signal in the co-purified PvAPs (Boulay et al., 2017). Another study reported that, after incubating acute brain slices with puromycin, ∼73% of the puromycin puncta were located more than 9 µm away from the centre of the cortical astrocyte nucleus, suggesting that translation occurs more in distal processes than in the soma (Sakers et al., 2017). More recently, quantification of the puromycin signal in hippocampal PAPs on acute brain sections showed that immunolabelled synapses that are found within 1 µm of puromycin- and GFP-labelled astrocytic ribosome signals accounted for ∼3% of all synapses contacted by eGFP-labelled astrocytic ribosomes. Although this proportion is not large and might be due to technical issues related to the low level of puromycin incorporated into astrocytes, these results indicate the presence of local translation in PAPs (Mazare et al., 2020a).

Identification of ribosome-bound mRNAs in astrocyte processes

To further analyse translation in PvAPs and PAPs, several recent studies focused on ribosome-bound mRNAs in astrocyte processes (Fig. 2). All the studies were based on the use of a transgenic mouse expressing the chimeric ribosomal protein L10A tagged to GFP under the control of the Aldh1l1 astrocyte-specific promoter (Aldh1l1:L10A–eGFP) and the purification of eGFP-tagged polysomes by so-called translating ribosome affinity purification (TRAP) (Doyle et al., 2008; Heiman et al., 2014, 2008). Importantly, this transgenic model has also been instrumental in the visualization of ribosomes in PAPs and PvAPs (Boulay et al., 2017; Mazare et al., 2020a; Sakers et al., 2017). Our initial study enabled the identification of the most abundant ribosome-bound mRNAs in PvAPs from whole brain (Boulay et al., 2017) (Fig. 2A). First, we extracted total mRNAs from purified brain vessels and brain vessels that had been partially depleted of PvAPs by basal lamina digestion. The comparison of these two samples allowed us to identify mRNAs that were relatively abundant in PvAPs, compared to the vascular compartment. Second, we investigated the ribosome-bound status of these mRNAs by comparing ribosome-bound mRNAs from whole astrocytes or PvAPs that were extracted by TRAP from either whole-brains or purified brain vessels from Aldh1l1:L10A–eGFP mice. Only mRNAs detected in both preparations were considered, since all mRNAs present in PvAPs should also be detected in whole astrocytes. The intersection between the total mRNA preparation and the TRAP preparation allowed us to identify 28 mRNAs that constituted the 'endfeetome', that is, the pool of most abundant ribosome-bound mRNAs in PvAPs (Boulay et al., 2017). Some of these mRNAs encoded proteins involved in vascular functions, such as Aqp4, Kir4.1 and Cx43 – all of which are transmembrane proteins known to have crucial roles in blood–brain barrier homeostasis. More details on the functions of these proteins can be found in a recent review (Cohen-Salmon et al., 2020). Interestingly, a comparison of total mRNA versus ribosome-bound mRNAs in PvAPs indicated that some PvAP mRNAs were not bound to ribosomes and so might remain silent after their transport (Boulay et al., 2017). Although the ribosome-bound status of an mRNA does not necessarily reflect its translation, as ribosome-bound mRNAs can also be silent if they are compacted in granules, our results were the first to highlight potential translation events in a distal compartment of mature astrocytes. Given that transcripts in the endfeetome are known to have critical roles in the regulation of the brain vascular systems, we hypothesized that local translation may be crucially involved in maintaining the vascular functions of astrocytes (Boulay et al., 2017). In a second study, a similar subtractive approach was used to identify ribosome-bound mRNAs that were abundant in PAPs from the cortex (Sakers et al., 2017) (Fig. 2B). Here, the pool of ribosome-bound mRNAs in PAPs was extracted by performing TRAP on Aldh1l1:L10A–eGFP purified cortical synaptoneurosomes, which in addition to PAPs comprise the pre- and post-synaptic compartments of neurons

Journal of Cell Science (2021) 134, jcs251629. doi:10.1242/jcs.251629

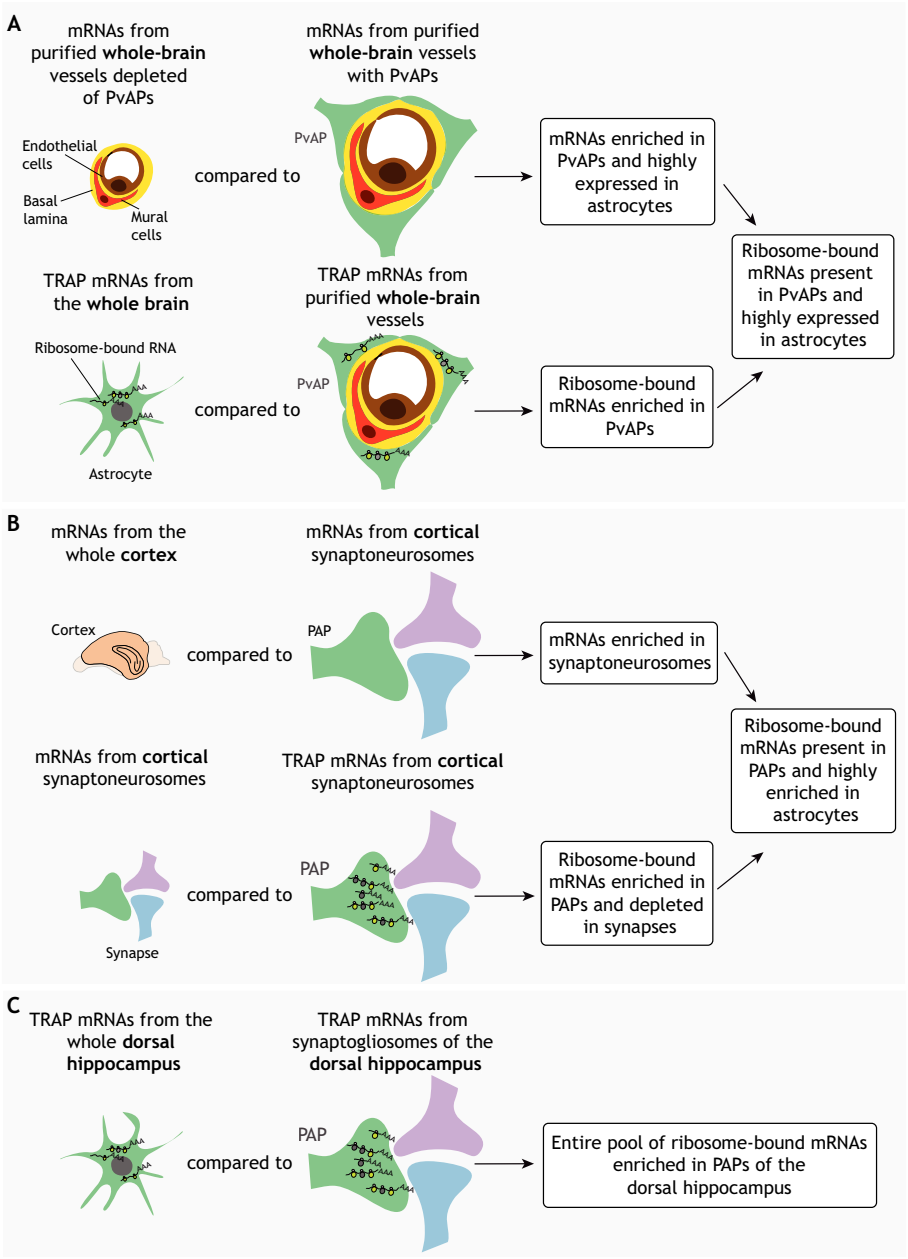

Fig. 2. Identification of ribosome-bound mRNAs in the perivascular and perisynaptic processes of astrocytes. (A) Identification of ribosome-bound mRNAs present in PvAPs and highly expressed in astrocytes in the whole brain. The experimental set up used in Boulay et al. (2017) to analyse ribosome-bound mRNAs in PvAPs from the whole brain. mRNAs from blood vessels (including the basal lamina, endothelial cells and mural cells) were mechanically purified from whole brain and thereby retained the PvAPs. They were then compared with mRNAs extracted from blood vessels after the basal lamina was enzymatically digested to remove PvAPs. mRNAs found to be more abundant in the preparation that retained PvAPs were identified. In parallel, translating ribosome affinity purification (TRAP) was applied to mechanically isolated blood vessels from whole brains of Aldh1l1:L10a–eGFP mice, which express an eGFP fusion to the ribosomal protein L10A specifically in astrocytes, in order to extract ribosome-bound mRNAs from PvAPs (second row). This preparation was then compared with the set of ribosome-bound mRNAs from whole astrocytes (extracted from whole brains using TRAP). Ribosome-bound mRNAs that were more abundant in PvAPs than in whole astrocytes were selected and then compared with ribosome-bound mRNAs in PvAPs. The overlapping mRNAs constituted the endfeetome, a set of highly expressed, ribosome-bound mRNAs in PvAPs. (B) Identification of ribosome-bound mRNAs present in PAPs and highly enriched in the synaptoneurosomes of the cortex. The experimental design used by (Sakers et al., 2017) to analyse ribosome-bound mRNAs in perisynaptic processes (PAPs) from the cortex. mRNAs from cortical synaptoneurosomes (including the PAP, pre-synapse and postsynapse) were purified and compared with mRNAs from whole cortices and the mRNAs that were more abundant in synaptoneurosomes were determined. In parallel, TRAP was used to extract the set of ribosome-bound mRNAs from cortical PAPs (the PAP-TRAP fraction, second row), and the latter were compared with mRNAs from whole cortical synaptoneurosomes to determine the mRNAs that are more abundant in the PAP-TRAP fraction. Next, mRNAs that were more abundant in synaptoneurosomes were compared with ribosome-bound mRNAs from PAPs; and overlap between the two sets yielded a set of ribosome-bound mRNAs present in PAPs and highly enriched in astrocytes. (C) Identification of the entire pool of ribosome-bound mRNAs enriched in PAPs of the dorsal hippocampus. The experimental design used by Mazaré et al. (2020a) to analyse ribosome-bound mRNAs that are more abundant in PAPs compared with their levels in whole astrocytes from the dorsal hippocampus. Starting with synaptogliosomes from dorsal hippocampi and whole dorsal hippocampi, a refined TRAP protocol was used to collect ribosome-bound mRNAs present in PAPs or whole astrocytes. The overlap between the two sets yielded the entire pool of ribosome-bound mRNAs that were enriched in PAPs from the dorsal hippocampus.

Journal of Cell Science (2021) 134, jcs251629. doi:10.1242/jcs.251629

(Sakers et al., 2017). The authors first compared the transcriptomes of total brain cortex and synaptoneurosomes, in order to identify mRNAs that were abundant in the latter structures. In parallel, they performed TRAP extraction on Aldh1l1:L10A–eGFP synaptoneurosomes and compared purified mRNAs with total mRNAs extracted from synaptoneurosomes, in order to identify ribosome-bound mRNAs that were highly abundant in PAPs (Sakers et al., 2017). Comparison of the two lists allowed the identification of 224 abundant ribosome-bound mRNAs in astrocyte PAPs (Sakers et al., 2017). These mRNAs coded for (1) proteins involved in glutamate metabolism, GABA metabolism and the biosynthesis of unsaturated fatty acids, (2) cytoskeletal proteins, such as ezrin, which might have a role in PAP remodelling (Lavialle et al., 2011), and (3) synaptogenic factors, such as the secreted protein acidic and rich in cysteine (Sparc), which regulates the synapse number (Lopez-Murcia et al., 2015). Taken as a whole, these two studies identified a set of ribosome-bound mRNAs that were more abundant in PvAPs and PAPs than in whole astrocytes. The results thus suggest that mRNA distribution and local translation could sustain the polarity of astrocytes at the perisynaptic and perivascular interfaces (Boulay et al., 2017; Sakers et al., 2017).

Despite these promising results, these initial studies focused solely on mRNAs that were either highly expressed in or were specific to astrocytes. In fact, the technical limitations of the TRAP protocol prevented the detection of ubiquitous transcripts. Further work was thus required to characterize the entire pool of local ribosome-bound mRNAs at the perisynaptic and perivascular interfaces. To overcome limitations of the two previous studies, we recently refined the TRAP protocol by adding additional precleaning and blocking steps that reduced the background noise caused by unspecific mRNA binding (Mazaré et al., 2020a) (Fig. 2C). The use of this protocol eliminated contamination by neuronal mRNA and enabled us to extract a pool of 844 astroglial ribosome-bound mRNAs in PAPs from dorsal hippocampus synaptogliosomes. It should be noted that our extraction protocol differed slightly from that used in the synaptoneurosome study by Sakers et al. because we did not include ultracentrifugation on discontinuous Percoll–sucrose density gradients (Westmark et al., 2011). By analogy with the above-mentioned ‘endfeetome’ in PvAPs, we referred to this repertoire as the ‘PAPome’ (Mazare et al., 2020a). Interestingly, our study revealed a wholly new, and unexpected, set of enriched ribosome-bound transcripts in PAPs compared to those found previously (Sakers et al., 2017); the most abundant mRNAs encoded ubiquitous proteins involved in iron homeostasis, translation, the cell cycle and the cytoskeleton [notably ezrin, as also identified by Sakers et al. (2017)] (Mazaré et al., 2020a). Remarkably, a large proportion of ribosome-bound transcripts in PAPs encoded ribosomal proteins and elongation factors (Mazaré et al., 2020a), which is reminiscent of observations in neuronal processes (Deglincerti and Jaffrey, 2012; Giustetto et al., 2003; Moccia et al., 2003; Shigeoka et al., 2019). Overall, our results strongly suggest that local translation in PAPs might be sustained by local synthesis of the translation machinery, with either the *de novo* assembly of translational complexes or the replacement of damaged proteins, as recently suggested for ribosomal proteins in axons (Shigeoka et al., 2019).

The subcellular organization of local protein synthesis and maturation in astrocytes

To become functional, most secreted and membrane proteins must undergo post-translational modifications. In PvAPs, most of the endfeetome mRNAs encode membrane proteins that require folding and/or glycosylation as they pass through the endoplasmic reticulum (ER) and the Golgi. Accordingly, we observed smooth, rough and mixed ERs in all PvAPs (Fig. 3). A full Golgi was also detected in 7% of PvAPs, and these specific PvAPs might therefore contain the same canonical translation machinery as the soma (Boulay et al., 2017). PAPs are extremely thin structures (<50 nm in diameter) (Reichenbach et al., 2010), and their subcellular organization has not yet been fully explored. However, by using

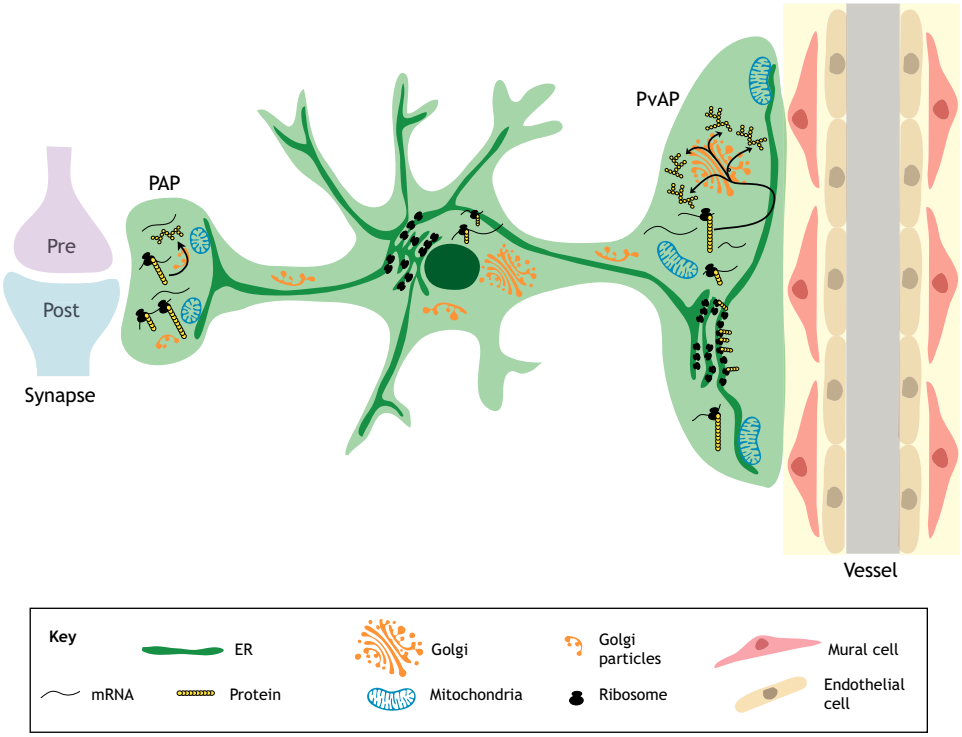

Fig. 3. Subcellular organization of perisynaptic and perivascular astrocytic processes. Astrocytes extend PAPs towards the synapse and PvAPs towards blood vessels. The astrocytic ER forms a continuous network that is in contact with both PAPs and PvAPs. PvAPs also contain rough ER to which ribosomes are bound, as well as mitochondria, ribosomes, mRNAs and mRNA-ribosome complexes that translate new proteins. A Golgi is observed in ∼7% of the PvAPs in the cortex and the hippocampus. In contrast, PAPs only contain small Golgi particles (pGolt particles), and small round mitochondria can also be observed.

an adeno-associated virus strategy, we were able to show that 32% of the hippocampal glutamatergic synapses in an astrocyte territory are contacted by PAPs containing ERGIC-53 (also known as LMAN1), an integral membrane protein located in the intermediate region between the ER and the Golgi (Mazare et al., 2020a). Furthermore, expression of the Golgi tracker pGolt (Mikhaylova et al., 2016) was detected in PAPs surrounding 38% of the glutamatergic synapses, suggesting the existence of detached Golgi particles (possibly outposts) in PAPs (Mazare et al., 2020a) (Fig. 3). A recent electron microscopy study provided evidence for ER in PvAPs and PAPs, and showed that the contact between the ER and mitochondria in PvAPs changed upon brain injury (Göbel et al., 2020). The authors suggested that the subcellular organization of astrocyte processes might be dynamically regulated (Göbel et al., 2020). Finally, to go further, it would be useful to determine whether polysomes and/or monosomes are present in PvAPs as well as PAPs. Indeed, monosomes display specific translational properties (Heyer and Moore, 2016) and have been shown to translate key synaptic transcripts in dendrites and axons (Biever et al., 2020).

Overall, the subcellular organization of PvAPs and PAPs is heterogenous; it is likely that the full functional diversity of translational and post-translational mechanisms in these structures has yet to be discovered (Rangaraju et al., 2017).

The molecular bases of translation in astrocytes

Local translation is mediated by *cis*-acting elements that include RNA motifs and secondary structures influencing the binding of *trans*-acting proteins, also known as RNA-binding proteins (RBPs) (Harvey et al., 2018). RNA-binding motifs are mostly present in UTRs in general and the 3′UTR in particular. Interestingly, a gene can give rise to different 3′UTR isoforms through alternative polyadenylation, which therefore modulates the ability of an mRNA to bind to an RBP. mRNAs bind to RBPs in the nucleus and soma to form ribonucleoparticles (RNPs, also referred to as granules). Depending on the nature of the *cis*- and *trans*-acting elements, the RNPs are transported along the cytoskeleton as cargo by kinesin and dynein molecular motor complexes (Pushpalatha and Besse, 2019). Although transcriptomic data indicate that RBPs are expressed in astrocytes (sometimes more strongly than in neurons), their roles in astrocytes have been poorly explored (Zhang et al., 2014) (Table 1). *Fmr1* encodes the fragile X mental retardation protein (FMRP) and is mutated in fragile X syndrome (FXS, a neurodevelopmental disorder resulting in intellectual disability and autism) (Penagarikano et al., 2007). One of the several possible functions of FMRP in neurons is its ability to act as an RBP and silence the translation of mRNAs encoding synaptic proteins (Darnell et al., 2011). Interestingly, FMRP might be more strongly expressed in astrocytes than in neurons (Table 1) (Zhang et al., 2014). It has been shown that FMRP controls mRNA transport in radial glia PvAPs *in vivo* and binds to mRNAs that encode autism-related signalling proteins and cytoskeletal regulators (Pilaz et al., 2016). In astrocytes, the selective loss of FMRP has been shown to dysregulate protein synthesis in general and expression of the glutamate transporter GLT1 (impairing neurotransmission and astrocytic glutamate uptake) in particular (Higashimori et al., 2016). In astrocytes, the expression of a pathological form of FMRP linked to late-onset FXS/ataxia syndrome has been found to impair motor performance in the mouse (Wenzel et al., 2019). These results strongly suggest that translational control by astroglial FMRP is involved in the pathogenesis of FXS.

The RBP quaking (QKI) is also strongly expressed in glial cells (Zhang et al., 2014). QKI was initially implicated in the regulation of *Mbp* mRNA transport in oligodendrocyte processes (Li et al., 2000; Doukhanine et al., 2010; Larocque et al., 2009; Wang et al., 2010). Furthermore, the QKI-7 cytosolic isoform was shown to regulate *Gfap* mRNA translation in human primary astrocytes (Radomska et al., 2013). More recently, it has been demonstrated that the ribosome-bound mRNAs that are preferentially found in PAPs contain a larger number of QKI-binding motifs (Sakers et al., 2017). This study also suggested that the inactivation of QKI-6 (another cytosolic isoform of QKI) in astrocytes altered the binding of certain mRNAs (e.g. *Sparc*) to ribosomes and thus influenced translation (Sakers et al., 2020 preprint). The role of QKI in brain development was recently studied in a conditional knockout (KO) model of *Qki* in neural stem cells (NSCs), which showed that QKI regulates the differentiation of NSCs into glial precursor cells by upregulating several genes involved in gliogenesis (Takeuchi et al., 2020). Finally, QKI has been reported as a candidate gene for schizophrenia susceptibility (Aberg et al., 2006). Thus, as with FXS, the regulation of QKI-mediated translation in astrocytes might be involved in schizophrenia.

Human antigen R (HuR, also referred to as ELAV-like protein 1) is one of the best-known RBPs in astrocytes. It binds to AU-rich elements (AREs) and stabilizes mRNAs (Brennan and Steitz, 2001). Although HuR is predominantly located in the nucleus, it translocates to the cytoplasm, transports the bound mRNAs to polysomes, and promotes their translation and stabilization (Fan and Steitz, 1998). This mode of translational regulation has been observed *in vivo* following spinal cord injury (Kwan et al., 2017a) and *in vitro* in a stretch injury model of primary astrocytes, in which HuR activated the expression of inflammatory mediators such as interleukin-1β, tumour necrosis factor (TNF), and matrix metalloproteinase 12 (Kwan et al., 2017b). Furthermore, translocation of HuR from the nucleus to the cytoplasm has been found to upregulate the translation of the cysteine-glutamate antiporter (Slc7a11, also known as the xCT system), following the treatment of mouse cortical primary astrocytes with interleukin-1β (Shi et al., 2016). HuR might therefore be a key factor for astrocyte translation in inflammatory contexts. Interestingly, HuR in primary astrocytes was also found to bind to the 3′UTR of *Tardbp*, which encodes TDP-43, an RBP linked to amyotrophic lateral sclerosis (ALS) (Lu et al., 2014). Finally, experiments in a glioma cell line showed that HuR bound to and stabilized the mRNA encoding B-cell lymphoma 2 (*Bcl2*, an important regulator of cell death) by activating its translation (Filippova et al., 2011). Consistent with this, the cytoplasmic level of HuR is positively correlated with the tumour grade in human glioma tissues (Bolognani et al., 2012).

Other known RBPs have been less extensively studied with regard to their possible effects on translation in astrocytes. This is the case for the cytoplasmic polyadenylation element binding protein 1 (CPEB1), which regulates poly(A) tail length and binds cytoplasmic polyadenylation elements (CPEs) in mRNA (Hake and Richter, 1994). CPEB1 also regulates synaptic plasticity (Alarcon et al., 2004) and binds to RNA granules in dendrites (Ohashi and Shiina, 2020). In primary astrocytes, *Fabp7* mRNA (containing CPEs in its 3′UTR) co-immunoprecipitates with CPEB1 (Gerstner et al., 2012). Interestingly, the length of the poly(A) tail in *Fabp7* mRNA in mouse brain samples varies with the time of day, and CPEB1 might thus have a role in the astrocyte-mediated neuronal plasticity linked to circadian rhythm, as previously suggested (Gerstner et al., 2012). Furthermore, CPEB1 controls the division of rat primary astrocytes (Kim et al., 2011). Upon the stimulation of cell division, CPEB1 is phosphorylated, binds to cyclin B1 mRNA and lengthens the mRNA poly(A) tail; in turn, this increases the rate

Journal of Cell Science (2021) 134, jcs251629. doi:10.1242/jcs.251629

Table 1. RNA-binding proteins in astrocytes

RBP	Gene	Expression level in astrocytes/ neurons*	Known roles	Astrocyte studies	Results	Reference(s)
FMRP	*Fmr1*	28.91/13.80	Alternative mRNA splicing; mRNA stability; mRNA transport (for a review, see Davis and Broadie, 2017)	*In vivo* mouse radial glia endfeet	FMRP binds autism-related mRNAs and controls active mRNA transport in radial glia.	Pilaz et al., 2016
				Inducible astrocyte-specific *Fmr1*-KO mouse	Decrease in GLT1 protein and glutamate uptake, resulting in increased neuronal excitability.	Higashimori et al., 2016
QKI	*Qki*	319.64/32.87	mRNA export; pre-mRNA splicing (for a review, see Darbelli and Richard, 2016)	*In vitro* primary human cortical astrocytes	QKI7 isoform binds *Gfap* mRNA; *Gfap* mRNA contains QKE. QKI increase leads to an elevated level of GFAP.	Radomska et al., 2013
				Astroglial QKI6 KO mouse	Impaired translation of *Sparc* mRNA. Increased synapse formation and delay in astrocyte maturation.	Sakers et al., 2020 preprint
				Quaking NSC-specific KO mouse	Quaking influences glial differentiation of NSCs by upregulating the expression of astrocyte and oligodendrocyte genes.	Takeuchi et al., 2020
HuR	*Elavl1*	10.23/11.16	mRNA stability (for a review, see Meisner and Filipowicz, 2011)	*In vivo* mouse spinal cord injury and *in vitro* stretch model of astrocytes	HuR translocates into the astrocyte cytoplasm upon injury. HuR increases the level of cytokine mRNAs.	Kwan et al., 2017a,b
				In vitro primary cortical astrocytes	IL-1 promotes HuR translocation to the cytoplasm. Binding of HuR to the 3′UTR of *xCT* mRNA increases the latter's half-life, protein level, and functions linked to the xCT system.	Shi et al., 2016
				In vitro primary cortical astrocytes from the G93A SOD1 mouse	HuR's binding to the 3′UTR of *Tardbp and Fus* mRNAs controls their translational efficiency. HuR KO in astrocytes leads to neuronal toxicity.	Lu et al., 2014
				In vitro U251 cells and glioblastoma xenograft	HuR upregulates *Bcl-2* mRNA translation and promotes cell survival.	Filippova et al., 2011
				Human glioma tissue and cell lines	The HuR protein level is increased in gliomas and correlates with the tumour grade.	Bolognani et al., 2012
CPEB1	*Cpeb1*	7.72/14.81	mRNA cytoplasmic polyadenylation mRNA transport (for a review, see Richter, 2007)	*In vivo* and *in vitro* PAPs from astrocytes in the mouse hippocampus and primary cortical	CPEB1 controls *Fabp7* mRNA translation in astrocytes via poly(A) tail length regulation in a time-of-day dependent manner.	Gerstner et al., 2012
				In vitro rat primary cortical astrocytes	CPEB1 regulates cyclin B1 translation and cell proliferation. CPEB1 KO enhances proliferation.	Kim et al., 2011
KSRP	*Khsrp*	14.17/19.78	Pre-mRNA splicing, mRNA decay, microRNA biogenesis (for a review, see Briata et al., 2016)	*In vitro* primary cortical astrocytes from KSRP-KO and WT mice	KSRP downregulates some cytokine mRNAs and mediates an inflammatory response in astrocytes.	Li et al., 2012

NSC, neural stem cell; WT, wild type.
*Expressed as the mean fragments per kilobase million (FPKM) (see Zhang et al., 2014).

of cyclin B1 translation and activates cell proliferation (Kim et al., 2011). The far upstream element-binding protein 2 [FUSE-binding protein 2 (FUBP2), also known as KH type-splicing regulatory protein (KSRP)] is an RBP that destabilizes ARE-containing mRNAs (Bird et al., 2013). In an *in vitro* luciferase reporter assay, FUBP2 was shown to downregulate the translation of cytokines. The knockdown of FUBP2 in rat primary astrocytes induces cortical neuron toxicity and astrocyte migration (Li et al., 2012).

In conclusion, only a few *in vivo* studies have been conducted regarding astrocytic RBPs, and data on their mode of action and their function in astrocytes are scarce. In particular, their possible role in the regulation of local translation remains to be addressed.

Conclusions and perspectives

Local translation in astrocytes is an emerging field of research, and many questions have yet to be addressed. First, the role of local translation in the establishment and maintenance of the functional polarity of astrocytes at their perivascular and perisynaptic interfaces is still an open question. Astrocyte heterogeneity constitutes a technical challenge in this respect. Indeed, astrocytes are diverse in terms of both morphology – for instance with voluminous, bushy, protoplasmic astroglia in the grey matter compared to elongated, fibrous astroglia in the white matter – and functionality, particularly with regard to their neuronal and vascular microenvironment (Farmer and Murai, 2017; Miller, 2018). For instance, the gliovascular interface greatly differs from one region of the brain to another and from one type of vessel to another, that is, capillaries, arteries or veins (Cohen-Salmon et al., 2020). The same reasoning applies to PAPs, which display functional and morphological differences throughout the brain. Another inherent difficulty in studies of astrocytes (compared to neurons) lies in the absence of *in vitro* systems in which astrocytes can reliably develop polarized

interfaces with vessels and/or neurons. The emergence of new *in vitro* microfluidic or organoid methods might offer greater opportunities in the future.

If local translation does sustain astrocyte polarity, it might occur differently in the soma and in the various processes. As mentioned above, the three TRAP studies found clear differences in the repertoire of ribosome-bound mRNAs between astrocyte soma and the processes, suggesting that local translation might sustain molecular polarity in PAPs and PvAPs (Boulay et al., 2017; Mazare et al., 2020a; Sakers et al., 2017). One of the most striking results obtained in our latest TRAP study of PAPs from the dorsal hippocampus is the enrichment in several ribosome-bound mRNAs encoding proteins of the large and small ribosomal subunits in PAPs compared to level of these mRNAs found in whole astrocytes (Mazare et al., 2020a). These results suggest that the ribosomal compositions of the astrocyte soma and PAPs could differ. Ribosomal proteins exhibit different functions in ribosomes (Castello et al., 2012), and mutations in individual ribosomal proteins give rise to distinct qualitative effects rather than an overall loss of protein synthesis (Shi and Barna, 2015). Hence, differences in ribosomal protein composition between astrocytic soma and PAPs might have important functional consequences. This question has yet to be resolved and will require a detailed proteomics study. The comparison of astrocytic interfaces might be an important way to determine the role of local translation in astrocyte polarity. PvAPs and PAPs differ in their subcellular organization; they both contain ER, but a full Golgi is observed only in ∼7% of PvAPs, suggesting that protein maturation is regulated differently (even among PvAPs) (Boulay et al., 2017). Interestingly, studies of dendrites have shown that membrane proteins bypassing the Golgi display atypical N-glycosylation profiles and thus probably have specific properties (Hanus et al., 2016). A link between Golgi outposts, microtubule branching, cell polarity and myelination was recently observed in oligodendrocytes (Fu et al., 2019). These findings suggest that the differences in ultrastructural organization between PvAPs and PAPs might underpin a diversity of translational, post-translational mechanisms and perhaps other functions yet to be discovered. Finally, and if local translation indeed sustains astrocyte polarity, PvAPs and PAPs might differ in the repertoire of ribosome-bound mRNAs. This question is still unresolved because the endfeetome has been characterized in whole brain and only covered transcripts that were abundant in astrocytes (Boulay et al., 2017), and the full ribosome-bound repertoire in PAPs was assessed specifically in the dorsal hippocampus (Mazaré et al., 2020a). Our recent refinement of the TRAP protocol now makes it possible to compare ribosome-bound mRNAs in PAPs and PvAPs from a given region of the brain (Mazaré et al., 2020a,b). Incidentally, this technical refinement might also be useful for reinvestigating ribosome-bound mRNAs in axons and dendrites because the earlier TRAP preparations of synapses or neurites contained astrocyte-specific mRNAs (Ouwenga et al., 2017; Shigeoka et al., 2016). Interestingly, our study of some of the most abundant mRNAs in the PAPome revealed differences between hippocampal PAPs and PvAPs, suggesting that local translation might indeed govern functional polarity (Mazaré et al., 2020a). One of the ribosome-bound mRNAs found to be more abundant in PAPs than in PvAPs was *Rplp1*, which encodes a ribosomal protein, suggesting that PvAPs and PAPs might also differ in the composition of their ribosomes, which might give rise to specific translational properties (Castello et al., 2012; Shi and Barna, 2015).

Besides polarity, there is a need for further investigations into the physiological and pathophysiological relevance of local translation in astrocytes. Interestingly, we observed that fear-conditioning in mice altered the levels of several enriched ribosome-bound mRNAs in dorsal hippocampal PAPs; this hints at a physiological role of astrocyte local translation in memory and learning and, more generally, in the cellular response to environmental cues (Mazaré et al., 2020a). During development, local translation in axons has a preponderant role in growth cone guidance, axon elongation and membrane remodelling (Wu et al., 2005; Yao et al., 2006; Campbell and Holt, 2001; Leung et al., 2006; Ming et al., 2002; Piper et al., 2006; Cagnetta et al., 2018; Hengst et al., 2009; Gracias et al., 2014). Results on axonal growth cone raised the intriguing possibility that local translation conditions the growth and formation of PvAPs and PAPs. Dysregulation of local translation in neurons has been linked to diseases such as FXS (Kao et al., 2010), spinal muscular atrophy (Jablonka et al., 2001; Zhang et al., 2003), ALS (Alami et al., 2014; Fallini et al., 2012) and Alzheimer's disease (Baleriola et al., 2014; Kobayashi et al., 2017; Li and Gotz, 2017; Walker et al., 2018). Furthermore, local translation might also be essential for the restoration of axon outgrowth after axon injury (Koley et al., 2019). With regard to the glia, translation of myelin basic protein in oligodendrocyte distal cell processes *in vitro* is impaired by exposure to amyloid β-peptide (Quintela-Lopez et al., 2019). We recently observed that the distribution of mRNAs encoding the GFAP isoforms α and δ differed in an Alzheimer's disease mouse model, particularly in astrocytes close to amyloid deposits (Oudart et al., 2020). As discussed above, most of the RBPs linked to neuronal dysfunction are also expressed in astrocytes. Alteration of astrocyte polarity is a hallmark in neuropathology (Cohen-Salmon et al., 2020; Dossi et al., 2018). Hence, changes in local translation in astrocytes are likely to be linked to diseases by altering the perivascular and perisynaptic functions of astrocytes.

In conclusion, the discovery of local translation in astrocytes raises a new repertoire of questions, in particular regarding the way astrocytes regulate their high level of polarity in normal and pathological contexts. Given the critical functions of astrocytes in the regulation of synaptic and vascular functions, characterization of local translation in these cells might also reveal important and novel aspects of the brain physiology.

Competing interests
The authors declare no competing or financial interests.

Funding
Our work in this area was funded by the Fondation pour la Recherche Médicale (FRM) (grant no. AJE20171039094), the Fondation pour l'aide à la recherche sur la sclérose en plaques (ARSEP), the Association Européenne contre les Leucodystrophies (ELA), and the Fondation France Alzheimer to M.C.-S. The work of N.M. was funded by the Ecole Doctorale Cerveau Cognition Comportement (ED3C) doctoral student program and the FRM (grant no. FDT201904008077). The work of M.O. was funded by the ED3C doctoral student program. The creation of the Center for Interdisciplinary Research in Biology (CIRB) was funded by the Fondation Bettencourt Schueller.

References

Aberg, K., Saetre, P., Lindholm, E., Ekholm, B., Pettersson, U., Adolfsson, R. and Jazin, E. (2006). Human QKI, a new candidate gene for schizophrenia involved in myelination. *Am. J. Med. Genet. B Neuropsychiatr. Genet.* **141B**, 84-90. doi:10.1002/ajmg.b.30243

Alami, N. H., Smith, R. B., Carrasco, M. A., Williams, L. A., Winborn, C. S., Han, S. S. W., Kiskinis, E., Winborn, B., Freibaum, B. D., Kanagaraj, A. et al. (2014). Axonal transport of TDP-43 mRNA granules is impaired by ALS-causing mutations. *Neuron* **81**, 536-543. doi:10.1016/j.neuron.2013.12.018

Alarcon, J. M., Malleret, G., Touzani, K., Vronskaya, S., Ishii, S., Kandel, E. R. and Barco, A. (2004). Chromatin acetylation, memory, and LTP are impaired in

CBP$^{+/-}$ mice: a model for the cognitive deficit in Rubinstein-Taybi syndrome and its amelioration. *Neuron* **42**, 947-959. doi:10.1016/j.neuron.2004.05.021
Allen, N. J. and Eroglu, C. (2017). Cell biology of astrocyte-synapse interactions. *Neuron* **96**, 697-708. doi:10.1016/j.neuron.2017.09.056
Alvarez, J. I., Katayama, T. and Prat, A. (2013). Glial influence on the blood brain barrier. *Glia* **61**, 1939-1958. doi:10.1002/glia.22575
Amiry-Moghaddam, M. and Ottersen, O. P. (2003). The molecular basis of water transport in the brain. *Nat. Rev. Neurosci.* **4**, 991-1001. doi:10.1038/nrn1252
Baleriola, J., Walker, C. A., Jean, Y. Y., Crary, J. F., Troy, C. M., Nagy, P. L. and Hengst, U. (2014). Axonally synthesized ATF4 transmits a neurodegenerative signal across brain regions. *Cell* **158**, 1159-1172. doi:10.1016/j.cell.2014.07.001
Berger, U. V., DeSilva, T. M., Chen, W. and Rosenberg, P. A. (2005). Cellular and subcellular mRNA localization of glutamate transporter isoforms GLT1a and GLT1b in rat brain by in situ hybridization. *J. Comp. Neurol.* **492**, 78-89. doi:10.1002/cne.20737
Bernardinelli, Y., Muller, D. and Nikonenko, I. (2014). Astrocyte-synapse structural plasticity. *Neural Plast.* **2014**, 232105. doi:10.1155/2014/232105
Bertrand, E., Chartrand, P., Schaefer, M., Shenoy, S. M., Singer, R. H. and Long, R. M. (1998). Localization of ASH1 mRNA particles in living yeast. *Mol. Cell* **2**, 437-445. doi:10.1016/S1097-2765(00)80143-4
Biever, A., Donlin-Asp, P. G. and Schuman, E. M. (2019). Local translation in neuronal processes. *Curr. Opin. Neurobiol.* **57**, 141-148. doi:10.1016/j.conb.2019.02.008
Biever, A., Glock, C., Tushev, G., Ciirdaeva, E., Dalmay, T., Langer, J. D. and Schuman, E. M. (2020). Monosomes actively translate synaptic mRNAs in neuronal processes. *Science* **367**, eaay4991. doi:10.1126/science.aay4991
Bindocci, E., Savtchouk, I., Liaudet, N., Becker, D., Carriero, G. and Volterra, A. (2017). Three-dimensional Ca^{2+} imaging advances understanding of astrocyte biology. *Science* **356**, eaai8185. doi:10.1126/science.aai8185
Bird, C. W., Gardiner, A. S., Bolognani, F., Tanner, D. C., Chen, C.-Y., Lin, W.-J., Yoo, S., Twiss, J. L. and Perrone-Bizzozero, N. (2013). KSRP modulation of GAP-43 mRNA stability restricts axonal outgrowth in embryonic hippocampal neurons. *PLoS ONE* **8**, e79255. doi:10.1371/journal.pone.0079255
Bolognani, F., Gallani, A. I., Sokol, L., Baskin, D. S. and Meisner-Kober, N. (2012). mRNA stability alterations mediated by HuR are necessary to sustain the fast growth of glioma cells. *J. Neurooncol.* **106**, 531-542. doi:10.1007/s11060-011-0707-1
Boulay, A.-C., Saubamea, B., Decleves, X. and Cohen-Salmon, M. (2015). Purification of mouse brain vessels. *J. Vis. Exp.* **105**, e53208. doi:10.3791/53208
Boulay, A.-C., Saubaméa, B., Adam, N., Chasseigneaux, S., Mazaré, N., Gilbert, A., Bahin, M., Bastianelli, L., Blugeon, C., Perrin, S. et al. (2017). Translation in astrocyte distal processes sets molecular heterogeneity at the gliovascular interface. *Cell Discov.* **3**, 17005. doi:10.1038/celldisc.2017.5
Brennan, C. M. and Steitz*, J. A. (2001). HuR and mRNA stability. *Cell Mol. Life Sci.* **58**, 266-277. doi:10.1007/PL00000854
Briata, P., Bordo, D., Puppo, M., Gorlero, F., Rossi, M., Perrone-Bizzozero, N. and Gherzi, R. (2016). Diverse roles of the nucleic acid-binding protein KHSRP in cell differentiation and disease: diverse roles of the nucleic acid-binding protein KHSRP. *Wiley Interdiscip. Rev. RNA* **7**, 227-240. doi:10.1002/wrna.1327
Cagnetta, R., Frese, C. K., Shigeoka, T., Krijgsveld, J. and Holt, C. E. (2018). Rapid cue-specific remodeling of the nascent axonal proteome. *Neuron* **99**, 29-46.e4. doi:10.1016/j.neuron.2018.06.004
Campbell, D. S. and Holt, C. E. (2001). Chemotropic responses of retinal growth cones mediated by rapid local protein synthesis and degradation. *Neuron* **32**, 1013-1026. doi:10.1016/S0896-6273(01)00551-7
Castello, A., Fischer, B., Eichelbaum, K., Horos, R., Beckmann, B. M., Strein, C., Davey, N. E., Humphreys, D. T., Preiss, T., Steinmetz, L. M. et al. (2012). Insights into RNA biology from an atlas of mammalian mRNA-binding proteins. *Cell* **149**, 1393-1406. doi:10.1016/j.cell.2012.04.031
Chen, W., Mahadomrongkul, V., Berger, U. V., Bassan, M., DeSilva, T., Tanaka, K., Irwin, N., Aoki, C. and Rosenberg, P. A. (2004). The glutamate transporter GLT1a is expressed in excitatory axon terminals of mature hippocampal neurons. *J. Neurosci.* **24**, 1136-1148. doi:10.1523/JNEUROSCI.1586-03.2004
Chung, W. S., Allen, N. J. and Eroglu, C. (2015). Astrocytes control synapse formation, function, and elimination. *Cold Spring Harb. Perspect. Biol.* **7**, a020370. doi:10.1101/cshperspect.a020370
Cohen-Salmon, M., Slaoui, L., Mazaré, N., Gilbert, A., Oudart, M., Alvear-Perez, R., Elorza-Vidal, X., Chever, O. and Boulay, A. C. (2020). Astrocytes in the regulation of cerebrovascular functions. *Glia*. doi:10.1002/glia.23924
Dallerac, G., Chever, O. and Rouach, N. (2013). How do astrocytes shape synaptic transmission? Insights from electrophysiology. *Front. Cell Neurosci.* **7**, 159. doi:10.3389/fncel.2013.00159
Dallérac, G., Zapata, J. and Rouach, N. (2018). Versatile control of synaptic circuits by astrocytes: where, when and how? *Nat. Rev. Neurosci.* **19**, 729-743. doi:10.1038/s41583-018-0080-6
Darbelli, L. and Richard, S. (2016). Emerging functions of the Quaking RNA-binding proteins and link to human diseases. *Wiley Interdiscip. Rev. RNA* **7**, 399-412. doi:10.1002/wrna.1344
Darnell, J. C., Van Driesche, S. J., Zhang, C., Hung, K. Y. S., Mele, A., Fraser, C. E., Stone, E. F., Chen, C., Fak, J. J., Chi, S. W. et al. (2011). FMRP stalls ribosomal translocation on mRNAs linked to synaptic function and autism. *Cell* **146**, 247-261. doi:10.1016/j.cell.2011.06.013
Davis, J. K. and Broadie, K. (2017). Multifarious functions of the fragile X mental retardation protein. *Trends Genet.* **33**, 703-714. doi:10.1016/j.tig.2017.07.008
Deglincerti, A. and Jaffrey, S. R. (2012). Insights into the roles of local translation from the axonal transcriptome. *Open Biol.* **2**, 120079. doi:10.1098/rsob.120079
Dossi, E., Vasile, F. and Rouach, N. (2018). Human astrocytes in the diseased brain. *Brain Res. Bull.* **136**, 139-156. doi:10.1016/j.brainresbull.2017.02.001
Doukhanine, E., Gavino, C., Haines, J. D., Almazan, G. and Richard, S. (2010). The QKI-6 RNA binding protein regulates actin-interacting protein-1 mRNA stability during oligodendrocyte differentiation. *Mol. Biol. Cell* **21**, 3029-3040. doi:10.1091/mbc.e10-04-0305
Doyle, J. P., Dougherty, J. D., Heiman, M., Schmidt, E. F., Stevens, T. R., Ma, G., Bupp, S., Shrestha, P., Shah, R. D., Doughty, M. L. et al. (2008). Application of a translational profiling approach for the comparative analysis of CNS cell types. *Cell* **135**, 749-762. doi:10.1016/j.cell.2008.10.029
Fallini, C., Bassell, G. J. and Rossoll, W. (2012). The ALS disease protein TDP-43 is actively transported in motor neuron axons and regulates axon outgrowth. *Hum. Mol. Genet.* **21**, 3703-3718. doi:10.1093/hmg/dds205
Fallon, R. F. and Goodenough, D. A. (1981). Five-hour half-life of mouse liver gap-junction protein. *J. Cell Biol.* **90**, 521-526. doi:10.1083/jcb.90.2.521
Fan, X. C. and Steitz, J. A. (1998). Overexpression of HuR, a nuclear-cytoplasmic shuttling protein, increases the in vivo stability of ARE-containing mRNAs. *EMBO J.* **17**, 3448-3460. doi:10.1093/emboj/17.12.3448
Farmer, W. T. and Murai, K. (2017). Resolving Astrocyte Heterogeneity in the CNS. *Front. Cell Neurosci.* **11**, 300. doi:10.3389/fncel.2017.00300
Filippova, N., Yang, X., Wang, Y., Gillespie, G. Y., Langford, C., King, P. H., Wheeler, C. and Nabors, L. B. (2011). The RNA-binding protein HuR promotes glioma growth and treatment resistance. *Mol. Cancer Res.* **9**, 648-659. doi:10.1158/1541-7786.MCR-10-0325
Fu, M. M., McAlear, T. S., Nguyen, H., Oses-Prieto, J. A., Valenzuela, A., Shi, R. D., Perrino, J. J., Huang, T. T., Burlingame, A. L., Bechstedt, S. et al. (2019). The golgi outpost protein TPPP nucleates microtubules and is critical for Myelination. *Cell* **179**, 132-146.e14. doi:10.1016/j.cell.2019.08.025
Garcia-Ladona, F. J., Huss, Y., Frey, P. and Ghandour, M. S. (1997). Oligodendrocytes express different isoforms of beta-amyloid precursor protein in chemically defined cell culture conditions: in situ hybridization and immunocytochemical detection. *J. Neurosci. Res.* **50**, 50-61. doi:10.1002/(SICI)1097-4547(19971001)50:1<50::AID-JNR6>3.0.CO;2-K
Gerstner, J. R., Vanderheyden, W. M., LaVaute, T., Westmark, C. J., Rouhana, L., Pack, A. I., Wickens, M. and Landry, C. F. (2012). Time of day regulates subcellular trafficking, tripartite synaptic localization, and polyadenylation of the astrocytic Fabp7 mRNA. *J. Neurosci.* **32**, 1383-1394. doi:10.1523/JNEUROSCI.3228-11.2012
Ghandour, M. S. and Skoff, R. P. (1991). Double-labeling in situ hybridization analysis of mRNAs for carbonic anhydrase II and myelin basic protein: expression in developing cultured glial cells. *Glia* **4**, 1-10. doi:10.1002/glia.440040102
Ghézali, G., Dallérac, G. and Rouach, N. (2016). Perisynaptic astroglial processes: dynamic processors of neuronal information. *Brain Struct. Funct.* **221**, 2427-2442. doi:10.1007/s00429-015-1070-3
Giustetto, M., Hegde, A. N., Si, K., Casadio, A., Inokuchi, K., Pei, W., Kandel, E. R. and Schwartz, J. H. (2003). Axonal transport of eukaryotic translation elongation factor 1alpha mRNA couples transcription in the nucleus to long-term facilitation at the synapse. *Proc. Natl. Acad. Sci. USA* **100**, 13680-13685. doi:10.1073/pnas.1835674100
Glock, C., Heumuller, M. and Schuman, E. M. (2017). mRNA transport & local translation in neurons. *Curr. Opin Neurobiol.* **45**, 169-177. doi:10.1016/j.conb.2017.05.005
GÖbel, J., Engelhardt, E., Pelzer, P., Sakthivelu, V., Jahn, H. M., Jevtic, M., Folz-Donahue, K., Kukat, C., Schauss, A., Frese, C. K. et al. (2020). Mitochondria-Endoplasmic Reticulum Contacts in Reactive Astrocytes Promote Vascular Remodeling. *Cell Metab.* **31**, 791-808.e8. doi:10.1016/j.cmet.2020.03.005
Gracias, N. G., Shirkey-Son, N. J. and Hengst, U. (2014). Local translation of TC10 is required for membrane expansion during axon outgrowth. *Nat. Commun.* **5**, 3506. doi:10.1038/ncomms4506
Hake, L. E. and Richter, J. D. (1994). CPEB is a specificity factor that mediates cytoplasmic polyadenylation during Xenopus oocyte maturation. *Cell* **79**, 617-627. doi:10.1016/0092-8674(94)90547-9
Hanus, C., Geptin, H., Tushev, G., Garg, S., Alvarez-Castelao, B., Sambandan, S., Kochen, L., Hafner, A. S., Langer, J. D. and Schuman, E. M. (2016). Unconventional secretory processing diversifies neuronal ion channel properties. *eLife* **5**, e20609. doi:10.7554/eLife.20609
Harvey, R. F., Smith, T. S., Mulroney, T., Queiroz, R. M. L., Pizzinga, M., Dezi, V., Villenueva, E., Ramakrishna, M., Lilley, K. S. and Willis, A. E. (2018). Trans-acting translational regulatory RNA binding proteins. *Wiley Interdiscip. Rev. RNA* **9**, e1465. doi:10.1002/wrna.1465
Heiman, M., Schaefer, A., Gong, S., Peterson, J. D., Day, M., Ramsey, K. E., Suárez-Fariñas, M., Schwarz, C., Stephan, D. A., Surmeier, D. J. et al. (2008). A translational profiling approach for the molecular characterization of CNS cell types. *Cell* **135**, 738-748. doi:10.1016/j.cell.2008.10.028

Heiman, M., Kulicke, R., Fenster, R. J., Greengard, P. and Heintz, N. (2014). Cell type-specific mRNA purification by translating ribosome affinity purification (TRAP). *Nat. Protoc.* **9**, 1282-1291. doi:10.1038/nprot.2014.085
Hengst, U., Deglincerti, A., Kim, H. J., Jeon, N. L. and Jaffrey, S. R. (2009). Axonal elongation triggered by stimulus-induced local translation of a polarity complex protein. *Nat. Cell Biol.* **11**, 1024-1030. doi:10.1038/ncb1916
Heyer, E. E. and Moore, M. J. (2016). Redefining the translational Status of 80S monosomes. *Cell* **164**, 757-769. doi:10.1016/j.cell.2016.01.003
Higashimori, H., Schin, C. S., Chiang, M. S., Morel, L., Shoneye, T. A., Nelson, D. L. and Yang, Y. (2016). Selective deletion of astroglial FMRP dysregulates glutamate transporter GLT1 and contributes to fragile X syndrome phenotypes *in vivo*. *J. Neurosci.* **36**, 7079-7094. doi:10.1523/JNEUROSCI.1069-16.2016
Holt, C. E. and Schuman, E. M. (2013). The central dogma decentralized: new perspectives on RNA function and local translation in neurons. *Neuron* **80**, 648-657. doi:10.1016/j.neuron.2013.10.036
Holt, C. E., Martin, K. C. and Schuman, E. M. (2019). Local translation in neurons: visualization and function. *Nat. Struct. Mol. Biol.* **26**, 557-566. doi:10.1038/s41594-019-0263-5
Horisawa, K. (2014). Specific and quantitative labeling of biomolecules using click chemistry. *Front. Physiol.* **5**, 457. doi:10.3389/fphys.2014.00457
Jablonka, S., Bandilla, M., Wiese, S., Buhler, D., Wirth, B., Sendtner, M. and Fischer, U. (2001). Co-regulation of survival of motor neuron (SMN) protein and its interactor SIP1 during development and in spinal muscular atrophy. *Hum. Mol. Genet.* **10**, 497-505. doi:10.1093/hmg/10.5.497
Jeffery, W. R., Tomlinson, C. R. and Brodeur, R. D. (1983). Localization of actin messenger RNA during early ascidian development. *Dev. Biol.* **99**, 408-417. doi:10.1016/0012-1606(83)90290-7
Kao, D. I., Aldridge, G. M., Weiler, I. J. and Greenough, W. T. (2010). Altered mRNA transport, docking, and protein translation in neurons lacking fragile X mental retardation protein. *Proc. Natl. Acad. Sci. USA* **107**, 15601-15606. doi:10.1073/pnas.1010564107
Kim, K. C., Oh, W. J., Ko, K. H., Shin, C. Y. and Wells, D. G. (2011). Cyclin B1 expression regulated by cytoplasmic polyadenylation element binding protein in astrocytes. *J. Neurosci.* **31**, 12118-12128. doi:10.1523/JNEUROSCI.1621-11.2011
Kobayashi, S., Tanaka, T., Soeda, Y., Almeida, O. F. X. and Takashima, A. (2017). Local somatodendritic translation and hyperphosphorylation of tau protein triggered by AMPA and NMDA receptor stimulation. *EBioMed.* **20**, 120-126. doi:10.1016/j.ebiom.2017.05.012
Koenig, E. (1965a). Synthetic mechanisms in the axon. I. local axonal synthesis of acetylcholinesterase. *J. Neurochem.* **12**, 343-355. doi:10.1111/j.1471-4159.1965.tb04235.x
Koenig, E. (1965b). Synthetic Mechanisms in the Axon. II. Rna in myelin-free axons of the cat. *J. Neurochem.* **12**, 357-361. doi:10.1111/j.1471-4159.1965.tb04236.x
Koenig, E. (1967a). Synthetic mechanisms in the axon. 3. Stimulation of acetylcholinesterase synthesis by actinomycin-D in the hypoglossal nerve. *J. Neurochem.* **14**, 429-435. doi:10.1111/j.1471-4159.1967.tb09541.x
Koenig, E. (1967b). Synthetic mechanisms in the axon. IV. In vitro incorporation of [3H]precursors into axonal protein and RNA. *J. Neurochem.* **14**, 437-446. doi:10.1111/j.1471-4159.1967.tb09542.x
Koley, S., Rozenbaum, M., Fainzilber, M. and Terenzio, M. (2019). Translating regeneration: Local protein synthesis in the neuronal injury response. *Neurosci. Res.* **139**, 26-36. doi:10.1016/j.neures.2018.10.003
Kristensson, K., Zeller, N. K., Dubois-Dalcq, M. E. and Lazzarini, R. A. (1986). Expression of myelin basic protein gene in the developing rat brain as revealed by in situ hybridization. *J. Histochem. Cytochem.* **34**, 467-473. doi:10.1177/34.4.2419396
Kuklin, E. A., Alkins, S., Bakthavachalu, B., Genco, M. C., Sudhakaran, I., Raghavan, K. V., Ramaswami, M. and Griffith, L. C. (2017). The Long 3'UTR mRNA of CaMKII Is essential for translation-dependent plasticity of spontaneous release in Drosophila melanogaster. *J. Neurosci.* **37**, 10554-10566. doi:10.1523/JNEUROSCI.1313-17.2017
Kwan, T., Floyd, C. L., Patel, J., Mohaimany-Aponte, A. and King, P. H. (2017a). Astrocytic expression of the RNA regulator HuR accentuates spinal cord injury in the acute phase. *Neurosci. Lett.* **651**, 140-145. doi:10.1016/j.neulet.2017.05.003
Kwan, T., Floyd, C. L., Kim, S. and King, P. H. (2017b). RNA binding protein human antigen r is translocated in astrocytes following spinal cord injury and promotes the inflammatory response. *J. Neurotrauma* **34**, 1249-1259. doi:10.1089/neu.2016.4757
Laird, D. W., Puranam, K. L. and Revel, J. P. (1991). Turnover and phosphorylation dynamics of connexin43 gap junction protein in cultured cardiac myocytes. *Biochem. J.* **273**, 67-72. doi:10.1042/bj2730067
Laird, D. W., Castillo, M. and Kasprzak, L. (1995). Gap junction turnover, intracellular trafficking, and phosphorylation of connexin43 in brefeldin A-treated rat mammary tumor cells. *J. Cell Biol.* **131**, 1193-1203. doi:10.1083/jcb.131.5.1193
Larocque, D., Fragoso, G., Huang, J., Mushynski, W. E., Loignon, M., Richard, S. and Almazan, G. (2009). The QKI-6 and QKI-7 RNA binding proteins block proliferation and promote Schwann cell myelination. *PLoS ONE* **4**, e5867. doi:10.1371/journal.pone.0005867
Lavialle, M., Aumann, G., Anlauf, E., Prols, F., Arpin, M. and Derouiche, A. (2011). Structural plasticity of perisynaptic astrocyte processes involves ezrin and metabotropic glutamate receptors. *Proc. Natl. Acad. Sci. USA* **108**, 12915-12919. doi:10.1073/pnas.1100957108
Leung, K. M., van Horck, F. P., Lin, A. C., Allison, R., Standart, N. and Holt, C. E. (2006). Asymmetrical beta-actin mRNA translation in growth cones mediates attractive turning to netrin-1. *Nat. Neurosci.* **9**, 1247-1256. doi:10.1038/nn1775
Li, C. and Götz, J. (2017). Somatodendritic accumulation of Tau in Alzheimer's disease is promoted by Fyn-mediated local protein translation. *EMBO J.* **36**, 3120-3138. doi:10.15252/embj.201797724
Li, Z., Zhang, Y., Li, D. and Feng, Y. (2000). Destabilization and mislocalization of myelin basic protein mRNAs in quaking dysmyelination lacking the QKI RNA-binding proteins. *J. Neurosci.* **20**, 4944-4953. doi:10.1523/JNEUROSCI.20-13-04944.2000
Li, X., Lin, W. J., Chen, C. Y., Si, Y., Zhang, X., Lu, L., Suswam, E., Zheng, L. and King, P. H. (2012). KSRP: a checkpoint for inflammatory cytokine production in astrocytes. *Glia* **60**, 1773-1784. doi:10.1002/glia.22396
López-Murcia, F. J., Terni, B. and Llobet, A. (2015). SPARC triggers a cell-autonomous program of synapse elimination. *Proc. Natl. Acad. Sci. USA* **112**, 13366-13371. doi:10.1073/pnas.1512202112
LoPresti, P., Szuchet, S., Papasozomenos, S. C., Zinkowski, R. P. and Binder, L. I. (1995). Functional implications for the microtubule-associated protein tau: localization in oligodendrocytes. *Proc. Natl. Acad. Sci. USA* **92**, 10369-10373. doi:10.1073/pnas.92.22.10369
Lu, L., Zheng, L., Si, Y., Luo, W., Dujardin, G., Kwan, T., Potochick, N. R., Thompson, S. R., Schneider, D. A. and King, P. H. (2014). Hu antigen R (HuR) is a positive regulator of the RNA-binding proteins TDP-43 and FUS/TLS: implications for amyotrophic lateral sclerosis. *J. Biol. Chem.* **289**, 31792-31804. doi:10.1074/jbc.M114.573246
Mathiisen, T. M., Lehre, K. P., Danbolt, N. C. and Ottersen, O. P. (2010). The perivascular astroglial sheath provides a complete covering of the brain microvessels: an electron microscopic 3D reconstruction. *Glia* **58**, 1094-1103. doi:10.1002/glia.20990
Mathur, C., Johnson, K. R., Tong, B. A., Miranda, P., Srikumar, D., Basilio, D., Latorre, R., Bezanilla, F. and Holmgren, M. (2018). Demonstration of ion channel synthesis by isolated squid giant axon provides functional evidence for localized axonal membrane protein translation. *Sci. Rep.* **8**, 2207. doi:10.1038/s41598-018-20684-8
Mazaré, N., Oudart, M., Moulard, J., Cheung, G., Tortuyaux, R., Mailly, P., Mazaud, D., Bemelmans, A. P., Boulay, A. C., Blugeon, C. et al. (2020a). Local translation in perisynaptic astrocytic processes is specific and changes after fear conditioning. *Cell Rep.* **32**, 108076. doi:10.1016/j.celrep.2020.108076
Mazaré, N., Oudart, M., Cheung G., Boulay, A. C. and Cohen-Salmon, M. (2020b). Immunoprecipitation of Ribosome-Bound mRNAs from Astrocytic Perisynaptic Processes of the Mouse Hippocampus. *STAR Protocols* **1**, e100198. doi:10.1016/j.xpro.2020.100198
McCaslin, A. F., Chen, B. R., Radosevich, A. J., Cauli, B. and Hillman, E. M. (2011). *In vivo* 3D morphology of astrocyte—vasculature interactions in the somatosensory cortex: implications for neurovascular coupling. *J. Cereb. Blood Flow Metab.* **31**, 795-806. doi:10.1038/jcbfm.2010.204
Meisner, N. C. and Filipowicz, W. (2011). Properties of the regulatory RNA-binding protein HuR and its role in controlling miRNA repression. *Adv. Exp. Med. Biol.* **700**, 106-123. doi:10.1007/978-1-4419-7823-3_10
Mikhaylova, M., Bera, S., Kobler, O., Frischknecht, R. and Kreutz, M. R. (2016). A dendritic golgi satellite between ERGIC and retromer. *Cell Rep.* **14**, 189-199. doi:10.1016/j.celrep.2015.12.024
Miller, S. J. (2018). Astrocyte Heterogeneity in the Adult Central Nervous System. *Front. Cell Neurosci.* **12**, 401. doi:10.3389/fncel.2018.00401
Ming, G. L., Wong, S. T., Henley, J., Yuan, X. B., Song, H. J., Spitzer, N. C. and Poo, M. M. (2002). Adaptation in the chemotactic guidance of nerve growth cones. *Nature* **417**, 411-418. doi:10.1038/nature745
Moccia, R., Chen, D., Lyles, V., Kapuya, E., Kalachikov, Y. E. S., Spahn, C. M., Frank, J., Kandel, E. R., Barad, M. and Martin, K. C. (2003). An unbiased cDNA library prepared from isolated Aplysia sensory neuron processes is enriched for cytoskeletal and translational mRNAs. *J. Neurosci.* **23**, 9409-9417. doi:10.1523/JNEUROSCI.23-28-09409.2003
Moeton, M., Stassen, O. M., Sluijs, J. A., van der Meer, V. W., Kluivers, L. J., van Hoorn, H., Schmidt, T., Reits, E. A., van Strien, M. E. and Hol, E. M. (2016). GFAP isoforms control intermediate filament network dynamics, cell morphology, and focal adhesions. *Cell Mol. Life Sci.* **73**, 4101-4120. doi:10.1007/s00018-016-2239-5
Murphy-Royal, C., Dupuis, J., Groc, L. and Oliet, S. H. R. (2017). Astroglial glutamate transporters in the brain: Regulating neurotransmitter homeostasis and synaptic transmission. *J. Neurosci. Res.* **95**, 2140-2151. doi:10.1002/jnr.24029
Nadarajah, B., Brunstrom, J. E., Grutzendler, J., Wong, R. O. and Pearlman, A. L. (2001). Two modes of radial migration in early development of the cerebral cortex. *Nat. Neurosci.* **4**, 143-150. doi:10.1038/83967
Ohashi, R. and Shiina, N. (2020). Cataloguing and selection of mRNAs localized to dendrites in neurons and regulated by RNA-binding proteins in RNA granules. *Biomolecules* **10**, 167. doi:10.3390/biom10020167

Oudart, M., Tortuyaux, R., Mailly, P., Mazaré, N., Boulay, A.-C. and Cohen-Salmon, M. (2020). AstroDot - a new method for studying the spatial distribution of mRNA in astrocytes. *J. Cell Sci.* **133**, jcs239756. doi:10.1242/jcs.239756

Ouwenga, R., Lake, A. M., O'Brien, D., Mogha, A., Dani, A. and Dougherty, J. D. (2017). Transcriptomic analysis of ribosome-bound mRNA in cortical neurites *in vivo*. *J. Neurosci.* **37**, 8688-8705. doi:10.1523/JNEUROSCI.3044-16.2017

Pannasch, U., Vargova, L., Reingruber, J., Ezan, P., Holcman, D., Giaume, C., Sykova, E. and Rouach, N. (2011). Astroglial networks scale synaptic activity and plasticity. *Proc. Natl. Acad. Sci. USA* **108**, 8467-8472. doi:10.1073/pnas.1016650108

Penagarikano, O., Mulle, J. G. and Warren, S. T. (2007). The pathophysiology of fragile x syndrome. *Annu. Rev. Genomics Hum. Genet.* **8**, 109-129. doi:10.1146/annurev.genom.8.080706.092249

Perng, M. D., Wen, S. F., Gibbon, T., Middeldorp, J., Sluijs, J., Hol, E. M. and Quinlan, R. A. (2008). Glial fibrillary acidic protein filaments can tolerate the incorporation of assembly-compromised GFAP-δ, but with consequences for filament organization and αB-crystallin association. *Mol. Biol. Cell* **19**, 4521-4533. doi:10.1091/mbc.e08-03-0284

Pestka, S. (1971). Inhibitors of ribosome functions. *Annu. Rev. Microbiol.* **25**, 487-562. doi:10.1146/annurev.mi.25.100171.002415

Pestka, S. and Brot, N. (1971). Studies on the formation of transfer ribonucleic acid-ribosome complexes. IV. Effect of antibiotics on steps of bacterial protein synthesis: some new ribosomal inhibitors of translocation. *J. Biol. Chem.* **246**, 7715-7722. doi:10.1016/S0021-9258(19)45834-1

Pilaz, L. J., Lennox, A. L., Rouanet, J. P. and Silver, D. L. (2016). Dynamic mRNA transport and local translation in radial glial progenitors of the developing brain. *Curr. Biol.* **26**, 3383-3392. doi:10.1016/j.cub.2016.10.040

Piper, M., Anderson, R., Dwivedy, A., Weinl, C., van Horck, F., Leung, K. M., Cogill, E. and Holt, C. (2006). Signaling mechanisms underlying Slit2-induced collapse of Xenopus retinal growth cones. *Neuron* **49**, 215-228. doi:10.1016/j.neuron.2005.12.008

Pushpalatha, K. V. and Besse, F. (2019). Local translation in Axons: when membraneless RNP granules meet membrane-bound organelles. *Front. Mol. Biosci.* **6**, 129. doi:10.3389/fmolb.2019.00129

Quintela-Lopez, T., Ortiz-Sanz, C., Serrano-Regal, M. P., Gaminde-Blasco, A., Valero, J., Baleriola, J., Sanchez-Gomez, M. V., Matute, C. and Alberdi, E. (2019). Aβ oligomers promote oligodendrocyte differentiation and maturation via integrin β1 and Fyn kinase signaling. *Cell Death Dis.* **10**, 445. doi:10.1038/s41419-019-1636-8

Radomska, K. J., Halvardson, J., Reinius, B., Lindholm Carlstrom, E., Emilsson, L., Feuk, L. and Jazin, E. (2013). RNA-binding protein QKI regulates Glial fibrillary acidic protein expression in human astrocytes. *Hum. Mol. Genet.* **22**, 1373-1382. doi:10.1093/hmg/dds553

Rakic, P. (2007). The radial edifice of cortical architecture: from neuronal silhouettes to genetic engineering. *Brain Res. Rev.* **55**, 204-219. doi:10.1016/j.brainresrev.2007.02.010

Rangaraju, V., Tom Dieck, S. and Schuman, E. M. (2017). Local translation in neuronal compartments: how local is local? *EMBO Rep.* **18**, 693-711. doi:10.15252/embr.201744045

Reichenbach, A., Derouiche, A. and Kirchhoff, F. (2010). Morphology and dynamics of perisynaptic glia. *Brain Res. Rev.* **63**, 11-25. doi:10.1016/j.brainresrev.2010.02.003

Richter, J. D. (2007). CBEP: a life in translation. *Trends Biochem. Sci.* **32**, 279-285. doi:10.1016/j.tibs.2007.04.004

Sakers, K., Lake, A. M., Khazanchi, R., Ouwenga, R., Vasek, M. J., Dani, A. and Dougherty, J. D. (2017). Astrocytes locally translate transcripts in their peripheral processes. *Proc. Natl. Acad. Sci. USA* **114**, E3830-E3838. doi:10.1073/pnas.1617782114

Sakers, K., Liu, Y., Llaci, L., Vasek, M. J., Rieder, M. J., Brophy, S., Tycksen, E., Lewis, R., Maloney, S. E. and Dougherty, J. D. (2020). CRISPR-TRAPSeq identifies the QKI RNA binding protein as important for astrocytic maturation and control of thalamocortical synapses. *BioRXiv*. doi:10.1101/2020.03.13.991224

Schmidt, E. K., Clavarino, G., Ceppi, M. and Pierre, P. (2009). SUnSET, a nonradioactive method to monitor protein synthesis. *Nat. Methods* **6**, 275-277. doi:10.1038/nmeth.1314

Shi, Z. and Barna, M. (2015). Translating the genome in time and space: specialized ribosomes, RNA regulons, and RNA-binding proteins. *Annu. Rev. Cell Dev. Biol.* **31**, 31-54. doi:10.1146/annurev-cellbio-100814-125346

Shi, J., He, Y., Hewett, S. J. and Hewett, J. A. (2016). Interleukin 1beta regulation of the system xc- substrate-specific subunit, xCT, in primary mouse astrocytes involves the RNA-binding protein HuR. *J. Biol. Chem.* **291**, 1643-1651. doi:10.1074/jbc.M115.697821

Shigeoka, T., Jung, H., Jung, J., Turner-Bridger, B., Ohk, J., Lin, J. Q., Amieux, P. S. and Holt, C. E. (2016). Dynamic axonal translation in developing and mature visual circuits. *Cell* **166**, 181-192. doi:10.1016/j.cell.2016.05.029

Shigeoka, T., Koppers, M., Wong, H. H.-W., Lin, J. Q., Cagnetta, R., Dwivedy, A., de Freitas Nascimento, J., van Tartwijk, F. W., Ströhl, F., Cioni, J.-M. et al. (2019). On-site ribosome remodeling by locally synthesized ribosomal proteins in axons. *Cell Rep.* **29**, 3605-3619.e10. doi:10.1016/j.celrep.2019.11.025

Si, K., Giustetto, M., Etkin, A., Hsu, R., Janisiewicz, A. M., Miniaci, M. C., Kim, J. H., Zhu, H. and Kandel, E. R. (2003). A neuronal isoform of CPEB regulates local protein synthesis and stabilizes synapse-specific long-term facilitation in aplysia. *Cell* **115**, 893-904. doi:10.1016/S0092-8674(03)01021-3

Stogsdill, J. A. and Eroglu, C. (2017). The interplay between neurons and glia in synapse development and plasticity. *Curr. Opin. Neurobiol.* **42**, 1-8. doi:10.1016/j.conb.2016.09.016

Takeuchi, A., Takahashi, Y., Iida, K., Hosokawa, M., Irie, K., Ito, M., Brown, J. B., Ohno, K., Nakashima, K. and Hagiwara, M. (2020). Identification of Qk as a Glial Precursor cell marker that governs the fate specification of neural stem cells to a glial cell lineage. *Stem Cell Rep.* **15**, 883-897. doi:10.1016/j.stemcr.2020.08.010

Thomsen, R., Pallesen, J., Daugaard, T. F., Borglum, A. D. and Nielsen, A. L. (2013a). Genome wide assessment of mRNA in astrocyte protrusions by direct RNA sequencing reveals mRNA localization for the intermediate filament protein nestin. *Glia* **61**, 1922-1937. doi:10.1002/glia.22569

Thomsen, R., Daugaard, T. F., Holm, I. E. and Nielsen, A. L. (2013b). Alternative mRNA splicing from the glial fibrillary acidic protein (GFAP) gene generates isoforms with distinct subcellular mRNA localization patterns in astrocytes. *PLoS ONE* **8**, e72110. doi:10.1371/journal.pone.0072110

Ventura, R. and Harris, K. M. (1999). Three-dimensional relationships between hippocampal synapses and astrocytes. *J. Neurosci.* **19**, 6897-6906. doi:10.1523/JNEUROSCI.19-16-06897.1999

Walker, C. A., Randolph, L. K., Matute, C., Alberdi, E., Baleriola, J. and Hengst, U. (2018). Abeta1-42 triggers the generation of a retrograde signaling complex from sentinel mRNAs in axons. *EMBO Rep.* **19**, e45435. doi:10.15252/embr.201745435

Wang, Y., Lacroix, G., Haines, J., Doukhanine, E., Almazan, G. and Richard, S. (2010). The QKI-6 RNA binding protein localizes with the MBP mRNAs in stress granules of glial cells. *PLoS ONE* **5**, e12824. doi:10.1371/journal.pone.0012824

Wang, M. X., Ray, L., Tanaka, K. F., Lliff, J. J. and Heys, J. (2020). Varying perivascular astroglial endfoot dimensions along the vascular tree maintain perivascular-interstitial flux through the cortical mantle. *Glia* **69**, 3715-3728. doi:10.1002/glia.23923

Wenzel, H. J., Murray, K. D., Haify, S. N., Hunsaker, M. R., Schwartzer, J. J., Kim, K., La Spada, A. R., Sopher, B. L., Hagerman, P. J., Raske, C. et al. (2019). Astroglial-targeted expression of the fragile X CGG repeat premutation in mice yields RAN translation, motor deficits and possible evidence for cell-to-cell propagation of FXTAS pathology. *Acta Neuropathol. Commun.* **7**, 27. doi:10.1186/s40478-019-0677-7

Westmark, P. R., Westmark, C. J., Jeevananthan, A. and Malter, J. S. (2011). Preparation of synaptoneurosomes from mouse cortex using a discontinuous percoll-sucrose density gradient. *J. Vis. Exp.* **55**, 3196. doi:10.3791/3196

Wu, K. Y., Hengst, U., Cox, L. J., Macosko, E. Z., Jeromin, A., Urquhart, E. R. and Jaffrey, S. R. (2005). Local translation of RhoA regulates growth cone collapse. *Nature* **436**, 1020-1024. doi:10.1038/nature03885

Yao, J., Sasaki, Y., Wen, Z., Bassell, G. J. and Zheng, J. Q. (2006). An essential role for beta-actin mRNA localization and translation in Ca^{2+}-dependent growth cone guidance. *Nat. Neurosci.* **9**, 1265-1273. doi:10.1038/nn1773

Zhang, H. L., Pan, F., Hong, D., Shenoy, S. M., Singer, R. H. and Bassell, G. J. (2003). Active transport of the survival motor neuron protein and the role of exon-7 in cytoplasmic localization. *J. Neurosci.* **23**, 6627-6637. doi:10.1523/JNEUROSCI.23-16-06627.2003

Zhang, Y., Chen, K., Sloan, S. A., Bennett, M. L., Scholze, A. R., O'Keeffe, S., Phatnani, H. P., Guarnieri, P., Caneda, C., Ruderisch, N. et al. (2014). An RNA-sequencing transcriptome and splicing database of glia, neurons, and vascular cells of the cerebral cortex. *J. Neurosci.* **34**, 11929-11947. doi:10.1523/JNEUROSCI.1860-14.2014

Bibliography

Aakalu, G., Smith, W.B., Nguyen, N., Jiang, C., and Schuman, E.M. (2001). Dynamic Visualization of Local Protein Synthesis in Hippocampal Neurons. Neuron *30*, 489–502. https://doi.org/10.1016/S0896-6273(01)00295-1.

Abelaira, H.M., Réus, G.Z., and Quevedo, J. (2013). Animal models as tools to study the pathophysiology of depression. Braz. J. Psychiatry *35*, S112–S120. https://doi.org/10.1590/1516-4446-2013-1098.

Adams, D.R., Ron, D., and Kiely, P.A. (2011). RACK1, A multifaceted scaffolding protein: Structure and function. Cell Communication and Signaling *9*, 22. https://doi.org/10.1186/1478-811X-9-22.

Agrawal, M., and Welshhans, K. (2021). Local Translation Across Neural Development: A Focus on Radial Glial Cells, Axons, and Synaptogenesis. Frontiers in Molecular Neuroscience *14*, 164. https://doi.org/10.3389/fnmol.2021.717170.

Agulhon, C., Sun, M.-Y., Murphy, T., Myers, T., Lauderdale, K., and Fiacco, T. (2012). Calcium Signaling and Gliotransmission in Normal vs. Reactive Astrocytes. Frontiers in Pharmacology *3*. .

Ainsley, J.A., Drane, L., Jacobs, J., Kittelberger, K.A., and Reijmers, L.G. (2014). Functionally diverse dendritic mRNAs rapidly associate with ribosomes following a novel experience. Nat Commun *5*, 4510. https://doi.org/10.1038/ncomms5510.

Allen, N.J., and Barres, B.A. (2009). Glia — more than just brain glue. Nature *457*, 675–677. https://doi.org/10.1038/457675a.

Alvarez-Castelao, B., Schanzenbächer, C.T., Hanus, C., Glock, C., tom Dieck, S., Dörrbaum, A.R., Bartnik, I., Nassim-Assir, B., Ciirdaeva, E., Mueller, A., et al. (2017). Cell-type-specific metabolic labeling of nascent proteomes in vivo. Nat Biotechnol *35*, 1196–1201. https://doi.org/10.1038/nbt.4016.

An, J.J., Gharami, K., Liao, G.-Y., Woo, N.H., Lau, A.G., Vanevski, F., Torre, E.R., Jones, K.R., Feng, Y., Lu, B., et al. (2008). Distinct Role of Long 3′UTR BDNF mRNA in Spine Morphology and Synaptic Plasticity in Hippocampal Neurons. Cell *134*, 175–187. https://doi.org/10.1016/j.cell.2008.05.045.

Andreassi, C., and Riccio, A. (2009). To localize or not to localize: mRNA fate is in 3′UTR ends. Trends in Cell Biology *19*, 465–474. https://doi.org/10.1016/j.tcb.2009.06.001.

Angenstein, F., Evans, A.M., Settlage, R.E., Moran, S.T., Ling, S.-C., Klintsova, A.Y., Shabanowitz, J., Hunt, D.F., and Greenough, W.T. (2002). A Receptor for Activated C Kinase Is Part of Messenger Ribonucleoprotein Complexes Associated with PolyA-mRNAs in Neurons. J. Neurosci. *22*, 8827–8837. https://doi.org/10.1523/JNEUROSCI.22-20-08827.2002.

Anlauf, E., and Derouiche, A. (2013). Glutamine Synthetase as an Astrocytic Marker: Its Cell Type and Vesicle Localization. Front Endocrinol (Lausanne) *4*, 144. https://doi.org/10.3389/fendo.2013.00144.

Araque, A., Carmignoto, G., Haydon, P.G., Oliet, S.H.R., Robitaille, R., and Volterra, A. (2014). Gliotransmitters Travel in Time and Space. Neuron *81*, 728–739. https://doi.org/10.1016/j.neuron.2014.02.007.

Arora, A., Goering, R., Lo, H.Y.G., Lo, J., Moffatt, C., and Taliaferro, J.M. (2022). The Role of Alternative Polyadenylation in the Regulation of Subcellular RNA Localization. Frontiers in Genetics *12*. .

Ashique, A.M., Kharazia, V., Yaka, R., Phamluong, K., Peterson, A.S., and Ron, D. (2006). Localization of the scaffolding protein RACK1 in the developing and adult mouse brain. Brain Research *1069*, 31–38. https://doi.org/10.1016/j.brainres.2005.11.018.

Bae, J.A., Bae, W.K., Kim, S.J., Ko, Y.-S., Kim, K.Y., Park, S.-Y., Yu, Y.H., Kim, E.A., Chung, I.J., Kim, H., et al. (2021). A new KSRP-binding compound suppresses distant metastasis of colorectal cancer by targeting the oncogenic KITENIN complex. Molecular Cancer *20*, 78. https://doi.org/10.1186/s12943-021-01368-w.

Bak, L.K., and Walls, A.B. (2018). CrossTalk opposing view: lack of evidence supporting an astrocyte-to-neuron lactate shuttle coupling neuronal activity to glucose utilisation in the brain. J Physiol *596*, 351–353. https://doi.org/10.1113/JP274945.

Baleriola, J., Walker, C.A., Jean, Y.Y., Crary, J.F., Troy, C.M., Nagy, P.L., and Hengst, U. (2014). Axonally synthesized ATF4 transmits a neurodegenerative signal across brain regions. Cell *158*, 1159–1172. https://doi.org/10.1016/j.cell.2014.07.001.

Ban, N., Beckmann, R., Cate, J.H., Dinman, J.D., Dragon, F., Ellis, S.R., Lafontaine, D.L., Lindahl, L., Liljas, A., Lipton, J.M., et al. (2014). A new system for naming ribosomal proteins. Curr Opin Struct Biol *24*, 165–169. https://doi.org/10.1016/j.sbi.2014.01.002.

von Bartheld, C.S., Bahney, J., and Herculano-Houzel, S. (2016). The Search for True Numbers of Neurons and Glial Cells in the Human Brain: A Review of 150 Years of Cell Counting. J Comp Neurol *524*, 3865–3895. https://doi.org/10.1002/cne.24040.

Barton, S.K., Gregory, J.M., Chandran, S., and Turner, B.J. (2019). Could an Impairment in Local Translation of mRNAs in Glia be Contributing to Pathogenesis in ALS? Front. Mol. Neurosci. *12*, 124. https://doi.org/10.3389/fnmol.2019.00124.

Batiuk, M.Y., Martirosyan, A., Wahis, J., de Vin, F., Marneffe, C., Kusserow, C., Koeppen, J., Viana, J.F., Oliveira, J.F., Voet, T., et al. (2020). Identification of region-specific astrocyte subtypes at single cell resolution. Nat Commun *11*. https://doi.org/10.1038/s41467-019-14198-8.

Bélanger, M., Allaman, I., and Magistretti, P.J. (2011). Brain Energy Metabolism: Focus on Astrocyte-Neuron Metabolic Cooperation. Cell Metabolism *14*, 724–738. https://doi.org/10.1016/j.cmet.2011.08.016.

Bernardinelli, Y., Randall, J., Janett, E., Nikonenko, I., König, S., Jones, E.V., Flores, C.E., Murai, K.K., Bochet, C.G., Holtmaat, A., et al. (2014a). Activity-Dependent Structural Plasticity of Perisynaptic Astrocytic Domains Promotes Excitatory Synapse Stability. Current Biology *24*, 1679–1688. https://doi.org/10.1016/j.cub.2014.06.025.

Bernardinelli, Y., Muller, D., and Nikonenko, I. (2014b). Astrocyte-Synapse Structural Plasticity. Neural Plast *2014*, 232105. https://doi.org/10.1155/2014/232105.

Besson, A., Wilson, T.L., and Yong, V.W. (2002). The Anchoring Protein RACK1 Links Protein Kinase Cε to Integrin β Chains: REQUIREMENT FOR ADHESION AND MOTILITY*. Journal of Biological Chemistry *277*, 22073–22084. https://doi.org/10.1074/jbc.M111644200.

Béthune, J., Jansen, R.-P., Feldbrügge, M., and Zarnack, K. (2019). Membrane-Associated RNA-Binding Proteins Orchestrate Organelle-Coupled Translation. Trends in Cell Biology *29*, 178–188. https://doi.org/10.1016/j.tcb.2018.10.005.

van Beuningen, S.F.B., Will, L., Harterink, M., Chazeau, A., van Battum, E.Y., Frias, C.P., Franker, M.A.M., Katrukha, E.A., Stucchi, R., Vocking, K., et al. (2015). TRIM46 Controls Neuronal Polarity and Axon Specification by Driving the Formation of Parallel Microtubule Arrays. Neuron *88*, 1208–1226. https://doi.org/10.1016/j.neuron.2015.11.012.

Biever, A., Glock, C., Tushev, G., Ciirdaeva, E., Dalmay, T., Langer, J.D., and Schuman, E.M. (2020). Monosomes actively translate synaptic mRNAs in neuronal processes. Science *367*, eaay4991. https://doi.org/10.1126/science.aay4991.

Bisht, K., Okojie, K.A., Sharma, K., Lentferink, D.H., Sun, Y.-Y., Chen, H.-R., Uweru, J.O., Amancherla, S., Calcuttawala, Z., Campos-Salazar, A.B., et al. (2021). Capillary-associated microglia regulate vascular structure and function through PANX1-P2RY12 coupling in mice. Nat Commun *12*, 5289. https://doi.org/10.1038/s41467-021-25590-8.

Blagden, S., Schneider, C., and Fischer, U. (2016). Loss of LARP4B , an early event in the tumorigenesis of brain cancer? Translational Cancer Research *5*. https://doi.org/10.21037/10581.

Bohlen, J., Roiuk, M., and Teleman, A.A. (2021). Phosphorylation of ribosomal protein S6 differentially affects mRNA translation based on ORF length. Nucleic Acids Research *49*, 13062–13074. https://doi.org/10.1093/nar/gkab1157.

Bolger, G.B. (2017). The RNA-binding protein SERBP1 interacts selectively with the signaling protein RACK1. Cellular Signalling *35*, 256–263. https://doi.org/10.1016/j.cellsig.2017.03.001.

Bonvento, G., Herard, A.-S., and Voutsinos-Porche, B. (2005). The Astrocyte—Neuron Lactate Shuttle: A Debated but still Valuable Hypothesis for Brain Imaging. J Cereb Blood Flow Metab *25*, 1394–1399. https://doi.org/10.1038/sj.jcbfm.9600127.

Boulay, A.-C., Mazeraud, A., Cisternino, S., Saubaméa, B., Mailly, P., Jourdren, L., Blugeon, C., Mignon, V., Smirnova, M., Cavallo, A., et al. (2015a). Immune quiescence of the brain is set by astroglial connexin 43. J. Neurosci. *35*, 4427–4439. https://doi.org/10.1523/JNEUROSCI.2575-14.2015.

Boulay, A.-C., Saubaméa, B., Declèves, X., and Cohen-Salmon, M. (2015b). Purification of Mouse Brain Vessels. JoVE 53208. https://doi.org/10.3791/53208.

Boulay, A.-C., Saubaméa, B., Adam, N., Chasseigneaux, S., Mazaré, N., Gilbert, A., Bahin, M., Bastianelli, L., Blugeon, C., Perrin, S., et al. (2017). Translation in astrocyte distal processes sets molecular heterogeneity at the gliovascular interface. Cell Discov *3*, 17005. https://doi.org/10.1038/celldisc.2017.5.

Browning, K.S., and Bailey-Serres, J. (2015). Mechanism of Cytoplasmic mRNA Translation. Arbo.j *2015*. https://doi.org/10.1199/tab.0176.

Brugier, A., Hafirrassou, M.L., Pourcelot, M., Baldaccini, M., Kril, V., Couture, L., Kümmerer, B.M., Gallois-Montbrun, S., Bonnet-Madin, L., Vidalain, P.-O., et al. (2022). RACK1 Associates with RNA-Binding Proteins Vigilin and SERBP1 to Facilitate Dengue Virus Replication. Journal of Virology *96*, e01962-21. https://doi.org/10.1128/jvi.01962-21.

Buensuceso, C.S., Woodside, D., Huff, J.L., Plopper, G.E., and O'Toole, T.E. (2001). The WD protein Rack1 mediates protein kinase C and integrin-dependent cell migration. Journal of Cell Science *114*, 1691–1698. https://doi.org/10.1242/jcs.114.9.1691.

Buoso, E., Ronfani, M., Galasso, M., Ventura, D., Corsini, E., and Racchi, M. (2019). Cortisol-induced SRSF3 expression promotes GR splicing, RACK1 expression and breast cancer cells migration. Pharmacological Research *143*, 17–26. https://doi.org/10.1016/j.phrs.2019.03.008.

Buoso, E., Masi, M., Long, A., Chiappini, C., Travelli, C., Govoni, S., and Racchi, M. (2020). Ribosomes as a nexus between translation and cancer progression: Focus on ribosomal Receptor for Activated C Kinase 1 (RACK1) in breast cancer. British Journal of Pharmacology *n/a*. https://doi.org/10.1111/bph.15218.

Bushong, E.A., Martone, M.E., Jones, Y.Z., and Ellisman, M.H. (2002). Protoplasmic Astrocytes in CA1 Stratum Radiatum Occupy Separate Anatomical Domains. J Neurosci *22*, 183–192. https://doi.org/10.1523/JNEUROSCI.22-01-00183.2002.

Buxbaum, A.R., Haimovich, G., and Singer, R.H. (2015). In the right place at the right time: visualizing and understanding mRNA localization. Nat Rev Mol Cell Biol *16*, 95–109. https://doi.org/10.1038/nrm3918.

Cagnetta, R., Frese, C.K., Shigeoka, T., Krijgsveld, J., and Holt, C.E. (2018). Rapid Cue-Specific Remodeling of the Nascent Axonal Proteome. Neuron *99*, 29-46.e4. https://doi.org/10.1016/j.neuron.2018.06.004.

Cajigas, I.J., Tushev, G., Will, T.J., tom Dieck, S., Fuerst, N., and Schuman, E.M. (2012). The Local Transcriptome in the Synaptic Neuropil Revealed by Deep Sequencing and High-Resolution Imaging. Neuron *74*, 453–466. https://doi.org/10.1016/j.neuron.2012.02.036.

Campagne, C., Reyes-Gomez, E., Picco, M.E., Loiodice, S., Salaun, P., Ezagal, J., Bernex, F., Commère, P.H., Pons, S., Esquerre, D., et al. (2017). RACK1 cooperates with NRAS Q61K to promote melanoma in vivo. Cellular Signalling *36*, 255–266. https://doi.org/10.1016/j.cellsig.2017.03.015.

Campbell, D.S., and Holt, C.E. (2001). Chemotropic responses of retinal growth cones mediated by rapid local protein synthesis and degradation. Neuron *32*, 1013–1026. https://doi.org/10.1016/s0896-6273(01)00551-7.

Campbell, S., and MacQueen, G. (2004). The role of the hippocampus in the pathophysiology of major depression. J Psychiatry Neurosci *29*, 417–426. .

Campbell, D.S., Regan, A.G., Lopez, J.S., Tannahill, D., Harris, W.A., and Holt, C.E. (2001). Semaphorin 3A Elicits Stage-Dependent Collapse, Turning, and Branching in Xenopus Retinal Growth Cones. J Neurosci *21*, 8538–8547. https://doi.org/10.1523/JNEUROSCI.21-21-08538.2001.

Canclini, L., Cal, K., Bardier, C., Ruiz, P., Mercer, J.A., and Calliari, A. (2020). Calcium triggers the dissociation of myosin-Va from ribosomes in ribonucleoprotein complexes. FEBS Letters *594*, 2311–2321. https://doi.org/10.1002/1873-3468.13813.

do Canto, A.M., Vieira, A.S., H B Matos, A., Carvalho, B.S., Henning, B., Norwood, B.A., Bauer, S., Rosenow, F., Gilioli, R., Cendes, F., et al. (2020). Laser microdissection-based microproteomics of the hippocampus of a rat epilepsy model reveals regional differences in protein abundances. Sci Rep *10*, 4412. https://doi.org/10.1038/s41598-020-61401-8.

Cao, J., Zhao, M., Liu, J., Zhang, X., Pei, Y., Wang, J., Yang, X., Shen, B., and Zhang, J. (2019). RACK1 Promotes Self-Renewal and Chemoresistance of Cancer Stem Cells in Human Hepatocellular Carcinoma through Stabilizing Nanog. Theranostics *9*, 811–828. https://doi.org/10.7150/thno.29271.

Cauli, B., and Hamel, E. (2010). Revisiting the Role of Neurons in Neurovascular Coupling. Front Neuroenergetics *2*, 9. https://doi.org/10.3389/fnene.2010.00009.

Ceci, M., Gaviraghi, C., Gorrini, C., Sala, L.A., Offenhäuser, N., Carlo Marchisio, P., and Biffo, S. (2003). Release of eIF6 (p27BBP) from the 60S subunit allows 80S ribosome assembly. Nature *426*, 579–584. https://doi.org/10.1038/nature02160.

Ceci, M., Welshhans, K., Ciotti, M.T., Brandi, R., Parisi, C., Paoletti, F., Pistillo, L., Bassell, G.J., and Cattaneo, A. (2012). RACK1 Is a Ribosome Scaffold Protein for β-actin mRNA/ZBP1 Complex. PLoS ONE *7*, e35034. https://doi.org/10.1371/journal.pone.0035034.

Cerezo, E., Plisson-Chastang, C., Henras, A.K., Lebaron, S., Gleizes, P.-E., O'Donohue, M.-F., Romeo, Y., and Henry, Y. (2019). Maturation of pre-40S particles in yeast and humans. WIREs RNA *10*, e1516. https://doi.org/10.1002/wrna.1516.

Chen, T., Wang, F., Wei, S., Nie, Y., Zheng, X., Deng, Y., Zhu, X., Deng, Y., Zhong, N., and Zhou, C. (2021). FGFR/RACK1 interacts with MDM2, promotes P53 degradation, and inhibits cell senescence in lung squamous cell carcinoma. Cancer Biology & Medicine *18*, 1–10. .

Chever, O., Dossi, E., Pannasch, U., Derangeon, M., and Rouach, N. (2016). Astroglial networks promote neuronal coordination. Science Signaling https://doi.org/10.1126/scisignal.aad3066.

Choudhuri, A., Maitra, U., and Evans, T. (2013). Translation initiation factor eIF3h targets specific transcripts to polysomes during embryogenesis. Proceedings of the National Academy of Sciences *110*, 9818–9823. https://doi.org/10.1073/pnas.1302934110.

Cioni, J.-M., Lin, J.Q., Holtermann, A.V., Koppers, M., Jakobs, M.A.H., Azizi, A., Turner-Bridger, B., Shigeoka, T., Franze, K., Harris, W.A., et al. (2019). Late Endosomes Act as mRNA Translation Platforms and Sustain Mitochondria in Axons. Cell *176*, 56-72.e15. https://doi.org/10.1016/j.cell.2018.11.030.

Clasadonte, J., and Haydon, P.G. (2014). Connexin 30 controls the extension of astrocytic processes into the synaptic cleft through an unconventional non-channel function. 4. .

Clavreul, S., Abdeladim, L., Hernández-Garzón, E., Niculescu, D., Durand, J., Ieng, S.-H., Barry, R., Bonvento, G., Beaurepaire, E., Livet, J., et al. (2019). Cortical astrocytes develop in a plastic manner at both clonal and cellular levels. Nat Commun *10*, 4884. https://doi.org/10.1038/s41467-019-12791-5.

Cohen-Salmon, M., Slaoui, L., Mazaré, N., Gilbert, A., Oudart, M., Alvear-Perez, R., Elorza-Vidal, X., Chever, O., and Boulay, A.-C. (2020). Astrocytes in the regulation of cerebrovascular functions. Glia https://doi.org/10.1002/glia.23924.

Connors, N.C., and Kofuji, P. (2006). Potassium channel Kir4.1 macromolecular complex in retinal glial cells. Glia *53*, 124–131. https://doi.org/10.1002/glia.20271.

Cooke, A., Schwarzl, T., Huppertz, I., Kramer, G., Mantas, P., Alleaume, A.-M., Huber, W., Krijgsveld, J., and Hentze, M.W. (2019). The RNA-Binding Protein YBX3 Controls Amino Acid

Levels by Regulating SLC mRNA Abundance. Cell Reports *27*, 3097-3106.e5. https://doi.org/10.1016/j.celrep.2019.05.039.

Cornell-Bell, A.H., Finkbeiner, S.M., Cooper, M.S., and Smith, S.J. (1990). Glutamate Induces Calcium Waves in Cultured Astrocytes: Long-Range Glial Signaling. Science *247*, 470–473. https://doi.org/10.1126/science.1967852.

Coyle, S.M., Gilbert, W.V., and Doudna, J.A. (2009). Direct Link between RACK1 Function and Localization at the Ribosome In Vivo. Molecular and Cellular Biology *29*, 1626–1634. https://doi.org/10.1128/MCB.01718-08.

Cui, Y., Yang, Y., Ni, Z., Dong, Y., Cai, G., Foncelle, A., Ma, S., Sang, K., Tang, S., Li, Y., et al. (2018). Astroglial Kir4.1 in the lateral habenula drives neuronal bursts in depression. Nature *554*, 323–327. https://doi.org/10.1038/nature25752.

Dahlberg, J.E. (2003). Nuclear translation: What is the evidence? RNA *9*, 1–8. https://doi.org/10.1261/rna.2121703.

Darnell, J.C., Van Driesche, S.J., Zhang, C., Hung, K.Y.S., Mele, A., Fraser, C.E., Stone, E.F., Chen, C., Fak, J.J., Chi, S.W., et al. (2011). FMRP Stalls Ribosomal Translocation on mRNAs Linked to Synaptic Function and Autism. Cell *146*, 247–261. https://doi.org/10.1016/j.cell.2011.06.013.

Das, S., Vera, M., Gandin, V., Singer, R.H., and Tutucci, E. (2021). Intracellular mRNA transport and localized translation. Nature Reviews Molecular Cell Biology 1–22. https://doi.org/10.1038/s41580-021-00356-8.

Dastidar, S.G., and Nair, D. (2022). A Ribosomal Perspective on Neuronal Local Protein Synthesis. Front Mol Neurosci *15*, 823135. https://doi.org/10.3389/fnmol.2022.823135.

David, A., Dolan, B.P., Hickman, H.D., Knowlton, J.J., Clavarino, G., Pierre, P., Bennink, J.R., and Yewdell, J.W. (2012). Nuclear translation visualized by ribosome-bound nascent chain puromycylation. The Journal of Cell Biology *197*, 45–57. https://doi.org/10.1083/jcb.201112145.

Davidovic, L., Jaglin, X.H., Lepagnol-Bestel, A.-M., Tremblay, S., Simonneau, M., Bardoni, B., and Khandjian, E.W. (2007). The fragile X mental retardation protein is a molecular adaptor between the neurospecific KIF3C kinesin and dendritic RNA granules. Human Molecular Genetics *16*, 3047–3058. https://doi.org/10.1093/hmg/ddm263.

De Conti, L., Baralle, M., and Buratti, E. (2017). Neurodegeneration and RNA-binding proteins. WIREs RNA *8*, e1394. https://doi.org/10.1002/wrna.1394.

Del Bigio, M.R. (2010). Ependymal cells: biology and pathology. Acta Neuropathol *119*, 55–73. https://doi.org/10.1007/s00401-009-0624-y.

Della Vecchia, S., Marchese, M., Santorelli, F.M., and Sicca, F. (2021). Kir4.1 Dysfunction in the Pathophysiology of Depression: A Systematic Review. Cells *10*, 2628. https://doi.org/10.3390/cells10102628.

Derouiche, A., and Geiger, K.D. (2019). Perspectives for Ezrin and Radixin in Astrocytes: Kinases, Functions and Pathology. IJMS *20*, 3776. https://doi.org/10.3390/ijms20153776.

Di Prisco, G.V., Huang, W., Buffington, S.A., Hsu, C.-C., Bonnen, P.E., Placzek, A.N., Sidrauski, C., Krnjević, K., Kaufman, R.J., Walter, P., et al. (2014). Translational control of mGluR-dependent

long-term depression and object-place learning by eIF2α. Nat Neurosci *17*, 1073–1082. https://doi.org/10.1038/nn.3754.

Dictenberg, J.B., Swanger, S.A., Antar, L.N., Singer, R.H., and Bassell, G.J. (2008). A Direct Role for FMRP in Activity-Dependent Dendritic mRNA Transport Links Filopodial-Spine Morphogenesis to Fragile X Syndrome. Developmental Cell *14*, 926–939. https://doi.org/10.1016/j.devcel.2008.04.003.

Djukic, B., Casper, K.B., Philpot, B.D., Chin, L.-S., and McCarthy, K.D. (2007). Conditional Knock-Out of Kir4.1 Leads to Glial Membrane Depolarization, Inhibition of Potassium and Glutamate Uptake, and Enhanced Short-Term Synaptic Potentiation. J Neurosci *27*, 11354–11365. https://doi.org/10.1523/JNEUROSCI.0723-07.2007.

Dong, Z.-F., Tang, L.-J., Deng, G.-F., Zeng, T., Liu, S.-J., Wan, R.-P., Liu, T., Zhao, Q.-H., Yi, Y.-H., Liao, W.-P., et al. (2014). Transcription of the Human Sodium Channel SCN1A Gene Is Repressed by a Scaffolding Protein RACK1. Mol Neurobiol *50*, 438–448. https://doi.org/10.1007/s12035-014-8633-9.

Donlin-Asp, P.G., Polisseni, C., Klimek, R., Heckel, A., and Schuman, E.M. (2021). Differential regulation of local mRNA dynamics and translation following long-term potentiation and depression. PNAS *118*. https://doi.org/10.1073/pnas.2017578118.

Dwane, S., Durack, E., O'Connor, R., and Kiely, P.A. (2014). RACK1 promotes neurite outgrowth by scaffolding AGAP2 to FAK. Cellular Signalling *26*, 9–18. https://doi.org/10.1016/j.cellsig.2013.08.036.

Einhorn, E. (2013). The scaffolding protein RACK1: multiple roles in human cancer. 9. .

El Fatimy, R., Tremblay, S., Dury, A.Y., Solomon, S., De Koninck, P., Schrader, J.W., and Khandjian, E.W. (2012). Fragile Mental Retardation Protein Interacts with the RNA-Binding Protein Caprin1 in Neuronal RiboNucleoProtein Complexes. PLoS ONE *7*, e39338. https://doi.org/10.1371/journal.pone.0039338.

Emmott, E., Jovanovic, M., and Slavov, N. (2019). Ribosome Stoichiometry: From Form to Function. Trends in Biochemical Sciences *44*, 95–109. https://doi.org/10.1016/j.tibs.2018.10.009.

Escartin, C., Galea, E., Lakatos, A., O'Callaghan, J.P., Petzold, G.C., Serrano-Pozo, A., Steinhäuser, C., Volterra, A., Carmignoto, G., Agarwal, A., et al. (2021). Reactive astrocyte nomenclature, definitions, and future directions. Nature Neuroscience 1–14. https://doi.org/10.1038/s41593-020-00783-4.

Fusco, C.M., Desch, K., Dörrbaum, A.R., Wang, M., Staab, A., Chan, I.C.W., Vail, E., Villeri, V., Langer, J.D., and Schuman, E.M. (2021). Neuronal ribosomes exhibit dynamic and context-dependent exchange of ribosomal proteins. Nat Commun *12*, 6127. https://doi.org/10.1038/s41467-021-26365-x.

Gallo, S., and Manfrini, N. (2015). Working hard at the nexus between cell signaling and the ribosomal machinery: An insight into the roles of RACK1 in translational regulation. Translation *3*, e1120382. https://doi.org/10.1080/21690731.2015.1120382.

Gallo, S., Ricciardi, S., Manfrini, N., Pesce, E., Oliveto, S., Calamita, P., Mancino, M., Maffioli, E., Moro, M., Crosti, M., et al. (2018). RACK1 Specifically Regulates Translation through Its Binding to Ribosomes. Mol Cell Biol *38*, e00230-18, /mcb/38/23/e00230-18.atom. https://doi.org/10.1128/MCB.00230-18.

Gamarra, M., Blanco-Urrejola, M., Batista, A.F.R., Imaz, J., and Baleriola, J. (2020). Object-Based Analyses in FIJI/ImageJ to Measure Local RNA Translation Sites in Neurites in Response to Aβ1-42 Oligomers. Front Neurosci *14*, 547. https://doi.org/10.3389/fnins.2020.00547.

Gamarra, M., de la Cruz, A., Blanco-Urrejola, M., and Baleriola, J. (2021). Local Translation in Nervous System Pathologies. Front Integr Neurosci *15*, 689208. https://doi.org/10.3389/fnint.2021.689208.

Gandin, V., Gutierrez, G.J., Brill, L.M., Varsano, T., Feng, Y., Aza-Blanc, P., Au, Q., McLaughlan, S., Ferreira, T.A., Alain, T., et al. (2013). Degradation of Newly Synthesized Polypeptides by Ribosome-Associated RACK1/c-Jun N-Terminal Kinase/Eukaryotic Elongation Factor 1A2 Complex. Mol Cell Biol *33*, 2510–2526. https://doi.org/10.1128/MCB.01362-12.

Gandini, M.A., Souza, I.A., Khullar, A., Gambeta, E., and Zamponi, G.W. (2021). Regulation of CaV3.2 channels by the receptor for activated C kinase 1 (Rack-1). Pflugers Arch - Eur J Physiol https://doi.org/10.1007/s00424-021-02631-1.

Garner, C.C., Tucker, R.P., and Matus, A. (1988). Selective localization of messenger RNA for cytoskeletal protein MAP2 in dendrites. Nature *336*, 674–677. https://doi.org/10.1038/336674a0.

Gerbasi, V.R., Weaver, C.M., Hill, S., Friedman, D.B., and Link, A.J. (2004). Yeast Asc1p and Mammalian RACK1 Are Functionally Orthologous Core 40S Ribosomal Proteins That Repress Gene Expression. Mol Cell Biol *24*, 8276–8287. https://doi.org/10.1128/MCB.24.18.8276-8287.2004.

Gerstner, J.R., Vanderheyden, W.M., LaVaute, T., Westmark, C.J., Rouhana, L., Pack, A.I., Wickens, M., and Landry, C.F. (2012). Time of day regulates subcellular trafficking, tripartite synaptic localization, and polyadenylation of the astrocytic Fabp7 mRNA. J. Neurosci. *32*, 1383–1394. https://doi.org/10.1523/JNEUROSCI.3228-11.2012.

Giaume, C., Koulakoff, A., Roux, L., Holcman, D., and Rouach, N. (2010). Astroglial networks: a step further in neuroglial and gliovascular interactions. Nat Rev Neurosci *11*, 87–99. https://doi.org/10.1038/nrn2757.

Gilbert, A., Elorza-Vidal, X., Rancillac, A., Chagnot, A., Yetim, M., Hingot, V., Deffieux, T., Boulay, A.-C., Alvear-Perez, R., Cisternino, S., et al. (2021). Megalencephalic leukoencephalopathy with subcortical cysts is a developmental disorder of the gliovascular unit. 2021.05.17.444434. .

Giuditta, A., Dettbarn, W.D., and Brzin, M. (1968). Protein synthesis in the isolated giant axon of the squid. Proc Natl Acad Sci U S A *59*, 1284–1287. https://doi.org/10.1073/pnas.59.4.1284.

Goetze, B., Tuebing, F., Xie, Y., Dorostkar, M.M., Thomas, S., Pehl, U., Boehm, S., Macchi, P., and Kiebler, M.A. (2006). The brain-specific double-stranded RNA-binding protein Staufen2 is required for dendritic spine morphogenesis. J Cell Biol *172*, 221–231. https://doi.org/10.1083/jcb.200509035.

González, C., Cornejo, V.H., and Couve, A. (2018). Golgi bypass for local delivery of axonal proteins, fact or fiction? Current Opinion in Cell Biology *53*, 9–14. https://doi.org/10.1016/j.ceb.2018.03.010.

Griemsmann, S., Höft, S.P., Bedner, P., Zhang, J., von Staden, E., Beinhauer, A., Degen, J., Dublin, P., Cope, D.W., Richter, N., et al. (2015). Characterization of Panglial Gap Junction Networks in the Thalamus, Neocortex, and Hippocampus Reveals a Unique Population of Glial Cells. Cereb Cortex *25*, 3420–3433. https://doi.org/10.1093/cercor/bhu157.

Gu, W., Deng, Y., Zenklusen, D., and Singer, R.H. (2004). A new yeast PUF family protein, Puf6p, represses ASH1 mRNA translation and is required for its localization. Genes & Development *18*, 1452. https://doi.org/10.1101/gad.1189004.

Guerra-Gomes, S., Sousa, N., Pinto, L., and Oliveira, J.F. (2018). Functional Roles of Astrocyte Calcium Elevations: From Synapses to Behavior. Frontiers in Cellular Neuroscience *11*. .

Hafner, A.-S., Donlin-Asp, P.G., Leitch, B., Herzog, E., and Schuman, E.M. (2019). Local protein synthesis is a ubiquitous feature of neuronal pre- and postsynaptic compartments. Science *364*, eaau3644. https://doi.org/10.1126/science.aau3644.

Hale, C.R., Sawicka, K., Mora, K., Fak, J.J., Kang, J.J., Cutrim, P., Cialowicz, K., Carroll, T.S., and Darnell, R.B. (2021). FMRP regulates mRNAs encoding distinct functions in the cell body and dendrites of CA1 pyramidal neurons. Elife *10*, e71892. https://doi.org/10.7554/eLife.71892.

Han, Y., Yu, H., Sun, M., Wang, Y., Xi, W., and Yu, Y. (2014). Astrocyte-restricted disruption of connexin-43 impairs neuronal plasticity in mouse barrel cortex. European Journal of Neuroscience *39*, 35–45. https://doi.org/10.1111/ejn.12394.

Hanus, C., Geptin, H., Tushev, G., Garg, S., Alvarez-Castelao, B., Sambandan, S., Kochen, L., Hafner, A.-S., Langer, J.D., and Schuman, E.M. (2016). Unconventional secretory processing diversifies neuronal ion channel properties. ELife *5*, e20609. https://doi.org/10.7554/eLife.20609.

Harbauer, A.B., Hees, J.T., Wanderoy, S., Segura, I., Gibbs, W., Cheng, Y., Ordonez, M., Cai, Z., Cartoni, R., Ashrafi, G., et al. (2022). Neuronal mitochondria transport Pink1 mRNA via synaptojanin 2 to support local mitophagy. Neuron https://doi.org/10.1016/j.neuron.2022.01.035.

He, D.-Y., Neasta, J., and Ron, D. (2010). Epigenetic Regulation of BDNF Expression via the Scaffolding Protein RACK1*. Journal of Biological Chemistry *285*, 19043–19050. https://doi.org/10.1074/jbc.M110.100693.

Heiman, M., Kulicke, R., Fenster, R.J., Greengard, P., and Heintz, N. (2014). Cell type–specific mRNA purification by translating ribosome affinity purification (TRAP). Nat Protoc *9*, 1282–1291. https://doi.org/10.1038/nprot.2014.085.

Herbert, A.L., Fu, M., Drerup, C.M., Gray, R.S., Harty, B.L., Ackerman, S.D., O'Reilly-Pol, T., Johnson, S.L., Nechiporuk, A.V., Barres, B.A., et al. (2017). Dynein/dynactin is necessary for anterograde transport of *Mbp* mRNA in oligodendrocytes and for myelination in vivo. Proc Natl Acad Sci USA *114*, E9153–E9162. https://doi.org/10.1073/pnas.1711088114.

Herculano-Houzel, S. (2014). The glia/neuron ratio: How it varies uniformly across brain structures and species and what that means for brain physiology and evolution. Glia *62*, 1377–1391. https://doi.org/10.1002/glia.22683.

Higashi, K., Fujita, A., Inanobe, A., Tanemoto, M., Doi, K., Kubo, T., and Kurachi, Y. (2001). An inwardly rectifying K(+) channel, Kir4.1, expressed in astrocytes surrounds synapses and blood vessels in brain. Am J Physiol Cell Physiol *281*, C922-931. https://doi.org/10.1152/ajpcell.2001.281.3.C922.

Higashimori, H., Schin, C.S., Chiang, M.S.R., Morel, L., Shoneye, T.A., Nelson, D.L., and Yang, Y. (2016). Selective Deletion of Astroglial FMRP Dysregulates Glutamate Transporter GLT1 and Contributes to Fragile X Syndrome Phenotypes In Vivo. J. Neurosci. *36*, 7079–7094. https://doi.org/10.1523/JNEUROSCI.1069-16.2016.

Horton, A.C., and Ehlers, M.D. (2003). Dual Modes of Endoplasmic Reticulum-to-Golgi Transport in Dendrites Revealed by Live-Cell Imaging. J Neurosci *23*, 6188–6199. https://doi.org/10.1523/JNEUROSCI.23-15-06188.2003.

Hösli, L., Zuend, M., Bredell, G., Zanker, H.S., Porto de Oliveira, C.E., Saab, A.S., and Weber, B. (2022). Direct vascular contact is a hallmark of cerebral astrocytes. Cell Reports *39*, 110599. https://doi.org/10.1016/j.celrep.2022.110599.

Hu, Y., Liu, J.-P., Li, X.-Y., Cai, Y., He, C., Li, N.-S., Xie, C., Xiong, Z.-J., Ge, Z.-M., Lu, N.-H., et al. (2019). Downregulation of tumor suppressor RACK1 by Helicobacter pylori infection promotes gastric carcinogenesis through the integrin β-1/NF-κB signaling pathway. Cancer Lett. *450*, 144–154. https://doi.org/10.1016/j.canlet.2019.02.039.

Huang, Y.-C., Lin, K.-F., He, R.-Y., Tu, P.-H., Koubek, J., Hsu, Y.-C., and Huang, J.J.-T. (2013). Inhibition of TDP-43 Aggregation by Nucleic Acid Binding. PLoS One *8*, e64002. https://doi.org/10.1371/journal.pone.0064002.

Hubbard, J.A., and Binder, D.K. (2016). History of Astrocytes. In Astrocytes and Epilepsy, (Elsevier), pp. 1–38.

Huber, K.M., Kayser, M.S., and Bear, M.F. (2000). Role for Rapid Dendritic Protein Synthesis in Hippocampal mGluR-Dependent Long-Term Depression. Science *288*, 1254–1256. https://doi.org/10.1126/science.288.5469.1254.

Huffels, C.F.M., Osborn, L.M., Hulshof, L.A., Kooijman, L., Henning, L., Steinhäuser, C., and Hol, E.M. (2021). Amyloid-β plaques affect astrocyte Kir4.1 protein expression but not function in the dentate gyrus of APP/PS1 mice. Glia *n/a*. https://doi.org/10.1002/glia.24137.

Ikeuchi, K., and Inada, T. (2016). Ribosome-associated Asc1/RACK1 is required for endonucleolytic cleavage induced by stalled ribosome at the 3′ end of nonstop mRNA. Scientific Reports *6*, 28234. https://doi.org/10.1038/srep28234.

Ivanov, A.I., Malkov, A.E., Waseem, T., Mukhtarov, M., Buldakova, S., Gubkina, O., Zilberter, M., and Zilberter, Y. (2014). Glycolysis and oxidative phosphorylation in neurons and astrocytes during network activity in hippocampal slices. J Cereb Blood Flow Metab *34*, 397–407. https://doi.org/10.1038/jcbfm.2013.222.

Iwasaki, S., and Ingolia, N.T. (2017). The Growing Toolbox for Protein Synthesis Studies. Trends in Biochemical Sciences *42*, 612–624. https://doi.org/10.1016/j.tibs.2017.05.004.

Izrael, M., Slutsky, S.G., and Revel, M. (2020). Rising Stars: Astrocytes as a Therapeutic Target for ALS Disease. Frontiers in Neuroscience *14*, 824. https://doi.org/10.3389/fnins.2020.00824.

Johnson, A.G., Lapointe, C.P., Wang, J., Corsepius, N.C., Choi, J., Fuchs, G., and Puglisi, J.D. (2019). RACK1 on and off the ribosome (Biochemistry).

Jung, H., Yoon, B.C., and Holt, C.E. (2012). Axonal mRNA localization and local protein synthesis in nervous system assembly, maintenance and repair. Nat Rev Neurosci *13*, 308–324. https://doi.org/10.1038/nrn3210.

Kang, H., and Schuman, E.M. (1996). A Requirement for Local Protein Synthesis in Neurotrophin-Induced Hippocampal Synaptic Plasticity. Science *273*, 1402–1406. https://doi.org/10.1126/science.273.5280.1402.

Kapur, M., Monaghan, C.E., and Ackerman, S.L. (2017). Regulation of mRNA Translation in Neurons–A Matter of Life and Death. Neuron *96*, 616–637. https://doi.org/10.1016/j.neuron.2017.09.057.

Kedersha, N., Stoecklin, G., Ayodele, M., Yacono, P., Lykke-Andersen, J., Fritzler, M.J., Scheuner, D., Kaufman, R.J., Golan, D.E., and Anderson, P. (2005). Stress granules and processing bodies are dynamically linked sites of mRNP remodeling. J. Cell Biol. *169*, 871–884. https://doi.org/10.1083/jcb.200502088.

Kershner, L., and Welshhans, K. (2017a). RACK1 is necessary for the formation of point contacts and regulates axon growth: RACK1 in Growth Cones. Devel Neurobio *77*, 1038–1056. https://doi.org/10.1002/dneu.22491.

Kershner, L., and Welshhans, K. (2017b). RACK1 regulates neural development. Neural Regen Res *12*, 1036. https://doi.org/10.4103/1673-5374.211175.

Kershner, L., Bumbledare, T., Cassidy, P., Bailey, S., and Welshhans, K. (2019). RACK1 is required for axon guidance and local translation at growth cone point contacts. BioRxiv 816017. https://doi.org/10.1101/816017.

Kettenmann, H., Backus, K.H., and Schachner, M. (1984). Aspartate, glutamate and γ-aminobutyric acid depolarize cultured astrocytes. Neuroscience Letters *52*, 25–29. https://doi.org/10.1016/0304-3940(84)90345-8.

Khandjian, E.W., Dury, A., De Koninck, P., El Fatimy, R., and Davidovic, L. (2015). RNA Granules: Functions Within Presynaptic Terminals and Postsynaptic Spines☆. In Reference Module in Biomedical Sciences, (Elsevier), p.

Kharade, S.V., Kurata, H., Bender, A.M., Blobaum, A.L., Figueroa, E.E., Duran, A., Kramer, M., Days, E., Vinson, P., Flores, D., et al. (2018). Discovery, Characterization, and Effects on Renal Fluid and Electrolyte Excretion of the Kir4.1 Potassium Channel Pore Blocker, VU0134992. Mol Pharmacol *94*, 926–937. https://doi.org/10.1124/mol.118.112359.

Kinboshi, M., Ikeda, A., and Ohno, Y. (2020). Role of Astrocytic Inwardly Rectifying Potassium (Kir) 4.1 Channels in Epileptogenesis. Frontiers in Neurology *11*. .

Koenig, E., and Koelle, G.B. (1960). Acetylcholinesterase Regeneration in Peripheral Nerve after Irreversible Inactivation. Science *132*, 1249–1250. https://doi.org/10.1126/science.132.3435.1249.

Koester, S.K., and Dougherty, J.D. (2022). A Proposed Role for Interactions between Argonautes, miRISC, and RNA Binding Proteins in the Regulation of Local Translation in Neurons and Glia. J. Neurosci. *42*, 3291–3301. https://doi.org/10.1523/JNEUROSCI.2391-21.2022.

KOFUJI, P., and NEWMAN, E.A. (2004). POTASSIUM BUFFERING IN THE CENTRAL NERVOUS SYSTEM. Neuroscience *129*, 1045–1056. https://doi.org/10.1016/j.neuroscience.2004.06.008.

Koley, S., Rozenbaum, M., Fainzilber, M., and Terenzio, M. (2019). Translating regeneration: Local protein synthesis in the neuronal injury response. Neuroscience Research *139*, 26–36. https://doi.org/10.1016/j.neures.2018.10.003.

Komar, A.A., and Hatzoglou, M. (2011). Cellular IRES-mediated translation: The war of ITAFs in pathophysiological states. Cell Cycle *10*, 229–240. https://doi.org/10.4161/cc.10.2.14472.

Koppers, M., Cagnetta, R., Shigeoka, T., Wunderlich, L.C., Vallejo-Ramirez, P., Qiaojin Lin, J., Zhao, S., Jakobs, M.A., Dwivedy, A., Minett, M.S., et al. (2019). Receptor-specific interactome as a hub for rapid cue-induced selective translation in axons. ELife *8*, e48718. https://doi.org/10.7554/eLife.48718.

Kosti, A., de Araujo, P.R., Li, W.-Q., Guardia, G.D.A., Chiou, J., Yi, C., Ray, D., Meliso, F., Li, Y.-M., Delambre, T., et al. (2020). The RNA-binding protein SERBP1 functions as a novel oncogenic factor in glioblastoma by bridging cancer metabolism and epigenetic regulation. Genome Biol *21*, 195. https://doi.org/10.1186/s13059-020-02115-y.

Kratz, A., Beguin, P., Kaneko, M., Chimura, T., Suzuki, A.M., Matsunaga, A., Kato, S., Bertin, N., Lassmann, T., Vigot, R., et al. (2014). Digital expression profiling of the compartmentalized translatome of Purkinje neurons. Genome Res *24*, 1396–1410. https://doi.org/10.1101/gr.164095.113.

Krichevsky, A.M., and Kosik, K.S. (2001). Neuronal RNA Granules: A Link between RNA Localization and Stimulation-Dependent Translation. Neuron *32*, 683–696. https://doi.org/10.1016/S0896-6273(01)00508-6.

Kugler, J.-M., and Lasko, P. (2009). Localization, anchoring and translational control of oskar, gurken, bicoid and nanos mRNA during Drosophila oogenesis. Fly *3*, 15–28. https://doi.org/10.4161/fly.3.1.7751.

Kuzniewska, B., Cysewski, D., Wasilewski, M., Sakowska, P., Milek, J., Kulinski, T.M., Winiarski, M., Kozielewicz, P., Knapska, E., Dadlez, M., et al. (2020). Mitochondrial protein biogenesis in the synapse is supported by local translation. EMBO Reports *n/a*, e48882. https://doi.org/10.15252/embr.201948882.

LaFontaine, E., Miller, C.M., Permaul, N., Martin, E.T., and Fuchs, G. (2020). Ribosomal protein RACK1 enhances translation of poliovirus and other viral IRESs. Virology *545*, 53–62. https://doi.org/10.1016/j.virol.2020.03.004.

Lagier-Tourenne, C., Polymenidou, M., and Cleveland, D.W. (2010). TDP-43 and FUS/TLS: emerging roles in RNA processing and neurodegeneration. Human Molecular Genetics *19*, R46–R64. https://doi.org/10.1093/hmg/ddq137.

Lagier-Tourenne, C., Polymenidou, M., Hutt, K.R., Vu, A.Q., Baughn, M., Huelga, S.C., Clutario, K.M., Ling, S.-C., Liang, T.Y., Mazur, C., et al. (2012). Divergent roles of ALS-linked proteins FUS/TLS and TDP-43 intersect in processing long pre-mRNAs. Nat Neurosci *15*, 1488–1497. https://doi.org/10.1038/nn.3230.

Langdon, E.M., and Gladfelter, A.S. (2018). A New Lens for RNA Localization: Liquid-Liquid Phase Separation. Annual Review of Microbiology *72*, 255–271. https://doi.org/10.1146/annurev-micro-090817-062814.

Langeswaran, K., Sugnya, N., and Sangavi, P. (2019). Study on recognition of novel RACK1 protein inhibitors for small cell lung cancer outlined by pharmacophore based virtual screening and Molecular Docking. Biocatalysis and Agricultural Biotechnology *21*, 101301. https://doi.org/10.1016/j.bcab.2019.101301.

Larburu, N., Montellese, C., O'Donohue, M.-F., Kutay, U., Gleizes, P.-E., and Plisson-Chastang, C. (2016). Structure of a human pre-40S particle points to a role for RACK1 in the final steps of 18S rRNA processing. Nucleic Acids Res. *44*, 8465–8478. https://doi.org/10.1093/nar/gkw714.

Lautier, O., Penzo, A., Rouvière, J.O., Chevreux, G., Collet, L., Loïodice, I., Taddei, A., Devaux, F., Collart, M.A., and Palancade, B. (2021). Co-translational assembly and localized translation of nucleoporins in nuclear pore complex biogenesis. Molecular Cell *81*, 2417-2427.e5. https://doi.org/10.1016/j.molcel.2021.03.030.

Lee, S., Park, D., Lim, C., Kim, J.-I., and Min, K.-T. (2022). mtIF3 is locally translated in axons and regulates mitochondrial translation for axonal growth. BMC Biology *20*, 12. https://doi.org/10.1186/s12915-021-01215-w.

Lesnik, C., Golani-Armon, A., and Arava, Y. (2015). Localized translation near the mitochondrial outer membrane: An update. RNA Biol *12*, 801–809. https://doi.org/10.1080/15476286.2015.1058686.

Leung, K.-M., van Horck, F.P., Lin, A.C., Allison, R., Standart, N., and Holt, C.E. (2006). Asymmetrical β-actin mRNA translation in growth cones mediates attractive turning to netrin-1. Nat Neurosci *9*, 1247–1256. https://doi.org/10.1038/nn1775.

Leung, K.-M., Lu, B., Wong, H.H.-W., Lin, J.Q., Turner-Bridger, B., and Holt, C.E. (2018). Cue-Polarized Transport of β-actin mRNA Depends on 3′UTR and Microtubules in Live Growth Cones. Front. Cell. Neurosci. *12*, 300. https://doi.org/10.3389/fncel.2018.00300.

Li, J.-J., and Xie, D. (2015). RACK1, a versatile hub in cancer. Oncogene *34*, 1890–1898. https://doi.org/10.1038/onc.2014.127.

Li, W., Zou, J., Shang, J., Gao, C., Sun, R., Liu, R., Cao, H., Wang, Y., and Zhang, J. (2022). Both the Complexity of Tight Junctions and Endothelial Transcytosis Are Increased During BBB Postnatal Development in Rats. Frontiers in Neuroscience *16*. .

Li, X., Lin, W.-J., Chen, C.-Y., Si, Y., Zhang, X., Lu, L., Suswam, E., Zheng, L., and King, P.H. (2012). KSRP: a checkpoint for inflammatory cytokine production in astrocytes. Glia *60*, 1773–1784. https://doi.org/10.1002/glia.22396.

Li, Z., Zhang, Y., Li, D., and Feng, Y. (2000). Destabilization and Mislocalization of Myelin Basic Protein mRNAs in *quaking* Dysmyelination Lacking the QKI RNA-Binding Proteins. J. Neurosci. *20*, 4944–4953. https://doi.org/10.1523/JNEUROSCI.20-13-04944.2000.

Lia, A., Henriques, V.J., Zonta, M., Chiavegato, A., Carmignoto, G., Gómez-Gonzalo, M., and Losi, G. (2021). Calcium Signals in Astrocyte Microdomains, a Decade of Great Advances. Front Cell Neurosci *15*, 673433. https://doi.org/10.3389/fncel.2021.673433.

Lin, A.C., and Holt, C.E. (2007). Local translation and directional steering in axons. EMBO J *26*, 3729–3736. https://doi.org/10.1038/sj.emboj.7601808.

Lind, B.L., Jessen, S.B., Lønstrup, M., Joséphine, C., Bonvento, G., and Lauritzen, M. (2018). Fast Ca2+ responses in astrocyte end-feet and neurovascular coupling in mice. Glia *66*, 348–358. https://doi.org/10.1002/glia.23246.

Liu, Y. (2020). A code within the genetic code: codon usage regulates co-translational protein folding. Cell Commun Signal *18*, 145. https://doi.org/10.1186/s12964-020-00642-6.

Liu, F., Shao, J., Yang, H., Yang, G., Zhu, Q., Wu, Y., Zhu, L., and Wu, H. (2021). Disruption of rack1 suppresses SHH-type medulloblastoma formation in mice. CNS Neuroscience & Therapeutics *n/a*. https://doi.org/10.1111/cns.13728.

Liu, W., Dou, F., Feng, J., and Yan, Z. (2011). RACK1 is involved in β-amyloid impairment of muscarinic regulation of GABAergic transmission. Neurobiol Aging *32*, 1818–1826. https://doi.org/10.1016/j.neurobiolaging.2009.10.017.

Lu, L., Zheng, L., Si, Y., Luo, W., Dujardin, G., Kwan, T., Potochick, N.R., Thompson, S.R., Schneider, D.A., and King, P.H. (2014). Hu antigen R (HuR) is a positive regulator of the RNA-binding proteins TDP-43 and FUS/TLS: implications for amyotrophic lateral sclerosis. J. Biol. Chem. *289*, 31792–31804. https://doi.org/10.1074/jbc.M114.573246.

Lu, R., Fan, B., Yin, D., Li, Y., Wang, B., Zhu, S., Chen, Y., and Xu, Z. (2019). Receptor for activated C kinase 1 mediates the chronic constriction injury-induced neuropathic pain in the rats' peripheral and central nervous system. Neuroscience Letters *712*, 134477. https://doi.org/10.1016/j.neulet.2019.134477.

Majzoub, K., Hafirassou, M.L., Meignin, C., Goto, A., Marzi, S., Fedorova, A., Verdier, Y., Vinh, J., Hoffmann, J.A., Martin, F., et al. (2014). RACK1 controls IRES-mediated translation of viruses. Cell *159*, 1086–1095. https://doi.org/10.1016/j.cell.2014.10.041.

Mamidipudi, V., Zhang, J., Lee, K.C., and Cartwright, C.A. (2004). RACK1 Regulates G1/S Progression by Suppressing Src Kinase Activity. Mol Cell Biol *24*, 6788–6798. https://doi.org/10.1128/MCB.24.15.6788-6798.2004.

Martineau, M., Parpura, V., and Mothet, J.-P. (2014). Cell-type specific mechanisms of D-serine uptake and release in the brain. Front Synaptic Neurosci *6*, 12. https://doi.org/10.3389/fnsyn.2014.00012.

Mathiisen, T.M., Lehre, K.P., Danbolt, N.C., and Ottersen, O.P. (2010). The perivascular astroglial sheath provides a complete covering of the brain microvessels: An electron microscopic 3D reconstruction. Glia *58*, 1094–1103. https://doi.org/10.1002/glia.20990.

Matsuda, R., Ikeuchi, K., Nomura, S., and Inada, T. (2014). Protein quality control systems associated with no-go and nonstop mRNA surveillance in yeast. Genes to Cells *19*, 1–12. https://doi.org/10.1111/gtc.12106.

Mazaré, N., Oudart, M., Moulard, J., Cheung, G., Tortuyaux, R., Mailly, P., Mazaud, D., Bemelmans, A.-P., Boulay, A.-C., Blugeon, C., et al. (2020a). Local translation in perisynaptic astrocytic processes is specific and regulated by fear conditioning (Neuroscience).

Mazaré, N., Oudart, M., Cheung, G., Boulay, A.-C., and Cohen-Salmon, M. (2020b). Immunoprecipitation of Ribosome-Bound mRNAs from Astrocytic Perisynaptic Processes of the Mouse Hippocampus. STAR Protocols *1*, 100198. https://doi.org/10.1016/j.xpro.2020.100198.

Mazaré, N., Oudart, M., and Cohen-Salmon, M. (2021). Local translation in perisynaptic and perivascular astrocytic processes – a means to ensure astrocyte molecular and functional polarity? Journal of Cell Science *134*, jcs251629. https://doi.org/10.1242/jcs.251629.

Merianda, T.T., Lin, A.C., Lam, J.S.Y., Vuppalanchi, D., Willis, D.E., Karin, N., Holt, C.E., and Twiss, J.L. (2009). A functional equivalent of endoplasmic reticulum and Golgi in axons for secretion of locally synthesized proteins. Mol Cell Neurosci *40*, 128–142. https://doi.org/10.1016/j.mcn.2008.09.008.

Meservey, L.M., Topkar, V.V., and Fu, M. (2021). mRNA Transport and Local Translation in Glia. Trends in Cell Biology https://doi.org/10.1016/j.tcb.2021.03.006.

Mestre, H., Hablitz, L.M., Xavier, A.L., Feng, W., Zou, W., Pu, T., Monai, H., Murlidharan, G., Castellanos Rivera, R.M., Simon, M.J., et al. (2018). Aquaporin-4-dependent glymphatic solute transport in the rodent brain. ELife *7*, e40070. https://doi.org/10.7554/eLife.40070.

Moor, A.E., Golan, M., Massasa, E.E., Lemze, D., Weizman, T., Shenhav, R., Baydatch, S., Mizrahi, O., Winkler, R., Golani, O., et al. (2017). Global mRNA polarization regulates translation efficiency in the intestinal epithelium. Science *357*, 1299–1303. https://doi.org/10.1126/science.aan2399.

Morel, L., Regan, M., Higashimori, H., Ng, S.K., Esau, C., Vidensky, S., Rothstein, J., and Yang, Y. (2013). Neuronal Exosomal miRNA-dependent Translational Regulation of Astroglial Glutamate Transporter GLT1. Journal of Biological Chemistry *288*, 7105–7116. https://doi.org/10.1074/jbc.M112.410944.

Morgello, S., Uson, R.R., Schwartz, E.J., and Haber, R.S. (1995). The human blood-brain barrier glucose transporter (GLUT1) is a glucose transporter of gray matter astrocytes. Glia *14*, 43–54. https://doi.org/10.1002/glia.440140107.

Müller, C., Bauer, N., Schäfer, I., and White, R. (2013). Making myelin basic protein -from mRNA transport to localized translation. Frontiers in Cellular Neuroscience *7*. .

Müntjes, K., Devan, S.K., Reichert, A.S., and Feldbrügge, M. (2021). Linking transport and translation of mRNAs with endosomes and mitochondria. EMBO Reports *22*. https://doi.org/10.15252/embr.202152445.

Nagano, S., Jinno, J., Abdelhamid, R.F., Jin, Y., Shibata, M., Watanabe, S., Hirokawa, S., Nishizawa, M., Sakimura, K., Onodera, O., et al. (2020). TDP-43 transports ribosomal protein mRNA to regulate axonal local translation in neuronal axons. Acta Neuropathol https://doi.org/10.1007/s00401-020-02205-y.

Nagy, J.I., Ionescu, A.-V., Lynn, B.D., and Rash, J.E. (2003). Coupling of astrocyte connexins Cx26, Cx30, Cx43 to oligodendrocyte Cx29, Cx32, Cx47: Implications from normal and connexin32 knockout mice. Glia *44*, 205–218. https://doi.org/10.1002/glia.10278.

Nakayama, K., Ohashi, R., Shinoda, Y., Yamazaki, M., Abe, M., Fujikawa, A., Shigenobu, S., Futatsugi, A., Noda, M., Mikoshiba, K., et al. (2017). RNG105/caprin1, an RNA granule protein for dendritic mRNA localization, is essential for long-term memory formation. ELife *6*, e29677. https://doi.org/10.7554/eLife.29677.

Nevo-Dinur, K., Nussbaum-Shochat, A., Ben-Yehuda, S., and Amster-Choder, O. (2011). Translation-Independent Localization of mRNA in E. coli. Science *331*, 1081–1084. https://doi.org/10.1126/science.1195691.

Nwaobi, S.E., Cuddapah, V.A., Patterson, K.C., Randolph, A.C., and Olsen, M.L. (2016). The role of glial specific Kir4.1 in normal and pathological states of the CNS. Acta Neuropathol *132*, 1–21. https://doi.org/10.1007/s00401-016-1553-1.

Oberheim, N.A., Wang, X., Goldman, S., and Nedergaard, M. (2006). Astrocytic complexity distinguishes the human brain. Trends in Neurosciences *29*, 547–553. https://doi.org/10.1016/j.tins.2006.08.004.

Oberheim, N.A., Tian, G.-F., Han, X., Peng, W., Takano, T., Ransom, B., and Nedergaard, M. (2008). Loss of Astrocytic Domain Organization in the Epileptic Brain. J Neurosci *28*, 3264–3276. https://doi.org/10.1523/JNEUROSCI.4980-07.2008.

Oberheim, N.A., Takano, T., Han, X., He, W., Lin, J.H.C., Wang, F., Xu, Q., Wyatt, J.D., Pilcher, W., Ojemann, J.G., et al. (2009). Uniquely Hominid Features of Adult Human Astrocytes. J Neurosci *29*, 3276–3287. https://doi.org/10.1523/JNEUROSCI.4707-08.2009.

Ogata, K., and Kosaka, T. (2002). Structural and quantitative analysis of astrocytes in the mouse hippocampus. Neuroscience *113*, 221–233. https://doi.org/10.1016/S0306-4522(02)00041-6.

Ohno, Y. (2018). Astrocytic Kir4.1 potassium channels as a novel therapeutic target for epilepsy and mood disorders. Neural Regen Res *13*, 651–652. https://doi.org/10.4103/1673-5374.230355.

Ohno, Y., Kinboshi, M., and Shimizu, S. (2018). Inwardly Rectifying Potassium Channel Kir4.1 as a Novel Modulator of BDNF Expression in Astrocytes. Int J Mol Sci *19*. https://doi.org/10.3390/ijms19113313.

Ohno, Y., Kunisawa, N., and Shimizu, S. (2021). Emerging Roles of Astrocyte Kir4.1 Channels in the Pathogenesis and Treatment of Brain Diseases. International Journal of Molecular Sciences *22*, 10236. https://doi.org/10.3390/ijms221910236.

Olguin, S.L., Patel, P., Buchanan, C.N., Dell'Orco, M., Gardiner, A.S., Cole, R., Vaughn, L.S., Sundararajan, A., Mudge, J., Allan, A.M., et al. (2022). KHSRP loss increases neuronal growth and synaptic transmission and alters memory consolidation through RNA stabilization. Commun Biol *5*, 1–15. https://doi.org/10.1038/s42003-022-03594-4.

Oliet, S.H.R., Piet, R., and Poulain, D.A. (2001). Control of Glutamate Clearance and Synaptic Efficacy by Glial Coverage of Neurons. Science https://doi.org/10.1126/science.1059162.

Oliet, S.H.R., Piet, R., Poulain, D.A., and Theodosis, D.T. (2004). Glial modulation of synaptic transmission: Insights from the supraoptic nucleus of the hypothalamus. Glia *47*, 258–267. https://doi.org/10.1002/glia.20032.

Ostroff, L.E., Botsford, B., Gindina, S., Cowansage, K.K., LeDoux, J.E., Klann, E., and Hoeffer, C. (2017). Accumulation of Polyribosomes in Dendritic Spine Heads, But Not Bases and Necks, during Memory Consolidation Depends on Cap-Dependent Translation Initiation. J. Neurosci. *37*, 1862–1872. https://doi.org/10.1523/JNEUROSCI.3301-16.2017.

Oudart, M., Tortuyaux, R., Mailly, P., Mazaré, N., Boulay, A.-C., and Cohen-Salmon, M. (2020). AstroDot – a new method for studying the spatial distribution of mRNA in astrocytes. J Cell Sci *133*. https://doi.org/10.1242/jcs.239756.

Oudart, M.-, Gutierrez, K.A., Moch, C., Dossi, E., Milior, G., Boulay, A.C., Gaudey, M., Moulard, J., Lombard, B., Loew, D., et al. (2022). Translational regulation by RACK1 in astrocytes represses KIR4.1 expression and regulates neuronal activity. 2022.07.16.500292. https://doi.org/10.1101/2022.07.16.500292.

Ouwenga, R., Lake, A.M., Aryal, S., Lagunas, T., and Dougherty, J.D. (2018). The Differences in Local Translatome across Distinct Neuron Types Is Mediated by Both Baseline Cellular Differences and Post-transcriptional Mechanisms. ENeuro *5*, ENEURO.0320-18.2018. https://doi.org/10.1523/ENEURO.0320-18.2018.

Pan, X., Rijnbeek, P., Yan, J., and Shen, H.-B. (2018). Prediction of RNA-protein sequence and structure binding preferences using deep convolutional and recurrent neural networks. BMC Genomics *19*, 511. https://doi.org/10.1186/s12864-018-4889-1.

Pan, X., Fang, Y., Li, X., Yang, Y., and Shen, H.-B. (2020). RBPsuite: RNA-protein binding sites prediction suite based on deep learning. BMC Genomics *21*, 884. https://doi.org/10.1186/s12864-020-07291-6.

Pannasch, U., and Rouach, N. (2013). Emerging role for astroglial networks in information processing: from synapse to behavior. Trends in Neurosciences *36*, 405–417. https://doi.org/10.1016/j.tins.2013.04.004.

Pannasch, U., Freche, D., Dallérac, G., Ghézali, G., Escartin, C., Ezan, P., Cohen-Salmon, M., Benchenane, K., Abudara, V., Dufour, A., et al. (2014). Connexin 30 sets synaptic strength by controlling astroglial synapse invasion. Nat Neurosci *17*, 549–558. https://doi.org/10.1038/nn.3662.

Pannicke, T., Iandiev, I., Uckermann, O., Biedermann, B., Kutzera, F., Wiedemann, P., Wolburg, H., Reichenbach, A., and Bringmann, A. (2004). A potassium channel-linked mechanism of glial cell swelling in the postischemic retina. Mol Cell Neurosci *26*, 493–502. https://doi.org/10.1016/j.mcn.2004.04.005.

Papouin, T., Henneberger, C., Rusakov, D.A., and Oliet, S.H.R. (2017). Astroglial versus Neuronal D-Serine: Fact Checking. Trends in Neurosciences *40*, 517–520. https://doi.org/10.1016/j.tins.2017.05.007.

Patterson, R.L., van Rossum, D.B., Barrow, R.K., and Snyder, S.H. (2004). RACK1 binds to inositol 1,4,5-trisphosphate receptors and mediates Ca2+ release. Proceedings of the National Academy of Sciences *101*, 2328–2332. https://doi.org/10.1073/pnas.0308567100.

Pellerin, L., and Magistretti, P.J. (1994). Glutamate uptake into astrocytes stimulates aerobic glycolysis: a mechanism coupling neuronal activity to glucose utilization. Proceedings of the National Academy of Sciences *91*, 10625–10629. https://doi.org/10.1073/pnas.91.22.10625.

Pelvig, D.P., Pakkenberg, H., Stark, A.K., and Pakkenberg, B. (2008). Neocortical glial cell numbers in human brains. Neurobiology of Aging *29*, 1754–1762. https://doi.org/10.1016/j.neurobiolaging.2007.04.013.

Petzold, G.C., and Murthy, V.N. (2011). Role of Astrocytes in Neurovascular Coupling. Neuron *71*, 782–797. https://doi.org/10.1016/j.neuron.2011.08.009.

Peyrl, A., Weitzdoerfer, R., Gulesserian, T., Fountoulakis, M., and Lubec, G. (2002). Aberrant expression of signaling-related proteins 14-3-3 gamma and RACK1 in fetal Down Syndrome brain (trisomy 21). ELECTROPHORESIS *23*, 152–157. https://doi.org/10.1002/1522-2683(200201)23:1<152::AID-ELPS152>3.0.CO;2-T.

Pilaz, L.-J., Lennox, A.L., Rouanet, J.P., and Silver, D.L. (2016). Dynamic mRNA Transport and Local Translation in Radial Glial Progenitors of the Developing Brain. Curr. Biol. *26*, 3383–3392. https://doi.org/10.1016/j.cub.2016.10.040.

Pilaz, L.-J., Joshi, K., Liu, J., Tsunekawa, Y., Alsina, F.C., Sethi, S., Suzuki, I.K., Vanderhaeghen, P., Polleux, F., and Silver, D.L. (2020). Subcellular mRNA localization and local translation of Arhgap11a in radial glial cells regulates cortical development. BioRxiv 2020.07.30.229724. https://doi.org/10.1101/2020.07.30.229724.

Puighermanal, E., Biever, A., Pascoli, V., Melser, S., Pratlong, M., Cutando, L., Rialle, S., Severac, D., Boubaker-Vitre, J., Meyuhas, O., et al. (2017). Ribosomal Protein S6 Phosphorylation Is Involved in Novelty-Induced Locomotion, Synaptic Plasticity and mRNA Translation. Frontiers in Molecular Neuroscience *10*. .

Purves, D., Augustine, G.J., Fitzpatrick, D., Hall, W.C., LaMantia, A.-S., and White, L.E. (2012). Neuroscience (Sunderland (Mass.), Etats-Unis d'Amérique: Sinauer).

Radomska, K.J., Halvardson, J., Reinius, B., Lindholm Carlström, E., Emilsson, L., Feuk, L., and Jazin, E. (2013). RNA-binding protein QKI regulates Glial fibrillary acidic protein expression in human astrocytes. Hum Mol Genet *22*, 1373–1382. https://doi.org/10.1093/hmg/dds553.

Rajgor, D., Purkey, A.M., Sanderson, J.L., Welle, T.M., Garcia, J.D., Dell'Acqua, M.L., and Smith, K.R. (2020). Local miRNA-Dependent Translational Control of GABAAR Synthesis during Inhibitory Long-Term Potentiation. Cell Reports *31*, 107785. https://doi.org/10.1016/j.celrep.2020.107785.

Rangaraju, V., Lauterbach, M., and Schuman, E.M. (2019). Spatially Stable Mitochondrial Compartments Fuel Local Translation during Plasticity. Cell *176*, 73-84.e15. https://doi.org/10.1016/j.cell.2018.12.013.

Re, A., Joshi, T., Kulberkyte, E., Morris, Q., and Workman, C.T. (2014). RNA–Protein Interactions: An Overview. In RNA Sequence, Structure, and Function: Computational and Bioinformatic Methods, J. Gorodkin, and W.L. Ruzzo, eds. (Totowa, NJ: Humana Press), pp. 491–521.

Reck-Peterson, S.L., Redwine, W.B., Vale, R.D., and Carter, A.P. (2018). The cytoplasmic dynein transport machinery and its many cargoes. Nat Rev Mol Cell Biol *19*, 382–398. https://doi.org/10.1038/s41580-018-0004-3.

Reid, D.W., and Nicchitta, C.V. (2012). The enduring enigma of nuclear translation. The Journal of Cell Biology *197*, 7–9. https://doi.org/10.1083/jcb.201202140.

Ribot, J., Breton, R., Calvo, C.-F., Moulard, J., Ezan, P., Zapata, J., Samama, K., Moreau, M., Bemelmans, A.-P., Sabatet, V., et al. (2021). Astrocytes close the mouse critical period for visual plasticity. Science *373*, 77–81. https://doi.org/10.1126/science.abf5273.

Rollins, M.G., Jha, S., Bartom, E.T., and Walsh, D. (2019). RACK1 evolved species-specific multifunctionality in translational control through sequence plasticity within a loop domain. Journal of Cell Science *132*, jcs228908. https://doi.org/10.1242/jcs.228908.

Ronzano, R., Roux, T., Thetiot, M., Aigrot, M.S., Richard, L., Lejeune, F.X., Mazuir, E., Vallat, J.M., Lubetzki, C., and Desmazières, A. (2021). Microglia-neuron interaction at nodes of Ranvier depends on neuronal activity through potassium release and contributes to remyelination. Nat Commun *12*, 5219. https://doi.org/10.1038/s41467-021-25486-7.

Rouach, N., Koulakoff, A., Abudara, V., Willecke, K., and Giaume, C. (2008). Astroglial Metabolic Networks Sustain Hippocampal Synaptic Transmission. Science *322*, 1551–1555. https://doi.org/10.1126/science.1164022.

Russo, A., Scardigli, R., La Regina, F., Murray, M.E., Romano, N., Dickson, D.W., Wolozin, B., Cattaneo, A., and Ceci, M. (2017). Increased cytoplasmic TDP-43 reduces global protein synthesis by interacting with RACK1 on polyribosomes. Hum Mol Genet *26*, 1407–1418. https://doi.org/10.1093/hmg/ddx035.

Sáez, J.C., Berthoud, V.M., Brañes, M.C., Martínez, A.D., and Beyer, E.C. (2003). Plasma Membrane Channels Formed by Connexins: Their Regulation and Functions. Physiological Reviews *83*, 1359–1400. https://doi.org/10.1152/physrev.00007.2003.

Sakers, K., Lake, A.M., Khazanchi, R., Ouwenga, R., Vasek, M.J., Dani, A., and Dougherty, J.D. (2017). Astrocytes locally translate transcripts in their peripheral processes. PNAS *114*, E3830–E3838. https://doi.org/10.1073/pnas.1617782114.

Sakers, K., Liu, Y., Llaci, L., Vasek, M.J., Rieger, M.A., Brophy, S., Tycksen, E., Lewis, R., Maloney, S.E., and Dougherty, J.D. (2020). CRISPR-TRAPSeq identifies the QKI RNA binding protein as important for astrocytic maturation and control of thalamocortical synapses. BioRxiv 2020.03.13.991224. https://doi.org/10.1101/2020.03.13.991224.

Sakers, K., Liu, Y., Llaci, L., Lee, S.M., Vasek, M.J., Rieger, M.A., Brophy, S., Tycksen, E., Lewis, R., Maloney, S.E., et al. (2021). Loss of Quaking RNA binding protein disrupts the expression of genes associated with astrocyte maturation in mouse brain. Nature Communications *12*, 1537. https://doi.org/10.1038/s41467-021-21703-5.

Sanderson, M.J., Charles, A.C., Boitano, S., and Dirksen, E.R. (1994). Mechanisms and function of intercellular calcium signaling. Molecular and Cellular Endocrinology *98*, 173–187. https://doi.org/10.1016/0303-7207(94)90136-8.

Sapkota, D., Sakers, K., Liu, Y., Lake, A.M., Khazanchi, R., Khankan, R.R., Zhang, Y., and Dougherty, J.D. (2020). Activity dependent translation in astrocytes. BioRxiv 2020.04.08.033027. https://doi.org/10.1101/2020.04.08.033027.

Schäffler, K., Schulz, K., Hirmer, A., Wiesner, J., Grimm, M., Sickmann, A., and Fischer, U. (2010). A stimulatory role for the La-related protein 4B in translation. RNA *16*, 1488–1499. https://doi.org/10.1261/rna.2146910.

Schousboe, A., Scafidi, S., Bak, L.K., Waagepetersen, H.S., and McKenna, M.C. (2014). Glutamate Metabolism in the Brain Focusing on Astrocytes. Adv Neurobiol *11*, 13–30. https://doi.org/10.1007/978-3-319-08894-5_2.

Semyanov, A., and Verkhratsky, A. (2021). Astrocytic processes: from tripartite synapses to the active milieu. Trends in Neurosciences *44*, 781–792. https://doi.org/10.1016/j.tins.2021.07.006.

Sengupta, J., Nilsson, J., Gursky, R., Spahn, C.M.T., Nissen, P., and Frank, J. (2004). Identification of the versatile scaffold protein RACK1 on the eukaryotic ribosome by cryo-EM. Nat Struct Mol Biol *11*, 957–962. https://doi.org/10.1038/nsmb822.

Serrels, B., Sandilands, E., Serrels, A., Baillie, G., Houslay, M.D., Brunton, V.G., Canel, M., Machesky, L.M., Anderson, K.I., and Frame, M.C. (2010). A Complex between FAK, RACK1, and PDE4D5 Controls Spreading Initiation and Cancer Cell Polarity. Current Biology *20*, 1086–1092. https://doi.org/10.1016/j.cub.2010.04.042.

Sharma, V., Sood, R., Khlaifia, A., Eslamizade, M.J., Hung, T.-Y., Lou, D., Asgarihafshejani, A., Lalzar, M., Kiniry, S.J., Stokes, M.P., et al. (2020). eIF2α controls memory consolidation via excitatory and somatostatin neurons. Nature 1–5. https://doi.org/10.1038/s41586-020-2805-8.

Sharma, V., Sood, R., Lou, D., Hung, T.-Y., Lévesque, M., Han, Y., Levett, J.Y., Wang, P., Murthy, S., Tansley, S., et al. (2021). 4E-BP2–dependent translation in parvalbumin neurons controls epileptic seizure threshold. PNAS *118*. https://doi.org/10.1073/pnas.2025522118.

Shen, S., Feng, H., Le, Y., Ni, J., Yu, L., Wu, J., and Bai, M. (2019). RACK1 affects the progress of G2/M by regulating Aurora-A. Cell Cycle *18*, 2228–2238. https://doi.org/10.1080/15384101.2019.1642065.

Shi, Z., Fujii, K., Kovary, K.M., Genuth, N.R., Röst, H.L., Teruel, M.N., and Barna, M. (2017). Heterogeneous Ribosomes Preferentially Translate Distinct Subpools of mRNAs Genome-wide. Molecular Cell *67*, 71-83.e7. https://doi.org/10.1016/j.molcel.2017.05.021.

Shigeoka, T., Jung, H., Jung, J., Turner-Bridger, B., Ohk, J., Lin, J.Q., Amieux, P.S., and Holt, C.E. (2016). Dynamic Axonal Translation in Developing and Mature Visual Circuits. Cell *166*, 181–192. https://doi.org/10.1016/j.cell.2016.05.029.

Shigeoka, T., Koppers, M., Wong, H.H.-W., Lin, J.Q., Cagnetta, R., Dwivedy, A., de Freitas Nascimento, J., van Tartwijk, F.W., Ströhl, F., Cioni, J.-M., et al. (2019). On-Site Ribosome Remodeling by Locally Synthesized Ribosomal Proteins in Axons. Cell Reports *29*, 3605-3619.e10. https://doi.org/10.1016/j.celrep.2019.11.025.

Shu, H., Donnard, E., Liu, B., Jung, S., Wang, R., and Richter, J.D. (2020). FMRP links optimal codons to mRNA stability in neurons. PNAS *117*, 30400–30411. https://doi.org/10.1073/pnas.2009161117.

Sibille, J., Dao Duc, K., Holcman, D., and Rouach, N. (2015). The Neuroglial Potassium Cycle during Neurotransmission: Role of Kir4.1 Channels. PLoS Comput Biol *11*, e1004137. https://doi.org/10.1371/journal.pcbi.1004137.

Sidibé, H., Khalfallah, Y., Xiao, S., Gómez, N.B., Fakim, H., Tank, E.M.H., Di Tomasso, G., Bareke, E., Aulas, A., McKeever, P.M., et al. (2021). TDP-43 stabilizes G3BP1 mRNA: relevance to amyotrophic lateral sclerosis/frontotemporal dementia. Brain *144*, 3461–3476. https://doi.org/10.1093/brain/awab217.

Simons, M., and Nave, K.-A. (2016). Oligodendrocytes: Myelination and Axonal Support. Cold Spring Harb Perspect Biol *8*, a020479. https://doi.org/10.1101/cshperspect.a020479.

Sklan, E.H., Podoly, E., and Soreq, H. (2006). RACK1 has the nerve to act: Structure meets function in the nervous system. Progress in Neurobiology *78*, 117–134. https://doi.org/10.1016/j.pneurobio.2005.12.002.

Sofroniew, M.V., and Vinters, H.V. (2010). Astrocytes: biology and pathology. Acta Neuropathol *119*, 7–35. https://doi.org/10.1007/s00401-009-0619-8.

Speth, C., and Laubinger, S. (2014). RACK1 and the microRNA pathway. Plant Signal Behav *9*. https://doi.org/10.4161/psb.27909.

Ströhl, F., Lin, J.Q., Laine, R.F., Wong, H.H.-W., Urbančič, V., Cagnetta, R., Holt, C.E., and Kaminski, C.F. (2017). Single Molecule Translation Imaging Visualizes the Dynamics of Local β-Actin Synthesis in Retinal Axons. Sci Rep *7*, 709. https://doi.org/10.1038/s41598-017-00695-7.

Sun, C., Nold, A., Fusco, C.M., Rangaraju, V., Tchumatchenko, T., Heilemann, M., and Schuman, E.M. (2021). The prevalence and specificity of local protein synthesis during neuronal synaptic plasticity. Science Advances *7*, eabj0790. https://doi.org/10.1126/sciadv.abj0790.

Sundaramoorthy, E., Leonard, M., Mak, R., Liao, J., Fulzele, A., and Bennett, E.J. (2017). ZNF598 and RACK1 Regulate Mammalian Ribosome-Associated Quality Control Function by Mediating Regulatory 40S Ribosomal Ubiquitylation. Molecular Cell *65*, 751-760.e4. https://doi.org/10.1016/j.molcel.2016.12.026.

Suzuki, A., Stern, S.A., Bozdagi, O., Huntley, G.W., Walker, R.H., Magistretti, P.J., and Alberini, C.M. (2011). Astrocyte-neuron lactate transport is required for long-term memory formation. Cell *144*, 810–823. https://doi.org/10.1016/j.cell.2011.02.018.

Takano, T., Wallace, J.T., Baldwin, K.T., Purkey, A.M., Uezu, A., Courtland, J.L., Soderblom, E.J., Shimogori, T., Maness, P.F., Eroglu, C., et al. (2020). Chemico-genetic discovery of astrocytic control of inhibition in vivo. Nature 1–7. https://doi.org/10.1038/s41586-020-2926-0.

Takeuchi, A., Takahashi, Y., Iida, K., Hosokawa, M., Irie, K., Ito, M., Brown, J.B., Ohno, K., Nakashima, K., and Hagiwara, M. (2020). Identification of Qk as a Glial Precursor Cell Marker that Governs the Fate Specification of Neural Stem Cells to a Glial Cell Lineage. Stem Cell Reports https://doi.org/10.1016/j.stemcr.2020.08.010.

Terenzio, M., Koley, S., Samra, N., Rishal, I., Zhao, Q., Sahoo, P.K., Urisman, A., Marvaldi, L., Oses-Prieto, J.A., Forester, C., et al. (2018). Locally translated mTOR controls axonal local translation in nerve injury. Science *359*, 1416–1421. https://doi.org/10.1126/science.aan1053.

Thomas, K.T., Gross, C., and Bassell, G.J. (2018). microRNAs Sculpt Neuronal Communication in a Tight Balance That Is Lost in Neurological Disease. Frontiers in Molecular Neuroscience *11*. .

Torvund-Jensen, J., Steengaard, J., Askebjerg, L.B., Kjaer-Sorensen, K., and Laursen, L.S. (2018). The 3'UTRs of Myelin Basic Protein mRNAs Regulate Transport, Local Translation and Sensitivity to Neuronal Activity in Zebrafish. Frontiers in Molecular Neuroscience *11*. .

Tushev, G., Glock, C., Heumüller, M., Biever, A., Jovanovic, M., and Schuman, E.M. (2018). Alternative 3′ UTRs Modify the Localization, Regulatory Potential, Stability, and Plasticity of mRNAs in Neuronal Compartments. Neuron *98*, 495-511.e6. https://doi.org/10.1016/j.neuron.2018.03.030.

Vainchtein, I.D., Chin, G., Cho, F.S., Kelley, K.W., Miller, J.G., Chien, E.C., Liddelow, S.A., Nguyen, P.T., Nakao-Inoue, H., Dorman, L.C., et al. (2018). Astrocyte-derived interleukin-33 promotes microglial synapse engulfment and neural circuit development. Science *359*, 1269–1273. https://doi.org/10.1126/science.aal3589.

Vasek, M.J., Deajon-Jackson, J.D., Liu, Y., Crosby, H.W., Yi, J., and Dougherty, J.D. (2021). Microglia perform local protein synthesis at perisynaptic and phagocytic structures. 2021.01.13.426577. https://doi.org/10.1101/2021.01.13.426577.

Verkhratsky, A., and Nedergaard, M. (2018). Physiology of Astroglia. Physiol Rev *98*, 151. .

Villarin, J.M., McCurdy, E.P., Martínez, J.C., and Hengst, U. (2016). Local synthesis of dynein cofactors matches retrograde transport to acutely changing demands. Nat Commun *7*, 13865. https://doi.org/10.1038/ncomms13865.

Volta, V., Beugnet, A., Gallo, S., Magri, L., Brina, D., Pesce, E., Calamita, P., Sanvito, F., and Biffo, S. (2013). RACK1 depletion in a mouse model causes lethality, pigmentation deficits and reduction in protein synthesis efficiency. Cell. Mol. Life Sci. *70*, 1439–1450. https://doi.org/10.1007/s00018-012-1215-y.

Wake, H., Lee, P.R., and Fields, R.D. (2011). Control of Local Protein Synthesis and Initial Events in Myelination by Action Potentials. Science *333*, 1647–1651. https://doi.org/10.1126/science.1206998.

Wang, H.-Y., and Friedman, E. (2001). Increased association of brain protein kinase C with the receptor for activated C kinase-1 (RACK1) in bipolar affective disorder. Biological Psychiatry *50*, 364–370. https://doi.org/10.1016/S0006-3223(01)01147-7.

Wang, M.X., Ray, L., Tanaka, K.F., Iliff, J.J., and Heys, J. (2021). Varying perivascular astroglial endfoot dimensions along the vascular tree maintain perivascular-interstitial flux through the cortical mantle. Glia *69*, 715–728. https://doi.org/10.1002/glia.23923.

Wehner, P., Shnitsar, I., Urlaub, H., and Borchers, A. (2011). RACK1 is a novel interaction partner of PTK7 that is required for neural tube closure. Development *138*, 1321–1327. https://doi.org/10.1242/dev.056291.

Wilcock, D.M., Vitek, M.P., and Colton, C.A. (2009). Vascular amyloid alters astrocytic water and potassium channels in mouse models and humans with Alzheimer's disease. Neuroscience *159*, 1055–1069. https://doi.org/10.1016/j.neuroscience.2009.01.023.

Wolf, S.A., Boddeke, H.W.G.M., and Kettenmann, H. (2017). Microglia in Physiology and Disease. Annu. Rev. Physiol. *79*, 619–643. https://doi.org/10.1146/annurev-physiol-022516-034406.

Wolosker, H., Balu, D.T., and Coyle, J.T. (2017). Astroglial Versus Neuronal D-Serine: Check Your Controls! Trends in Neurosciences *40*, 520–522. https://doi.org/10.1016/j.tins.2017.06.010.

Wu, K.Y., Hengst, U., Cox, L.J., Macosko, E.Z., Jeromin, A., Urquhart, E.R., and Jaffrey, S.R. (2005). Local translation of RhoA regulates growth cone collapse. Nature *436*, 1020–1024. https://doi.org/10.1038/nature03885.

Xie, J., Han, Y., and Wang, T. (2021). RACK1 modulates polyglutamine-induced neurodegeneration by promoting ERK degradation in Drosophila. PLOS Genetics *17*, e1009558. https://doi.org/10.1371/journal.pgen.1009558.

Xiong, Z., Zhang, K., Ren, Q., Chang, L., Chen, J., and Hashimoto, K. (2019). Increased expression of inwardly rectifying Kir4.1 channel in the parietal cortex from patients with major depressive disorder. Journal of Affective Disorders *245*, 265–269. https://doi.org/10.1016/j.jad.2018.11.016.

Xu, A., and Barna, M. (2020). Cleaning up stalled ribosome-translocon complexes with ufmylation. Cell Res *30*, 1–2. https://doi.org/10.1038/s41422-019-0249-1.

Xu, K., Zhong, G., and Zhuang, X. (2013). Actin, Spectrin, and Associated Proteins Form a Periodic Cytoskeletal Structure in Axons. Science *339*, 452–456. https://doi.org/10.1126/science.1232251.

Xu, X., Yang, X., Xiong, Y., Gu, J., He, C., Hu, Y., Xiao, F., Chen, G., and Wang, X. (2015). Increased expression of receptor for activated C kinase 1 in temporal lobe epilepsy. Journal of Neurochemistry *133*, 134–143. https://doi.org/10.1111/jnc.13052.

Yaka, R., Thornton, C., Vagts, A.J., Phamluong, K., Bonci, A., and Ron, D. (2002). NMDA receptor function is regulated by the inhibitory scaffolding protein, RACK1. Proc Natl Acad Sci U S A *99*, 5710–5715. https://doi.org/10.1073/pnas.062046299.

Yaka, R., He, D.-Y., Phamluong, K., and Ron, D. (2003). Pituitary Adenylate Cyclase-activating Polypeptide (PACAP(1–38)) Enhances N-Methyl-d-aspartate Receptor Function and Brain-derived Neurotrophic Factor Expression via RACK1*. Journal of Biological Chemistry *278*, 9630–9638. https://doi.org/10.1074/jbc.M209141200.

Yang, H., Zhu, Q., Cheng, J., Wu, Y., Fan, M., Zhang, J., and Wu, H. (2019a). Opposite regulation of Wnt/β-catenin and Shh signaling pathways by Rack1 controls mammalian cerebellar development. Proc Natl Acad Sci USA *116*, 4661–4670. https://doi.org/10.1073/pnas.1813244116.

Yang, H., Yang, C., Zhu, Q., Wei, M., Li, Y., Cheng, J., Liu, F., Wu, Y., Zhang, J., Zhang, C., et al. (2019b). Rack1 Controls Parallel Fiber–Purkinje Cell Synaptogenesis and Synaptic Transmission. Front Cell Neurosci *13*. https://doi.org/10.3389/fncel.2019.00539.

Yewdell, J.W., and David, A. (2013). Nuclear translation for immunosurveillance. Proceedings of the National Academy of Sciences *110*, 17612–17613. https://doi.org/10.1073/pnas.1318259110.

Yip, M.C.J., and Shao, S. (2021). Detecting and Rescuing Stalled Ribosomes. Trends in Biochemical Sciences *46*, 731–743. https://doi.org/10.1016/j.tibs.2021.03.008.

Yoon, Y.J., Wu, B., Buxbaum, A.R., Das, S., Tsai, A., English, B.P., Grimm, J.B., Lavis, L.D., and Singer, R.H. (2016). Glutamate-induced RNA localization and translation in neurons. Proceedings of the National Academy of Sciences *113*, E6877–E6886. https://doi.org/10.1073/pnas.1614267113.

Yoshimura, A., Fujii, R., Watanabe, Y., Okabe, S., Fukui, K., and Takumi, T. (2006). Myosin-Va Facilitates the Accumulation of mRNA/Protein Complex in Dendritic Spines. Current Biology *16*, 2345–2351. https://doi.org/10.1016/j.cub.2006.10.024.

Younts, T.J., Monday, H.R., Dudok, B., Klein, M.E., Jordan, B.A., Katona, I., and Castillo, P.E. (2016). Presynaptic Protein Synthesis Is Required for Long-Term Plasticity of GABA Release. Neuron *92*, 479–492. https://doi.org/10.1016/j.neuron.2016.09.040.

Yousefi, R., Fornasiero, E.F., Cyganek, L., Jakobs, S., Rizzoli, S.O., Rehling, P., and Pacheu-Grau, D. (2020). Local translation in synaptic mitochondria influences synaptic transmission. BioRxiv 2020.07.22.215194. https://doi.org/10.1101/2020.07.22.215194.

Yu, X., and Khakh, B.S. (2022). SnapShot: Astrocyte interactions. Cell *185*, 2. https://doi.org/10.1016/j.cell.2021.09.029.

Yu, J., Chen, M., Huang, H., Zhu, J., Song, H., Zhu, J., Park, J., and Ji, S.-J. (2018). Dynamic m6A modification regulates local translation of mRNA in axons. Nucleic Acids Res *46*, 1412–1423. https://doi.org/10.1093/nar/gkx1182.

Zhang, H., and Verkman, A.S. (2008). AQUAPORIN-4 INDEPENDENT Kir4.1 K+ CHANNEL FUNCTION IN BRAIN GLIAL CELLS. Mol Cell Neurosci *37*, 1–10. https://doi.org/10.1016/j.mcn.2007.08.007.

Zhang, J., Hou, L., Klann, E., and Nelson, D.L. (2009). Altered Hippocampal Synaptic Plasticity in the *Fmr1* Gene Family Knockout Mouse Models. Journal of Neurophysiology *101*, 2572–2580. https://doi.org/10.1152/jn.90558.2008.

Zhang, L., Lv, Y., Rong, Y., Chen, W., Fang, Y., Mao, W., Lou, W., Jin, D., and Xu, X. (2019a). Downregulated expression of RACK1 results in pancreatic cancer growth and metastasis. OTT *Volume 12*, 1007–1020. https://doi.org/10.2147/OTT.S176101.

Zhang, Y., Chen, K., Sloan, S.A., Bennett, M.L., Scholze, A.R., O'Keeffe, S., Phatnani, H.P., Guarnieri, P., Caneda, C., Ruderisch, N., et al. (2014). An RNA-sequencing transcriptome and splicing database of glia, neurons, and vascular cells of the cerebral cortex. J Neurosci *34*, 11929–11947. https://doi.org/10.1523/JNEUROSCI.1860-14.2014.

Zhang, Z., Ma, Z., Zou, W., Guo, H., Liu, M., Ma, Y., and Zhang, L. (2019b). The Appropriate Marker for Astrocytes: Comparing the Distribution and Expression of Three Astrocytic Markers in Different Mouse Cerebral Regions. Biomed Res Int *2019*, 9605265. https://doi.org/10.1155/2019/9605265.

Zhao, W., Zhang, S., Zhu, Y., Xi, X., Bao, P., Ma, Z., Kapral, T.H., Chen, S., Zagrovic, B., Yang, Y.T., et al. (2022). POSTAR3: an updated platform for exploring post-transcriptional regulation coordinated by RNA-binding proteins. Nucleic Acids Res *50*, D287–D294. https://doi.org/10.1093/nar/gkab702.

Zhou, X., Liao, W.-J., Liao, J.-M., Liao, P., and Lu, H. (2015). Ribosomal proteins: functions beyond the ribosome. J Mol Cell Biol *7*, 92–104. https://doi.org/10.1093/jmcb/mjv014.

Zhu, Q., Chen, L., Li, Y., Huang, M., Shao, J., Li, S., Cheng, J., Yang, H., Wu, Y., Zhang, J., et al. (2021). Rack1 is essential for corticogenesis by preventing p21-dependent senescence in neural stem cells. Cell Reports *36*, 109639. https://doi.org/10.1016/j.celrep.2021.109639.

Résumé

Dans le système nerveux central, les neurones sont en intéraction avec une autre population cellulaire : les cellules gliales. Parmi ces cellules, les astrocytes intéragissent avec les synapses, lieu de communication entre 2 neurones où elles régulent la transmission synaptique. Cette interface s'accompagne d'un polarité moléculaire soutenue par la synthèse locale, c'est à dire au niveau de cette interface, de protéines spécifiques. Pendant ma thèse j'ai voulu comprendre les mécanisme de cette synthèse locale dans les astrocytes. J'ai identifié une protéine, RACK1, comme régulant la synthèse d'un canal au potassium, KIR4.1, crucial dans la bonne transmission nerveuse. En effet, dans une souris transgénique où RACK1 est inactivé dans les astrocytes, les propriétés synaptiques des neurones étaient modifié dues à une modification des échanges de potassium. Ma thèse met en lumière de nouveaux mécanismes moléculaires des astrocytes dans la régulation des fonctions cérébrales.

Abstract

In the central nervous system, neurons interact with another cell population : glial cells. Among these cells, astrocytes interact with synapses, communication hub between 2 neurons where they regulate synaptic transmission for instance. This interface display a molecular polarity sustained by the local synthesis, meaning at the level of this interface, of specific proteins. During my PhD, I wanted to uncover mechanisms of this local synthesis in astrocytes. I identified RACK1 as a protein regulating the synthesis of KIR4.1, a potassium channel, crucial for the good nervous transmission. Indeed, in a transgenic mouse in which RACK1 is inactivated in astrocytes, the synaptiques properties of neurons were changed due to a potassium exchange modification. My thesis highlights new molecular pathways in astrocytes in the regulation of brain functions.